Modelling flow and transport in the Chalk unsaturated zone

by

Simon Alexander Mathias

A thesis submitted for the degree of Doctor of Philosophy
of the University of London

Department of Civil and Environmental Engineering
Imperial College London

September 13, 2005

Abstract

The Chalk is an important aquifer representing 20% of all national water supplies in the United Kingdom (UK Groundwater Forum, 1998). Much of the aquifer is unconfined and in places overlain by a deep unsaturated zone which may be 10's of metres thick. Understanding flow and transport processes within the unsaturated zone is important as they dictate the fate and behaviour of groundwater contaminants and the quality of aquifer recharge.

This thesis develops a unified physics-based modelling framework for unsaturated chalk that is consistent with observed (often apparently contradictory) phenomena at chalk sites. These include: a fast water table response to rainfall events (in days) and an absence of surface run-off (*Headworth*, 1972); slow solute migration (in tens of years) with very little dispersion (*Oakes et al.*, 1981); specific yields that can vary by an order of magnitude during droughts (*Price et al.*, 2000).

Flow in unsaturated chalk is described using a modified Richards' equation for dual-permeability, whereby fast flow occurs in fractures and much slower flow occurs in the matrix. Hydraulic characterisation of the matrix is achieved using existing mercury intrusion data. The fractures are characterised by consideration of existing *in situ* hydraulic conductivity data.

Hypothetical coupled transient flow and solute transport simulations of the model are presented. A key finding is that the system is highly non-linear causing different temporal sampling rates of the precipitation time-series to yield very different results. The simulations support the widely accepted hypothesis that peak preservation in observed solute profiles is an artefact of very little fracture flow. The model further suggests that the Chalk unsaturated zone possesses significant storage properties (excluding the intergranular pores of the matrix) which attenuate infiltration to a rate which can be absorbed by the matrix and provide greater storage than that identified from conventional pumping test analyses.

Acknowledgements

Thanks to the Engineering and Physical Sciences Research Council for funding this project.

Thanks to Denis Peach, Daren Gooddy, Paul Shand, John Bloomfield and Alex Gallagher at the British Geological Survey (BGS). Throughout the duration of this project I have visited the BGS on more than ten occasions and made numerous presentations discussing the progress of this project. Their field experience has made an invaluable contribution to my conceptual understanding of the Chalk unsaturated zone. Similar thanks must also be made to David Cooper at the Centre of Ecology and Hydrology, especially for his guided tour around instrumented sites in Oxfordshire and Berkshire where much of the relevant fieldwork detailed in the literature was undertaken.

Thanks to John Barker and Tim Atkinson at University College London for showing me how easy it is to numerically invert Laplace transforms and for showing me the benefits of normalising to an advective travel time as opposed to a characteristic block diffusion time. Thanks also to Robert Zimmerman at the Royal School of Mines, Imperial College London for his thoughtful guidance offered during my transfer exam and many times after. Thanks also to Geoff Stephenson (Imperial College Maths Advice Centre) for getting my maths up to scratch.

I would like to thank my PhD examiners, John Barker and Peter Jackson for thoroughly reviewing and commenting on this thesis.

Special thanks must be made to Bethanna Jackson from this department for her patience with all the mathematical, numerical and soil physical support she has offered throughout this project. I am also entirely grateful for the professional guidance provided to me by my supervisors, Howard Wheater, Adrian Butler and Neil McIntyre.

Finally, I must thank my beautiful wife and wonderful son for putting up with having a 'student' husband/dad for the last four years. Without their support none of this would have been possible.

Note that Chapters 3 and 5 along with Appendix B have been (or are in the process of being) published in multi-author papers. While the respective co-authors have been invaluable to the development of these papers and this thesis, I would like to confirm that their role has always been advisory and that the work discussed in this thesis was carried out by myself, unless otherwise stated.

Contents

List of Figures

List of Tables

Notation

a	fracture half-width;	$[L]$
a_0	contact point half-width;	$[L]$
a_1	contact point half-spacing;	$[L]$
b	matrix block half-width;	$[L]$
b_1	bedding plane half-spacing;	$[L]$
c	solute concentration;	$[ML^{-3}]$
c_f	solute concentration in the fractures;	$[ML^{-3}]$
c_m	solute concentration in the matrix;	$[ML^{-3}]$
$\overline{c}_m$	mean solute concentration in the matrix over the X direction;	$[ML^{-3}]$
c_{max}	amplitude of oscillation (a solute concentration);	$[ML^{-3}]$
$f(T)$	arbitrary function;	$[-]$
g	gravitational acceleration;	$[LT^{-2}]$
$g(T)$	arbitrary function;	$[-]$
h	hydraulic head;	$[L]$
k	intrinsic permeability;	$[L]$
k_r	relative permeability;	$[-]$
m	van Genuchten parameter;	$[-]$
n	van Genuchten parameter, $n = \lambda + 1$ for $m = 1 - 1/n$ and $\psi << \psi_s$;	$[-]$
q	water flux;	$[LT^{-1}]$
q_f	water flux in the fractures;	$[LT^{-1}]$
q_{fm}	solute exchange flux between fractures and matrix;	$[ML^{-3}T^{-1}]$
q_m	water flux in the matrix;	$[LT^{-1}]$
q_{re}	recharge;	$[LT^{-1}]$
q_w	water flux;	$[LT^{-1}]$
q_s	solute flux;	$[ML^{-2}T^{-1}]$
r	pore-radius (which is analogous to fracture-aperture);	$[L]$
r_s	the largest sized pore with a significant presence, $r_s = -2\kappa \cos\Theta/\rho g\psi_s$;	$[L]$
s	Laplace transform variable;	$[-]$

t	time;	$[T]$
t_a	advective travel time (or centroid), $t_a = (L/v_f)(1+\sigma)$ for a dual-porosity model and $t_a = (L/v_f)(1+\sigma)/(1+\beta\sigma)$ for a dual-permeability model;	$[T]$
t_d	delay time;	$[T]$
t_r	residence time;	$[T]$
t_{cb}	characteristic block diffusion time, $t_{cb} = b^2/D_A$;	$[T]$
t^*_{cb}	equivalent characteristic block diffusion time accounting for flow in the matrix;	$[T]$
t_p	period of oscillation;	$[T]$
v	pore-water velocity;	$[LT^{-1}]$
$\overline{v}$	composite mean velocity of a fractured porous medium;	$[LT^{-1}]$
v_f	pore-water velocity in the fractures;	$[LT^{-1}]$
v_m	pore-water velocity in the matrix;	$[LT^{-1}]$
v_{peak}	displacement of a solute peak over one day;	$[LT^{-1}]$
v_∞	downward velocity of a contaminant assuming fractures and matrix are in equilibrium (i.e. when $D_A \to \infty$);	$[LT^{-1}]$
w_f	fracture-matrix volumetric weighting factor, $w_f = a/(a+b)$	$[-]$;
x	horizontal distance (normally from the centre of a matrix block);	$[L]$
y	horizontal distance;	$[L]$
z	vertical distance (normally depth);	$[L]$
z_0	depth of zero flux plane;	$[L]$
z_{wt}	depth of water table;	$[L]$
AE	actual evaporation;	$[L]$
C	specific capacity, $C = d\theta/d\psi$;	$[L^{-1}]$
C_1	root constant;	$[L]$
C_2	wilting point;	$[L]$
C_3	empirical constant relating actual to potential evapotranspiration;	$[-]$
C_f	specific capacity in the fractures;	$[L^{-1}]$
C_m	specific capacity in the matrix;	$[L^{-1}]$
D	dispersion coefficient;	$[L^2T^{-1}]$

D_A	apparent diffusion coefficient;	$[L^2T^{-1}]$
D_L	longitudinal dispersion coefficient;	$[L^2T^{-1}]$
D_T	transverse dispersion coefficient;	$[L^2T^{-1}]$
E	Young's modulus;	$[ML^{-1}T^{-2}]$
J	hydraulic gradient;	$[-]$
K	hydraulic conductivity;	$[LT^{-1}]$
K_a	matrix hydraulic conductivity close to fracture interface;	$[LT^{-1}]$
K_{eff}	block-scale hydraulic conductivity;	$[LT^{-1}]$
K_f	hydraulic conductivity in the fractures;	$[LT^{-1}]$
$K_{f,s}$	saturated hydraulic conductivity in the fractures;	$[LT^{-1}]$
K_m	hydraulic conductivity in the matrix;	$[LT^{-1}]$
$K_{m,s}$	saturated hydraulic conductivity in the matrix;	$[LT^{-1}]$
K_s	saturated hydraulic conductivity;	$[LT^{-1}]$
L	a length;	$[L]$
N	number of identical continuously stirred tank reactors in series;	$[-]$
P	precipitation;	$[L]$
Pe	Peclet number, $Pe = vL/D_L$;	$[-]$
PE	potential evapotranspiration;	$[L]$
Q	flow;	$[L^3T^{-1}]$
R	largest pore-radius that contains water at a given pressure head, $R = -2\kappa\cos\Theta/\rho g\psi$;	$[L]$
S_e	effective saturation, $S_e = (\theta - \theta_r)/(\theta_s - \theta_r)$;	$[-]$
S_s	specific storage (associated with compressibility);	$[L^{-1}]$
S_y	specific yield, $S_y = \Delta V_w/\Delta z_{wt}$;	$[-]$
SMD	soil moisture deficit;	$[L]$
T	dimensionless time, in Chapter 2 and Appendix A, $T = t/t_{cb}$ and in Chapter 3 and Appendix B, $T = t/t_a$;	$[-]$
T_d	dimensionless delay time, $T_d = t_d/t_a$;	$[-]$
T_r	dimensionless delay time, $T_r = t_r/t_a$;	$[-]$
V	total water content;	$[L]$
X	dimensionless horizontal distance, $X = x/b$;	$[-]$
Z	dimensionless depth, $Z = z/L$;	$[-]$

α	van Genuchten parameter, $\alpha = \psi_s^{-1}$ for $\psi << \psi_s$;	$[L^{-1}]$
α_s	solute mass transfer coefficient, $\alpha_s = \omega D_A / b^2$;	$[T^{-1}]$
α_w	water mass transfer coefficient, $\alpha_w = \omega \gamma_w K_a / b^2$;	$[T^{-1}]$
β	matrix-fracture pore-water velocity ratio, $\beta = v_m / v_f$;	$[-]$
γ	advective-diffusive time ratio, $\gamma = t_a / t_{cb}$;	$[-]$
γ_1	compressibility of rock;	$[M^{-1}LT^2]$
γ_2	compressibility of water;	$[M^{-1}LT^2]$
γ_w	empirical factor;	$[-]$
δ	dimensionless phase angle;	$[-]$
$\delta(T)$	Dirac delta function;	$[-]$
ϵ	Poisson's ratio;	$[-]$
ζ	location of the solute front on the X axis;	$[-]$
η	tortuosity parameter;	$[-]$
η_f	tortuosity parameter for the fractures;	$[-]$
η_m	tortuosity parameter for the matrix;	$[-]$
θ	moisture content;	$[-]$
θ_f	moisture content in the fractures;	$[-]$
θ_m	moisture content in the matrix;	$[-]$
θ_r	residual moisture content;	$[-]$
θ_s	saturated moisture content;	$[-]$
κ	surface tension;	$[MT^{-2}]$
λ	Brooks and Corey parameter;	$[-]$
λ_f	Brooks and Corey parameter for the fractures;	$[-]$
λ_m	Brooks and Corey parameter for the matrix;	$[-]$
μ_1'	first absolute moment;	$[-]$
μ_2	second central moment;	$[-]$
μ_3	third central moment;	$[-]$
ν	kinematic viscosity;	$[L^2T^{-1}]$
ρ	radial distance from the centre of a contact point;	$[L]$
ρ_w	density of water;	$[ML^{-3}]$
σ	porosity ratio, $\sigma = \phi b / a$;	$[-]$
ϕ	porosity (normally of the matrix);	$[-]$
ϕ_f	fracture porosity;	$[-]$

ϕ_m	matrix porosity;	$[-]$
χ	dispersivity;	$[L]$
ψ	pressure head;	$[L]$
ψ_0	a constant boundary pressure head;	$[L]$
ψ_1	a constant boundary pressure head;	$[L]$
ψ_c	air entry pressure head;	$[L]$
ψ_f	pressure head in fractures;	$[L]$
ψ_m	pressure head in the matrix;	$[L]$
$\psi_{f,s}$	air entry pressure head of the largest sized aperture with a significant presence in the fractures;	$[L]$
$\psi_{m,s}$	air entry pressure head of the largest sized pore with a significant presence in the matrix;	$[L]$
ψ_s	air entry pressure head of the largest sized pore with a significant presence;	$[L]$
ω	block geometry coefficient;	$[-]$
Γ_s	solute mass transfer term;	$[ML^{-3}T^{-1}]$
Γ_w	water mass transfer term;	$[T^{-1}]$
Δv	difference between fracture and matrix pore-water velocities, $\Delta v = v_f - v_m$;	$[LT^{-1}]$
Δx	finite space step;	$[L]$
Δz	finite space step;	$[L]$
Δz_{wt}	change in depth of water table;	$[L]$
ΔT	finite dimensionless time step;	$[-]$
ΔX	finite dimensionless space step;	$[-]$
ΔV_w	change in total water content;	$[L]$
Θ	contact angle;	$[-]$
Λ	normalised fracture-matrix exchange term, in Chapter 2, $\Lambda = t_{cb} q_{fm}/\sigma$ and in Chapter 3, $\Lambda = t_a q_{fm}/\sigma$;	$[ML^{-3}]$
Λ^*	normalised fracture-matrix exchange term specific for a unit step change in fracture concentration, i.e. a block geometry function;	$[ML^{-3}]$
Ω	characteristic frequency, $\Omega = 2\pi t_{cb}/t_p$;	$[-]$

Chapter 1

Introduction

About 35 million years ago, during the Late Cretaceous period, sea levels were several hundred metres higher than today and Northern Europe was arid. These conditions significantly limited rates of erosion, which allowed the formation of a soft white ooze on the seabed from the accumulation of coccoliths (the exoskeletons of planktonic algae). This ooze layer then hardened to form the limestone lithostratigraphic unit known as the Chalk. The depositional, diagenetic and tectonic history that followed gave rise to an aquifer with a fine-grained porous matrix traversed by a network of fractures (*Downing et al.*, 1993).

This type of aquifer is often referred to as a dual-porosity aquifer whereby the aquifer possesses a matrix porosity and a fracture porosity. Note that within the literature, the term dual-porosity is commonly used to describe models where flow occurs in the fractures but not in the matrix while dual-permeability is used to describe models where flow occurs in both the fractures and the matrix (see Figure 1.1). In the Chalk, the matrix porosity ranges between 0.3 to 0.4 whereas the fracture porosity is typically no more than 0.01. In contrast, the matrix hydraulic conductivity is around 0.1 cm/day whereas the hydraulic conductivity of fractures can be up to 100 cm/day. Hence the Chalk represents a system whereby, under saturated conditions, water is mostly stored in the matrix while flow mostly occurs in fractures (*Price et al.*, 1993).

The Chalk is an important aquifer representing 20% of all national water supplies in the United Kingdom (UK Groundwater Forum, 1998). Much of the aquifer is unconfined and, in places, overlain by a deep unsaturated zone which may be 10's of metres thick. Understanding flow and transport processes within the unsaturated zone is important as they dictate the fate and behaviour of groundwater contaminants and the quality of aquifer recharge. This thesis sets out to develop a unified physically-based modelling framework for unsaturated

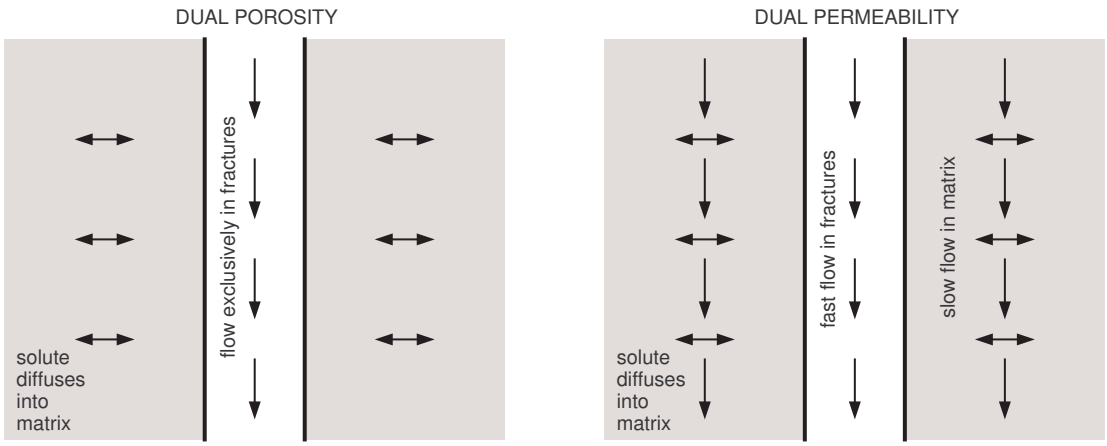

Figure 1.1 Schematic diagram of dual-porosity and dual-permeability systems.

Chalk.

1.1 Current understanding of the Chalk unsaturated zone

Flow in the unsaturated zone of the Chalk was originally believed to be predominantly through fractures. Evidence to support this included the observed rapid response of the water table after high intensity rainfall events (*Headworth*, 1972) and the appearance of bacteria in boreholes (*Maclean*, 1969). This was largely unquestioned prior to a 1968 study of tritium content in pore-water from the unsaturated zone at a Berkshire site which led *Smith et al.* (1970) to suggest that 85% of the total flow through the unsaturated zone was by intergranular seepage through the matrix at a mean rate of less than 0.9 m/year. This rate of solute movement has been widely supported by many other similar studies (e.g. *Oakes*, 1977; *Wellings*, 1984b; *Barraclough et al.*, 1994). The rapid observed response of water tables was then explained by a 'piston-displacement' mechanism whereby water arriving at the water table had been displaced from the bottom of the unsaturated zone instead of travelling quickly through it (*Price et al.*, 1993).

However, the saturated hydraulic conductivity of the Chalk matrix is consistently observed to be less than 10 mm/day (e.g. *Wellings*, 1984a; *Cooper et al.*, 1990; *Hodnett and Bell*, 1990) in contrast to measurements of daily rainfall, which can be up to 100 mm in the United Kingdom. Noting that observations of surface runoff in Chalk catchments are rare, it follows that despite the evidence of slow solute migration, significant amounts of water must be absorbed by fracture flow (*Foster*, 1975). The model suggested by *Smith et al.* (1970)

implicitly assumed that the tritium entering the unsaturated zone is areally uniform. *Foster* (1975) speculated that it was more likely that tritium input to the unsaturated zone (after infiltration through a thin soil cover) would be focused on fracture openings within the Chalk. The concentration gradients between the contaminated fracture water and the cleaner matrix water would then cause lateral diffusion of the solute into the matrix, thus greatly retarding its downward movement. This mechanism presented a means by which fracture-dominated flow could be reconciled with a much slower observed downward movement of tritium.

Building on the ideas of *Foster* (1975), *Young et al.* (1976) developed a simple solute transport model which assumed that flow occurred exclusively in fractures while solutes diffused instantaneously into the matrix. This idea is often referred to as the local equilibrium assumption (e.g. *Valocchi*, 1985) in that it is assumed that the fractures and matrix have the same solute concentration (i.e. are in equilibrium). The advantage of such an approach is that only one concentration field need be considered and no parameters are required to describe solute transfer between the two domains. *Young et al.* (1976), *Oakes* (1977) and *Oakes et al.* (1981) had significant success in calibrating their model to a range of solute profiles describing different solutes at different places.

Invoking Fickian diffusion provides a more rigourous model to describe fracture-matrix transfer (*Barker and Foster*, 1981; *Barker*, 1982, 1991; *Sudicky and Frind*, 1982; *Lever et al.*, 1983) (the subject of fracture-matrix transfer including the governing equation is discussed further in Chapter 2). *Barker and Foster* (1981) set up some simple numerical experiments to compare the local equilibrium model with a Fickian (or diffusive) representation of a Chalk matrix block. They found that for typical fracture spacings, the Fickian model invoked significant solute dispersion for apparent diffusion coefficients $< 10^{-8}\mathrm{m}^2/\mathrm{s}$. Note that in the absence of hydrodynamic dispersion, the local equilibrium assumption invokes zero dispersion.

This presented a conundrum because measured values of apparent diffusion coefficients for conservative solutes (e.g. chloride, nitrate and tritium) ranged between 10^{-11} and 10^{-10} m^2/s (*Hill*, 1984; *Gooddy et al.*, 1995). Furthermore, field data indicate very low levels of dispersion (through strong peak preservation) over pore-water profiles as deep as 40 m (*Smith et al.*, 1970; *Young et al.*, 1976; *Oakes*, 1977; *Oakes et al.*, 1981; *Barraclough et al.*, 1994). This subject is discussed further in Chapter 3 where it is speculated that the failure of the *Barker and Foster* (1981) model to accommodate these field observations is due to the fact that they assumed that flow in the matrix is negligible.

While work carried out in the 1970s and early 80s focused on solute transport, the work of the 1980s was more focused on flow. *Wellings and Bell* (1980) presented measurements

of the annual cycle of changes in water content and potential in the 40 m thick unsaturated zone of the Upper Chalk at a site in southern England. They found that throughout the year, below 5 or 6 m into the unsaturated zone, pressure heads ranged between -50 cm and -150 cm H_2O. Applying the capillary theory of *Marshall* (1959), *Wellings and Bell* (1980) calculated that almost no flow took place in the fractures throughout the year.

Wellings (1984a) presented measurements of unsaturated hydraulic conductivity against pressure head for the same site down to a depth of 3 m. The hydraulic conductivity remained almost constant around 2 to 6 mm/day and then sharply rose as the pressure head exceeded -50 cm. These features are consistent with observations made at a number of other sites in the Chalk (*Cooper et al.*, 1990; *Hodnett and Bell*, 1990; *Mahamood-ul-Hassan and Gregory*, 2002). The sharp rise is associated with the onset of fracture flow, while the almost constant values of hydraulic conductivity are associated with the saturated hydraulic conductivity of the Chalk matrix.

It has often been assumed that fractures drain instantaneously giving rise to a close association of fracture porosity with specific yield (ordinarily obtained from pumping tests) (*Price et al.*, 1993). However, *Lewis et al.* (1993) found that during drought periods, estimates of groundwater storage, obtained by determining the volume of Chalk in an interval between two potentiometric surfaces on various dates and multiplying it by an assumed value of specific yield, were an order of magnitude smaller than estimates from base-flow calculated from catchment outlet data. It is unlikely that extra water could have drained from the Chalk matrix because intergranular pores are typically less than a micron in diameter, suggesting that they are unlikely to drain until pressure heads drop below -30 m (*Price et al.*, 1976).

But if the fractures had drained completely and the matrix was never going to drain, it is difficult to understand where this extra water could have come from. From a series of core-scale drainage measurements, *Price et al.* (2000) concluded that substantial storage of water could occur in the unsaturated zone within films generated on the surface irregularities of matrix blocks. It was suggested that as pressure heads increase, continuously larger depressions on a fracture face fill with water until the fracture becomes completely filled and fracture flow is initiated. Because the occurrence of completely filled fractures is rare, it follows that drainage of smaller depressions must be predominantly due to the suction of water into the matrix (matrix imbibition) followed by downward flow through the matrix (*Price et al.*, 2000).

Further reviews of the literature regarding flow and transport in the Chalk unsaturated zone are offered in Chapters 3 and 4 although the above is considered enough to establish

the current understanding of the Chalk unsaturated zone. To summarise, the Chalk is a fractured porous medium. Flow can occur in the fractures and to a lesser extent in the matrix. A number of the observations detailed above are difficult to reconcile. These include: a fast water table response to rainfall events (in days) and an absence of surface run-off (*Headworth*, 1972); slow solute migration (in tens of years) with very little dispersion (*Oakes et al.*, 1981); specific yields that can vary by an order of magnitude during droughts (*Price et al.*, 2000). Representing these processes in a consistent quantitative model is non-trivial. Consequently, as demonstrated in the following section, modellers have generally resorted to over simplistic representations.

1.2 A history of modelling the Chalk unsaturated zone

The first models of contaminant transport in the Chalk unsaturated zone utilised the uniform solute velocity model suggested by *Young et al.* (1976). These authors also prescribed a 10 to 15% solute bypass to the water table to account for extreme infiltration events when fracture flow is too fast to allow solute exchange with the matrix. This model has been successful in describing nitrate, tritium and chloride profiles in unsaturated Chalk at various sites across the UK (*Young et al.*, 1976; *Oakes*, 1977; *Oakes et al.*, 1981). A steady-state flow field was assumed. Tritium input pulses were derived from knowledge of tritium contents in rainfall, nitrate inputs were translated from land management histories and model outputs were calibrated against the observed profiles to obtain parameters describing the system.

The same framework was also used by *Carey and Lloyd* (1985) to obtain a nitrate input for a regional saturated zone nitrate model. The model proved to be highly efficient in predicting long-term trends but failed to represent the small-scale fluctuations of observed nitrate concentration. This is believed to be due to the assumption of steady state flow. Interestingly, sensitivity analyses showed unsaturated zone travel times to be the most dominant factor.

The *Young et al.* (1976) model, which invokes the local equilibrium assumption in conjunction with a 10 to 15% bypass function, is inconsistent with itself. The conceptual model assumes that all flow occurs in the fractures and solute concentrations diffuse instantaneously into the matrix so as to justify a uniform solute front movement. However, it also assumes that some flow occurs which is so fast that the fractures and matrix are no longer in equilibrium and completely independent (to account for the presence of extreme infiltration events, personal communications with J. A. Barker, 2005). In this way it represents the two extreme conditions of solute transport in a dual-porosity model. However, if we assume (as with

Smith et al., 1970) that 85% of water is flowing through the matrix and the remaining 10 to 15% flows in the fractures we have a model that is mathematically analogous to *Young et al.* (1976), but conceptually makes more reasonable sense.

Andrews et al. (1997) considered a transient flow field derived from daily recharge estimates using the Penman-Grindley model (a two-store soil moisture accounting model) (*Penman*, 1950; *Grindley*, 1969). Nitrate was assumed to enter the matrix at a rate defined by the daily recharge with an upper limit of 3.75 mm/day (i.e. the saturated hydraulic conductivity of the matrix). Any remaining recharge and its associated nitrate was bypassed directly to the water table. This idea is based on the hydraulic conductivity relationships observed by *Wellings* (1984a) and *Cooper et al.* (1990).

The *Andrews et al.* (1997) model has a more consistent theory than the previous models and allows us to understand better the physical assumptions that are being made. A key departure from the *Young et al.* (1976) model is the assumption that there is no interaction of solutes between the fractures and the matrix. This would make sense if the fractures were coated with some impregnable substance (such as a clay). However, no studies detailing significant fracture coatings in the Chalk unsaturated zone of the United Kingdom have been noted.

Andrews et al. (1997) describe their model output as comparing well (but not perfectly) with observed solute profiles. A question arises as to how well should they compare, or even if this is the right methodology for model validation. This model remains unsatisfactory because its assumption that fracture and matrix concentrations are independent remains to be proven. The consequence for getting it wrong could be dramatic. Consider a scenario where nitrate input is stopped. The *Andrews et al.* (1997) model would predict that currently residing nitrate will leave the unsaturated zone only at a rate up to the matrix saturated hydraulic conductivity. But if the fractures were interacting with the matrix, fast flowing water in the fractures could skim off nitrates from the existing matrix profile, giving rise to much earlier breakthrough times.

Attempts to model the Chalk unsaturated zone have also been driven by landfill contamination issues. *Fretwell et al.* (2000) describe a modelling study carried out to explain an apparent accumulation of chloride in the seasonal unsaturated zone (SUZ) beneath a landfill site in southern England. They describe the SUZ as "that part of an aquifer that lies between the highest and lowest water stands". Analysis of pore water profiles showed that chloride concentrations were highest within the SUZ (*Fretwell et al.*, 2000).

Fretwell et al. (2000) sought to explain this phenomenon using a semi-analytical formula-

tion of the dual-porosity solute transport problem described by *Barker et al.* (2000). *Fretwell et al.* (2000) describe the model as follows: The model domain consists of a one-dimensional vertical column divided into layers of uniform thickness. Each layer contains elements of both fracture and matrix. Matrix flow is ignored and solutes are transported into and out of the matrix by diffusion. The fractures and matrix are assumed to be homogenous throughout. As the water table rises and falls, contaminant mass enters and leaves the fracture component via source and sink terms so as to avoid the need of a two-dimensional representation. The simulation consisted of a period of solute injection (10 years) followed by a period of flushing with clean water. It was found that the peak concentration in the profile moved to the vertical centre of the SUZ.

Within the *Fretwell et al.* (2000) model, flow is not explicitly considered. A water table fluctuation is specified *a priori*, which is used to dictate how much water enters the model domain. As a result, the velocity direction changes throughout the year. As the water table moves up, it is assumed that water in the fractures moves up. (Generally, water tables move up due to water moving down from the surface of the unsaturated zone. This is not the case here because of an overlying concrete cover.) Similarly as the water table moves down, the water in the fractures moves down. Consequently, once solute enters the SUZ it remains trapped and concentrates in the middle.

1.3 Modelling flow and transport in unsaturated fractured rocks

Whilst models of flow and transport in the Chalk unsaturated zone are relatively under developed, much progress has been made in the field of unsaturated fractured rock as a whole. These models can be broadly classified into continuum and fracture network models:

In the continuum approach, fractures are considered to be sufficiently ubiquitous and distributed in such a manner that they can be meaningfully described statistically (*Bear*, 1993). The role of individual fractures in fractured media is considered to be similar to that of individual pores in porous media. Connected fractures and rock matrix are viewed as two or more overlapped interacting continua. In other words, at a 'point', two or more continua are considered to coexist (*Liu et al.*, 2003b).

The fracture network approach involves the generation, by computer simulation, of synthetic fracture networks, and the subsequent modelling of flow and transport in these networks (*Pruess et al.*, 1999). This approach has been applied under unsaturated conditions by

a number of authors (e.g. *Kwicklis and Healey*, 1993; *Zimmerman and Bodvarsson*, 1996; *Liu et al.*, 2003a). Fracture network models can be useful as tools to explore specific mechanistic concepts. However, the geometric parameters that most strongly impact flow and transport, such as fracture-apertures and connectivity, are almost impossible to constrain from field data (*Pruess et al.*, 1999).

Much work has gone into the development of process understanding and modelling of flow through unsaturated fractured rocks due to the proposed high level nuclear waste repository at Yucca Mountain, Nevada, USA (*Liu et al.*, 1998, 2003a,b,c; *Pruess*, 1999; *Pruess et al.*, 1999). Most of the literature discussed in this section was motivated by the Yucca Mountain Project. Yucca Mountain is comprised of a series of layered welded and non-welded tuffs associated with volcanic events at the site and subject to faulting. Away from the fault zones, welded tuffs are regarded as dual-permeability media with a matrix of moderate porosity and very low permeability, which has been subjected to fracturing (*Wang and Narasimhan*, 1993). The area is arid with an average annual rainfall of 170 mm (*Flint et al.*, 2001). For comparison, average annual rainfall in south-east England is around 750 mm (www.worldclimate.com, 2004).

As with *Wellings and Bell* (1980) and the Chalk, *Wang and Narasimhan* (1985) recognised that while fractures with large apertures will drain relatively easily, water is likely to remain in the matrix. This intuition stems from the knowledge that large pores cannot sustain large capillary suction forces (e.g. *Marshall and Holmes*, 1979; *Hillel*, 1980). In studies of saturated fracture flow, a parallel-plate model is frequently used (*Snow*, 1968; *Barker*, 1991, 1993). However, the parallel plate model implies that fractures are either completely filled or completely drained. This is an inadequate representation for the unsaturated zone. Because fractures have rough surfaces, different portions of a given fracture will be water filled depending on the local aperture and matric potential (*Wang and Narasimhan*, 1985). Based on this concept, *Wang and Narasimhan* (1985) built one of the first numerical models of unsaturated flow through fractured rocks. Both fractures and matrix continua were modelled using separate (but coupled) Richards' equations (*Richards*, 1931). A moisture retention function in the fracture domain was derived by assuming that the fracture-aperture distribution approximated to a gamma distribution function. Closed form relationships were then obtained for relative permeability (the normalised variation of permeability with pressure head) by applying a model similar to *Burdine* (1953) which assumed that permeability is cubically related to aperture size (see Chapter 4).

Kwicklis and Healey (1993) noticed that the moisture retention and relative permeability

functions of *Wang and Narasimhan* (1985) behaved very similarly to those presented by *van Genuchten* (1980) for porous soils. Consequently, the *van Genuchten* (1980) relationships have widely been used to describe both fractures and matrix blocks throughout both fracture network- and (e.g. *Kwicklis and Healey*, 1993; *Zimmerman and Bodvarsson*, 1996; *Liu et al.*, 2003a) continuum-based modelling studies (*Gerke and van Genuchten*, 1993a; *Zimmerman et al.*, 1996; *Liu et al.*, 1998, 2003c; *Doughty*, 1999).

Richards' equation based models typically predict downward water migration as proceeding in the form of smooth sheets (*Pruess et al.*, 1999). Due to the assumed large interaction area between flowing fractures and matrix block, these models tend to predict that water in fractures is quickly imbibed (or sucked) into the matrix, resulting in flow rates controlled by the much smaller matrix permeability (e.g. *Wang and Narasimhan*, 1985, 1993; *Nitao and Buscheck*, 1991). For average net infiltration on the order of 5 mm/year, volume-averaged pore velocities, predicted by such models, at 10% water-filled porosity are on the order of 50 mm/year (*Pruess et al.*, 1999). Waters percolating piston-style would then require thousands of years to reach the water table at Yucca Mountain, at a nominal depth of 600 m beneath the land surface (*Pruess et al.*, 1999). These model predictions were largely unquestioned prior to the finding of 'Bomb Pulse' (1963) Chlorine 36 deep within the Yucca Mountain unsaturated zone formation (*Fabryka-Martin et al.*, 1996). This would indicate pore-velocities of 10 m/year or even larger (*Pruess et al.*, 1999).

A corollary of applying capillary theory to fractures is that large fractures will only flow at large, close to atmospheric, pressures. *Tokunaga and Wan* (1997) proposed that flow in these fractures could potentially occur at much lower pressures through thin films along the fracture walls. However, their laboratory measurements of film thickness around an unconfined block of Bishop tuff showed that significant film flow did not occur until pressure heads exceeded -2.5 cm.

A problem with these models (both continuum and fracture-network) is that the assumption that downward water migration proceeds in the form of smooth sheets is false. Laboratory studies on unsaturated fracture replicas (normally made of epoxy resin or glass) have shown, without exception, that flow proceeds along localised preferential flow paths, or 'fingers' (e.g. *Nicholl et al.*, 1994; *Su et al.*, 1999, 2001). Furthermore, these flow paths are highly unstable, even under steady infiltration scenarios (*Nicholl et al.*, 1994; *Su et al.*, 1999).

Similar observations have been made in the Chalk unsaturated zone of the Negev desert in Israel. Over the last 18 years the northern Negev has become a prime target for siting a variety of chemical industries that have been rejected by or transferred from more populated areas

(*Nativ et al.*, 1995). Furthermore, the national site for treatment and isolation of hazardous waste has been operating there since 1975. The aridity of the area (50-200 mm/year rainfall) and the presumed low permeability of the underlying chalk formations of the Eocene Avdat Group have been considered major assets in preventing potential groundwater contamination resulting from these activities (*Nativ et al.*, 1995).

This hypothesis was thrown into question when *Nativ and Nissim* (1992) calculated pore-water velocities of up to 2.4 m/year, based on the presence of tritium and significant levels of heavy metals in the groundwater just ten years after operations had begun (the unsaturated zone in this area ranges in thickness from 20 to 60 m). However, pore-water profiles at the same site detected the bomb-pulse (1963) tritium peaks in a number of core-holes at just 2.5 m below ground surface inferring a much lower velocity of between 0.016 and 0.066 m/year (*Nativ et al.*, 1995).

To reconcile the two findings, *Nativ et al.* (1995) speculated that the tritium peaks may not have been produced exclusively by the 1963 pulse. Instead, they assumed that the peaks represent a mixture of modern (with low tritium content) and old (1963) water. *Nativ et al.* (1995) suggested that this hypothesis could be explained using a mechanism similar to the matrix diffusion theory of *Foster* (1975). However, as with the pore-water profiles obtained by *Smith et al.* (1970), *Oakes* (1977) and others, there is very little evidence of the solute spreading associated with this mechanism (see Chapter 3). Note that *Nativ et al.* (1995) do not support their hypothesis with any numerical studies.

In an attempt to further explain the conundrum presented by the conflicting results of *Nativ and Nissim* (1992) and *Nativ et al.* (1995), *Dahan et al.* (1998, 1999, 2001) set out to explicitly observe the flow processes within their chalk unsaturated zone. The experimental setup allowed complete control of the flow domain inlet and outlet of a single *in situ* fracture. Water flux into and out of the fracture was measured in small segments of the fracture openings, and flow trajectories were identified using seven flurobenzoic acid tracers. A 5-day percolation experiment on a 5.3 m long fracture showed significant spatial and temporal variability in the flow regime.

Flow through fracture openings did not reach steady state either in individual segments or across the entire flow domain, although the boundary conditions were kept relatively steady throughout the test. It appeared that over 70% of the flux was transmitted through <20% of the studied fracture openings *Dahan et al.* (1999). The authors end statement was that "it appears that no simple model for transient water flow through fractures can be directly applied to this data. Rather, a new conceptualisation is needed to define predictive and

quantitative models better".

While it is widely acknowledged that the capillary theory models are unable to represent this behaviour (e.g. *Glass et al.*, 1995; *Liu et al.*, 1998; *Pruess*, 1999; *Dahan et al.*, 1999), none of these experiments have offered data sufficient to parameterise a reasonable alternative. *Su et al.* (2001) was able to calibrate some arbitrary transfer-function relationships (log-normal distribution function, cells in series, etc.) to breakthrough curves obtained from laboratory scale tracer tests on a synthetic, unsaturated fracture. But it is difficult to conceive how such models could be appropriately extrapolated to the field-scale problems of interest.

There is also a question as to the applicability of these various findings to the Chalk unsaturated zone in the United Kingdom. The laboratory experiments were conducted on replica fractures where matrix imbibition would not occur. Conversely, the Chalk matrix is permeable, suggesting that matrix imbibition should be an important process. Numerical simulations suggest that matrix imbibition is likely to have a strong stabilising effect on flow in fractures (*Pruess*, 1999).

The field study presented by *Dahan et al.* (1999) and others in the Negev Chalk unsaturated zone is also far from the conditions expected in the United Kingdom. *Dahan et al.* (1999) removed the top three metres of surface material to obtain a horizontal, clean massive rock bench. Water was then irrigated directly into a single fracture at a continuous rate for five days. In the United Kingdom, chalk fractures are often covered by a thin soil layer. Furthermore, generally the top three metres is often weathered and gravelly (*Jones and Robins*, 1999). Such a layer could provide a significant storage component giving rise to flow attenuation and stabilisation.

It is interesting to note that within the Yucca Mountain Total System Performance Assessment (TSPA), YMUZ (Yucca Mountain Unsaturated Zone) is characterised by a continuum Richards' equation dual continua model where fracture-matrix transfer is characterised by a first-order transfer expression (also known as the quasi-steady-state model, see Chapter 2) (*Bechtel SAIC Company*, 2003). Furthermore, despite the known episodicity of the rainfall in the area (*Flint et al.*, 2001), flow is assumed to be steady state due to the presumed attenuating properties of a thick layer of non-welded tuff known as the Paintbrush Tuff (*Bechtel SAIC Company*, 2003). Solute transport is then routed through the steady state flow-field using the advection dispersion equation (*Bechtel SAIC Company*, 2003).

A limitation of the above methodology is the recognition that preferential flow pathways in unsaturated fractured rock have been observed to occur (e.g. *Nicholl et al.*, 1994; *Su et al.*, 1999, 2001). This limitation in the YMUZ flow model led to the development of the 'active

fracture' concept (*Liu et al.*, 1998), where it was postulated that because preferential flow pathways form, water only flows in a subset of the fractures, the active fractures.

Active fractures are not necessarily saturated and are assumed to have the same hydraulic characteristics as inactive fractures. Whereas conventional Richards' equation models predict that water flow takes place in progressively narrower pores with reducing saturation, the active fracture model also provides that water flow takes place in progressively fewer fractures, regardless of pore-size.

Liu et al. (1998) assume that the fraction of fractures that are active f_a is related to a power function of the effective water saturation, S_e (i.e. $f_a = S_e^{\gamma}$). This approach is attractive as it only introduces one additional parameter (γ) and has the properties that at $S_e = 0$ no fractures are flowing and at saturation, $S_e = 1$, flow takes place in all fractures. The relative permeability of the overall network of fractures is then given by f_a times the relative permeability of the active fracture system (considered by itself). The f_a factor also provides a saturation dependant, fracture-matrix interaction-area reduction-factor for calculating matrix imbibition of water and matrix diffusion of solutes.

A potential problem with this approach is that there is no physical basis for assuming the fraction of active-fractures is a function of saturation (let alone a power law) or even constant for constant levels of saturation.

There are clearly many more limitations with the modelling procedure above. However, given all the resources that were available throughout the 30 year (to date) project, the scientists involved have been unable to offer a more practical alternative. Consequently, for this project we have considered it prudent to follow a similar route by adopting a Richards' equation, continuum approach. This method is particularly attractive for developing a model of flow of the Chalk unsaturated zone because the soil physics data (moisture content and matric potential) it requires are reasonably available in the literature (e.g. *Cooper et al.*, 1990; *Price et al.*, 2000; *Mahamood-ul-Hassan and Gregory*, 2002; *Haria et al.*, 2003) and much more data is currently being collected at a number of Chalk sites as part of the NERC (Natural Environment Research Council) thematic program, LOCAR (Lowland Catchment Research). Once a flow-field is defined, solute transport can then be dealt with by routing solutes through a modelled flow-field using the advection dispersion equation (e.g. *Gerke and van Genuchten*, 1993a, 1996; *Liu et al.*, 2003b; *Bechtel SAIC Company*, 2003).

1.4 Catchment-scale nutrient models and their applicability to Chalk catchments

As part of the European Union legislation that includes the Nitrates Directive (91/676/EC) and the Water Framework Directive (2000/60/EC), it is necessary to regulate the nutrient (Nitrogen, N and Phosphate, P) loads entering groundwater, lake and river systems considered sensitive to nutrient inputs. Given the costs involved in reducing N and P loads, catchment-scale nutrient models (CSNM) are commonly used to aid the understanding of freshwater N and P dynamics and to make predictions of future changes in the water-quality and ecology under likely scenarios (*Wade et al.*, 2004).

In lowland UK river systems dominated by intensive agriculture, enhanced N and P loads can have a detrimental impact on river ecology since both are linked to problems of eutrophication at local, catchment and regional scales (*Hayes and Greene*, 1984). Most freshwater systems are P limited and hence there are concerns that increased P loads to a water body can affect the composition and diversity of aquatic plant species by changing the competitive balance (*Wade et al.*, 2004). Nitrate is of concern because elevated concentrations render water unsuitable for drinking and many of the permeable catchments of south and east England are subject to rising concentrations in both surface and groundwater (*Heathwaite et al.*, 1993).

In urban areas, nutrient pollution is largely due to point sources derived from domestic and industrial wastewater effluent. In rural areas the main nitrate problems are from non-point sources from agricultural inputs. Nitrate concentrations in rivers and groundwaters have increased substantially since the 1940s. The changes since the 1940s are linked to changing agricultural practices, such as using nitrogen fertiliser to grow higher yielding crops and high animal stocking rates , which allows organic manure production to increase. This, combined with more land being cultivated each year, has increased losses of nitrogen from the land (*Heathwaite et al.*, 1993).

In 2003, 27% of rivers had high concentrations of nitrate (greater than 30mg/l) (Environment Agency, 2004). Note that the Drinking Water Directive (COM 80/788/EC) recommends a guide and maximum admissible concentration of 25 and 50 mg NO_3 l^{-1} respectively.

CSNMs, as with other hydrological models, can be broadly classified into metric, conceptual and physically-based models (*Wheater et al.*, 1993). Metric models are essentially statistical relationships that relate an input data-set to an output data-set. Conceptual models, involve specifying a model structure *a priori*, normally on the basis of a system

of conceptual stores characterised by a set of empirical parameters obtained by calibration against an observed data-set. Physically-based models seek to capture a system's response by incorporating the necessary processes through fundamental physical equations (Darcy's Law, Advection Dispersion, Navier-Stokes, etc.) and require parameters that can be theoretically measured in the field (hydraulic conductivity, dispersivity, river channel dimensions, etc.).

An example of a physically-based catchment-scale water-quality model is SHETRAN (*Ewen et al.*, 2000). SHETRAN is powered by the hydrological modelling framework, SHE (Systeme Hydrologique Europeen) (*Abbot et al.*, 1986b) where the unsaturated zone is described using Richards' equation, the saturated zone is described using the Boussinesq equation while surface runoff and channel flow are described using the St Venant equations. SHETRAN extends SHE by applying the advection dispersion equation to route solutes through the hydrological flow field. NITS (*Birkinshaw and Ewen*, 2000) provides another module for coupling various nitrogen cycling process into the SHETRAN solute transport-field. While this approach appears comprehensive, it is not popular due to its heavy computation requirement and parameter identification issues, discussed below.

The UP Model (*Ewen*, 1997; *Sloan and Ewen*, 1999) aimed to resolve the computation issue. The UP Model splits a watershed into UP elements typically less than 100 km^2. The resulting UP elements can be then be represented using simple lumped conceptual models. The philosophy is that rather than parameterising the UP elements by calibration against observed data, they are calibrated against model output from a physically-based model of the area. However, the issue of parameter identification still remains.

In principle the parameters used in physically-based models are physically measurable. However, due to the natural constraints of field investigations, only sparsely placed point measurements are normally obtained. Physically-based models generally discretise a model into a grid of elements or nodes. Despite the observation of heterogeneity, modellers are forced to extrapolate point measurements to elements where no measurements exist (*Wheater et al.*, 1993). Furthermore, heterogeneity often occurs at a scale smaller than the specified model grid (*Beven*, 1989). The extent to which subgrid-scale heterogeneity can be represented by effective properties of a uniform element is not well understood (*Binley et al.*, 1989; *Binley and Beven*, 1989; *Zhu et al.*, 1990). This gives rise to a large number of unknown parameters with degrees of freedom so great that parameters cannot be uniquely identified (*Wheater et al.*, 1993).

The export coefficient model (ECM) initially developed in the USA (*Beaulac and Reckhow*, 1982) is a metric approach to CSNM that has been widely used in the United Kingdom

(*Johnes*, 1996; *Johnes et al.*, 1996; *Johnes and Heathwaite*, 1997; *Whitehead et al.*, 2002). The annual load of diffuse nutrient runoff is predicted based on land use data for the upstream catchment using coefficients derived from small, generally plot- and field-scale studies (*Smith et al.*, 2004).

By developing a land use map of the catchment being modelled, export coefficients can be applied for each land use to calculate an areally weighted measure of annual catchment nutrient loss in kg ha^{-1} $year^{-1}$ (*Johnes*, 1996). The model output is the sum of the relative contributions from different non-point sources.

ECMs offer a cheap and fast approach to nutrient modelling. The data required is easily obtained and because these models are calibrated against total nitrogen and total phosphorous they are uninhibited by the difficulties associated with individual nutrient fractions (*Trudgill*, 1995). However, because ECMs do not explicitly consider hydro-chemical processes they are incapable of representing seasonal and diurnal dynamics. Consequently, ECMs are limited to annual time step studies (*Smith et al.*, 2004).

Conceptual models are becoming increasingly more popular for catchment-scale nutrient modelling (e.g. *Whitehead et al.*, 2002; *Wade et al.*, 2004). For a review of available conceptual modelling approaches the reader is referred to *Johnes and Burt* (1993), *Trudgill* (1995) and *Smith and Wheater* (2004). The normal procedure is to route the contaminant of interest through a hydrological regime derived from a lumped-response rainfall runoff model. These typically calculate a hydrologically effective rainfall (HER) from precipitation and potential evaporation through a soil moisture accounting model such as MORECS (*Hough and Jones*, 1997). HER is then routed to a catchment or (sub-catchment) outlet using a system of linear stores (e.g. two parallel stores for fast and slow catchment responses, *Smith et al.*, 2004).

Conceptual models are arguably the preferable option. Whilst being computationally and parametrically cheaper than physically-based models, they retain the flexibility to deal with sub-annual time scales. It has been contested that physically-based models (with their physically measured parameters) are more suitable for simulating effects of land use changes and predicting hydrology in ungauged catchments (*Abbot et al.*, 1986a). However, this contention is challenged by the fact that appropriate measurable parameters are rarely obtainable, giving rise to a need for calibrating physically-based models analogous to conceptual models but with greatly increased numbers of degrees of freedom (*Beven*, 1989).

INCA (Integrated Nitrogen model for multiple source assessment in Catchments) is an example of a conceptual CSNM. It separates catchments into sub-catchments. Each sub-catchment is then further separated into three hydrological components, a reactive soil zone,

groundwater zone and river zone (*Whitehead et al.*, 1998). The hydrological flow regime is described by residence times calculated from HER and base-flow indices. A nitrogen input is calculated for each sub-catchment using a GIS system detailing the land-use in the area. With the nitrogen input and flow in each element defined, solute transport is then simulated using a series of continuously stirred tank reactors (CSTR) and various nitrogen transformations in the soil and river zones (nitrification, denitrification etc.) are described by a set of reaction kinetic equations. INCA has previously been extensively applied in the United Kingdom, Europe and worldwide for evaluating nitrogen sources, transport and fate at the catchment scale (e.g. *Neal*, 2002, and papers therein).

Representation of solute transport derived through the unsaturated and saturated zones is typically poor in conceptual CSNMs. For example, in INCA both zones are represented by a single residence time derived from the hydrological water balance. Similarly weak representations can be seen in other models (e.g. *Neitsch et al.*, 2002; *Dunn et al.*, 2004). The reason lies in the fact that most of these models are based on older river quality models (*Trudgill*, 1995). These models were more concerned with point-sources (such as sewage treatment works) as opposed to non-point sources. In such cases, while groundwater might be important for the hydrology, in terms of solute transport, it is less relevant.

Integrating appropriate representations of groundwater response has not been easy because of a clear difference in modelling philosophy and expectation between surface- and groundwater modellers. When dealing with point-source pollution in rivers, a well defined input/output system can generally be defined. Water-quality data can be collected at the various point sources being considered (the input) and at the river outlet (the output). Previously, models relating input to output in rivers have been physically based using variations of the St Venant equations coupled with the advection dispersion equation. Conceptual stores-in-series approaches have become more favourable because they require only data from simple tracer experiments as opposed to detailed channel information which is often unavailable (*Whitehead et al.*, 1986). Solute transport can then be considered by calculating a residence time for a given reach and applying a CSTR. There has been wide success using such models in a range of different point-source studies (e.g. *Whitehead et al.*, 1997; *Lees et al.*, 1998).

Conversely, when studying groundwater contaminants, a problem is that the outputs are not easily defined. Often the emphasis is on predicting the arrival time of a plume (e.g. *Bechtel SAIC Company*, 2003) or defining a well vulnerability zone (e.g. *Wheater et al.*, 2000). Unlike in rivers, tracer tests can not be used in the same way because travel times are often of the order of decades for nutrients (e.g. *Carey and Lloyd*, 1985) or in the context of

radioactive waste, thousands of years (*Bechtel SAIC Company*, 2003). Consequently, model predictions rely heavily on physically-based models characterised by a spatial distribution of point measurements.

Representing the hydrological response of chalk catchments within conceptual rainfall runoff models is quite well established although difficulties arise due to uncertainty in catchment area (*Wheater et al.*, 2002). However, as was discussed in Section 1.1, the hydrological and solute transport responses in Chalk catchments are very different due to the presence of a deep, fractured unsaturated zone. While the water table level can respond to a rainfall event in just a few days, contaminants can take twenty to fifty years to leach to the saturated zone (*Foster*, 1993; *Price et al.*, 1993). Consequently, conceptual CSNMs must make some special considerations when dealing with Chalk catchments (note that this is less important with P because, P tends to bypass the groundwater system, e.g. *Smith and Wheater*, 2004). The importance of this extended unsaturated zone residence time was touched upon by *Jackson et al.* (2004), who through a sensitivity analysis of INCA applied to the Chalk catchment, the Kennet, found that initial groundwater conditions were overwhelmingly the most important parameters. The importance of the unsaturated zone in respect to nitrate travel times in Chalk catchments is well established (*Oakes et al.*, 1981; *Carey and Lloyd*, 1985; *Andrews et al.*, 1997). However, understanding how to represent the Chalk unsaturated zone in such a simplified manner, appropriate for conceptual CSNMs, is not. An issue is that there is no bench mark physically-based model with which to make comparisons.

1.5 Research objective

The objective of this thesis is to develop a unified physically-based modelling framework for unsaturated Chalk that is consistent with observed phenomena (often contradicting) at Chalk sites. These include: a fast water table response to rainfall events (in days) and an absence of surface run-off (*Headworth*, 1972); slow solute migration (in tens of years) with very little dispersion (*Oakes et al.*, 1981); specific yields that can vary an order of magnitude during droughts (*Price et al.*, 2000). Our motivation for this work is the need to guide the development of models for nutrient management, as discussed in Section 1.4 above.

1.6 Thesis outline

To further investigate flow and transport processes in the Chalk unsaturated zone we need a numerical dual-porosity model. With conventional dual-porosity models, even for a one-dimensional representation, the matrix blocks must be discretised in two-dimensions. There are several methodologies in the literature for avoiding this that involve lumping the distributed matrix response into a single mean value. In Chapter 2 the limitations of these approaches are assessed so as to ascertain the most appropriate representation of matrix diffusion in numerical dual-porosity models for use in this thesis.

Throughout the literature concerning flow and solute transport in unsaturated Chalk there has been much debate as to whether the dominant element of flow occurs in the fractures or the matrix. In Chapter 3, a detailed study of the literature is undertaken followed by some simple modelling analyses so as to arrive at a well-founded conclusion regarding the significance of flow in the matrix of the Chalk unsaturated zone.

Chapter 3 is limited to solute transport studies with steady state flow. The flow regime in the Chalk unsaturated zone is transient due to the episodic nature of infiltration. There is therefore a need to study solute transport under a transient flow regime. This requires a model that describes flow through a variably saturated fractured porous medium. Modelling flow in unsaturated fractured porous media (other than the Chalk) has been extensively explored using Richards' equation. Such a methodology should be equally appropriate for the Chalk. Chapter 4 concerns itself with how to parameterise the moisture retention and hydraulic conductivity relationships, associated with Richards' equation, for application to the Chalk.

Chapter 5 puts everything together into a one-dimensional coupled flow and transport model. Parameter sensitivity and the effects of different temporal sampling regimes are explored through a hypothetical scenario whereby a variable recharge time-series is applied for a number of years. The first year of recharge is tagged with a conservative solute (that could be tritium, chloride or nitrate) such that a set of simulated solute profiles and breakthrough curves are developed.

Chapter 6 summarises and concludes the thesis as a whole.

Chapter 2

Representing matrix diffusion in numerical dual-porosity models

2.1 Introduction

To further investigate flow and transport processes in the Chalk unsaturated zone we need a numerical dual-porosity model. When studying flow and/or transport in fractured rocks it is common to apply some form of numerical dual-porosity model. Dual-porosity models assume that longitudinal flow (parallel to the fractures) is negligible in the rock matrix due to its much lower hydraulic conductivity (the sensibility of doing this in the unsaturated zone is discussed in the next chapter). Consequently longitudinal flow occurs exclusively in the fractures, coupled with a lateral exchange of water or solute into and out of the matrix. *Barker* (1991) distinguishes between two types of dual-porosity model; the Fickian and the quasi-steady-state (QSS) (*Barenblatt et al.*, 1960; *Warren and Root*, 1963). Fickian models describe this exchange mechanism through Fick's 2nd Law (into and) within the matrix block (*Bibby*, 1981; *Barker*, 1982; *Sudicky and Frind*, 1982). QSS models characterise the matrix block using a single potential (concentration or pressure head). The diffusive flux between the fractures and matrix is then taken to be proportional to the difference between their potentials, where the proportionality is characterised by an empirical mass transfer coefficient.

QSS models have generally attracted more attention (*Vogel et al.*, 2000; *Landereau et al.*, 2001; *Simunek et al.*, 2003) due to their ability to lump a distributed matrix response into a single mean value, making it attractive to equate the QSS equations with the Fickian model to obtain relationships between the physical properties of the matrix and the mass transfer

coefficient. This has been done within the context of solute transport (*van Genuchten and Dalton*, 1986; *Dykhuizen*, 1987) and flow (*Dykhuizen*, 1990; *Gerke and van Genuchten*, 1993b, 1996). For the remainder of this study, literature regarding flow or solute transport will be used interchangeably and converted to the context of solute transport.

When viewed as an approximation to the Fickian model, the QSS model is valid only when changes within the fractures are slow in relation to the time for diffusive equilibrium across a matrix block (*Barker*, 1991). This happens at early times when dealing with very fine fracture spacing or macroscopically aggregated soils, but for the scenarios involving the Chalk (*Bibby*, 1981) or Tuff (*Zimmerman et al.*, 1993) it can take several months or even years. In order to deal with these particular issues, two specific lumped response models have been developed, the integral representation (*Bibby*, 1981) and the Vermeulen model (*Zimmerman et al.*, 1993).

In this chapter these alternative modelling approaches are compared to a Fickian model, within the context of conservative solute diffusing into Chalk blocks, so as to ascertain which is the most appropriate representation of Fickian matrix diffusion for numerical dual-porosity models.

2.2 Fickian models

Barker (1982) presents a set of assumptions and equations to describe solute transport in a fractured porous medium using a Fickian model. Identical slabs of matrix material are separated by equally spaced, planar fractures. The matrix is homogenous and saturated with immobile water. Solute transfer between the fractures and matrix and within the matrix occurs by molecular diffusion in the immobile water in a direction perpendicular to the plane of the fractures. There is no concentration gradient across the fractures. The flow velocity in the fractures is uniform while no flow occurs in the matrix. Longitudinal dispersion in the fractures is assumed negligible.

Because of the symmetry of the model only a single, semi-infinite unit extending from the centre of a matrix block to the centre of a neighbouring fracture need be considered. Let $c_f(z,t)$ be the solute concentration in the fracture water and $c_m(x,z,t)$ be the concentration in the matrix water. The movement of a conservative non-sorbing solute in a fracture is then described by

$$\frac{\partial c_f}{\partial t} + v_f \frac{\partial c_f}{\partial z} + q_{fm} = 0 \tag{2.1}$$

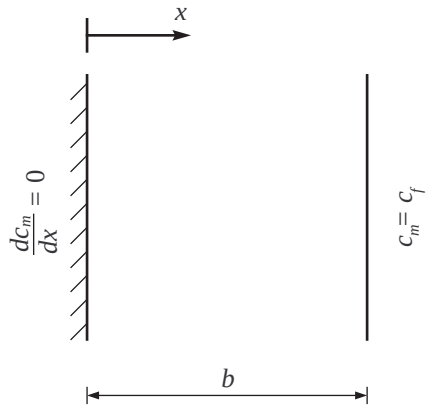

Figure 2.1 Schematic diagram of the model used to describe the diffusion of solute from a fracture into a matrix block.

where q_{fm} is the solute exchange flux between the fractures and the matrix found from

$$q_{fm} = \frac{\phi}{a} D_A \left.\frac{\partial c_m}{\partial x}\right|_{x=b} = \frac{\phi}{a} \int_0^b \frac{\partial c_m}{\partial t} dx \tag{2.2}$$

and x is lateral distance from the centre of the matrix block, z is longitudinal distance, t is time, a is the half-width of the fracture, b is the half-width of the matrix block, ϕ is the matrix porosity, v_f is the velocity of water flowing in the fracture and D_A is the apparent molecular diffusion coefficient for solute in the matrix.

Solute concentration in the matrix can then be described by Fick's 2nd Law:

$$\frac{\partial c_m}{\partial t} - D_A \frac{\partial^2 c_m}{\partial x^2} = 0 \tag{2.3}$$

subjected to the boundary conditions

$$\left.\frac{\partial c_m}{\partial x}\right|_{x=0} = 0; \quad c_m(b, z, t) = c_f(z, t) \tag{2.4}$$

As we are specifically interested in how to represent lateral diffusion in the matrix, it is therefore helpful to assume that $dc_f/dz = 0$ (as changes in concentration parallel to the fracture are beyond the scope of this chapter). The system being considered is now that described in Figure 2.1.

Applying the following transformations:

$$T = \frac{t}{t_{cb}}; \quad X = \frac{x}{b} \tag{2.5}$$

yields the dimensionless form of equation (2.3):

$$\frac{\partial c_m}{\partial T} - \frac{\partial^2 c_m}{\partial X^2} = 0 \tag{2.6}$$

$$\left.\frac{\partial c_m}{\partial X}\right|_{X=0} = 0; \quad c_m(1,T) = c_f(T) \tag{2.7}$$

where $t_{cb} = b^2/D_A$ is often described as the characteristic block diffusion time (*Barker et al.*, 2000).

The quantity of interest is the dimensionless fracture-matrix exchange term Λ found from

$$\Lambda(T) = \frac{at_{cb}}{\phi b} q_{fm} = \left.\frac{\partial c_m}{\partial X}\right|_{X=1} = \int_0^1 \frac{\partial c_m}{\partial T} dX = \frac{\partial \overline{c}_m}{\partial T} \tag{2.8}$$

where $\overline{c}_m$ is the mean concentration of the matrix in the X direction.

The characteristic block diffusion time is approximately the time it takes for an uncontaminated matrix block to equilibrate with a fracture at a fixed concentration. This can be better understood by considering the analytical solution to equations (2.6) and (2.7) when

$$\begin{aligned} c_m &= 0, && 0 \leq X \leq 1, \quad T = 0 \\ c_m &= c_f = 1, && X = 1, \quad T > 0 \end{aligned} \tag{2.9}$$

which is (*Carslaw and Jaeger*, 1980, p. 100)

$$c_m(X,T) = 1 - 2\sum_{n=0}^{\infty} \frac{(-1)^n}{A_n^{1/2}} e^{-A_n T} \cos(A_n^{1/2} X) \tag{2.10}$$

where c_f is assumed to be constant with time and $A_n = (2n+1)^2\pi^2/4$.

It follows that the mean concentration in the matrix in the X direction is found from

$$\overline{c}_m(T) = 1 - 2\sum_{n=0}^{\infty} \frac{1}{A_n} e^{-A_n T} \tag{2.11}$$

Differentiating in respect to T then yields the dimensionless fracture-matrix exchange term

$$\Lambda^*(T) = 2\sum_{n=0}^{\infty} e^{-A_n T} \tag{2.12}$$

Here the $*$ superscript denotes an exchange function for a unit step change in fracture concentration (i.e. $c_f = 1$ and $c_m(X, T=0) = 0$).

Figure 2.2 shows the response of the fracture-matrix exchange term with time according to equation (2.12) where it can be seen that exchange term sharply declines once $T > 1$ (i.e. $t > t_{cb}$), suggesting that the system is now very close to equilibrium.

2.3 Quasi-steady-state models

It is often assumed that the solute exchange flux between the fractures and the matrix is proportional to the averaged concentration gradient between the fracture and the matrix

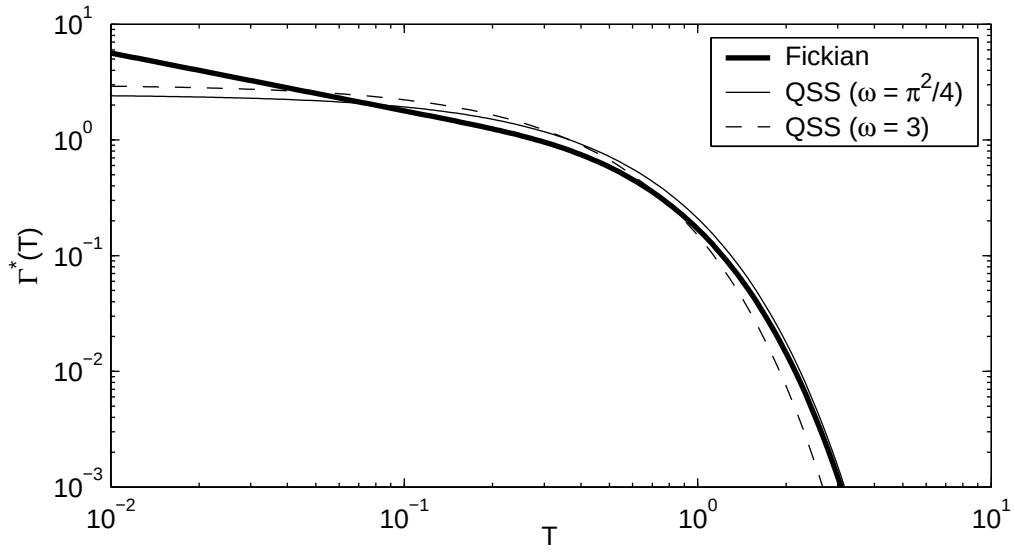

Figure 2.2 Comparison of dimensionless fracture-matrix exchange fluxes predicted by the Fickian model for a slab matrix subjected to a unit step change in concentration (equation 2.12) and the QSS models (i.e. equation 2.19) with $\omega = \pi^2/4$ and $\omega = 3$.

such that (e.g. *Warren and Root*, 1963)

$$\Lambda(T) = \frac{\partial \overline{c}_m}{\partial T} = \omega(c_f - \overline{c}_m) \tag{2.13}$$

where ω is a dimensionless transfer coefficient dependant on the geometry of the matrix being considered.

This model is often referred to as the quasi-steady-state (QSS) model because its approximation only becomes valid when changes within the fractures are slow in relation to the time required for diffusive equilibrium to occur within the matrix (*Barker*, 1991). The reason is that the QSS model implicitly assumes that $dc_m/dx = 0$ (i.e. that $\overline{c}_m(z) = c_m(x, z)$).

The transfer coefficient ω can be obtained from calibration against observed data or by assuming a geometric diffusion model (such as the diffusion model for a slab in equation 2.6) and equating equivalent analytical solutions.

2.3.1 Evaluation of ω via integral method

Assuming that the fracture concentration varies smoothly and monotonically at large values of time, *Dykhuizen* (1990) suggests that the fundamental mode of the matrix solution (i.e. equation 2.10) will be dominant. *Dykhuizen* (1990) then proposed the following functional

form for matrix diffusion at large times:

$$\frac{c_m(X,T) - c_{mi}}{c_f(T) - c_{mi}} = 1 - f(T)\cos\left[\frac{\pi X}{2}\right] \tag{2.14}$$

where $c_m(X,T)$ is the matrix concentration, $c_m(X,0 = c_{mi})$ is a uniform initial condition in the X direction, $c_f(T)$ is the fracture concentration, $f(T)$ is some unknown function.

The derivative of equation (2.14) at $X = 1$ is

$$\left.\frac{\partial c_m}{\partial x}\right|_{X=1} = \frac{\partial \overline{c}_m}{\partial T} = [c_f(T) - c_{mi}]\frac{\pi}{2}f(T) \tag{2.15}$$

The mean concentration in the X direction can be obtained from

$$\frac{\overline{c}_m(T) - c_{mi}}{c_f(T) - c_{mi}} = \int_0^1 \frac{c_m(X,T) - c_{mi}}{c_f(T) - c_{mi}} dX = 1 - \frac{2}{\pi}f(T) \tag{2.16}$$

Equating equations (2.15) and (2.16), the function, $f(T)$ is eliminated and we have a governing equation for large times (*Dykhuizen*, 1990):

$$\Lambda(T) = \frac{\partial \overline{c}_m}{\partial T} = \omega(c_f - \overline{c}_m) \tag{2.17}$$

where $\omega = \pi^2/4$.

2.3.2 Evaluation of ω via Laplace transforms

Consider the solution of equation (2.13) for the boundary and initial conditions described in (2.9),

$$\overline{c}_m(T) = 1 - e^{-\omega T} \tag{2.18}$$

The dimensionless exchange term is then given by

$$\Lambda^*(T) = \omega e^{-\omega T} \tag{2.19}$$

Gerke and van Genuchten (1993b) found a slightly different value of ω for slab matrix blocks by considering the Laplace transforms of equations (2.12) and (2.19):

$$\hat{\Lambda}^*(s) = \frac{1}{s^{1/2}}\tanh(s^{1/2}) \tag{2.20}$$

and

$$\hat{\Lambda}^*(s) = \frac{\omega}{s + \omega} \tag{2.21}$$

where the Laplace transform of $\hat{\Lambda}(s)$ is related to $\Lambda(T)$ by the integral

$$\hat{\Lambda}(s) = \int_0^\infty \Lambda(T)e^{-sT}dT \tag{2.22}$$

and s is a complex variable sometimes referred to as the Laplace transform variable.

Steps needed to obtain equation (2.20) are as follows. The Laplace transform of equation (2.12) is

$$\hat{\Lambda}^*(s) = 2\sum_{n=0}^{\infty} \frac{1}{s + A_n} = \frac{1}{s^{1/2}} \sum_{n=0}^{\infty} \frac{2s^{1/2}}{s + A_n} \tag{2.23}$$

From the identity (*Bromwich and Macrobert*, 1947, p.296)

$$\tanh y = \sum_{n=0}^{\infty} \frac{2y}{y^2 + (2n+1)^2\pi^2/4} \tag{2.24}$$

we then have equation (2.20).

It is interesting to note that the expression for $\hat{\Lambda}^*(s)$ in equation (2.20) is the block geometry function for a slab matrix presented by *Barker* (1985).

Using another expansion, $\tanh(y) = y - (y^3/3) + ...$ we find that the Laurent expansion of equation (2.20) about $s = 0$ is

$$\hat{\Lambda}^*(s) = 1 - \frac{s}{3} + ... \tag{2.25}$$

while the Laurent expansion of equation (2.21) is

$$\hat{\Lambda}^*(s) = 1 - \frac{s}{\omega} + ... \tag{2.26}$$

Gerke and van Genuchten (1993b) assume that as $T \to \infty$, $s \to 0$ suggesting that higher order terms of both Laurent expansions can be neglected. Accordingly, *Gerke and van Genuchten* (1993b) equate just the first two terms of both expansions which leads to the result that $\omega = 3$.

However, any sum of decaying exponentials gives rise to a term in the Laurent series for the Laplace transform proportional to s (as can be seen in equations 2.25 and 2.26). One cannot expect therefore to identify uniquely the decaying exponentials from the term proportional to s in the Laurent series. The analysis of *Gerke and van Genuchten* (1993b) is therefore flawed.

2.3.3 Evaluation of ω via asymptotic expansion

Nevertheless, *Carslaw and Jaeger* (1949) provide a credible method for obtaining large time approximations from a Laplace transform solution. Let s_0 be the singularity of $\hat{\Lambda}(s)$ having the largest real part. Assume that $\hat{\Lambda}(s)$ can be expanded in the neighbourhood of s_0 as follows (*Carslaw and Jaeger*, 1949, p.280):

$$\hat{\Lambda}(s) = \sum_{n=0}^{\infty} a_n(s - s_0)^{n-1} + (s - s_0)^{\beta-1} \sum_{n=0}^{\infty} b_n(s - s_0)^n, \quad 0 < \beta < 1 \tag{2.27}$$

The asymptotic expansion of $\Lambda(T)$ for large values of T is then given by (*Carslaw and Jaeger*, 1949, p.280)

$$\Lambda(T) \approx e^{s_0 T} \left\{ a_0 + \frac{\sin \pi\beta}{\pi} \sum_{n=0}^{\infty} (-1)^n b_n \Gamma(\beta + n) t^{-\beta - n} \right\} \tag{2.28}$$

where Γ is the gamma function.

Let us first consider the asymptotic expansion of the QSS Laplace transform in equation (2.21). Comparison of equation (2.21) and (2.27) reveals that

$$a_0 = \omega; \quad s_0 = -\omega \tag{2.29}$$

and all other terms are absent. Hence equation (2.28) shows that the asymptotic behaviour of the QSS model, for large times is given by (as with equation 2.19) (*Mathias and Zimmerman*, 2003)

$$\Lambda^*(T) \approx \omega e^{-\omega T} \tag{2.30}$$

Now we will consider the asymptotic expansion of equation (2.20). Substituting equation (2.24) into equation (2.20) we get

$$\hat{\Lambda}^*(s) = 2 \sum_{n=0}^{\infty} \frac{1}{s + A_n} \tag{2.31}$$

It follows that the singularities are

$$s_n = -A_n = -(2n+1)^2 \pi^2 / 4 \tag{2.32}$$

and the singularity with the largest real part is

$$s_0 = -\pi^2 / 4 \tag{2.33}$$

The residue is obtainable from

$$a_0 = \lim_{s \to s_0} (s - s_0) \Lambda^*(s) = 2 \tag{2.34}$$

and the resulting asymptotic solution is (*Mathias and Zimmerman*, 2003)

$$\Lambda^*(T) \approx 2e^{-(\pi^2/4)T} \tag{2.35}$$

which is identical to the first term in the series solution shown in equation 2.12. Comparison of equations (2.31) and (2.35) tells us (as with *Dykhuizen*, 1990) that setting $\omega = \pi^2/4$ causes the QSS model to have the same asymptotic behaviour as that of the Fickian model.

2.3.4 Evaluation of ω via convolution

Interestingly, a value of $\omega = 3$ can also be obtained by conventional methods. If solute concentrations in the fractures and matrix are initially zero and c_f is no longer constant but some arbitrary function of T (except that $c_f = 0$ at $T = 0$, note that this does not apply to the conditions outlined in equation 2.9), it can be said that (*Lever et al.*, 1983, Appendix D)

$$\Lambda(T) = 2\int_0^T \frac{dc_f}{d\tau}\sum_{n=0}^{\infty} e^{-A_n(T-\tau)}d\tau \tag{2.36}$$

where c_f is no longer constant but some arbitrary function of T.

Lever et al. (1983) suggest that if $T >> 1$ (i.e. $t >> t_{cb}$) and $\partial c_f/\partial T$ is relatively small, $\partial c_f/\partial\tau$ can be expanded in a Taylor series about $\tau = T$

$$\frac{\partial c_f}{\partial \tau} = \frac{\partial c_f}{\partial T} - (T-\tau)\frac{\partial^2 c_f}{\partial T^2} + O(T-\tau)^2 \tag{2.37}$$

This can be substituted into equation (2.36) and the terms can be evaluated to provide an expansion of the integral (*Lever et al.*, 1983)

$$\Lambda(T) = 2\frac{\partial c_f}{\partial T}\sum_{n=0}^{\infty}\frac{1}{A_n} - 2\frac{\partial^2 c_f}{\partial T^2}\sum_{n=0}^{\infty}\frac{1}{A_n^2} + O\left(\frac{\partial^3 c_f}{\partial T^3}\right) \tag{2.38}$$

It can be shown that

$$\sum_{n=0}^{\infty}\frac{1}{A_n} = \frac{1}{2}; \quad \sum_{n=0}^{\infty}\frac{1}{A_n^2} = \frac{1}{6} \tag{2.39}$$

and so

$$\Lambda(T) = \frac{\partial c_f}{\partial T} - \frac{1}{3}\frac{\partial^2 c_f}{\partial T^2} + O\left(\frac{\partial^3 c_f}{\partial T^3}\right) \tag{2.40}$$

As $T >> 1$, we can ignore the higher order terms such that

$$\Lambda(T) = \frac{\partial \overline{c}_m}{\partial T} = \frac{\partial c_f}{\partial T} - \frac{1}{3}\frac{\partial^2 c_f}{\partial T^2} \tag{2.41}$$

which can be integrated to give

$$\frac{\partial c_f}{\partial T} = 3(c_f - \overline{c}_m) \tag{2.42}$$

Invoking the assumption

$$\frac{d\overline{c}_m}{dT} \approx \frac{dc_f}{dT} \tag{2.43}$$

Lever et al. (1983) then finds, as with *Gerke and van Genuchten* (1993a)

$$\Lambda(T) = \frac{\partial \overline{c}_m}{\partial T} = \omega(c_f - \overline{c}_m) \tag{2.44}$$

where $\omega = 3$.

However, the usefulness of this result is not clear. The derivation implies that it represents a relatively uninteresting case, namely:

$$T >> 1; \quad \frac{\partial c_f}{\partial T} \rightarrow 0; \quad \frac{\partial c_f}{\partial T} \approx \frac{\partial \overline{c}_m}{\partial T}. \tag{2.45}$$

Figure 2.2 shows comparisons of equation (2.11) with (2.19) using $\omega = \pi^2/4$ and $\omega = 3$. It can be seen that both QSS solutions are not good at representing Fickian behaviour during early times. During large times, the QSS solution with $\omega = 3$ underestimates the exchange flux while the QSS solution with $\omega = \pi^2/4$ shows a progressive improvement in its approximation of the Fickian model solution. This is because when $\omega = \pi^2/4$, the QSS solution has the same asymptotic behaviour to that of the Fickian model (*Mathias and Zimmerman*, 2003).

2.4 Early time models

Zimmerman et al. (1996) explain that the reason why the QSS model can only be used for slowly varying transient conditions is because it assumes that all solute entering the matrix block is instantaneously distributed uniformly throughout it. The consequence of this is that during early times, after a small amount of solute has entered the block, the average concentration, $\overline{c}_m$ is essentially unchanged from its initial value, causing the predicted exchange flux to remain almost constant (see Figure 2.3).

2.4.1 Via the integral method

Dykhuizen (1990) points out that in reality, the solute entering the block is initially localised in a small boundary layer, giving rise to large gradients, and consequently, large fluxes within the matrix at early times. Following from equation (2.14), *Dykhuizen* (1990) speculates that an early time concentration profile in the matrix will take the form

$$\frac{c_m(X,T) - c_{mi}}{c_f(T) - c_{mi}} = \begin{cases} 1 - \cos\left[\frac{\pi(X-\zeta(T))}{2(1-\zeta(T))}\right], & X > \zeta(T) \\ 0, & X < \zeta(T) \end{cases} \tag{2.46}$$

where ζ denotes the location of the solute front on the X axis.

The derivative of equation (2.46) at $X = 1$ is

$$\left.\frac{\partial c_m}{\partial x}\right|_{X=1} = \frac{\partial \overline{c}_m}{\partial T} = [c_f(T) - c_{mi}]\frac{\pi}{2}\frac{1}{[1-\zeta(T)]} \tag{2.47}$$

The mean concentration in the X direction can be obtained from

$$\frac{\overline{c}_m(T) - c_{mi}}{c_f(T) - c_{mi}} = \int_{\zeta(T)}^{1} \frac{c_m(X,T) - c_{mi}}{c_f(T) - c_{mi}} dX = \frac{[\pi - 2][1-\zeta(T)]}{\pi} \tag{2.48}$$

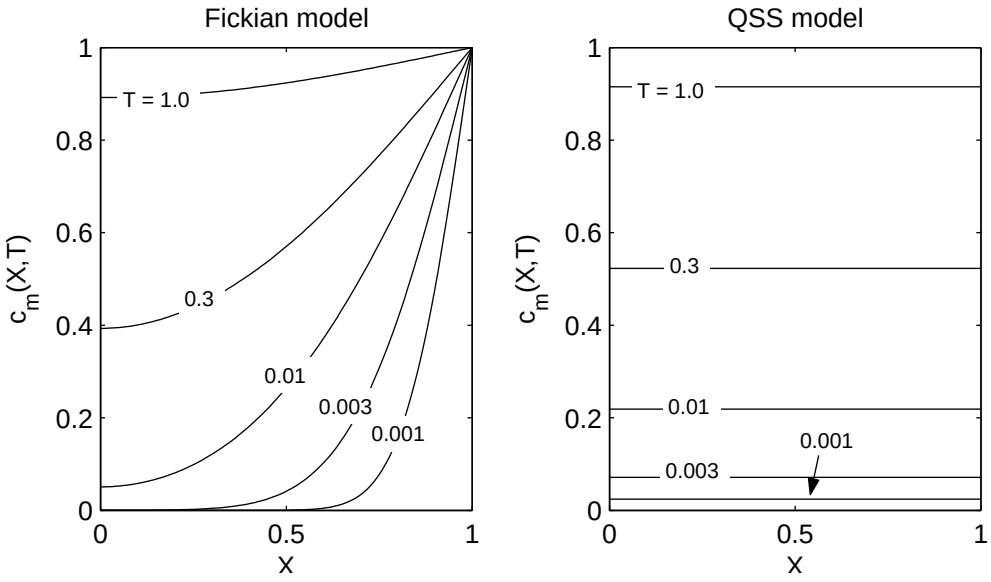

Figure 2.3 Comparison of concentration distributions predicted by the Fickian model (equation 2.10) and the QSS model (equation 2.18 with $\omega = \pi^2/4$) for a slab matrix subjected to a unit step change in concentration.

Equating equations (2.47) and (2.48), the function, $\zeta(T)$ is eliminated and we have a governing equation for early times (*Dykhuizen*, 1990):

$$\Lambda(T) = \frac{\partial \overline{c}_m}{\partial T} = \left(\frac{\pi}{2} - 1\right) \frac{[c_f(T) - c_{mi}]^2}{[\overline{c}_m(T) - c_{mi}]} \tag{2.49}$$

Application of the boundary and initial conditions in equation (2.9) into equation (2.49) gives the solution for mean concentration

$$\frac{\overline{c}_m - c_{mi}}{c_f - c_{mi}} = [(\pi - 2)T]^{1/2} \tag{2.50}$$

which can be differentiated in respect to time to yield

$$\Lambda^* = \left[\frac{4T}{\pi - 2}\right]^{-1/2} \tag{2.51}$$

2.4.2 Via assuming an infinitely thick matrix block

While the above approach appears very clever, it does not yield the correct result. A more direct route to the early time exchange flux can be obtained by considering the physics of the system. During early times, before the solute front has reached the centre of the matrix block, the block can be assumed to be infinitely thick (see Figure 2.3). The solution to equation (2.6) subjected to the boundary and initial conditions

$$c_m(0, T) = c_f(T) = 1; \quad c_m(\infty, T) = 0; \quad c_m(X, 0) = 0 \tag{2.52}$$

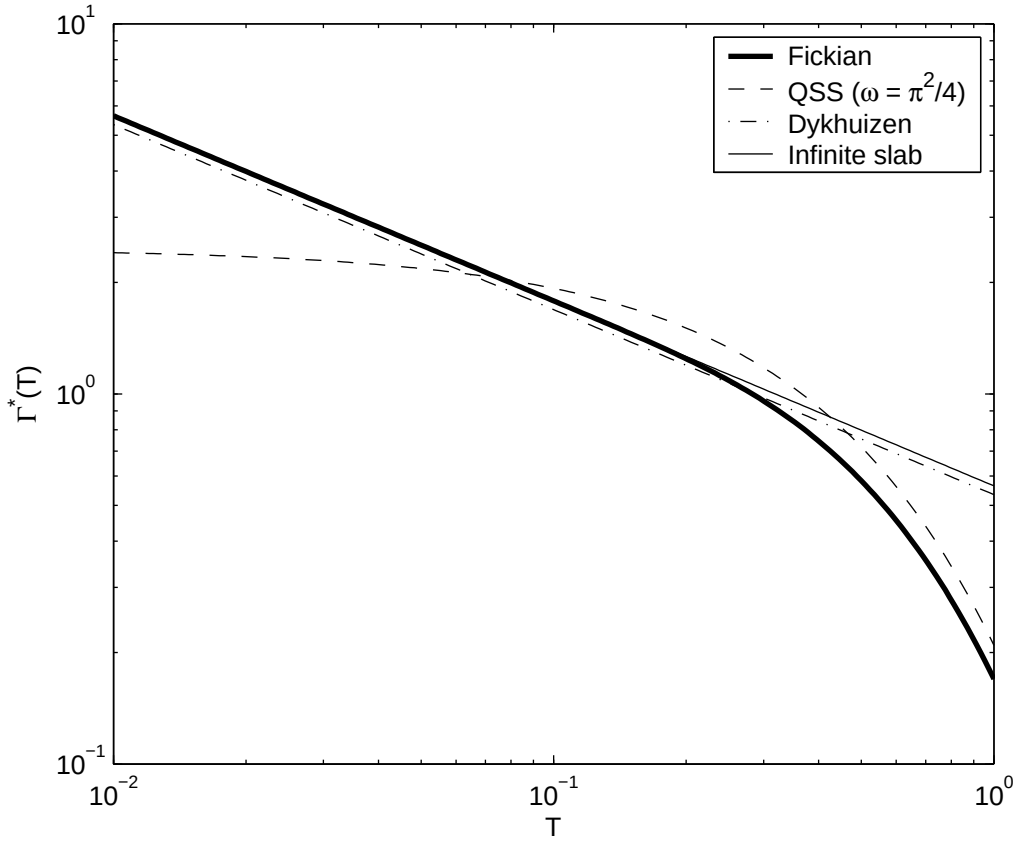

Figure 2.4 Comparison of dimensionless fracture-matrix exchange fluxes predicted by the Fickian model for a slab matrix subjected to a unit step change in concentration (equation 2.12), the QSS models with $\omega = \pi^2/4$ (equation 2.19), the Dykhuizen early time model (equation 2.51), and the infinite matrix model (equation 2.54).

is

$$c_m(X,T) = \text{erfc}\left(\frac{X}{2T^{1/2}}\right) \tag{2.53}$$

It follows that during early times (*Carrera et al.*, 1998)

$$\Lambda^*(T) = -\left.\frac{\partial c_m}{\partial X}\right|_{X=0} = (\pi T)^{-1/2} \tag{2.54}$$

That $\Lambda^*(T) \propto T^{-1/2}$ for $T << 1$ also suggests that it is the matrix concentration distribution at small times that largely determines the speed at which a solute plume moves through the fractures. (Note that the X axis has been reversed. Hereafter, it is reverted back to as before.)

Figure 2.4 compares the Fickian model with the early time formula developed by *Dykhuizen* (1990) and that developed by considering an infinite matrix block. The QSS model with $\omega = \pi^2/4$ is also shown for comparison. It can be seen that for early times, both early time

models have the same and correct slope but the *Dykhuizen* (1990) model underestimates the Fickian exchange flux by a factor of $[(\pi - 2)\pi/4]^{1/2} = 0.8966$.

As time passes, the boundary layer will travel from the fracture interface to the centre of the matrix block, beyond which *Dykhuizen* (1990) suggests that the late time approximation of equation (2.13) with $\omega = \pi^2/4$ becomes valid. The point at which this occurs is where the early-time equations diverge from the Fickian solution in Figure 2.4. It is interesting to note that the QSS model is still overestimating the Fickian exchange flux at this stage. Furthermore, the intersection points of the QSS and early-time models are far from smooth.

2.4.3 The Vermeulen function

Zimmerman et al. (1993) were interested in developing this idea further with a view to obtaining a lumped response relationship that describes the lateral diffusion behaviour of equations (2.6) and (2.7) for both early and late times in a continuous single differential equation. Their starting point was the work of *Vermeulen* (1953) who found by inspection (no mathematical rationale is given) that the spherical equivalent of equation (2.11) (*Crank*, 1975, p. 91)

$$\overline{c}_m(T) = 1 - 6\sum_{n=1}^{\infty} \frac{1}{B_n} e^{-B_n T} \tag{2.55}$$

(where $B_n = n^2\pi^2$) could be accurately approximated over all times by (see Figure 2.5)

$$\overline{c}_m(T) = \left[1 - e^{-\pi^2 T}\right]^{1/2} \tag{2.56}$$

Note that the *Vermeulen* (1953) approximation is only appropriate for spherical matrix block geometries (*Zimmerman et al.*, 1993). However, conceptualising matrix blocks as spheres is arguably no less appropriate than conceptualising them as slabs.

Zimmerman et al. (1993) differentiate equation (2.56) with respect to T to get the more general expression

$$\Lambda(T) = \frac{d\overline{c}_m}{dT} = \frac{\pi^2}{2}\left[\frac{(c_f - c_{mi})^2 - (\overline{c}_m - c_{mi})^2}{(\overline{c}_m - c_{mi})}\right] \tag{2.57}$$

Zimmerman et al. (1996) suggest that, at late times when $\overline{c}_m$ is close to c_f (i.e. the matrix and fractures are nearly in equilibrium), equation (2.57) takes a form similar to (2.13). During early times, the matrix concentration has not had sufficient time to respond to changes in c_f so that equation (2.57) takes a form more similar to (2.49).

Zimmerman et al. (1993) verified that equation (2.57) accurately models fracture-matrix diffusive transfer for a wide variety of monotonically varying fracture concentration histories.

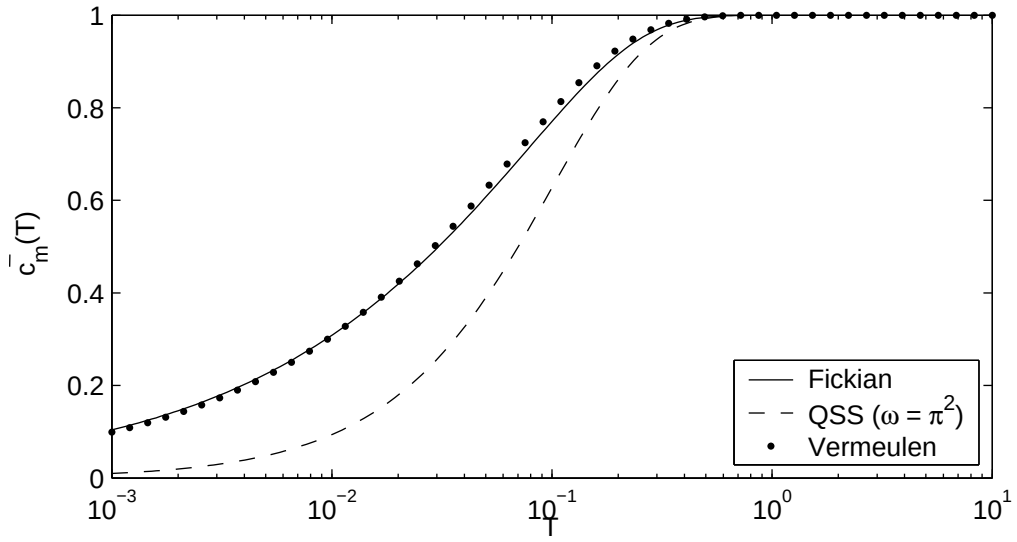

Figure 2.5 Comparison of mean matrix concentrations predicted by the Fickian model for a spherical matrix subjected to a unit step change in concentration (equation 2.55), the QSS model (equation 2.18 with $\omega = \pi^2$), and the Vermeulen model (equation 2.56).

However, to get it to work for non-monotonic functions, they needed to insert absolute values such that

$$\frac{d\bar{c}_m}{dT} = \frac{\pi^2}{2}\left[\frac{[(c_f - c_{mi}) - (\bar{c}_m - c_{mi})][|c_f - c_{mi}| + |\bar{c}_m - c_{mi}|]}{|\bar{c}_m - c_{mi}|}\right] \tag{2.58}$$

The non-monotonic example that *Zimmerman et al.* (1993) present is that for when

$$\left.\frac{\partial c_m}{\partial x}\right|_{X=0} = 0; \quad c_m(1,T) = c_f(T) = \sin(\Omega T); \quad c_m(X,0) = 0 \tag{2.59}$$

which for the Fickian model with spherical geometry yields (*Zimmerman et al.*, 1993)

$$\bar{c}_m(T) = 6\sum_{n=1}^{\infty} \frac{B_n \sin(\Omega T)e^{B_n T} - \Omega\cos(\Omega T)e^{B_n T} + \Omega e^{-B_n T}}{B_n^2 + \Omega^2} \tag{2.60}$$

and for the QSS model yields (*Zimmerman et al.*, 1993)

$$\bar{c}_m(T) = \frac{\omega^2 \sin(\Omega T) - \omega\Omega\cos(\Omega T) + \omega\Omega e^{-\omega T}}{\omega^2 + \Omega^2} \tag{2.61}$$

where $\omega = \pi^2$ for spherical geometries (assuming b is the radius of the sphere), $\Omega = 2\pi t_{cb}/t_p$ is a characteristic frequency and t_p is the period of oscillation. *Zimmerman et al.* (1993) solved equation (2.58) numerically.

Zimmerman et al. (1993) found that the *Vermeulen* (1953) approximation (equation 2.58) was able to achieve a much better wave amplitude accuracy than the QSS model with Ω values as large as 100. Limited information is given about the complete study as this was not their main focus. Accordingly we will investigate this process further.

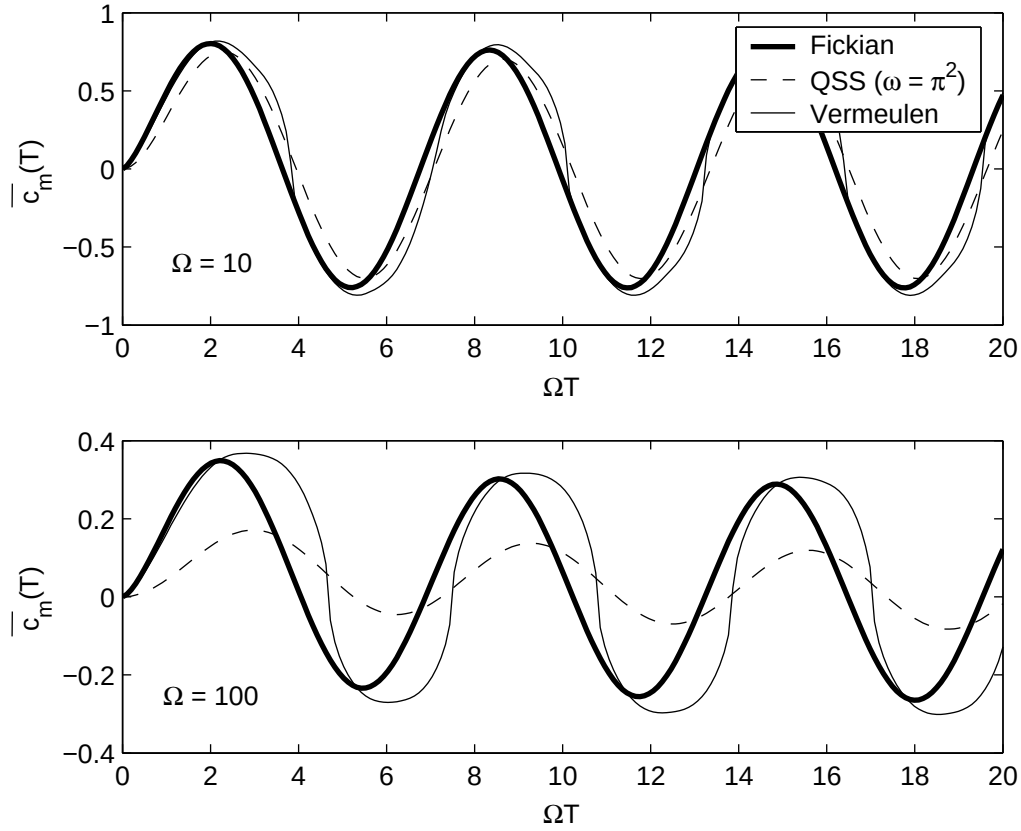

Figure 2.6 Comparison of mean matrix concentrations predicted by the Fickian model for a spherical matrix subjected to a sinusoidal change in concentration (equation 2.60), the QSS models with $\omega = \pi^2$ (equation 2.61), and the Vermeulen model (equation 2.58, numerically inverted with ODE45 from MATLAB).

Plotted responses of the Fickian model (with spherical geometry), the QSS model with $\omega = \pi^2$, and the Vermeulen model subjected to a sinusoidal change in concentration (i.e. equations 2.60, 2.61 and 2.58) for $\Omega = 10$ and 100 are shown in Figure 2.6. When $\Omega = 10$ the QSS models approximates the Fickian model reasonably well although its is slightly out of phase and underestimates the wave amplitude. When $\Omega = 100$ this becomes worse.

For $\Omega = 10$ (the example given by *Zimmerman et al.*, 1993) the Vermeulen model yields an approximation which appears arguably as good as the QSS model. However, when $\Omega = 100$, the Vermeulen model can be seen to behave in an unusual way. Unlike the QSS model, the Vermeulen model has a very similar amplitude to the Fickian model. Furthermore, it accurately approximates the initial rise in concentration. Afterwards, the Vermeulen model generates a non-sinusoidal wave-shape (in contrast to the other models). This is because, although the Vermeulen model has the right time dependence to represent a unidirectional

solute front (as with *Dykhuizen*, 1990), no consideration has been given for its return (although this has been attempted by the provision of absolute signs in equation 2.58). Clearly, this is an inappropriate method for representing Fickian matrix diffusion when fracture concentrations are non-monotonic.

2.5 The QSS models and smoothly varying functions

So far in this chapter, attention has mostly been made to the Fickian model subjected to a step increase in fracture concentration. This is an unrealistic scenario as generally, solute functions are much smoother suggesting that not all the early time regime is important. Natural solute functions are often periodic in nature due to climatic, seasonal or anthropogenic activities. It is therefore interesting to examine at which frequencies the QSS models cease to be accurate representations of Fickian behaviour. To this end, we will follow the thoughts of *Zimmerman et al.* (1993) and compare the response of the QSS model to the Fickian model when $c_f = \sin(\Omega T)$

To obtain an analytical solution for the Fickian model with a slab geometry (i.e. equations 2.6 and 2.7), consider the generalised analytical solution (*Carslaw and Jaeger*, 1980, p.104)

$$c_m(X,T) = 2\sum_{n=0}^{\infty} e^{-A_n T}\cos\left(A_n^{1/2}X\right) \cdot\left\{A_n^{1/2}(-1)^n\int_0^T e^{A_n\tau}c_f(\tau)d\tau + \int_0^1 c_m(X,0)\cos\left(A_n^{1/2}\xi\right)d\xi\right\} \tag{2.62}$$

where again $A_n = (2n+1)^2\pi^2/4$.

The mean concentration is then obtained by integration with respect to X from 0 to 1. Knowing that

$$\int_0^1 \cos(A_n^{1/2}X)dX = \frac{1}{A_n^{1/2}}(-1)^n \tag{2.63}$$

and assuming that $c_m(X,0) = c_{m,i}$ the mean concentration is therefore

$$\overline{c}_m(Z,T) = c_{m,i} + 2\sum_{n=0}^{\infty} e^{-A_n T}\int_0^T c_f(Z,\tau)e^{A_n\tau}d\tau \tag{2.64}$$

To find the solution for $\overline{c}_m(Z,T)$ when $c_f(Z,T) = \sin(\Omega T)$ we evaluate the time integral (*Zimmerman et al.*, 1993)

$$\int_0^T \sin(\Omega\tau)e^{A_n\tau}d\tau = \frac{A_n\sin(\Omega T)e^{A_n T} - \Omega\cos(\Omega T)e^{A_n T} + \Omega}{A_n^2 + \Omega^2} \tag{2.65}$$

Substituting this into equation (2.64) and assuming $c_{m,i} = 0$ it follows that

$$\overline{c}_m(T) = 2\sum_{n=0}^{\infty}\frac{A_n\sin(\Omega T) - \Omega\cos(\Omega T) + \Omega e^{-A_n T}}{A_n^2 + \Omega^2} \tag{2.66}$$

Zimmerman et al. (1993) points out that removing the exponential term in the above equation then yields the solution when the matrix block has reached a 'dynamic balance' such that

$$\overline{c}_m(T) = 2\sum_{n=0}^{\infty} \frac{A_n \sin(\Omega T) - \Omega \cos(\Omega T)}{A_n^2 + \Omega^2} \tag{2.67}$$

Inspection of equation (2.11) then yields

$$\overline{c}_m(T) = c_{max}[\cos(\delta)\sin(\Omega T) - \sin(\delta)\cos(\Omega T)] = c_{max}\sin(\Omega T - \delta) \tag{2.68}$$

where A and δ are the amplitude and phase angle of oscillation respectively.

Further inspection of equation (2.11) then suggests that

$$\delta = \arctan\left[\left(\sum_{n=0}^{\infty} \frac{\Omega}{A_n^2 + \Omega^2}\right)\left(\sum_{n=0}^{\infty} \frac{A_n}{A_n^2 + \Omega^2}\right)^{-1}\right] \tag{2.69}$$

and

$$c_{max} = \frac{2}{\cos\delta}\sum_{n=0}^{\infty} \frac{A_n}{A_n^2 + \Omega^2} = \frac{2}{\sin\delta}\sum_{n=0}^{\infty} \frac{\Omega}{A_n^2 + \Omega^2} \tag{2.70}$$

Similarly, for the QSS model (recall equation 2.61)

$$\delta = \arctan\left[\frac{\Omega}{\omega}\right]; \quad c_{max} = \frac{\omega^2}{\cos\delta(\omega^2 + \Omega^2)} = \frac{\omega\Omega}{\sin\delta(\omega^2 + \Omega^2)} \tag{2.71}$$

Figure 2.7 shows plots of wave amplitude, c_{max} and phase angle, δ for the Fickian model and the QSS model with $\omega = \pi^2/4$ and $\omega = 3$ for a range of Ω. It can be seen that as Ω gets smaller the QSS models approximate the Fickian model with increasing accuracy. This is because as Ω gets smaller the period of oscillation t_p is becoming larger relative to the characteristic block diffusion time t_{cb}. It is also interesting to note that the QSS model with $\omega = \pi^2/4$ reproduces the correct amplitude at higher values of Ω than the model with $\omega = 3$. Conversely, the phase angle for the QSS model with $\omega = 3$ converges to that of the Fickian model with small Ω where as the model with $\omega = \pi^2/4$ always overestimates it. This is presumably because the condition in equation (2.45) has finally been satisfied.

To establish what values of Ω might be appropriate for the Chalk we will consider the case of nitrate migration in the unsaturated Chalk. Elevated concentrations generally originate from fertiliser application which would be typically applied on an annual basis giving a $t_p = 1$ year. From laboratory analysis of nitrate diffusing into Chalk cores $10^{-10} > D_A > 10^{-11}$ m^2/s (*Hill*, 1984; *Gooddy et al.*, 1995). Fracture spacing at a site in the Chalk can potentially vary from 0.05 to 2 m (i.e. $0.025 < b < 1$ m) (*Bloomfield*, 1996). This yields a range of characteristic block diffusion times $10^{-1} < t_{cb} < 10^3$ years, which then yields a range of characteristic frequencies $10^{-1} < \Omega < 10^4$. From Figure 2.7 it can be seen that once $\Omega > 10$,

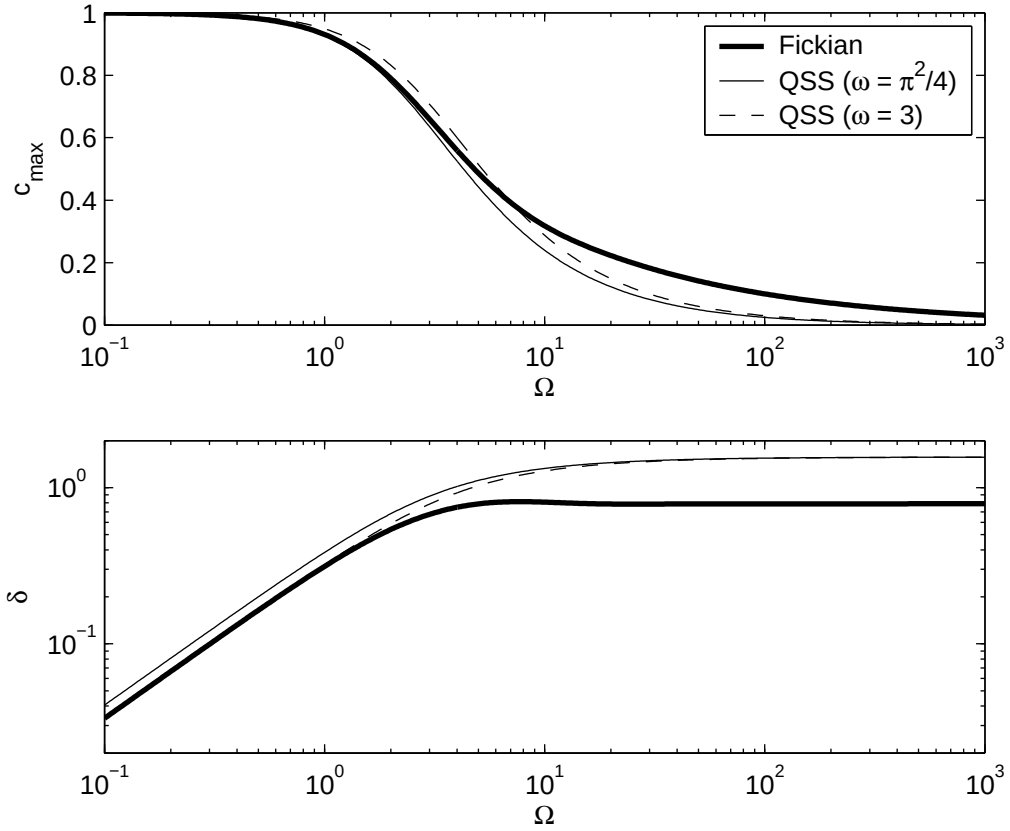

Figure 2.7 Comparison of wave amplitudes, c_{max} and dimensionless phase angles, δ for the Fickian model (equations 2.69 and 2.70) and the QSS model (equation 2.71) with $\omega = \pi^2/4$ and $\omega = 3$ subjected to a sinusoidal change in concentration for a range of dimensionless frequencies, Ω.

the phase angle is out by 0.6 which corresponds to a lag time of $0.6t_p/2\pi$, which corresponds to just over one month for $t_p = 1$ year. Furthermore, when $\Omega > 100$, the amplitudes predicted by the QSS model are less than half that of the Fickian model. Consequently it can be seen that for values of $\Omega > 10$, the QSS model is an increasingly poor approximation of the Fickian model. From this we can conclude that the QSS model is an inappropriate alternative for a Fickian model when simulating solute transport in fractured rock where t_{cb} is potentially greater than a year, such as in the Chalk.

2.6 Integral representations

An alternative approach of evaluating equations (2.6) and (2.7) using an integral representation has been presented by *Bibby* (1981) and *Little et al.* (1996). Their starting point was

Duhamel's formula

$$c_m = c_f(T_0)A(X,T) + \int_0^T \frac{dc_f}{d\tau} A(X, T-\tau)d\tau \tag{2.72}$$

where from equation (2.10)

$$A(X,T) = 1 - 2\sum_{n=0}^{\infty} \frac{(-1)^n}{A_n^{1/2}} e^{-A_n T} \cos(A_n^{1/2} X) \tag{2.73}$$

Bibby (1981) then found that the mean matrix concentration, $\overline{c}_m$ could be evaluated from

$$\begin{aligned}\overline{c}_m = c_f(T_0)\left[1 - 2\sum_{n=0}^{\infty} \frac{1}{A_n} e^{-A_n T}\right] + \sum_{i=1}^{M}\{c_f(T_i) - c_f(T_{i-1})\} \\ \cdot \left\{1 - \frac{2}{\Delta T_i}\sum_{n=0}^{\infty} \frac{1}{A_n^2}\left[e^{-A_n(T-T_i)} - e^{-A_n(T-T_{i-1})}\right]\right\}\end{aligned} \tag{2.74}$$

Equation (2.74) involves the summation over the whole history of the simulation, which means that all previous nodal concentrations at all time steps must be stored throughout a simulation. This has traditionally made the integral representation unattractive as significantly less information would be needed to calculate $\overline{c}_m$ from an equivalent finite difference representation. To overcome this problem *Bibby* (1981) truncates the summation over i. Only an optimum number of retained terms is needed, dependant on t_{cb} and ΔT, to minimise any error incurred.

A reworking of the development of these equations shows that this truncation can be avoided completely. Because $A(X, T-\tau)$ in equation (2.72) is essentially an exponential function, it is possible to separate it by considering $\exp(T-\tau) = \exp(T)\exp(-\tau)$, allowing the convolution integral to be transformed to a cumulative integral which only requires knowledge of the value of the integral from the previous time step as opposed to all previous nodal concentrations at all time steps.

Consider again equation (2.64). This can be evaluated from

$$\overline{c}_m(T_k) = \overline{c}_m(T_0) + 2\sum_{n=0}^{N} e^{-A_n T_k} I_{n,k} \tag{2.75}$$

where the integral, $I_{i,n}$ is defined by

$$I_{n,k} = I_{n,k-1} + c_f(T_k)e^{A_n T_k}\Delta T \quad \text{and} \quad I_0 = 0 \tag{2.76}$$

Because $e^{A_n T_i}$ becomes hard to compute as T_i becomes large it is better instead, to write this as

$$\overline{c}_m(T_k) = c_m(T_0) + 2\sum_{n=0}^{N} \Upsilon_{n,k} \tag{2.77}$$

with

$$\Upsilon_{n,k} = e^{-A_n \Delta T} \Upsilon_{n,k-1} + c_f(T_k)\Delta T \quad \text{and} \quad \Upsilon_{n,0} = 0 \tag{2.78}$$

which is similar to the result presented by *Carrera et al.* (1998).

It follows that

$$\Lambda(T_k) = \frac{\overline{c}_m(T_k) - \overline{c}_m(T_{k-1})}{\Delta T} \tag{2.79}$$

where ΔT is the length of a discrete time step and N is the number of terms considered for the approximation to the infinite series.

This algorithm can enable a fully analytical treatment of the fracture-matrix transfer, requiring only knowledge of the integral from the previous time. It should therefore follow that there is little point in adopting any of the aforementioned lumped response models since the integral naturally provides excellent approximations during large and small times due to the fact that it is a complete representation of equations (2.6) and (2.7). Its accuracy will only be dependant on the time step and number of terms incorporated into its infinite series.

However, almost exactly the same statement could be made about an equivalent finite difference representation except that its accuracy will be dependant on the number of nodes used in its spatial discretisation as opposed to the number of terms in an infinite series. A question then arises as to which method is more accurate with the same number of nodes or terms, because both affect computation efficiency due to their demands on memory storage.

A simple finite difference scheme needed to obtain the fracture-matrix exchange flux would be

$$\Lambda(T_k) = \frac{c_f(T_k) - c_{N,k-1}}{\Delta X/2} \tag{2.80}$$

where

$$c_{N,k} = \frac{\Delta T}{\Delta X^2}\left[c_{N-1,k-1} - \left(3 - \frac{\Delta X^2}{\Delta T}\right) c_{n,k-1} + 2c_f(T_k)\right] \tag{2.81}$$

$$c_{1,k} = \frac{\Delta T}{\Delta X^2}\left[-\left(1 - \frac{\Delta X^2}{\Delta T}\right) c_{1,k-1} + c_{2,k-1}\right] \tag{2.82}$$

$$c_{n,k} = \frac{\Delta T}{\Delta X^2}\left[c_{n-1,k-1} - \left(2 - \frac{\Delta X^2}{\Delta T}\right) c_{n,k-1} + c_{n+1,k-1}\right], \quad n = 2 \ldots N-1 \tag{2.83}$$

and $\Delta X = 1/N$.

Note that the above scheme is often referred to as an explicit time-stepping scheme whereby values for one time-step are calculated explicitly from values from the previous time-step. This scheme will become unstable when the middle term in equation (2.83) becomes negative. Consequently, it is necessary to keep ΔT sufficiently small such that

$$\frac{\Delta X^2}{\Delta T} > 2 \tag{2.84}$$

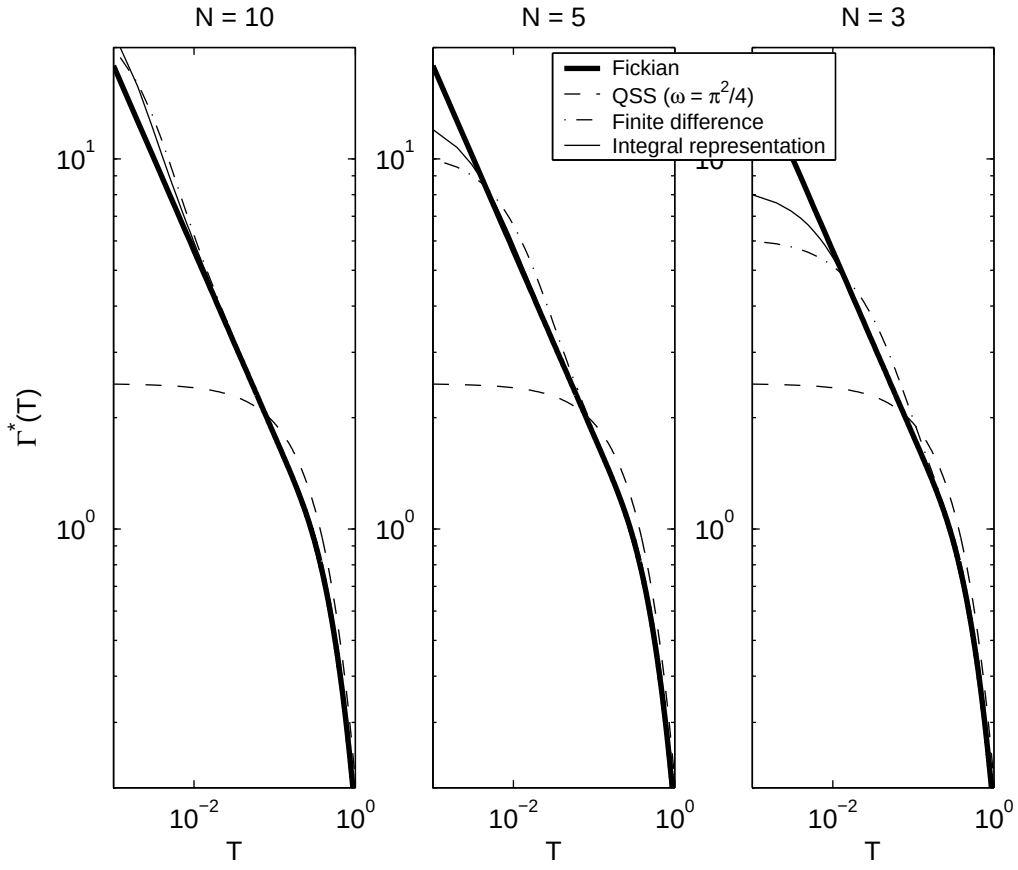

Figure 2.8 Plotted responses of the analytical solution, a finite difference solution and an integral representation solution for the Fickian model (with a slab geometry) subjected to a step change in concentration. The different subplots show the finite difference and integral representation solutions with $N = 10$, 5 and 3 where N is the number of terms in the infinite series or nodes in the finite difference discretisation.

although this issue can be avoided if an adaptive time grid is used (such as *Cash and Karp* (1990) scheme used with ODE45 in MATLAB).

To investigate this further, both the finite difference and integral representation methods were set up to solve the step change in concentration problem described by the analytical solution in equation (2.12) using an explicit time integration scheme with a uniform time step of $\Delta T = 0.001$. Plotted responses of the models are shown in Figure 2.8. The QSS model with ($\omega = \pi^2/4$) is also shown for completeness. The different subplots show the finite difference and integral representation solutions with $N = 10$, 5 and 3 where N is the number of terms in the infinite series or nodes in the finite difference discretisation. It can be seen that the integral representation consistently converges onto the Fickian model at earlier times than the finite difference.

2.7 Conclusions

Many geological systems exhibit dual-porosity behaviour which exerts an important control on contaminant travel times. It is therefore important that this property is represented appropriately in numerical models of these systems. Within such models it is common to assume that fracture/matrix transfer is governed by Fickian diffusion.

To avoid explicitly representing the matrix in terms of finite differences, many workers have sought to find approximations that lump a distributed matrix response into a single mean value that varies only in the direction of the fracture flow. One method of doing this is to assume that the fractures and matrix are in a quasi-steady-state (QSS) (*Barenblatt et al.*, 1960; *Warren and Root*, 1963). The diffusive flux between the fractures and matrix is then taken to be proportional to the difference between their concentrations. The problem is that when subjected to a step increase in fracture concentration, the QSS model is unable to replicate Fickian behaviour during early times. *Dykhuizen* (1990) and *Zimmerman et al.* (1993) (the Vermeulen model) proposed two alternative methods that work well during early times but are limited to monotonic fracture concentrations.

A step increase in fracture concentration is an unrealistic scenario as generally solute changes are less rapid. However, in systems where the characteristic block diffusion time is comparable to or greater than the timescale of change, the early time regime is still important. In addition, natural solute functions are often periodic (i.e. not monotonic) in nature due to climatic, seasonal or anthropogenic activities. In this chapter, a study was conducted to find out at what frequencies the QSS model cease to be a good approximation to Fickian diffusion by application of a sinusoidal fracture concentration. It was found that for dimensionless frequencies of $\Omega > 10$, the QSS model becomes an increasingly poor approximation of the Fickian model. In the context of conservative solute diffusing into Chalk blocks, this corresponds to a time period of $0.12 < t_p < 2000$ years. From this we conclude that the QSS model is an inappropriate alternative for a Fickian model when simulating solute transport in fractured rocks where the characteristic block diffusion time, t_{cb} is greater than a year (such as in the Chalk).

Bibby (1981), *Little et al.* (1996) and *Carrera et al.* (1998) presented another lumped response model that works well for non-monotonic fracture concentrations and large values of t_{cb} because it represents a fully analytical solution to the Fickian model. However, their model considers an integral representation of Fick's second law. This requires the evaluation of a number of terms for its approximation to an infinite series. The number of terms required

can be equated to the number of nodes needed for an equivalent finite difference solution. Nevertheless, our comparison study shows that the integral representation consistently offers more accurate results than the simple finite difference scheme (described in the previous section) with the same number of nodes/terms.

However, two major drawbacks of the integral representation are that it requires that the processes within the matrix are linear and that advective flow in the matrix is negligible. While the former is arguably true for the Chalk, in the following chapter it is concluded that the latter is not. Consequently, the finite difference method is used to represent matrix diffusion in numerical model simulations described in the remainder of this thesis.

Chapter 3

The significance of flow in the matrix of the Chalk unsaturated zone

Adapted from *Mathias et al.* (2005)

3.1 Introduction

Throughout the literature concerning flow and solute transport in the unsaturated zone of the Chalk there has been much debate as to whether the dominant element of flow occurs in the fractures or the matrix. As discussed in Chapter 1, flow in the unsaturated zone of the Chalk was originally believed to be predominantly through fractures. Evidence to support this included the observed rapid response of the water table after high intensity rainfall events (*Headworth*, 1972) and the appearance of bacteria in boreholes (*Maclean*, 1969). This was largely unquestioned prior to a 1968 study of tritium content in pore-water from the unsaturated zone at a Berkshire site, which led *Smith et al.* (1970) to suggest that 85% of the total flow through the unsaturated zone was by intergranular seepage through the matrix at a mean rate of less than 0.9 m/year. This rate of solute movement has been widely supported by many other similar studies (e.g. *Oakes*, 1977; *Wellings*, 1984b; *Barraclough et al.*, 1994). The rapid observed response of water tables was then explained by a 'piston-displacement' mechanism whereby water arriving at the water table had been displaced from the bottom of the unsaturated zone instead of travelling quickly through it (*Price et al.*, 1993).

Since the analysis of *Smith et al.* (1970), there have been parallel schools of thought

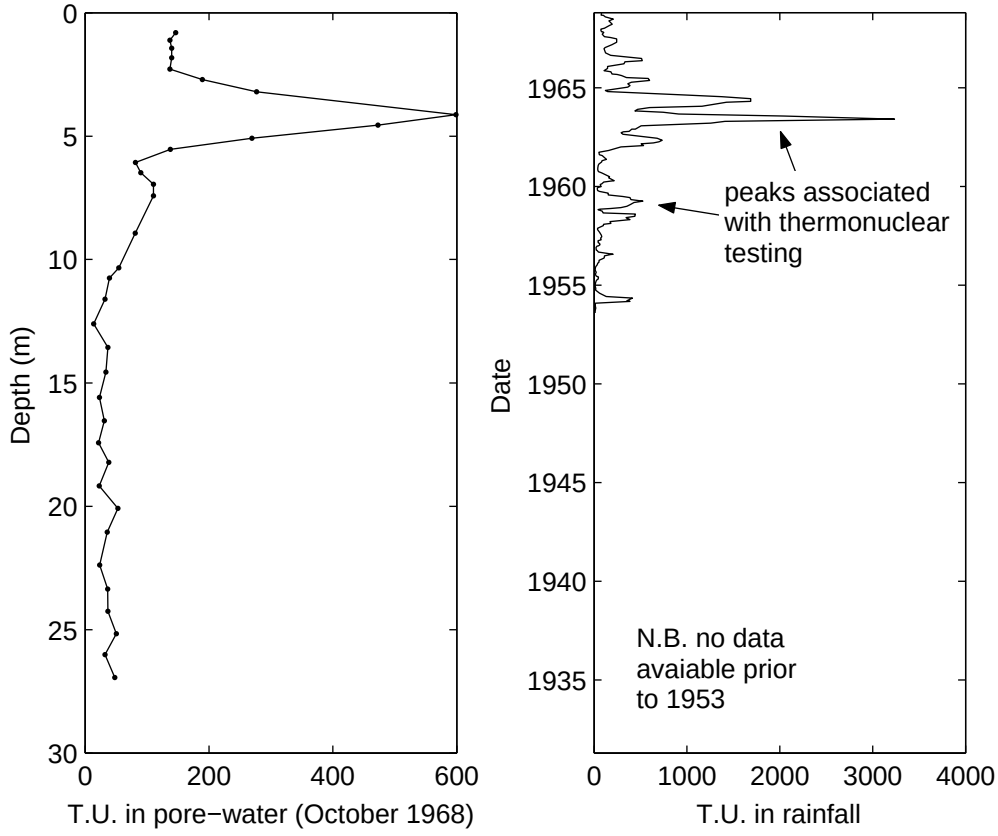

Figure 3.1 A Chalk unsaturated zone pore-water tritium profile from a Berkshire site in October 1968 alongside a plot of tritium content in UK rainfall against time, after *Smith et al.* (1970).

with regard to whether flow in the matrix of the Chalk unsaturated zone is significant (e.g. *Wellings*, 1984a; *Hodnett and Bell*, 1990; *Haria et al.*, 2003) or not (e.g. *Oakes et al.*, 1981; *Barker and Foster*, 1981; *Fretwell et al.*, 2000). *Foster* (1975) made an important contribution by highlighting the fact that solutes in fractures can be greatly retarded by lateral diffusion into adjacent matrix blocks. This provided an integrated theory of flow and transport, but one in which the role of matrix flow was not seen as significant. By studying the literature and performing some simple modelling analyses this chapter aims to resolve this issue to arrive at a well-founded conclusion regarding the significance of flow in the matrix of the Chalk unsaturated zone.

3.2 Pore water profiles

The findings of *Smith et al.* (1970) are based on the tritium profile presented in Figure 3.1. A sharp peak can be seen at 4 m depth followed by a broader peak at between 7 and 9 m

depth. These two peaks are thought to be associated with the very high tritium levels found in rainfall during the periods of 1963 to 1964 and 1958 to 1959. *Smith et al.* (1970) speculate that the existence of these peaks shows that downward movement of water is predominately by intergranular seepage through the matrix. From the position of these peaks the mean seepage velocity can be calculated at around 0.8 m/year. On this basis it should be expected that any tritium observed below 13 m depth has travelled via faster pathways in the fractures. This portion represents around 15% of the total mass present in the profile. Furthermore, an implicit assumption was made that all tritium travelling through fractures was still present within the unsaturated zone. However, this ignores the possibility that very fast flowing tritiated water may have flowed through the unsaturated zone and into the saturated zone. This was probably overlooked because the estimate of tritium input mass (corrected for evaporation) appeared to be less than the total mass measured from the profile.

The total amount of tritium in the profile was estimated to be 863 T.U.m. By contrast, the total amount of tritium which had fallen on the catchment in precipitation from 1954 to 1968 has been estimated at 2400 T.U.m (*Smith et al.*, 1970). To equate the total mass in the profile with the input mass, *Smith et al.* (1970) applied a simple soil moisture accounting model to calculate an effective rainfall. Through the evaporation of tritiated water, an effective tritium input can be obtained using the ratio of effective to actual rainfall. Effective rainfall was calculated from the difference between monthly values of precipitation and evaporation with surface runoff assumed to be negligible. Actual evaporation was calculated as potential evaporation using Penman's formula (*Penman*, 1950), but with an upper limit of soil moisture deficit of 120 mm. *Smith et al.* (1970) found that a mass balance could only be achieved between the tritium profile and the input time-series by reducing the calculated evaporation by 25%.

Furthermore, *Smith et al.* (1970) do not report any consideration of decay (tritium has a half-life of around 12.3 years) in their mass-balance calculation. *Smith et al.* (1970) apparently equate the mass of solute in the rainfall directly with that in the chalk profile. However, solute in the profile would have decayed since the time of entry (which would have been when the rainfall concentration was recorded). For example, assuming a constant vertical movement of 0.8 m/year and neglecting any diffusion/dispersion, solute found at a 10 m depth would have experienced 12.5 years of decay since the corresponding rainfall measurement was made. To perform the mass-balance correctly, one would therefore need to decay the rainfall tritium concentrations to the date when the core-measurements were made. This would suggest that Smith's evaporation estimate would need to be reduced even further before mass-balance

could be obtained.

The required reduction in evaporation is probably due in part to inadequacies associated with their evaporation calculation and because the estimate of UK rainfall tritium content was derived from data collected in Ireland (see *Foster and Smith-Carington*, 1980).

Smith et al. (1970) also overlook the significance of background tritium levels. It has been estimated that prior to initiation of atmospheric nuclear testing in 1952, the natural content of precipitation was in the range of about 5-20 T.U. (*Payne*, 1972). The tritium measurements below 13 m in Figure 3.1 range between 10 and 40 T.U. Bearing in mind that *Smith et al.* (1970) suggest that the accuracy of their tritium measurements was around ±10%, the value of 15% associated with fracture flow must therefore be taken very tentatively.

Another observation that has been consistently made on Chalk outcrop sites is an almost complete absence of surface runoff (*Foster*, 1975). Rainfall across the UK can be up to 10 cm/day whereas the hydraulic conductivity of the Chalk matrix is unlikely to be larger than 1 cm/day (e.g. *Wellings*, 1984a; *Cooper et al.*, 1990; *Hodnett and Bell*, 1990). *Foster* (1975) was concerned that this phenomena was incompatible with a matrix flow dominated system. He therefore concluded that substantial fracture flow must be occurring to absorb these higher rainfall events.

The model suggested by *Smith et al.* (1970) implicitly assumes that the tritium entering the unsaturated zone is areally uniform. *Foster* (1975) speculated that tritium input to the unsaturated zone (after infiltration through a thin soil cover) would be focused on fracture openings within the Chalk. The concentration gradients between the contaminated fracture water and the cleaner matrix water would then cause lateral diffusion of the solute into the matrix, thus greatly retarding its downward movement. This mechanism presented a means by which fracture-dominated flow could be reconciled with a much slower observed downward movement of tritium.

Provided there is time for sufficient diffusion to take place, solutes in the fracture water would appear to be in local equilibrium with the less mobile waters of the matrix (*Young et al.*, 1976). Assuming zero longitudinal dispersion, no flow in the matrix and that solute in the fractures and matrix are in local equilibrium, the ratio of the downward velocity of the contaminant front, v_∞ to the velocity of the water in the fractures, v_f is (*Oakes*, 1977)

$$\frac{v_\infty}{v_f} = \frac{a}{\phi b + a} \tag{3.1}$$

where ϕ is the matrix porosity, b is the mean half-width of the matrix and a is the mean half-width of the fractures. The properties of the unsaturated Chalk are such that the infiltrating

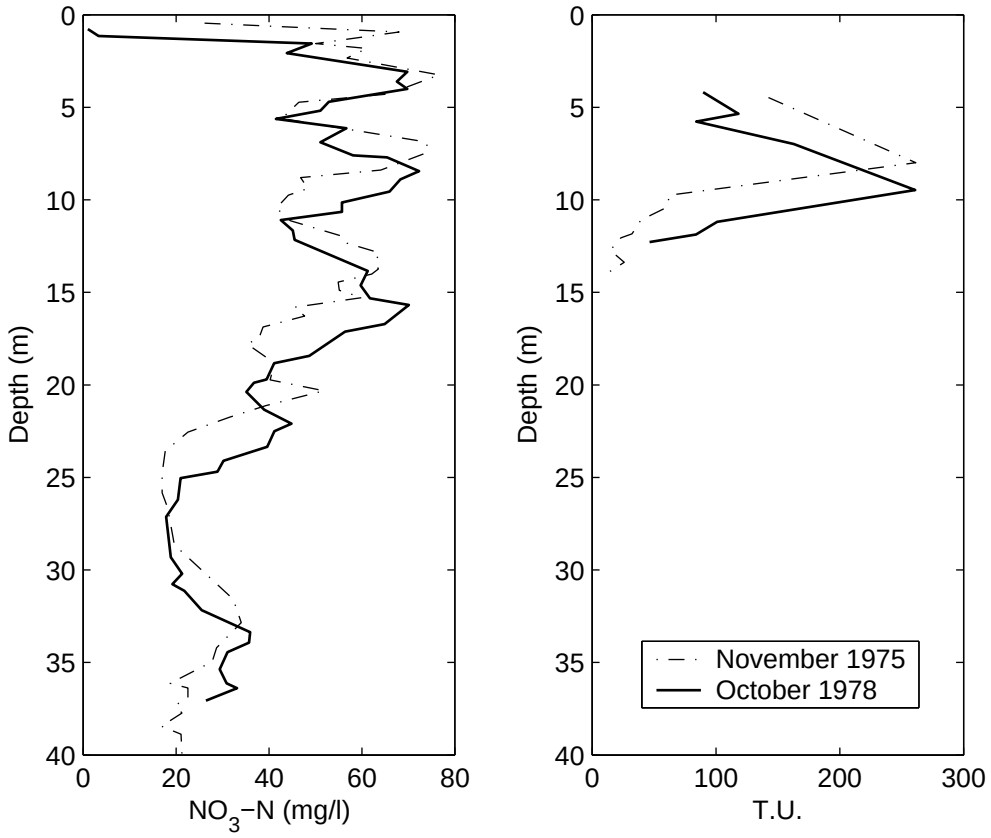

Figure 3.2 Chalk unsaturated zone pore-water nitrate and tritium profiles from repeated drilling in Kent, after *Oakes et al.* (1981).

water would therefore move downwards at a rate some 20 to 40 times faster than the associated contaminants. Sharp input peaks would persist in the matrix concentrations during downward migration provided that rapid equilibrium is attained, although some blurring would be expected due to longitudinal dispersion. This can be seen in the nitrate and tritium profiles obtained by *Oakes et al.* (1981) from repeated drilling at a site in Kent (see Figure 3.2).

Contaminant transport by such a mechanism could be well described by a uniform velocity, downward-flow model. *Young et al.* (1976) also suggest that 10 to 15% of water and solute should be bypassed directly to the water table to account for extreme infiltration events when fracture flow is too fast to allow solute exchange with the matrix. This model has been used with some success to simulate nitrate, tritium and chloride profiles in unsaturated Chalk at various sites in the UK (*Young et al.*, 1976; *Oakes*, 1977; *Oakes et al.*, 1981). Tritium input pulses were derived from knowledge of tritium content in rainfall, nitrate inputs were translated from land management histories and model outputs were calibrated against the observed profiles to obtain parameters describing the system. It is interesting that while

this model assumes no flow in the matrix, because of the local equilibrium assumption, it is mathematically analogous to the matrix-dominated flow model of *Smith et al.* (1970).

Wellings (1984b) studied pore-waters from samples taken at 20 cm intervals down to 2.9 m depth every 10 weeks from 1979 to 1981 at three different spring barley plots on an Upper Chalk outcrop in Hampshire. It was found that nitrate and chloride moved at about the same velocity as the water calculated in a soil physics study by *Wellings* (1984a). Flow was assumed to occur almost exclusively in the matrix for two reasons. Firstly, because measurements of pressure head rarely exceeded -50 cm, implying that any fracture with an aperture greater than 0.03 mm would be unable to hold water (*Wellings and Bell*, 1980). Secondly, because the estimated mean annual infiltration could easily be accommodated by an estimate of saturated matrix hydraulic conductivity (*Wellings*, 1984a).

However, fractures possess rough surfaces with apertures that can vary from zero to tens of millimetres (e.g. *Wang and Narasimhan*, 1985; *Bloomfield*, 1996). A significant percentage of the fracture surface (from a hydraulic perspective) could potentially transmit water at these pressure heads. Admittedly, observed hydraulic conductivities obtained by *Wellings* (1984a) also suggest that fracture flow does not occur until pressure heads exceed -50 cm (also see Section 3.4). However, these estimates are based on infrequent measurements of moisture content using neutron probes and daily rainfall. Continuous logging equipment (say hourly) may yield quite different answers. Furthermore, the fact that infiltration is transient suggests that the peaks could be orders of magnitude larger than the annual mean. Such events could only be absorbed through fractures.

Barraclough et al. (1994) studied the recovery of surface-applied Cl^- and ^2H at the same site over a four year period. Fractures in the Chalk have been subjectively subdivided by *Reeves* (1979) into microfissures with apertures less than 20 μm and macrofissures with apertures greater than 20 μm. *Barraclough et al.* (1994) use this subdivision to define three flow patterns: matrix flow through all or part of the matrix; microfissure flow which, although bypassing the matrix, is slow enough to allow some solute equilibration with the matrix; and macrofissure flow which is sufficiently rapid to preclude significant solute exchange with the matrix. *Barraclough et al.* (1994) found that the mass recovery of Cl^- and ^2H from solute profiles taken down to 600cm depth was almost 100%, from which they conclude that no macrofissure flow took place. However smearing of the seasonal peaks of background ^2H suggested to them that some microfissure flow had taken place.

The non-observation of macrofissure flow (as defined by *Barraclough et al.*, 1994) is interesting. However, the differentiation between micro and macrofissures is not particularly

helpful as *Barraclough et al.* (1994) present no evidence of aperture size having some threshold value beyond which solute exchange with the matrix is significantly reduced.

3.3 Fracture-matrix solute transfer

Barker (1982) presents a set of assumptions and equations to describe solute transport in a fractured porous medium through which the topic of fracture-matrix solute transfer and equilibration can be more systematically explored. Identical slabs of matrix material are separated by regularly spaced, planar fractures. The matrix is homogenous and saturated with immobile water. Solute transfer between the fractures and matrix and within the matrix occurs by molecular diffusion in the immobile water in a direction perpendicular to the plane of the fractures. There is no concentration gradient across the fractures. The flow velocity in the fractures is uniform, while no flow occurs in the matrix. Longitudinal dispersion in the fractures is assumed negligible.

Because of the symmetry of the model only a single, semi-infinite unit extending from the centre of a matrix block to the centre of a neighbouring fracture need be considered. Let $c_f(z,t)$ be the solute concentration in the fracture water and $c_m(x,z,t)$ be the concentration in the matrix water. The movement of a conservative non-sorbing solute in a fracture is then described by

$$\frac{\partial c_f}{\partial t} + v_f \frac{\partial c_f}{\partial z} + \frac{\phi D_A}{a} \left.\frac{\partial c_m}{\partial x}\right|_{x=b} = 0 \tag{3.2}$$

where x is lateral distance from the centre of the matrix block, z is longitudinal distance, t is time, a is the half-width of the fracture, b is the half-width of the matrix block , ϕ is the matrix porosity, v_f is the velocity of water flowing in the fracture and D_A is the apparent molecular diffusion coefficient for solute in the matrix. See Figure 3.3 for a schematic diagram.

Solute concentrations in the matrix are then described by

$$\frac{\partial c_m}{\partial t} - D_A \frac{\partial^2 c_m}{\partial x^2} = 0 \tag{3.3}$$

subject to the boundary conditions

$$\left.\frac{\partial c_m}{\partial x}\right|_{x=0} = 0; \quad c_m(b,z,t) = c_f(z,t) \tag{3.4}$$

Following *Barker et al.* (2000), we introduce a porosity ratio, σ, an advective travel time, t_a and a characteristic block diffusion time, t_{cb}, which are found from

$$\sigma = \phi \frac{b}{a}; \quad t_a = \frac{L}{v_f}(1+\sigma); \quad t_{cb} = \frac{b^2}{D_A} \tag{3.5}$$

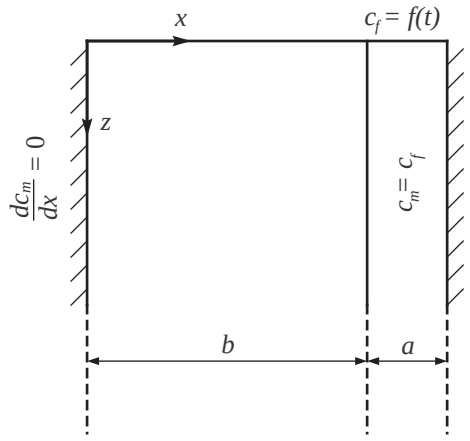

Figure 3.3 Schematic diagram of the parallel-fracture dual-porosity model.

where L is the distance along a fracture being considered.

Applying the following transformations

$$T = \frac{t}{t_a}; \quad Z = \frac{z}{L}; \quad X = \frac{x}{b}; \quad \gamma = \frac{t_a}{t_{cb}} \tag{3.6}$$

then yields the set of dimensionless equations

$$\frac{\partial c_f}{\partial T} + (1+\sigma)\frac{\partial c_f}{\partial Z} + \sigma\gamma \left.\frac{\partial c_m}{\partial X}\right|_{X=1} = 0 \tag{3.7}$$

$$\frac{\partial c_m}{\partial T} - \gamma \frac{\partial^2 c_m}{\partial X^2} = 0 \tag{3.8}$$

$$\left.\frac{\partial c_m}{\partial X}\right|_{X=0} = 0; \quad c_m(1, Z, T) = c_f(Z, T) \tag{3.9}$$

If the input of concentration in the fracture is a known function of time, $f(T)$, the initial concentration distribution a known function of distance in the flow direction, $g(Z)$, and the matrix concentration is initially uniform in the X direction, it can be said that

$$c_f(0, T) = f(T) \quad \text{and} \quad c_m(X, Z, 0) = c_f(Z, 0) = g(Z) \tag{3.10}$$

The above set of equations conform to the local equilibrium assumption used by *Oakes* (1977) as $D_A \to \infty$. *Barker and Foster* (1981) were interested in determining what finite values of D_A were needed for a given fracture-matrix geometry to behave in this fashion. To this end, *Barker and Foster* (1981) explored the movement of a Gaussian distributed profile by solving equations (3.7) to (3.10) using finite differences with

$$f(T) = 0 \quad \text{and} \quad g(Z) = \exp\left[\frac{-(Z-\mu_1')^2}{2\mu_2}\right] \tag{3.11}$$

where μ_1' represents the initial position of the solute peak and μ_2 represents the variance of the distribution.

Oakes (1977) assumed that the bulk rate of movement of a solute plume (denoted v_∞ in equation 3.1) could be measured from the displacement of peaks in a pore-water profile. *Barker and Foster* (1981) studied the ratio v_{peak}/v_∞ for a range of D_A values in various scenarios, where v_{peak} was the displacement of the peak for their Gaussian distribution over one simulation day.

The scenarios studied included two geometries, $a = 0.5$ mm with $b = 10$ cm and $a = 1$ mm with $b = 5$ cm, both with $\phi = 0.35$, and $v_f = 1$ m/day and 5 m/day used in both scenarios. Plots of v_{peak}/v_∞ against D_A showed that v_{peak}/v_∞ converged to unity only when $D_A > 10^{-8}$ m^2/s. For smaller fracture spacings or fracture flows, the assumption would work for smaller diffusion coefficients. This is reflected by the characteristic block diffusion time, t_{cb}, which is approximately the time for a solute to diffuse through the matrix block. The lower this diffusion time, the closer the fractures and matrix are to equilibrium, for any fixed value of time.

The specific interest in apparent diffusion coefficients at that time was in response to an empirically-obtained value for chloride in a laboratory sample of Chalk of 1.3×10^{-9} m^2/s by *Oakes* (1977). Bearing in mind that the free water diffusion coefficient for chloride is around 1.92×10^{-9} m^2/s (*Parsons*, 1959) this is anomalously large as the tortuosity of Chalk should have a large inhibiting effect, decreasing any observed molecular diffusion (e.g. *Hill*, 1984). Since then, techniques for determining diffusion coefficients in Chalk have become better established and the accepted values of D_A for tritium, nitrate and chloride are between 10^{-10} and 10^{-11} m^2/s (*Hill*, 1984; *Gooddy et al.*, 1995). Clearly, *Barker and Foster* (1981) demonstrated the inadequacy of the local equilibrium assumption in the Chalk.

Barker and Foster (1981) also studied model simulations where $g(Z) = 0$ and $f(T) = 1$ and found, for certain combinations of a, b, D_A and v_f, that the diffusion exchange mechanism was extremely effective in transferring solute from fracture water to the matrix, as suggested by *Foster* (1975). The mechanism also provided a possible explanation of how solutes present in the unsaturated zone in the matrix of fractured porous media migrate across near-horizontal discontinuities such as bedding planes.

It is instructive to undertake a sensitivity analysis of the model defined by equations (3.7) to (3.10). From the experimental work of *Gooddy et al.* (1995) we can be more confident about assuming an apparent diffusion coefficient $D_A \sim 10^{-10}$ m^2/s. A parameter of greater interest is therefore the fracture spacing (double the half-width of the matrix block, b). Fracture

spacing at a site in the Chalk can potentially vary from 5 to 200 cm (*Bloomfield*, 1996).

To perform this sensitivity analysis, equations (3.7) to (3.10) were solved using Laplace transforms and a numerical Laplace transform inversion algorithm as recommended by *Barker* (1982). Assuming $g(Z) = 0$ and $c_f(\infty, T) = 0$, the Laplace transform solution describing solute concentrations in the fracture is (*Barker*, 1982)

$$\hat{c}_f(Z, s) = F(s) \exp(-Z\hat{\lambda}(s)) \tag{3.12}$$

where

$$\hat{\lambda}(s) = \frac{s}{(1+\sigma)}[1 + \sigma\hat{\Lambda}^*(s)] \tag{3.13}$$

with $\hat{\Lambda}^*(s)$ being a block geometry function (*Barker*, 1985), which for a slab-like matrix is

$$\hat{\Lambda}^*(s) = \frac{\gamma^{1/2}}{s^{1/2}} \tanh\left(\frac{s^{1/2}}{\gamma^{1/2}}\right) \tag{3.14}$$

and s, $\hat{c}_f$, $F(s)$ are the corresponding Laplace transforms of T, c_f and $f(T)$.

The solute concentration that one would expect from sampling matrix pore-water would more likely represent the mean concentration in the matrix, $\overline{c}_m$ where

$$\overline{c}_m(Z, T) = \int_0^1 c_m(X, Z, T) dX \tag{3.15}$$

This can be obtained from (*Barker*, 1982)

$$\hat{\overline{c}}_m(Z, s) = \hat{\Lambda}^*(s)\hat{c}_f(Z, s) \tag{3.16}$$

Taking a recharge q_{re}, providing that $a << b$, the velocity of flow in the fracture is

$$v_f = q_{re} b/a \tag{3.17}$$

To generate plots easily comparable with the tritium profiles of *Oakes et al.* (1981) presented in Figure 3.2, pore-water profiles in the matrix were simulated using equations (3.12) and (3.16) at 10 and 13 years after an instantaneous injection of solute $f(T) = \delta(T)$, where δ denotes the Dirac delta function, which has the Laplace transform $F(s) = 1$, for fracture spacings of 5, 25 and 50 cm. A steady recharge of $q_{re} = 0.25$ m/year was applied with the fracture velocity v_f calculated from equation (3.17). The apparent diffusion coefficient was taken as $D_A = 10^{-10}$ m^2/s, the fracture half-width as $a = 1$ mm and the matrix porosity $\phi = 0.35$. Laplace transform solutions were inverted using a MATLAB implementation of the *de Hoog et al.* (1982) algorithm developed by *Hollenbeck* (1998). The plots are presented in Figure 3.4.

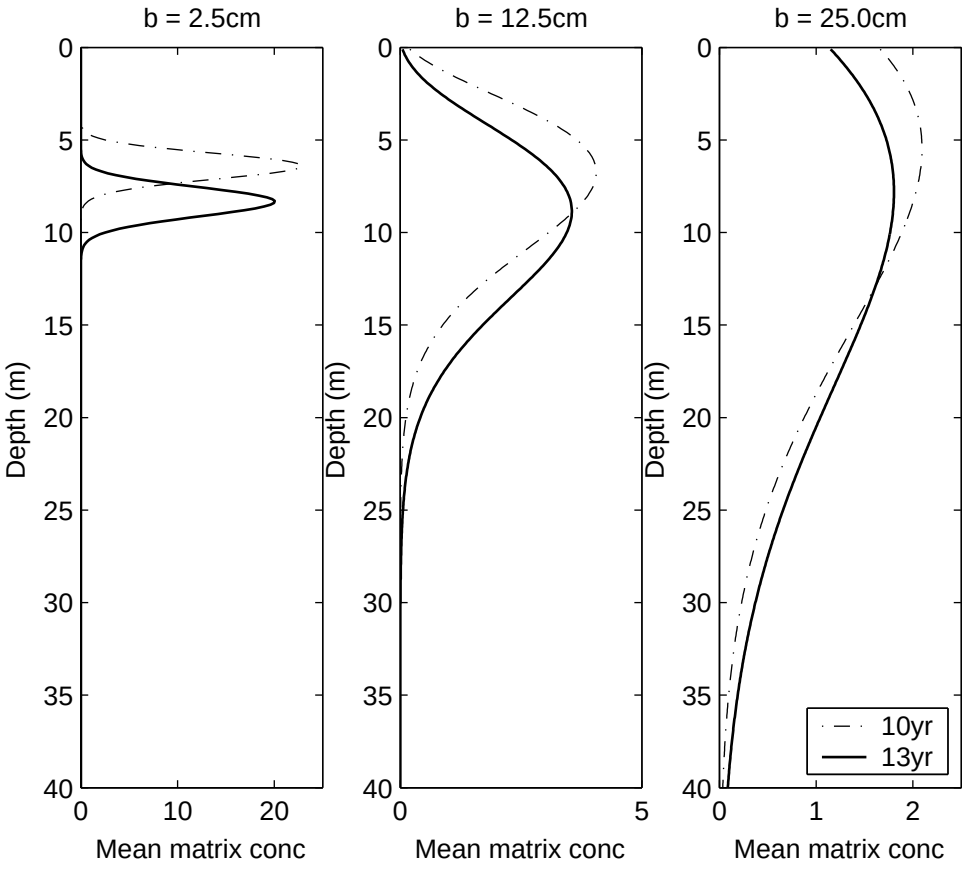

Figure 3.4 Matrix pore-water profiles generated from a dual-porosity model with $f(T) = \delta(T)$, $q_{re} = 0.25$ m/year, $D_A = 10^{-10}$ m^2/s, $a = 1$ mm, $\phi = 0.35$ after 10 and 13 years for matrix block half-widths, b as indicated in the subplot titles.

For the lower values of fracture spacings ($2b = 5$ cm) the profiles look very much like the tritium profiles presented in Figure 3.2. However, with fracture spacings greater than 50 cm, the extent of spreading within the profile is incompatible with the observed reality. While fracture spacings of 5 cm are probably common in the upper 3 m of the Chalk due to weathering, below 5 m depth at least the mid-range of the stated fracture spacings would be expected. Unless significant solute spreading of this kind is demonstrated in observed solute profiles, it is unlikely that equations (3.7) to (3.9) represent the system of interest with physically-consistent parameters.

3.4 Flow in the matrix

In order to provide an explanation for why the profiles simulated in Figure 3.4 are so unrealistic, it is useful to consider an alternative representation where longitudinal flow in the

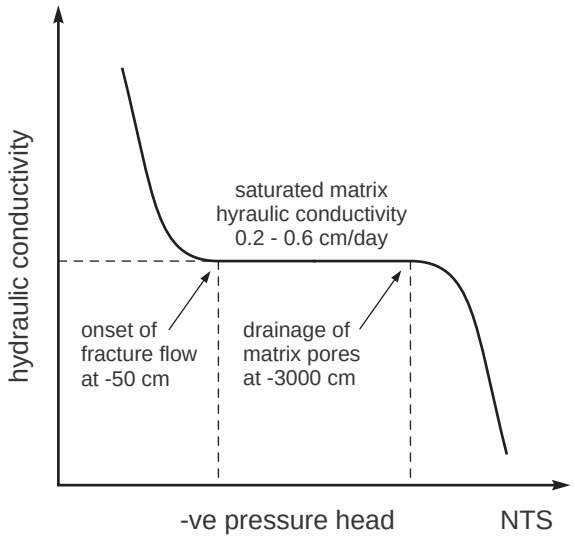

Figure 3.5 Conceptual diagram of a hydraulic conductivity curve for the Chalk

matrix is explicitly considered.

Wellings (1984a) presented measurements of hydraulic conductivity against pressure head down to a depth of 3 m from the unsaturated zone of the Upper Chalk at a site in southern England. The hydraulic conductivity remained almost constant around 0.2 to 0.6 cm/day and then appeared to increase asymptotically as the pressure heads exceeded -50 cm. These features are consistent with observations made at a number of other sites in the Chalk (*Cooper et al.*, 1990; *Hodnett and Bell*, 1990; *Mahamood-ul-Hassan and Gregory*, 2002). The rapid increase in hydraulic conductivity is associated with the onset of fracture flow, while the almost constant values are associated with the saturated hydraulic conductivity of the Chalk matrix. These findings are summarised in the conceptual hydraulic conductivity curve illustrated in Figure 3.5.

Mercury intrusion experiments carried out by *Price et al.* (1976) imply that the pore-throat diameters in the Chalk matrix are mostly less than 1 μm, suggesting that matrix pores are unlikely to drain for pressure heads greater than -30 m. This further implies that the Chalk matrix must be almost completely saturated throughout the unsaturated zone of the Chalk in the UK. Flow should therefore occur through the matrix blocks at a rate of up to its saturated hydraulic conductivity (0.2 to 0.6 cm/day). However, cutting through the matrix blocks are numerous near horizontal air phase discontinuities. In the unsaturated zone, these will remain mostly empty of water, allowing flow to take place only at points where matrix blocks make contact with each other (*Hodnett and Bell*, 1990; *Wang and Narasimhan*, 1985)

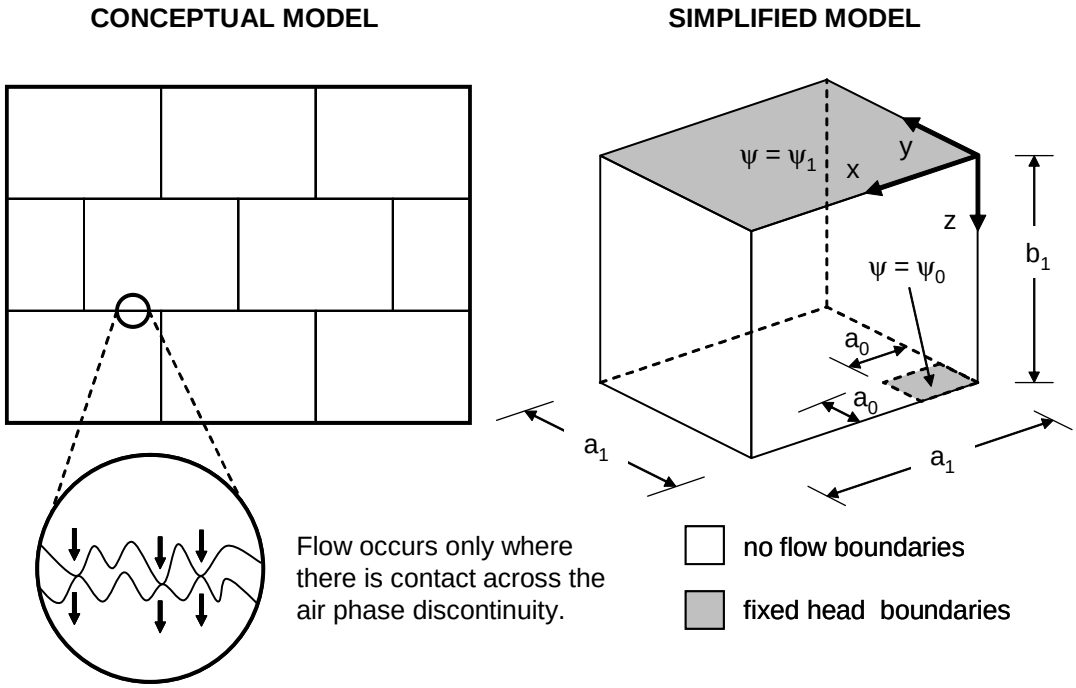

Figure 3.6 Conceptual model of flow across air phase discontinuities.

(see Figure 3.6). It is therefore important to consider how a pressure wave would be able to traverse such a discontinuity as would be required for the piston-displacement mechanism associated with matrix flow.

Hodnett and Bell (1990) suggest that as water flux increases, contact points wet up and therefore the hydraulic conductivity increases such that they do not form a restriction to flow. However, as these air phase discontinuities represent capillary barriers which may only be overcome once pressure heads exceed their air entry pressures (*Wellings and Bell*, 1980) it is arguable as to the extent of this effect. Because chalk blocks generally have rough surfaces (*Bloomfield*, 1996; *Price et al.*, 2000), this would suggest that for most of the time, even if inter-block films have developed, there will still only be partial connection between the matrix blocks. The issue therefore is the relationship between connectivity and its effect on inter-block conductance.

Because the Chalk matrix is likely to remain fully saturated throughout most of the unsaturated zone, if we assume that the matrix is homogenous and isotropic and flow is steady, the effect of inter-block connectivity on flow reduction can be meaningfully explored

using the three-dimensional Laplace equation

$$\frac{\partial^2\psi}{\partial x^2} + \frac{\partial^2\psi}{\partial y^2} + \frac{\partial^2\psi}{\partial z^2} = 0 \tag{3.18}$$

If all points of contact between the matrix blocks are assumed to be equally sized and equally spaced within an orthogonal grid that lies in the plane of the discontinuity we need only consider the quarter-block defined by the boundary conditions:

$$\begin{array}{llll}
\frac{\partial\psi}{\partial x} = 0, & x = 0, & y \geq 0, & z \geq 0; \\
\frac{\partial\psi}{\partial x} = 0, & x = a_1, & y \geq 0, & z \geq 0; \\
\frac{\partial\psi}{\partial y} = 0, & x \geq 0, & y = 0, & z \geq 0; \\
\frac{\partial\psi}{\partial y} = 0, & x \geq 0, & y = a_1, & z \geq 0; \\
\frac{\partial\psi}{\partial z} = 0, & x > a_0, & y \geq 0, & z = b_1; \\
\frac{\partial\psi}{\partial z} = 0, & 0 < x < a_0, & y > a_0, & z = b_1; \\
\psi = \psi_0, & 0 \leq x \leq a_0, & 0 \leq y \leq a_0, & z = b_1; \\
\psi = \psi_1, & x \geq 0, & y \geq 0, & z = 0.
\end{array} \tag{3.19}$$

where ψ is pressure head, x, y, z, a_0, a_1 and b_1 are as defined in the simplified model illustrated in Figure 3.6.

Hereafter connectivity will be defined as the ratio $(a_0/a_1)^2$. The quantity of interest for a corresponding connectivity is the reduction factor on the local rock hydraulic conductivity K_{eff}/K.

The total flow through the block can be found from

$$Q = -K \int_0^{a_1} \int_0^{a_1} \frac{d\psi}{dz} dxdy \tag{3.20}$$

where K is the pore-scale hydraulic conductivity.

The total flow can also be found from

$$Q = -K_{eff} \left(\frac{\psi_1 - \psi_0}{b_1} \right) a_1^2 \tag{3.21}$$

where K_{eff} is the block-scale hydraulic conductivity accounting for partial connection between underlying matrix blocks.

Equating equation (3.20) with equation (3.21) then yields the reduction factor on the local rock hydraulic conductivity

$$\frac{K_{eff}}{K} = \left(\frac{b_1}{\psi_1 - \psi_0} \right) \frac{1}{a_1^2} \int_0^{a_1} \int_0^{a_1} \frac{d\psi}{dz} dxdy \tag{3.22}$$

A three-dimensional contour visualisation from a typical simulation is shown in Figure 3.7, while the plotted variations of K_{eff}/K with $(a_0/a_1)^2$ for a range of aspect ratios b_1/a_1

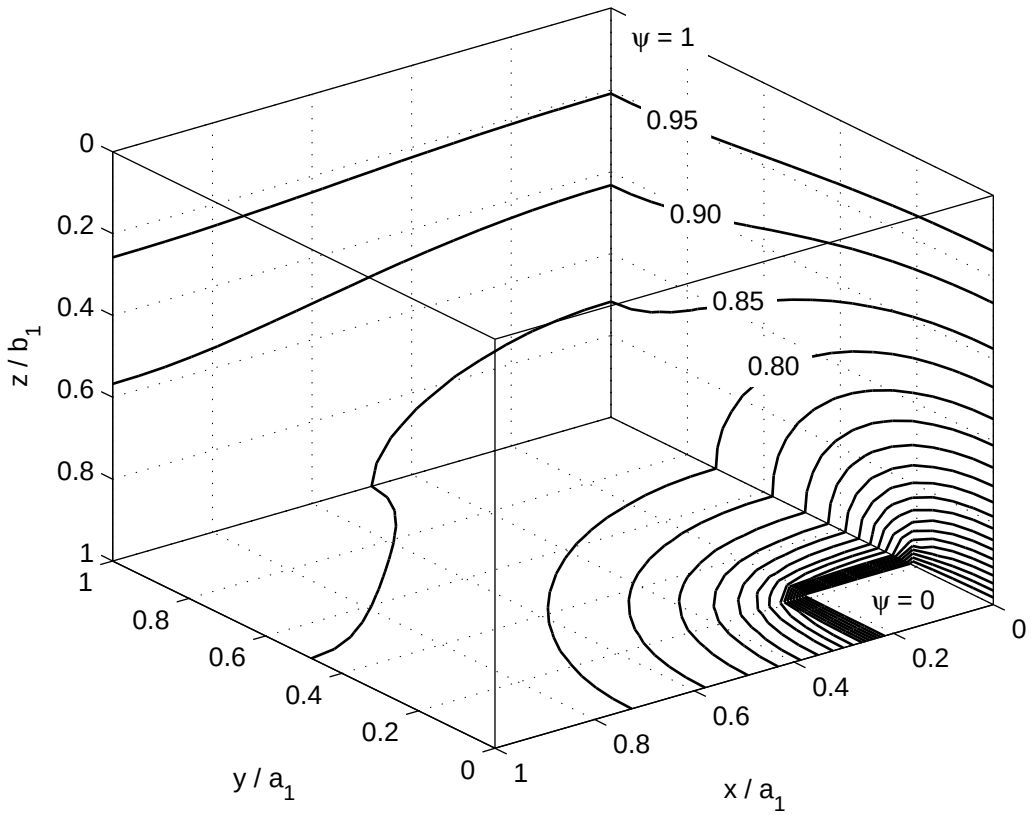

Figure 3.7 Contour plot showing pressure heads in a matrix block with $(a_0/a_1)^2 = 0.04$ and $b_1/a_1 = 1$.

are shown in Figure 3.8. These were obtained by solving equations (3.18) to (3.22) using finite difference discretisation and Gaussian elimination (see *Chapra and Canale*, 1998, p.812). It is of interest to note that, for small connectivities, the relationship of the effective and actual hydraulic conductivity approximates to a power law. Furthermore, the effect of connectivity diminishes with increasing aspect ratio.

In practice, the aspect ratio, b_1/a_1 is unlikely to be less than two as this would represent a matrix block where the contact spacing is equal to its depth. Figure 3.8 would therefore suggest that just 1% connectivity represents an effective pathway equivalent to at least 18% of the local rock hydraulic conductivity. *Pyrak-Nolte et al.* (1987) found that contact area within a single Stripa granite fracture ranged from 10% to 40% (depending on the effective stress). It can therefore be concluded that the piston-displacement mechanism will be only partially impeded by air-phase discontinuities.

It follows that an expression of steady state water mass balance for a fractured porous medium with dual-permeability (the term dual-permeability model being used to describe a

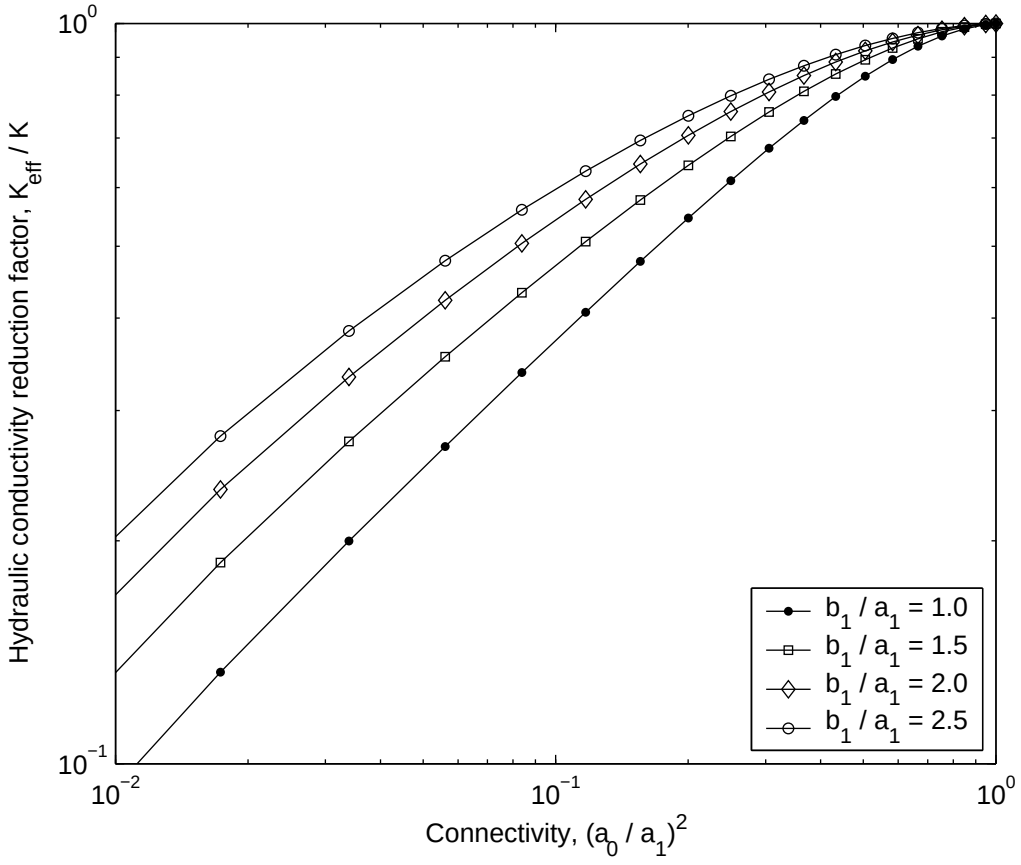

Figure 3.8 Plot of hydraulic conductivity reduction factor against connectivity for a range of aspect ratios.

dual-porosity model where a portion of flow occurs in the matrix) would be

$$bq_{re} = \phi b v_m + a v_f \quad \text{for} \quad q_{re} > \phi_m v_m \tag{3.23}$$

which can be rearranged to get

$$\beta \equiv \frac{v_m}{v_f} = \frac{1}{\sigma}\left(\frac{\phi v_m}{q_{re} - \phi v_m}\right) \tag{3.24}$$

where v_f and v_m are the pore-water velocities of the fractures and matrix respectively, q_{re} is the recharge and the ratio, β quantitatively represents the significance of flow in the matrix. By inspection, the significance of flow in the matrix will decrease with increasing q_{re}.

3.4.1 Further comment on the numerical scheme

To simplify the numerical scheme used to obtain Figure 3.8, a uniform space step was applied in all three dimensions. For suitable computation times, the matrix blocks were then discretised into $20 \times 20 \times (b_1/a_1)20$ nodes (the number of nodes in the vertical direction were

increased with increasing aspect ratio). Consequently, for very small connectivities, very few nodes were used to represent the contact point. In fact, to explore a connectivity of 0.02, the contact point was represented with a single node such that its flux distribution was assumed completely uniform.

Copson (1947) found that the flux distribution across a disk of unit potential with no external field is defined by (also described in *Sneddon*, 1966, p.72)

$$\frac{1}{\pi^2\sqrt{1-(\rho/a_0)^2}}, \quad r < a_0 \tag{3.25}$$

where a_0 is the radius of the disk and ρ is the distance from its origin. This essentially represents a laterally infinite matrix block with an infinite aspect ratio and only one circular point of contact of radius, a_0, to an underlying matrix block. Of interest is that the flux goes to infinity at the edge of the contact point suggesting that the majority of flow comes from its outer rim. In short, the distribution of flux across the point of connectivity is far from uniform.

The flux approaches infinity at the edge because all flow pathways originating from $\rho >> a_0$ hit the no-flow boundary at the base of the block and then travel near-horizontally to the contact point. Consequently, the horizontal hydraulic gradients at the edge of the contact point become exceptionally high (infinite in this case). In contrast, the flux near the centre of the contact point is much lower (zero at the absolute centre) because this region only collects near-vertical flow from the zone immediately above.

The effect of the coarse mesh used in our finite difference scheme would lead to a reduction in hydraulic gradients (and consequently flow) at the contact point edge because the pressure distribution in its close proximity is smoothed by the volume averaging. It therefore follows that block-scale hydraulic conductivities for blocks with small connectivities may be even larger than those presented in Figure 3.8.

3.5 The significance of flow in the matrix

To explore the significance of flow in the matrix we consider again the equations and assumptions presented by *Barker* (1982) but with a portion of vertical flow in the matrix. For mathematical tractability, it is assumed that concentrations in the matrix are fully mixed in the x direction (i.e. $dc_m/dx \rightarrow 0$). Furthermore, transfer of solutes between the fractures and the matrix is assumed to be linearly dependant on the concentration difference between the two domains. This approximation is often referred to as the quasi-steady-state (QSS) model (*Barker*, 1991).

Ignoring longitudinal dispersion, and assuming that fracture-matrix transfer conforms to the QSS model, the governing equations become

$$\frac{\partial c_f}{\partial t} + v_f \frac{\partial c_f}{\partial z} + \sigma \frac{\omega}{t_{cb}}(c_f - c_m) = 0 \tag{3.26}$$

and

$$\frac{\partial c_m}{\partial t} + \beta v_f \frac{\partial c_m}{\partial z} - \frac{\omega}{t_{cb}}(c_f - c_m) = 0 \tag{3.27}$$

where ω is a block geometry factor.

When there is flow in the matrix, the advective travel time is found from

$$t_a = \frac{L}{v_f} \frac{(1+\sigma)}{(1+\beta\sigma)} \tag{3.28}$$

and applying the relationships given in (3.6), the dimensionless problem can be written as

$$\frac{\partial c_f}{\partial T} + \frac{(1+\sigma)}{(1+\beta\sigma)} \frac{\partial c_f}{\partial Z} + \sigma\omega\gamma(c_f - c_m) = 0 \tag{3.29}$$

and

$$\frac{\partial c_m}{\partial T} + \beta \frac{(1+\sigma)}{(1+\beta\sigma)} \frac{\partial c_m}{\partial Z} - \omega\gamma(c_f - c_m) = 0 \tag{3.30}$$

The Laplace transform solution describing solute concentrations in the fracture under the boundary conditions

$$c_f(0,T) = c_m(0,T) = \delta(T), \quad \text{and} \quad c_f(\infty,T) = c_m(\infty,T) = 0 \tag{3.31}$$

and the initial condition

$$c_f(Z,0) = c_m(Z,0) = 0 \tag{3.32}$$

is

$$\begin{aligned} \hat{c}_f(Z,s) = \Bigg[& \exp\left(\frac{-Z}{2\beta} \frac{(1+\beta\sigma)}{(1+\sigma)} (A_1 - A_2^{1/2}) \right) \\ & + \exp\left(\frac{-Z}{2\beta} \frac{(1+\beta\sigma)}{(1+\sigma)} (A_1 + A_2^{1/2}) \right) \Bigg] \end{aligned} \tag{3.33}$$

where

$$A_1 = s(1+\beta) + \omega\gamma(1+\beta\sigma) \tag{3.34}$$

and

$$A_2 = (1+\beta\sigma)^2\omega\gamma^2 + 2\omega\gamma s(1-\beta\sigma)(1-\beta) + (1-\beta)^2 s^2 \tag{3.35}$$

When there is no longitudinal flow in the matrix, $\beta = 0$ and the solution reduces to equation (3.12) but with

$$\hat{\Lambda}(s) = \frac{\omega\gamma}{\omega\gamma + s} \tag{3.36}$$

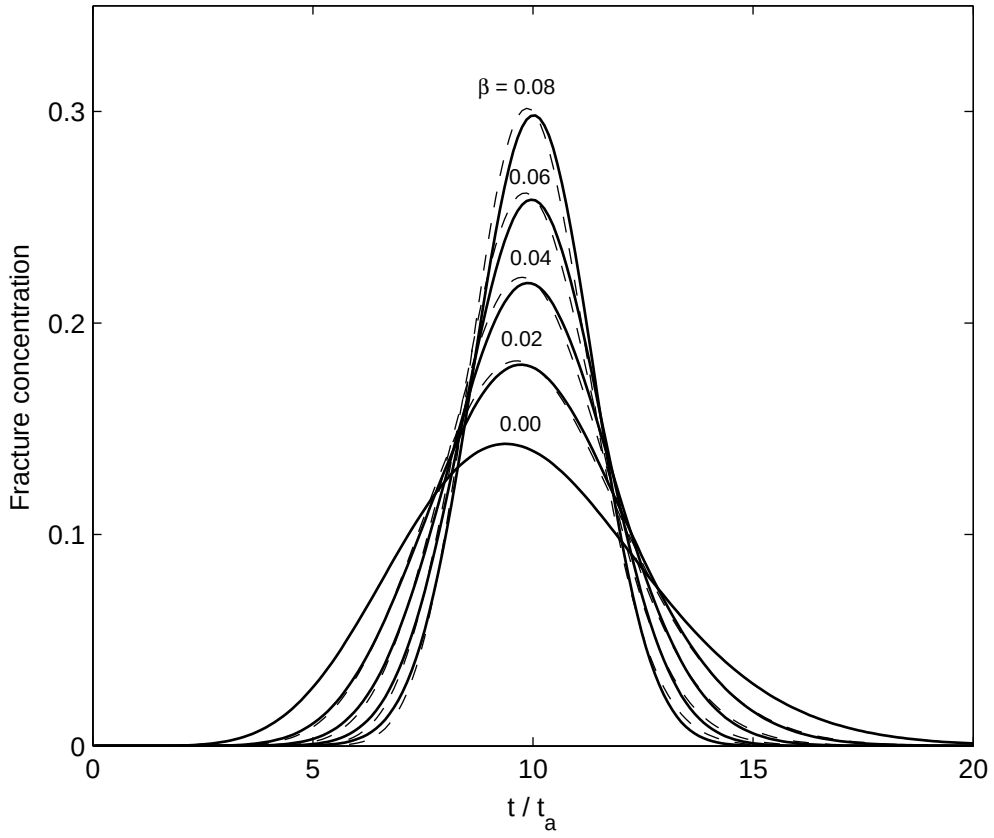

Figure 3.9 Breakthrough curves of dual-permeability models showing the effect of increasing the portion of flow in the matrix by varying the ratio $\beta = v_m/v_f$. Also shown in dashed lines are dual-porosity models using equivalent effective characteristic block diffusion times (t^*_{cb}) obtained from equation (3.46).

Figure 3.9 shows the sensitivity of breakthrough curves to β with $\sigma = 140$, $Z = 10$, $\omega = \pi^2/4$ (see Section 2.3) and $\gamma = 10$ (suggesting a slab-type matrix block with $t_a = t_{cb}$). As β increases, the spread of the breakthrough curve decreases, suggesting that solute concentrations in the fractures and the matrix are becoming closer to a local equilibrium. The reason is that as β approaches unity, the solutes in the matrix are moving at a more similar rate to those in the fracture. If $\beta = 1$, the breakthrough curve would simply translate the uncorrupted input function the distance dictated by the advective travel time.

Equations (3.12) and (3.36) can approximate any breakthrough curve (BTC) generated by (3.33) when the centroid and variance of the BTCs are matched. This can be achieved analytically as follows:

Absolute temporal moments (those about the origin) for a given function, $\eta(t)$ can be

obtained from

$$\mu'_m = \int_0^\infty t^m \eta(t) dt \tag{3.37}$$

Similarly, central moments (those about the mean) can be obtained from

$$\mu_m = \int_0^\infty (t - \mu'_1)^m \eta(t) dt \tag{3.38}$$

Providing these moments exist, the same absolute moments can be obtained from a function's Laplace transform using (*Aris*, 1958)

$$\mu'_m = (-1)^m \left[\frac{d^m}{ds^m} \hat{\eta}(s) \right]_{s=0} \tag{3.39}$$

By application of a binomial transform, the 2nd central moment can then be retrieved from (*Papoulis*, 1984, p.146)

$$\mu_2 = -{\mu'_1}^2 + \mu'_2 \tag{3.40}$$

Assuming that $f(T) = \delta(T)$, it can be shown that the moments of interest for equation (3.33) are

$$\mu'_1 = Z + \frac{Z}{\beta} \frac{(1 - \beta^2 \sigma)}{(1 + \sigma)} A_3 \tag{3.41}$$

$$\begin{aligned} \mu_2 = & \frac{2Z}{\omega\gamma} \frac{\sigma}{(1+\sigma)} \left(\frac{1-\beta}{1+\beta\sigma} \right)^2 (1 - A_3) \\ & + \frac{Z^2}{\beta^2(1+\beta\sigma)} \left(\frac{1+\beta^2\sigma}{1+\sigma} \right)^2 (A_3 - A_3^2) \\ & - \frac{2Z^2}{\beta} \left(\frac{1+\beta^2\sigma}{1+\sigma} \right) A_3 \end{aligned} \tag{3.42}$$

where

$$A_3 = \exp \left[\frac{-Z\omega\gamma}{\beta} \frac{(1+\beta\sigma)^2}{(1+\sigma)} \right] \tag{3.43}$$

which, when $A_3 \to 0$ reduce to

$$\mu'_1 = Z \quad \text{and} \quad \mu_2 = \frac{2Z}{\omega\gamma} \frac{\sigma}{(1+\sigma)} \left(\frac{1-\beta}{1+\beta\sigma} \right)^2 \tag{3.44}$$

The limits when $\beta \to 0$ further yield the moments for the dual-porosity model (equations 3.12 and 3.36) (compare *Valocchi*, 1985)

$$\mu'_1 = Z \quad \text{and} \quad \mu_2 = \frac{2Z}{\omega\gamma} \frac{\sigma}{(1+\sigma)} \tag{3.45}$$

Interestingly, the first moments, μ'_1, of both models are independent of D_A. This appears strange because intuitively we know that when $D_A = 0$ (i.e. $\gamma = 0$), the matrix pore-space is no longer connected to the fractures, and therefore μ'_1 should be equal to $Z(1 + \beta\sigma)/(1 + \sigma)$

for the dual-permeability model and $Z/(1+\sigma)$ for the dual-porosity model. However, this intuitive analysis is wrong. The first moments are independent of D_A because diffusion is a second-order process. When D_A is infinitesimally small, an infinitesimal part of solute will diffuse into the matrix. Because D_A is so small, it will then take an infinitely long time to come out. Consequently, this infinitesimal part of solute causes the variance and skewness of a breakthrough curve to increase such that its centroid remains at $\mu_1' = Z$ (this is further demonstrated using a Fickian model for matrix diffusion in Appendix B.4).

Equating the second central moments of the two models then gives the expression for an effective matrix block diffusion time t_{cb}^* which would be needed in a dual-porosity model (a model that ignores matrix flow) to simulate a BTC expected from an equivalent dual-permeability model (a model that incorporates matrix flow)

$$\frac{t_{cb}^*}{t_{cb}} = \left(\frac{1-\beta}{1+\beta\sigma}\right)^2 = \left(\phi_f \frac{\Delta v}{\overline{v}}\right)^2 \tag{3.46}$$

Note that

$$\frac{1-\beta}{1+\beta\sigma} = \frac{a(v_f - v_m)}{av_f + \phi b v_m} = \phi_f \frac{\Delta v}{\overline{v}} \tag{3.47}$$

where ϕ_f is the fracture porosity, Δv is the difference between the fracture and matrix velocities, and $\overline{v}$ is the composite mean velocity of the fractured porous medium.

BTCs derived from equations (3.12) and (3.36) using the correction factor in equation (3.46) are also presented in Figure 3.9 as dashed lines. It can be seen that the dual-porosity model can potentially approximate the dual-permeability model very well.

Equation (3.46) formalises the previous statement made about the effect of β on the equilibrium status between the fractures and matrix. When $\beta = 1$, $v_m = v_f$ and $t_{cb}^* = 0$ because the solute fronts in both the matrix and the fractures are moving at the same rate. When $\beta = 0$, $v_m = 0$ and $t_{cb}^* = t_{cb}$ because the system is appropriately described by a dual-porosity model. The intermediate behaviour can be understood by examination of Figure 3.10. It can be seen that the matrix flow velocity becomes more important with increasing matrix-fracture volumetric ratio, σ.

A physical explanation for equation (3.46) is that the dual-porosity model has to compensate for the extra longitudinal-flux in the matrix by increasing the diffusive-flux from the fractures. The increased diffusivity then results in a reduction in the time to equilibrium.

If we consider an annual recharge rate of 0.25 m/year, equation (3.24) yields a negative number because all the flow can easily be absorbed by the matrix. However, within the United Kingdom, daily rainfall can vary from 0 to over 10 cm/day, and this emphasises the need to explore these processes under a transient flow regime.

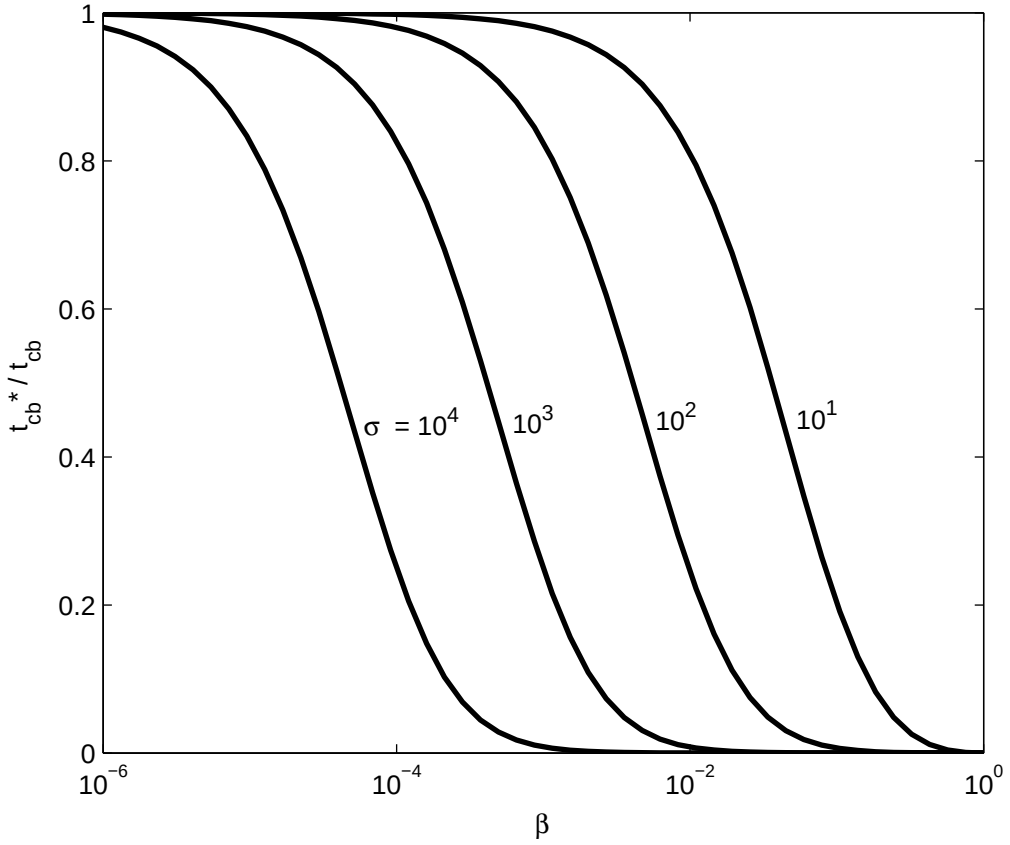

Figure 3.10 Plots of characteristic block diffusion time correction factor, t^*_{cb}/t_{cb} against β for a range of σ values as indicated by the labels.

Note that using t^*_{cb} implies that the Z axis has been transformed to one where water in the matrix appears stationary. As a result, the top boundary is essentially moving, with time, behind the origin of the transformed axis. This is not an issue when $c_f(0,T) = \delta(T)$ because the boundary position becomes irrelevant when $T > 0$. However, this would suggest that the expression in equation (3.46) is only valid for the instantaneous injection case (i.e. when $c_f(0,T) = \delta(T)$).

3.6 Conclusions

The respective contributions of flow in fractures and matrix to the behaviour of unsaturated Chalk has been the subject of much debate. Although many modelling studies cite the work of *Smith et al.* (1970) as a good reason for using a fracture flow bypass of around 15%, it has been shown that this work is unsatisfactory in at least four respects:

Firstly, the calculation of tritium input involved the assumption that actual evapotranspiration is the same as potential evaporation (albeit with an upper limit of soil moisture

deficit). This could potentially result in an underestimation of tritium input. Secondly, *Smith et al.* (1970) do not report any consideration of decay in their mass-balance calculation, which would result in an overestimation of tritium input. Thirdly, it assumes that all tritium that had travelled through fractures remained present in the unsaturated zone profile shown in Figure 3.1. In reality, very fast flowing tritium may have flowed through the unsaturated zone and into the saturated zone. Fourthly, the error associated with the measurements of tritium content were around $\pm 10\%$ while the values of tritium below 13m depth were only slightly elevated from values associated with background levels.

However, even if the analysis of *Smith et al.* (1970) was infallible, there is little evidence to suggest that the 15% bypass can be assumed to occur in Chalk outcrops elsewhere in the UK, as has been done in many previous conceptual models of the Chalk (e.g. *Oakes et al.*, 1981; *Rushton et al.*, 1989; *Ragab et al.*, 1997).

By contrast, the analysis of *Barker and Foster* (1981) presented results that indicated that a fracture flow dominant model could also explain the retardation of solute profiles in unsaturated Chalk through diffusive exchange between fractures and matrix. However, the consequence of ignoring matrix flow has been indicated in Figure 3.4. It is shown that an increase in fracture spacing results in an increase in solute spreading. The extent of solute spreading for a fracture spacing of just 25cm is incompatible with the well preserved peaks in solute profiles presented by *Smith et al.* (1970), *Young et al.* (1976), *Oakes* (1977), *Oakes et al.* (1981) and *Barraclough et al.* (1994).

The subject of how water can move through a matrix block, across an air phase discontinuity, and then into an underlying block has also been examined. As has been pointed out by *Wang and Narasimhan* (1985) and *Hodnett and Bell* (1990), these discontinuities are frequently interrupted by points of connectivity between matrix blocks. *Hodnett and Bell* (1990) suggest that as water flux increases the contact points wet up and the hydraulic conductivity increases such that they do not form a restriction to flow. However, these air phase discontinuities represent capillary barriers which may only be overcome once pressure heads exceed their air entry pressures. Furthermore, chalk blocks generally have rough surfaces suggesting that for most the time there will still only be partial connection between the matrix blocks. Nevertheless, a simple analysis of the Laplace equation has shown that just 1% connectivity represents an effective pathway equivalent to 18% of the local rock hydraulic conductivity.

The impact of flow in the matrix has been explicitly analysed by comparing a dual-porosity model and an equivalent dual-permeability model. It has been found that the dual-permeability breakthrough curves can be well approximated by the dual-porosity model with

a reduced characteristic block diffusion time. This is because as movement of water in the matrix reaches a similar velocity to water in the fractures, the two domains become closer to equilibrium with each another. Clearly, when there is no fracture flow, solute spreading is significantly reduced. However, this analysis shows that matrix flow reduces solute spreading in the presence of persistent fracture flow as well.

All the above studies suggest that flow in the matrix of the Chalk unsaturated zone is significant and that ignoring it may result in a serious misunderstanding of the system. However, the modelling analyses described in this article assume steady state flow conditions, necessitating the use of annual mean estimates of infiltration. This makes it difficult to sensibly estimate the proportion of total infiltration that enters the matrix. The assumption of steady state flow also forces fracture flow to be either negligible or persistent whereas in reality it is likely to be intermittent (*Price et al.*, 2000). More work is therefore needed to understand how the system works under transient flow conditions.

Chapter 4

Modelling flow in the Chalk unsaturated zone

4.1 Introduction

In the previous chapter, solute transport studies were limited to steady state flow regimes. The flow regime in the Chalk unsaturated zone is transient due to the episodic nature of infiltration. There is therefore a need to study solute transport under a transient flow regime which means we need a model that describes flow through a variably saturated fractured porous medium.

As discussed in Chapter 1, modelling flow in unsaturated fractured porous media has been extensively explored using Richards' equation (e.g. *Wang and Narasimhan*, 1985; *Kwicklis and Healey*, 1993; *Liu et al.*, 1998, 2003a,c). Such a methodology should be equally appropriate for the Chalk. This chapter concerns itself with how to parameterise the moisture retention and hydraulic conductivity relationships, associated with Richards' equation, for application to the Chalk.

In what follows, attempts to acquire data describing the Chalk unsaturated zone are reviewed. Different methods used to conceptualise and parameterise fracture continua in the literature are discussed. Parameters describing the Chalk matrix are obtained by considering pore-size distribution data. Parameters describing fractures in the Chalk are then obtained by calibration against some observed hydraulic conductivity data. Finally, parameter sensitivity is explored via a simple drainage simulation.

4.2 Studies of flow in the Chalk unsaturated zone

Wellings and Bell (1980) presented measurements of the annual cycle of changes in water content and potential in the 40 m thick unsaturated zone of the Upper Chalk at a site in southern England. They found that throughout the year, below 5 or 6 m into the unsaturated zone, pressure heads continually ranged between −50cm and −150 cm. Applying the capillary theory of *Marshall* (1959), *Wellings and Bell* (1980) calculated that almost no flow took place in the fractures throughout the year. This can be explained as follows:

Capillary theory dictates the pressure head, ψ_c that a cylindrical tube of radius (or the space between two parallel plates separated by a distance of) r will drain (*Massey*, 1995, p.24)

$$\psi_c = -\frac{2\kappa \cos(\Theta)}{\rho_w g r} \tag{4.1}$$

where ρ_w is fluid density, κ is surface tension and Θ is the angle between the fluid and solid surfaces (see Figure 4.1).

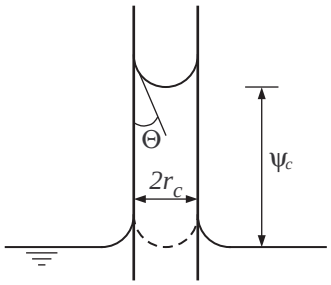

Figure 4.1 Schematic diagram of a capillary tube.

Capillary tube radii are often equated with soil-pore radii (e.g. *Hillel*, 1980) while distances of separation between two parallel plates are often equated with fracture apertures (*Wellings and Bell*, 1980; *Wang and Narasimhan*, 1985).

Foster (1975) suggested that typical fracture-apertures within the Chalk might vary between 0.1 and 1.0 mm. Taking $\Theta = 0$, $\kappa = 0.072$ kg/s^2, $\rho_w = 1000$ kg/m^3, $g = 9.8$ m/s^2, pressure heads greater than -14.7 cm are needed before such fractures can hold water. Hence the conclusion that fracture flow is unlikely to occur in the presence of pressure heads less than -50 cm (*Wellings and Bell*, 1980).

Wellings (1984a) presented measurements of unsaturated hydraulic conductivity against pressure head for the same site down to a depth of 3 m. The hydraulic conductivity remained almost constant around 0.2 to 0.6 cm/day and then appeared to increase dramatically as the pressure heads exceeded -50 cm. These features are consistent with observations made at a

number of other sites in the Chalk (*Cooper et al.*, 1990; *Hodnett and Bell*, 1990; *Mahamood-ul-Hassan and Gregory*, 2002). The dramatic rise is associated with the onset of fracture flow, while the almost constant values of hydraulic conductivity are associated with the saturated hydraulic conductivity of the Chalk matrix. The value of 0.2 to 0.6 cm/day is also consistent with the 3 mm/day calculated by *Hodnett and Bell* (1990) from intrinsic permeability data for a saturated laboratory sample of Chalk presented by *Price et al.* (1976).

Price et al. (1976) were particularly interested in the pore-size distribution of the Chalk matrix derived using a mercury intrusion technique (*Ritter and Drake*, 1945). *Price et al.* (1976) found that at least 95% of pores were smaller than 1 μm suggesting that the Chalk matrix would remain largely saturated until pressure heads dropped below -30 m.

These studies build a picture of the Chalk unsaturated zone whereby the entire water storage is immobile for pressure heads ranging between $-0.5 > \psi > -30$ m. For a 30 m deep unsaturated zone, even if enough time elapsed between infiltration events such that hydrostatic conditions were attained, the inter-granular pores of the Chalk matrix would never drain. In contrast, it is generally assumed that the fractures drain almost instantaneously with a fall in water table level. This gives rise to a close association of fracture porosity with specific yield (the fraction of the saturated bulk volume consisting of water which will drain by gravity when the water table drops). The specific yield in the Chalk is typically between 0.01 and 0.02 (*Price et al.*, 1993).

Assuming the above statement to be true, an estimate of 'apparent' change in groundwater storage (ACGS) can be obtained by determining the volume of Chalk in an interval between two potentiometric surfaces on various dates and multiplying it by an assumed value of specific yield (see Figure 4.2). *Lewis et al.* (1993) calculated the ACGS at two catchments situated in the outcrop of the Chalk in southern England during the drought periods of 1975, 1976, 1988 and 1989. They found that the ACGS was, consistently, at least an order of magnitude smaller than the estimates for baseflow volumes derived from catchment outlet data. The most likely explanation for the discrepancy was thought to be slow release of water by drainage of Chalk in the unsaturated zone. Calculations suggested that drainage of water equivalent to around 0.25-0.30% of the volume of rock in the unsaturated zone would be sufficient to account for the anomaly (*Lewis et al.*, 1993).

But if the fractures had drained completely and the matrix was never going to drain, it is difficult to understand where this extra water could have come from. From laboratory drainage (air-water capillary pressure) measurements, *Price et al.* (2000) found that more water drained from Chalk blocks with rougher surfaces, supported by the observance of

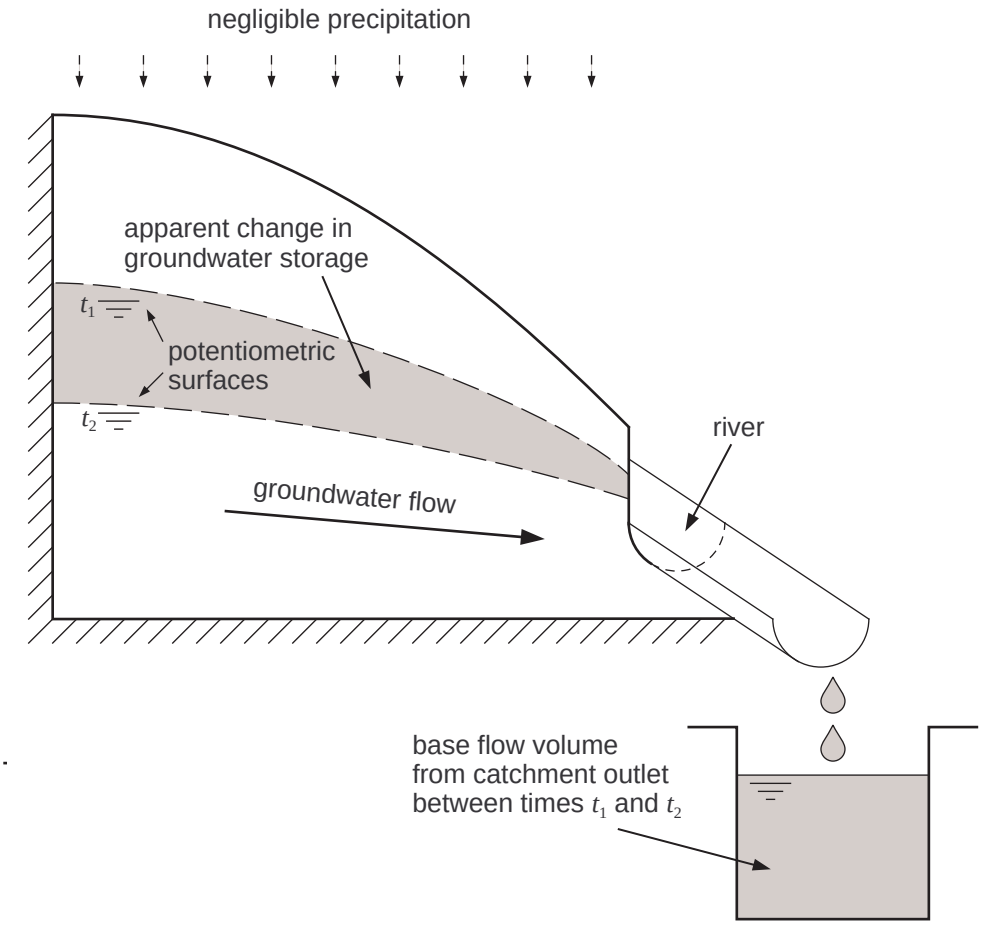

Figure 4.2 Schematic diagram illustrating the concept of equating apparent change in groundwater storage with base flow volumes during periods of negligible precipitation.

smaller blocks (hence larger surface areas) having larger specific yields. From this, *Price et al.* (2000) concluded that substantial storage of water could occur in the unsaturated zone within films generated on the surface irregularities of matrix blocks. It was suggested that as pressure heads increase, continuously larger depressions on a fracture face fill with water until the fracture becomes completely filled and fracture flow is initiated. Because the occurrence of completely filled fractures is rare, it follows that drainage of smaller depressions must be predominantly due to the suction of water into the matrix (matrix imbibition) followed by downward flow through the matrix. This concept is analogous to the fracture flow model suggested by *Wang and Narasimhan* (1985) discussed later in this chapter.

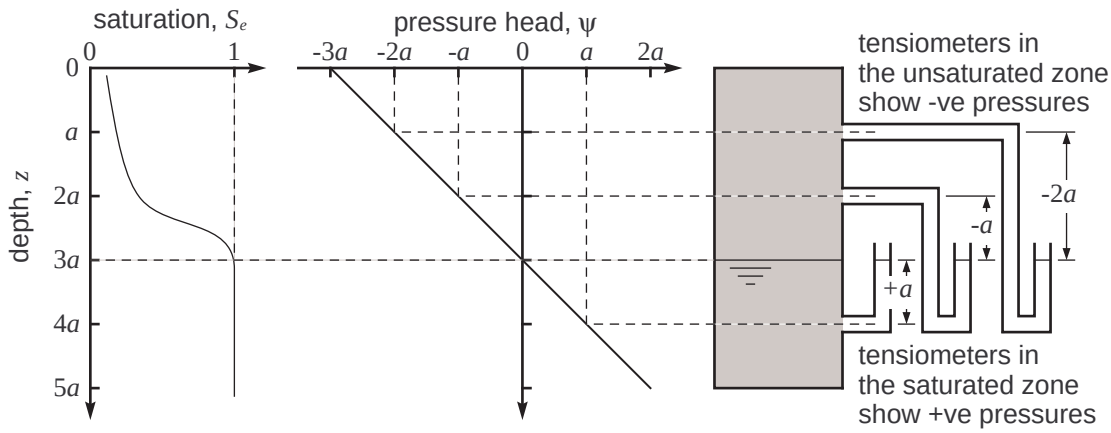

Figure 4.3 Schematic diagram illustrating the concept of a negative pressure head for a hydrostatic soil-column.

4.2.1 On the concept of negative pressure head

At the water-table, the water-pressure is zero (i.e. atmospheric). Below the water-table, the water-pressure is positive due to the weight of water above. Above the water-table, water can still be held within pores/fractures against the force of gravity due to surface tension. This manifests itself as negative water pressure (i.e. sub-atmospheric).

In the unsaturated zone, flow is governed by Darcy's Law, an occurs in response to a hydraulic head gradient as it is in the saturated zone (*Price et al.*, 1993). Hydraulic head, h is related to pressure head, ψ and depth, z through

$$h = \psi - z \tag{4.2}$$

Consider a porous formation where enough time has elapsed without precipitation such that the system has become hydrostatic. Such a system has a uniform hydraulic gradient of $dh/dz = 0$. From equation (4.2) it follows that the pressure gradient will be $d\psi/dz = 1$. Given that the pressure at the water-table is zero, if the depth of water-table is $3a$, the pressure head at the ground surface will be $-3a$ (see Figure 4.3).

For more information on this subject see *Marshall and Holmes* (1979) or *Hillel* (1980).

4.3 A model of unsaturated flow for the Chalk

One-dimensional flow through a partially saturated, single porous medium can be described by (*Richards*, 1931)

$$\frac{\partial \theta}{\partial t} = C\frac{\partial \psi}{\partial t} = \frac{\partial}{\partial z}\left[K\left(\frac{\partial \psi}{\partial z} - 1\right)\right] \tag{4.3}$$

where $\theta(\psi)$ is moisture content, $C(\psi)$ is specific capacity, $K(\psi)$ is hydraulic conductivity, t is time, z is depth and ψ is pressure head.

Modelling unsaturated flow in the Chalk is further complicated by the presence of fractures. Fractured porous media, where fast flow occurs in the fractures and much slower flow occurs in the matrix, is often modelled using dual-permeability models (e.g. *Gerke and van Genuchten*, 1993b; *Doughty*, 1999). However, the Chalk (in the UK) presents a special characteristic that allows flow to be adequately modelled, under certain circumstances, using only a single-permeability model (such as that stated in equation 4.3) as discussed below.

Because the Chalk matrix can generally be assumed constantly saturated, an estimate of the time taken for pressures in the fractures to equilibrate with pressures in the matrix can be found from (*Barker*, 1993)

$$t_{cb} = b^2\frac{S_s}{K} \tag{4.4}$$

where b is the matrix block half-width and S_s is the specific storage (*de Marsily*, 1986, p. 108)

$$S_s = \rho_w g(\gamma_1 + \phi\gamma_2) \tag{4.5}$$

with γ_1 being the rock compressibility and γ_2, the compressibility of water (around $5 \times 10^{-10}\text{Pa}^{-1}$).

The compressibility of rock can be related to more commonly measured material properties using (*Ross*, 1996, p.69)

$$\gamma_1 = \frac{3(1-2\epsilon)}{E} \tag{4.6}$$

where E is Young's modulus and ϵ is Poisson's ratio. *Bell et al.* (1990) obtained core scale values for Lower, Middle and Upper Chalk at sites in Yorkshire, Norfolk and Kent. Young's modulus values ranged between $10^9 < E < 10^{10}$ Pa while Poisson's ratios ranged between $0.2 < \epsilon < 0.4$. This gives a compressibility range of $10^{-11} < \gamma_1 < 10^{-9}$ Pa^{-1}. The specific storage of the Chalk matrix must therefore range between $10^{-6} < S_s < 10^{-5}$ m^{-1}. It follows that the time to equilibrium $t_{cb} < 10^{-2}$ days.

Under such conditions, when dealing with time steps $> 10^{-2}$ days, it is appropriate to assume that pressures in the matrix and the fractures are in local equilibrium such that only

one pressure field need be considered. This allows bulk properties for use in equation (4.3) to be obtained from (*Peters and Klavetter*, 1988)

$$\theta = \theta_f + \theta_m; \quad C = C_f + C_m; \quad K = K_f + K_m \tag{4.7}$$

where the subscripts f and m denote properties of the fracture and matrix continua respectively.

4.4 Effective saturation and relative permeability

The rates at which moisture content and hydraulic conductivity decrease with pressure head are often summarised by effective saturation, S_e and relative permeability, k_r functions:

$$S_e = \frac{\theta - \theta_r}{\theta_s - \theta_r}; \quad k_r = \frac{K}{K_s} \tag{4.8}$$

where θ, θ_r and θ_s are the actual, residual and saturated moisture contents and K and K_s are the actual and saturated hydraulic conductivities.

Effective saturation can be related to a pore-size distribution, $f(r)$ as follows (*Wang and Narasimhan*, 1985)

$$S_e(R) = \frac{\int_{R_{min}}^{R} r f(r) dr}{\int_{R_{min}}^{R_{max}} r f(r) dr} \tag{4.9}$$

where R is the radius of the largest pore that contains water at a given pressure head.

Permeability is often related to pore-size by the Poiseuille equation for steady, laminar flow through a smooth capillary tube of radius r (see *Massey*, 1995, p.157)

$$Q = -\frac{\pi r^4}{8} \frac{g}{\nu} J \tag{4.10}$$

where J is the hydraulic gradient and ν is now the kinematic viscosity.

If we now consider a block of cross-sectional area W^2 containing n number of identical tubes, the flow per unit area of medium can be found from $q = -kgJ/\nu$ where $k = \epsilon r^2/8$ is the intrinsic permeability and $\epsilon = \theta_s - \theta_r = n\pi r^2/W^2$ is the hydraulically significant porosity.

For a porous media containing a random distribution of different sized capillary tubes an expression of relative permeability k_r would take the form (*Wang and Narasimhan*, 1985)

$$k_r = \tau(R) \frac{\int_{R_{min}}^{R} r^3 f(r) dr}{\int_{R_{min}}^{R_{max}} r^3 f(r) dr} \tag{4.11}$$

where $\tau < 1$ is a tortuosity factor. If $\tau = 1$, this would imply that all the tubes were perfectly smooth and parallel.

It is common to assume that τ is a power function of S_e (e.g. *Mualem*, 1976; *Burdine*, 1953). Rewriting equation (4.11) in terms of S_e (recall equation 4.9) yields (*Burdine*, 1953)

$$k_r = S_e^{\eta} \frac{\int_0^{S_e} r^2 dS_e}{\int_0^1 r^2 dS_e} = S_e^{\eta} \frac{\int_0^{S_e} \psi^{-2} dS_e}{\int_0^1 \psi^{-2} dS_e} \tag{4.12}$$

where $\eta \geq 0$ is an exponent to describe the tortuosity factor.

Mualem (1976) set out to obtain a more tractable expression of relative permeability. Consider two capillary tubes of radii r and ρ and lengths l_1 and l_2 respectively. Under steady and laminar conditions, flow in the two tubes can be described by equation (4.10). If both tubes lie in series, flow through the two tubes can be adequately represented by an equivalent tube of radius R and length L. Providing that the lengths of the tubes are proportional to the radii (i.e. $l_1/l_2 = r/\rho$) it can be shown that $R^2 = r\rho$ (see section 4.4.1 and Figure 4.4).

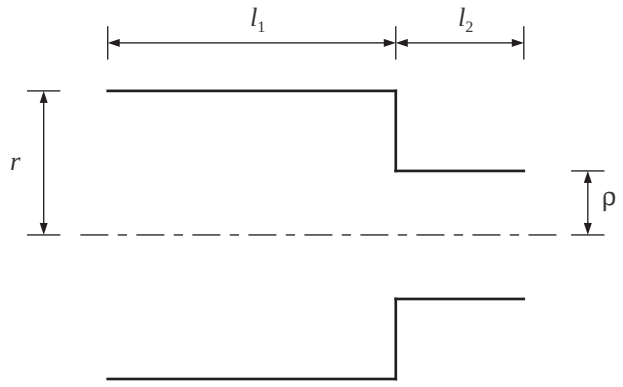

Figure 4.4 Schematic diagram of Mualem's tubes.

Mualem (1976) then considers a porous slab of thickness, Δx ($x \rightarrow x + \Delta x$ along the axis) where Δx is a similar order of magnitude as the pore-radii. The probability of pores of radii $r \rightarrow r + dr$ at x connecting with pores of radii $\rho \rightarrow \rho + d\rho$ at $x + \Delta x$ can then be described by (*Mualem*, 1976)

$$a(r, \rho) = G(R, r, \rho) r f(r) \rho f(\rho) dr d\rho \tag{4.13}$$

where $G(R, r, \rho)$ is a correction factor accounting for partial correlation between pores r and ρ at a given effective saturation $S_e(R)$.

Applying an additional correction factor $T(R, r, \rho) < 1$ to account for the eccentricity of the flow path, the contribution of the $r \rightarrow \rho$ element to the relative permeability, k_r is found from (*Mualem*, 1976)

$$dk_r(r, \rho) = \frac{T(R, r, \rho) r \rho G(R, r, \rho) r f(r) \rho f(\rho) dr d\rho}{\int_{R_{min}}^{R_{max}} \int_{R_{min}}^{R_{max}} T(R_{max}, r, \rho) r \rho G(R_{max}, r, \rho) r f(r) \rho f(\rho) dr d\rho} \tag{4.14}$$

Mualem (1976) then assumes that the correlation and eccentricity correction factors are power functions of S_e, thus depending solely on R. Re-writing equation (4.14) in terms of S_e then yields (*Mualem*, 1976)

$$k_r(S_e) = S_e^{\eta}\left[\frac{\int_0^{S_e} r dS_e}{\int_0^1 r dS_e}\right]^2 = S_e^{\eta}\left[\frac{\int_0^{S_e} \psi^{-1} dS_e}{\int_0^1 \psi^{-1} dS_e}\right]^2 \tag{4.15}$$

The *Mualem* (1976) model is easier to apply than the *Burdine* (1953) model because it involves integrating $\psi(S_e)$ as opposed to $\psi^2(S_e)$. A more general expression for relative permeability proposed by *Hoffmann-Reim et al.* (1999) is

$$k_r(S_e) = S_e^{\eta}\left[\frac{\int_0^{S_e} \psi^{-m_1} dS_e}{\int_0^1 \psi^{-m_1} dS_e}\right]_2^m \tag{4.16}$$

where $m_1 = 2$ and $m_2 = 1$ yields the *Burdine* (1953) model, $m_1 = 1$ and $m_2 = 2$ yields the *Mualem* (1976) model while $m_1 = 0$ and $m_2 = 0$ yields a more simple model:

$$k_r = S_e^{\eta} \tag{4.17}$$

known as the Kozeny model (*Brutsaert*, 1967).

A commonly used effective saturation function is that of *Brooks and Corey* (1966)

$$S_e = \begin{cases} (r/r_s)^{\lambda}, & r < r_s \\ 1, & r \geq r_s \end{cases} = \begin{cases} (\psi_s/\psi)^{\lambda}, & \psi < \psi_s \\ 1, & \psi \geq \psi_s \end{cases} \tag{4.18}$$

where λ is an exponent that describes the variation of a pore-size distribution, r_s is the radius of the largest sized pore and ψ_s is its air entry pressure (found from equation 4.1).

The corresponding relative permeability function using the *Burdine* (1953) model is

$$k_r = S_e^{\eta+1+2/\lambda} \tag{4.19}$$

and using the *Mualem* (1976) model is

$$k_r = S_e^{\eta+2+2/\lambda} \tag{4.20}$$

Some researchers dislike the *Brooks and Corey* (1966) function because of the discontinuity at $\psi = \psi_s$. *van Genuchten* (1980) suggested an alternative function that avoids this

$$S_e = \left[\frac{1}{1+|\alpha\psi|^n}\right]^m \quad (m = 1 - 1/n) \tag{4.21}$$

where α and n are empirical parameters obtained from calibration against observed moisture content data.

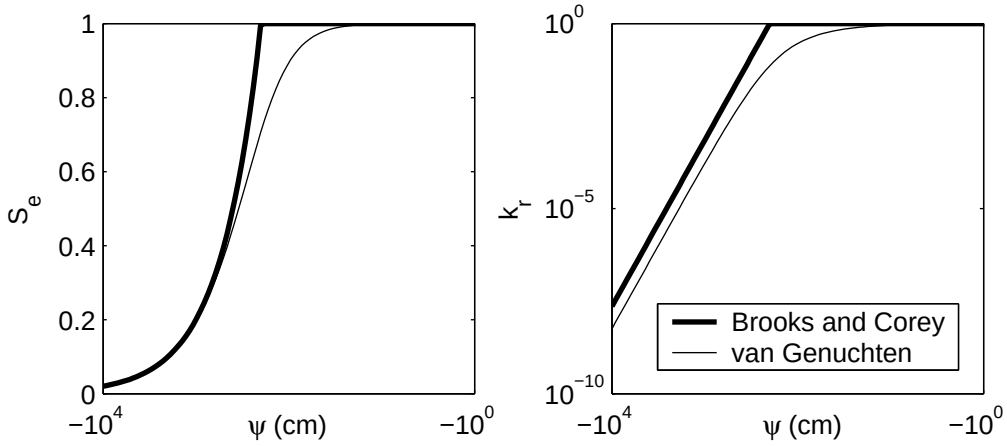

Figure 4.5 Comparison of the *Brooks and Corey* (1966) and *van Genuchten* (1980) models in conjunction with the *Mualem* (1976) model where $\alpha = 0.005$ cm^{-1}, $n = 2$, $\psi_s = -200$ cm, $\lambda = 1$ and $\eta = 0.5$.

The *Burdine* (1953) model can only be applied to the *van Genuchten* (1980) function when $m = 1 - 2/n$ whereas the *Mualem* (1976) model can be applied for a broader variety of different m relationships. When $m = 1 - 1/n$, the *Mualem* (1976) model yields the relative permeability function

$$k_r = S_e^{\eta}[1 - (1 - S_e^{1/m})^m]^2 \tag{4.22}$$

It can be seen that for large values of negative ψ, equation (4.21) reduces to (4.18) when $\psi_s = -1/\alpha$ and $\lambda = mn$ (*van Genuchten*, 1980). A comparison of the two models is presented in Figure 4.5. Although the *van Genuchten* (1980) model avoids the discontinuity at $\psi = \psi_s$, a drawback is that α and n have a strong cross-correlation making them difficult to identify when calibrating to observed data.

When using equation (4.15) it is often assumed *a priori* that $\eta = 0.5$ because *Mualem* (1976) found it was an optimum value for a data set of 45 disturbed and undisturbed samples. The sensitivity of relative permeability to the η parameter is illustrated in Figure 4.6. Higher η values yield lower permeabilities at low pressure heads which implies a more tortuous flow pathway. Note that when using the *Brooks and Corey* (1966) function, the exponent in the *Burdine* (1953) relative permeability function is less than in the *Mualem* (1976) function (see equations 4.19 and 4.20). This is because the *Burdine* (1953) model assumes a system of parallel capillary tubes which is less tortuous than the system of tubes in series assumed by *Mualem* (1976).

More recently, a study by *Schaap and Leij* (2000) on 235 soil samples has shown that there is no benefit in setting $\eta = 0.5$ and much better results can be obtained by calibrating it to

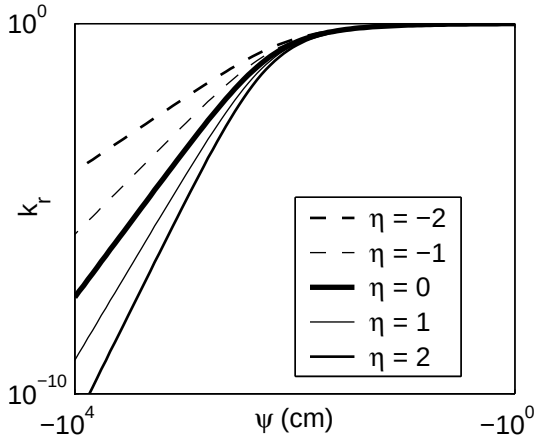

Figure 4.6 An illustration of the sensitivity of relative permeability to the tortuosity parameter, η.

observed hydraulic conductivity data. Furthermore, *Schaap and Leij* (2000) often found that negative values of η (which would suggest an 'anti tortuosity') achieved better objective function values. *Schaap and Leij* (2000) concluded that this ultimately suggests that the models proposed by *Mualem* (1976) and *Burdine* (1953) are overly simplified conceptualisations.

4.4.1 On Mualem's equivalent radius

Consider two tubes of radii r and ρ and length l_1 and l_2 with head losses of Δh_1 and Δh_2 respectively. If flow is laminar and steady, flow in the tubes is described by the Poiseuille equation (recall equation 4.10). If the two tubes lie in series, their composite response can be represented by an equivalent tube of radius, R and length L.

From flow continuity we have

$$R^4 \frac{(\Delta h_1 + \Delta h_2)}{L} = r^4 \frac{\Delta h_1}{l_1} = \rho^4 \frac{\Delta h_2}{l_2} \tag{4.23}$$

From volume equivalency we have

$$L = \frac{r^2 l_1 + \rho^2 l_2}{R^2} \tag{4.24}$$

Substituting equation (4.24) into (4.23) and solving for R we then get

$$R^6 = \rho^4 r^4 \left(\frac{r^2 l_1 + \rho^2 l_2}{r^4 l_2 + \rho^4 l_1} \right) \tag{4.25}$$

Mualem (1976) assumes that lengths of tubes are proportional to their radii (i.e. $l_1/l_2 = r/\rho$) such that equation (4.25) reduces to

$$R^2 = \rho r \tag{4.26}$$

4.5 Applicability of capillary theory to fracture flow

Natural fractures are characterised by rough surfaces, suggesting that fracture-apertures become very small near asperities (points where the two fracture faces meet). From consideration of equation (4.1), as fluid pressure decreases, portions of the fracture continuum with continuously smaller apertures will drain (analogous to the drainage of surface irregularities suggested by *Price et al.*, 2000) (see Figure 4.7). Consequently, *Wang and Narasimhan* (1985) suggest that an S_e function for a fracture continuum can be obtained by consideration of its aperture distribution (via equation 4.9).

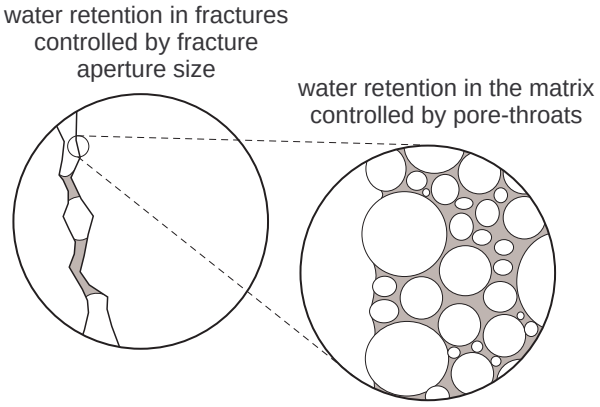

Figure 4.7 Conceptual model of water retention in a fractured porous medium.

Pruess and Tsang (1990) developed a numerical model to describe unsaturated flow through a single rough walled fracture. The model consisted of an array of elements each assigned a different fracture-aperture by a random model. The random model assumed a log-normal distribution of fracture-apertures based on empirical observations made by *Gentier* (1986). Each element was then assigned an air-entry pressure and a hydraulic conductivity by considerations of capillary theory and the cubic law (discussed later in this section). If the local pressure at a given element was greater than its air entry pressure, the element was considered fully saturated and flow through the element was defined by Darcy's law using its assigned hydraulic conductivity. If the local pressure was less than the air entry pressure, the element was assumed empty and impermeable to flow.

From a series of steady state simulations with a range of fixed head boundaries, *Pruess and Tsang* (1990) obtained a data set of moisture content with corresponding pressure head that described the averaged characteristics of the fracture domain as a whole. An analytical S_e function was then obtained by application of equation (4.9) to the log-normal distribution

function which provided a very accurate correspondence with the observed numerical data.

Kwicklis and Healey (1993) were interested in obtaining analytical relative permeability functions that could describe numerical experiments similar to *Pruess and Tsang* (1990) using the *Mualem* (1976) model.

Permeability is often related to fracture-apertures by the cubic law (*Snow*, 1968; *Wang and Narasimhan*, 1985; *Barker*, 1993; *Bloomfield*, 1996). The origins of this law lies in the governing equation of steady, laminar flow through a smooth, planar fracture of aperture r and width W (see *Massey*, 1995, p.163)

$$Q = -\frac{Wr^3}{12}\frac{g}{\nu}J \tag{4.27}$$

where J is the hydraulic gradient.

If a block of cross-sectional area W^2 contains n number of identical fractures of aperture r, then the flow per unit area of media is $q = -kgJ/\nu$ where $k = \epsilon r^2/12$ is the intrinsic permeability and $\epsilon = \theta_s - \theta_r = nr/W$ is the hydraulically active porosity. These results are almost identical to those derived from the Poiseuille equation. Inspection of the derivations of *Burdine* (1953) and *Mualem* (1976) models for pore-size distributions would suggest that they are also applicable to fracture-aperture distributions.

The problem with the S_e function derived by *Pruess and Tsang* (1990) is that it contained a complementary error function (erfc), rendering the *Mualem* (1976) model intractable. However, *Kwicklis and Healey* (1993) realised that the *van Genuchten* (1980) function behaves in a similar way to an erfc function. They then performed a series of more detailed simulations analogous to *Pruess and Tsang* (1990) and calibrated the *van Genuchten* (1980) function to the model output. It was found that the Mualem model, with the *a priori* calibrated van Genuchten parameters (against the analytically derived erfc function), yielded good correspondence with the relative hydraulic conductivity obtained from the detailed fracture model.

All the above studies assume that a rough-surfaced fracture can be adequately described by a single averaged value of aperture in conjunction with the cubic law. *Brown et al.* (1995) compared predictions using the Reynolds equation (analogous to the cubic law) with a more rigourous Navier-Stokes flow model for a two-dimensional channel constructed with an idealised sinusoidal roughness on each wall. The Reynolds equation was found to overestimate fluid velocity as the amplitude of surface roughness increased relative to its wavelength. This would suggest that cubic law-based relative permeability models overestimate the drop in permeability with decreasing pressure. Hence they need an 'anti tortuosity' factor if they are to mimic reality as was observed in soils by *Schaap and Leij* (2000).

However, providing that an effective saturation function is a power function of pressure head, it seems sensible to assume that relative permeability will be a power function as well (see equations 4.19 and 4.20). Consequently, we will use the Kozeny model (equation 4.17) to characterise the relative permeability of the Chalk where η is treated as an empirical parameter to be calibrated against field data.

Laboratory and field studies have demonstrated that flow proceeds along localised preferential flow paths, or fingers, through unsaturated fractures (e.g. *Nicholl et al.*, 1994; *Su et al.*, 1999; *Dahan et al.*, 1999). Furthermore, these flow paths are highly unstable, even under steady infiltration scenarios (*Nicholl et al.*, 1994; *Su et al.*, 1999). While it is acknowledged that the capillary theory models are unable to represent this behaviour (e.g. *Glass et al.*, 1995; *Liu et al.*, 1998; *Pruess*, 1999), none of these experiments have offered data sufficient to parameterise a reasonable alternative.

Bertels et al. (2003) performed a heavily simplified laboratory experiment analogous to the numerical experiments of *Pruess and Tsang* (1990) and *Kwicklis and Healey* (1993). An artificial fracture was induced along a 120 mm long cylindrical basalt core of 70 mm diameter. High-resolution measurements of aperture distribution were then obtained using a computed tomography technique. The distribution was found to be positively skewed and bi-modal. Of particular concern is that the effective saturation and relative permeability relationships with pressure head were non-monotonic. However, representing unsaturated flow using conventional monotonic capillary theory is the obvious route to explore (*Liu et al.*, 1998, 2003a,c).

4.6 Characterising the matrix

Characterising the Chalk matrix is relatively straightforward. Mercury intrusion curves can be converted to effective saturation curves by $S_e = 1 - V/100$ where V is volume of mercury intrusion as a % of pore volume (*Wellings and Bell*, 1980). *Price et al.* (2000) obtained mercury intrusion curves for Chalk cores of approximately 9 mm diameter from Cherry Hinton Quarry, near Cambridge (CH2 and CH3), Play Hatch Quarry, near Reading (PH6) and Shoreham Cement Works Quarry (SH3). These are presented in Figure 4.8.

Mercury intrusion tests (MIT) rely on the phenomena that a non-wetting fluid will not invade a pore-throat unless the fluid is pressurised, and that the size of the pore-throat or capillary that is invaded is inversely proportional to the capillary pressure. As pressure is increased, successively smaller pore-throats will be invaded by the non-wetting phase.

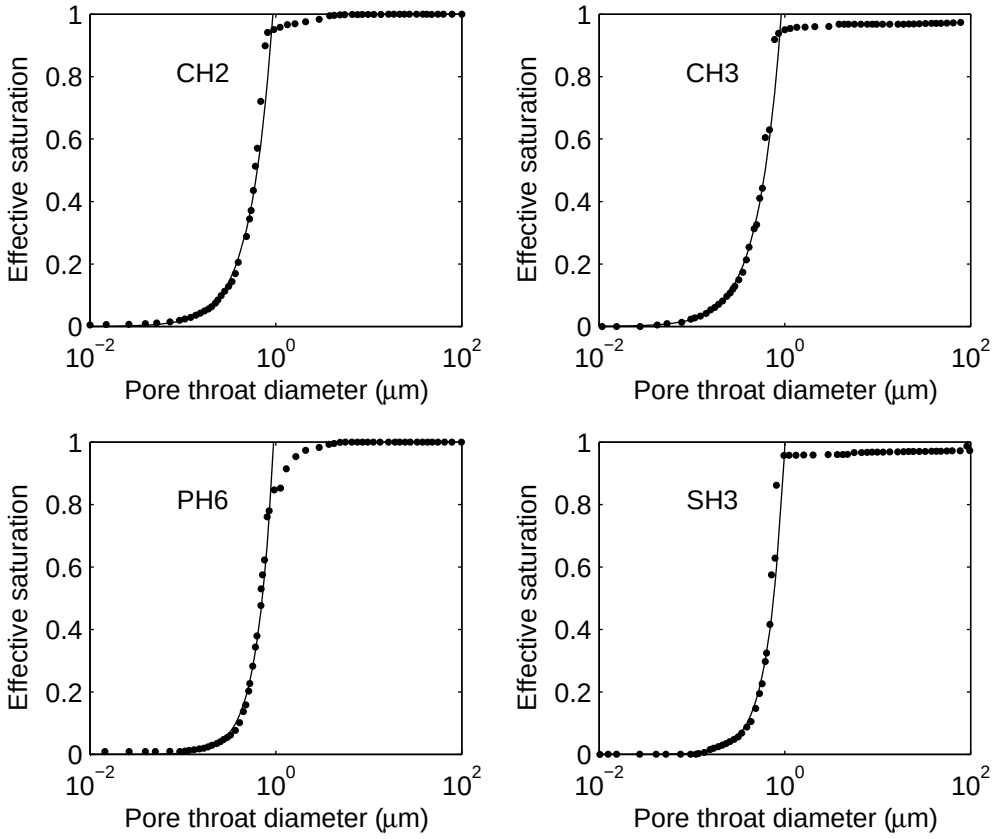

Figure 4.8 Effective saturation curves derived from mercury intrusion curves for samples of Chalk obtained by *Price et al.* (2000). The dots represent the observed data and the solid lines represent the calibrated S_e functions.

Gooddy (2003) describes the MIT as follows: A sample is placed in a glass vial, placed under a vacuum, and the annulus between the wall of the vial and the sample is filled with mercury. At this stage no mercury has entered the sample as the mercury is non-wetting with respect to the sample. The mercury is then pressurised hydrostatically in a series of steps, and the amount of mercury intruded into the sample at each pressure step is recorded. Once intrusion is complete the fractional pore volume intruded at each pressure step can be calculated using the total intruded volume.

A disadvantage of the MIT is that it tends not to recognise the larger pore-sizes present because the large pores cannot fill until they are connected by a continuous or percolated pathway. These are generally controlled by the smaller pores, or pore-throats. However, while MIT will not obtain a true pore-size distribution, it does indicate the accessibility of the overall porosity as a function of pore-size (*Winslow et al.*, 1994) which is arguably the quantity of interest when developing an S_e function for an unsaturated flow model.

By inspection, it can be seen that for pore-throats smaller than 1 μm diameter, the pore-

throat distributions are well approximated by a power law lending themselves well to the *Brooks and Corey* (1966) model (equation 4.18). The low negative pressure 'tails' present for pore-throats greater than 1 μm diameter, is associated with the filling of irregularities on the chalk sample surfaces (*Price et al.*, 2000). In the oil industry this is known as conformance (*Vavra et al.*, 1992). *Price et al.* (2000) suggested that these 'tails' were evidence of the significant storage capacity available in surface irregularities on fracture walls. In this study, it is reasonable to ignore the 'tails' because we are using pore-throat diameter data to characterise only the matrix. Fracture storage is explicitly dealt with later in this section using alternative data.

Estimates of ψ_s and λ were obtained by fitting equation (4.18) to the observed effective saturations from the four data-sets CH2, CH3, PH6 and SH3 using linear regression. The curve fits are also shown in Figure 4.8 as solid lines. The derived parameter sets are listed in Table 4.1. For all four samples it seems that $\lambda = 2$ and $\psi_s = -30$ m are reasonably representative parameters.

During the linear regression, mercury intrusion data was ignored where $S_e > 0.8$ or $S_e < 0.02$. Data was ignored where $S_e > 0.8$ so as to avoid incorporating any conformance effects. The data was graphically recovered from plots presented by *Price et al.* (2000) where S_e was plotted on a linear scale. Consequently, data where $S_e < 0.02$ was considered to be unreliably recovered and was also ignored.

Table 4.1 Matrix parameter sets from linear regression of mercury intrusion data

Sample	λ	r_s (μm)	ψ_s (m)
CH2	1.78	0.464	-31.6
CH3	1.71	0.460	-31.9
PH6	2.45	0.473	-31.0
SH3	2.43	0.503	-29.2

4.7 Characterising the fractures

Many researchers have used the *van Genuchten* (1980) model in conjunction with the *Mualem* (1976) model to characterise rough surfaced unsaturated fractures. *Gerke and van Genuchten* (1993b) derived van Genuchten parameters by likening fractures to a highly permeable sand. *Zimmerman et al.* (1996) used van Genuchten parameters derived from characteristic curves

obtained from similar numerical experiments as described by *Pruess and Tsang* (1990) and *Kwicklis and Healey* (1993). *Liu et al.* (1998) obtained van Genuchten parameters by calibrating a steady state flow model to moisture content profiles observed in the unsaturated zone of Yucca Mountain, Nevada, USA. In this section, parameters describing fractures are acquired using in situ unsaturated hydraulic conductivity measurements obtained at Chalk sites in southern England.

Cooper et al. (1990) observed variations of hydraulic conductivity with pressure head at two grass crop sites on the Middle Chalk outcrop in the vicinity of Cambridge, UK. The first site was close to Fleam Dyke Pumping station and the second was situated in the Gog Magog Golf Course. Moisture contents were measured using neutron probes and pressure heads were measured using mercury manometer tensiometers. Further details concerning site and instrumentation description are offered in Table 4.2.

Table 4.2 Site Details

	Fleam Dyke	Golf Course
Grid reference	TL 549549	TL 487542
Monitoring period	1978-1983	1980-1982
Soil depth (m)	0.3	0.25
Depth to unweathered material (m)	2.1	1
Groundwater depth (approx.) (m)	20	40
Monitoring frequency (week $^{-1}$)	5	2
No. of neutron probe access tubes	8	4
No. of tensiometer profiles	4	2

Cooper et al. (1990) calculated their estimates of hydraulic conductivity using a combination of two modified versions of the instantaneous profile (IP) method (*Watson*, 1966), the zero flux plane (ZFP) method and the water balance method. The IP method works as follows. Providing there is zero rainfall and zero evaporation (i.e. zero net infiltration), and the water table is deep enough not to affect moisture flow, the total water content change per unit time can be described by

$$\left[\frac{\partial V_w}{\partial t}\right]_z = K(z)\left[\frac{\partial h}{\partial z}\right]_z \tag{4.28}$$

where h is hydraulic head, K is hydraulic conductivity, t is time, z is the soil depth to which the measurement applies and V_w is the total water content obtained from

$$V_w = \int_0^z \theta d\zeta \tag{4.29}$$

Hydraulic conductivity can then be obtained from (*Watson*, 1966)

$$K(z) = \left[\frac{\partial V_w}{\partial t}\right]_z \left[\frac{\partial h}{\partial z}\right]_z^{-1} \tag{4.30}$$

In reality, net infiltration is not zero, consequently the instantaneous profile method must be modified. When evaporation exceeds rainfall, it is expected that the upper part of the soil moisture profile moves upwards towards crop roots or the soil surface. Below, water continues to drain towards the water table. Dividing the zones of upward and downward flow is a zero flux plane (ZFP), which can be identified where the hydraulic gradient exhibits a stationary point. It follows that under these conditions, the IP method remains valid providing that (*Cooper et al.*, 1990)

$$V_w = \int_{z_0}^{z} \theta d\zeta \tag{4.31}$$

where z_0 is the depth to the zero flux plane.

This modified form of the IP method is known as the ZFP method (*Wellings*, 1984a; *Cooper et al.*, 1990; *Mahamood-ul-Hassan and Gregory*, 2002). A problem with this approach is that it is only valid when a ZFP is apparent. However, periods when a ZFP is not apparent are commonly in the winter when evaporation is small and the water potential is relatively high. It can therefore be assumed that values of actual evaporation will be close to the potential rate for the crop being considered. This gives rise to the water balance method which allows estimates of hydraulic conductivity from (*Cooper et al.*, 1990)

$$K(z) = \left\{P - PE + \left[\frac{\partial V_w}{\partial t}\right]_z\right\} \left[\frac{\partial h}{\partial z}\right]_z^{-1} \tag{4.32}$$

where P and PE are rates of precipitation and potential evaporation and $z_0 = 0$.

Plots of hydraulic conductivity against pressure head are shown for the Golf Course (at 2.1 m depth) and Fleam Dyke (at 3.0 m depth) in Figure 4.9. Because the results do not include values corresponding to pressure heads less than -30 m, it is appropriate to assume the matrix was constantly saturated. It follows that all observed changes in hydraulic conductivity can be attributed exclusively to the fractures (or any pores greater than a micron in diameter). Assuming that the fractures can be adequately represented using the Kozeny model (equation 4.17), an expression of hydraulic conductivity for the composite medium would be

$$K(\psi) = \begin{cases} K_{f,s}(\psi_{f,s}/\psi)^{\lambda_f \eta_f} + K_{m,s}, & \psi < \psi_{f,s} \\ K_{f,s} + K_{m,s}, & \psi \geq \psi_{f,s} \end{cases} \tag{4.33}$$

where $K_{f,s}$ is the saturated hydraulic conductivity of the fracture continuum, $K_{m,s}$ is the saturated hydraulic conductivity of the matrix while $\psi_{f,s}$ and λ_f are the Brooks and Corey parameters and η_f is the tortuosity parameter for the fracture continuum.

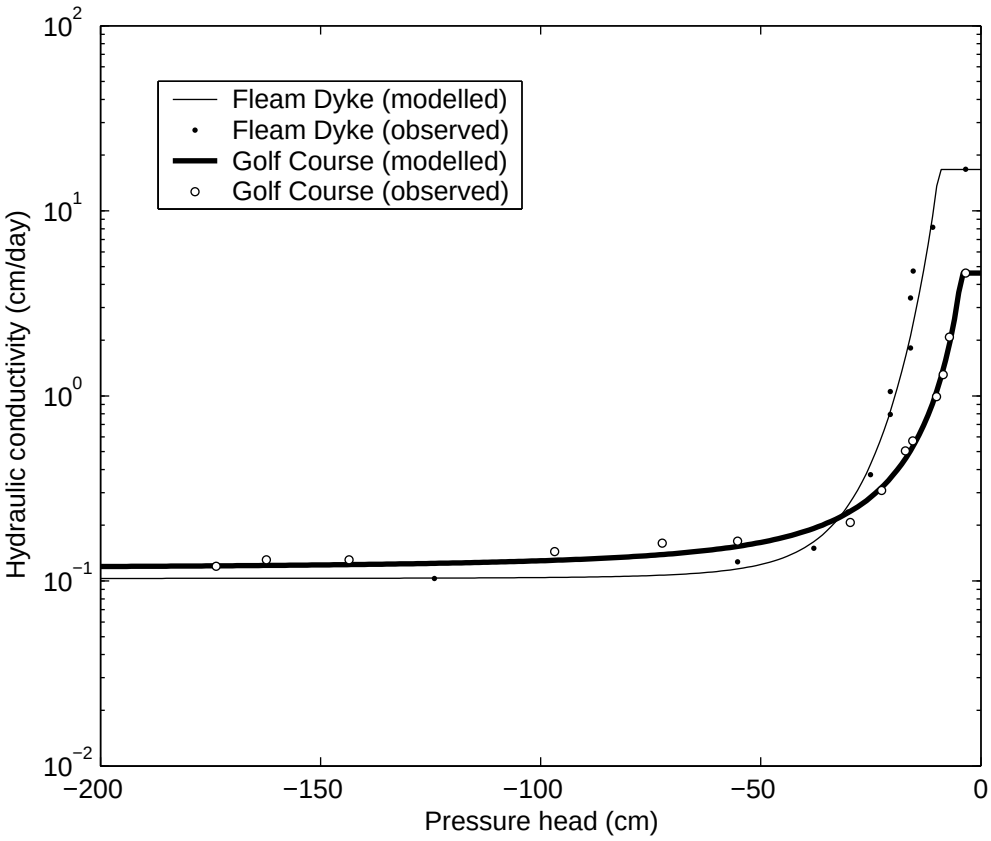

Figure 4.9 Hydraulic conductivity curves obtained at Fleam Dyke and Golf Course (aquired by *Cooper et al.*, 1990).

Estimates of $\psi_{f,s}$, $\lambda_f \eta_f$, $K_{m,s}$ and $K_{f,s}$ were obtained by minimising the RMSNE between values from equation (4.33) and observed hydraulic conductivities. The objective function was minimised using GBLSOLVE (*Jones et al.*, 1993). The optimum parameter sets are shown in Table 4.3 and the corresponding function outputs are plotted alongside the observed data in Figure 4.9.

The RMSNE was calculated using

$$\text{RMSNE} = \sqrt{\frac{1}{N}\sum_{n=1}^{N}\left(\frac{K_{mod,n} - K_{obs,n}}{K_{obs,n}}\right)^2} \tag{4.34}$$

where N is the number of samples, $K_{mod,n}$ and $K_{obs,n}$ are modelled and observed hydraulic conductivity respectively.

Generally, $\lambda_f \eta_f$ and $K_{m,s}$ are reasonably identifiable while $\psi_{f,s}$ and $K_{f,s}$ are highly correlated. To explore this further, contour plots of the parameter surface were plotted with $\lambda_f \eta_f$ and $K_{m,s}$ fixed at their optimum values (see Figure 4.10). It can be seen that overestimates of $K_{f,s}$ can be compensated for by increasing $\psi_{f,s}$.

Table 4.3 Optimised parameter sets from calibration against hydraulic conductivity data

Site	$\psi_{f,s}$ (cm)	$\lambda_f \eta_f$	$K_{m,s}$ (cm/day)	$K_{f,s}$ (cm/day)	RMSNE
Fleam Dyke	-9.51	4.06	0.10	16.62	0.201
Golf Course	-4.38	1.89	0.12	4.50	0.096

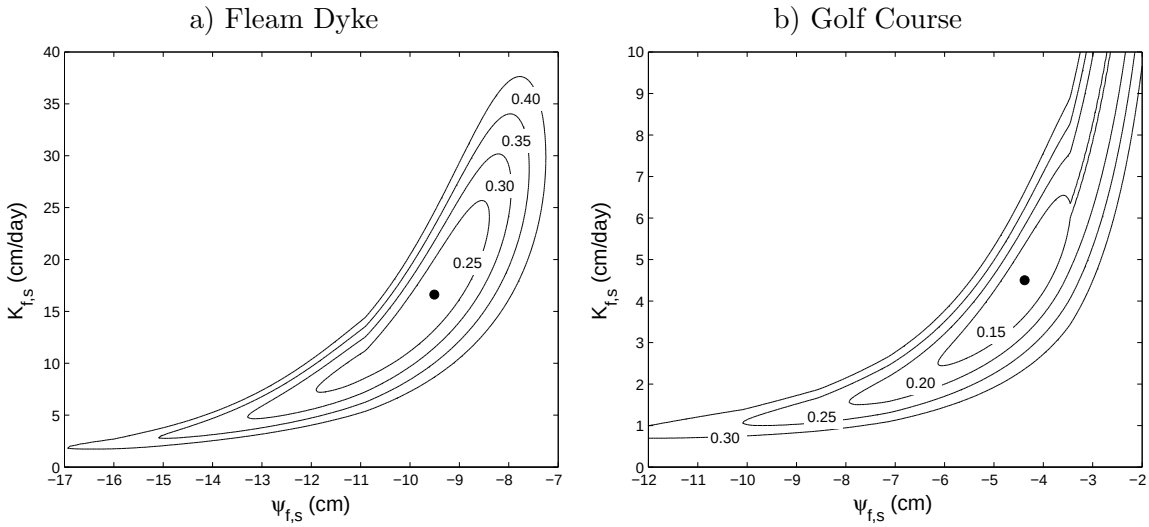

Figure 4.10 Contour plot illustrating the correlation between $\psi_{f,s}$ and $K_{f,s}$. The contour values are RMSNE values (obtained from 4.34) and the dot marks the minimum point found by GBLSOLVE.

An upper bound of $\psi_{f,s}$ can be found by considering the limit at which capillary theory remains valid. As apertures become very large, the radius of curvature approaches infinite causing the capillary effect to become negligible. For a wetting fluid with a contact angle of $\Theta = 0$, the hemispherical surface can no longer be defined when $r > -\psi_c$. Thus the maximum aperture (or pore-radii) that can be considered will be dictated by (*Wang and Narasimhan*, 1993)

$$r_{max} = \left(\frac{2\kappa}{\rho_w g}\right)^{1/2} \tag{4.35}$$

Taking the aforementioned values of κ, ρ_w and g, the maximum aperture size (or air entry pressure) is $r_{max} = -\psi_{c,max} = 4$ mm. Therefore $\psi_{f,s} \leq -4$ mm.

When fractures become close to saturated conditions, thin films of water are known to develop on their sides. Flow through films can be extremely fast (*Dragila and Wheatcraft*, 2003), hence it can be assumed that once film flow has been initiated, the hydraulic conductivity of the system will be a similar order of magnitude to when it is saturated.

Laboratory measurements of film thickness around an unconfined block of Bishop tuff

showed that significant film flow occurred once pressure heads exceeded -2.5 cm (*Tokunaga and Wan*, 1997). Similar experiments on a sheet of roughened glass showed film flow to occur with pressure heads as small as -10 cm (due to the absence of matrix imbibition) (*Tokunaga et al.*, 2000). Bearing this in mind, we can further reduce our upper bound for $\psi_{f,s}$ to around -2.5 cm. Interestingly, the estimates of $\psi_{f,s}$ at Fleam Dyke and the Golf Course lie in the range $-10 < \psi_{f,s} < -2.5$ cm.

The optimum estimates of $K_{f,s}$ at Fleam Dyke and the Golf Course from our calibration are 16.62 and 4.5 cm/day. These are smaller than what would be expected, probably because of the close correlation of $K_{f,s}$ and $\psi_{f,s}$ and the scarcity of data detailing close to saturated conditions. Data detailing this condition was rarely obtained because the data sampling was so coarse (between two and five times a week, see Table 4.2). Note that the sampling rate at Fleam Dyke was double as compared to that of Golf Course and the estimate of $K_{f,s}$ at Fleam Dyke is four times larger. It is hoped that this issue will be addressed in the NERC thematic programme, LOCAR, where many Chalk sites have been instrumented with automatic logging equipment that sample every 15 minutes.

A more generic approach to parameterising a fracture continuum for the Chalk unsaturated zone would be to consider a series of assumptions that force the model to be consistent with observations recorded in the literature.

If the largest pore-size considered to be relevant in the matrix has an air entry pressure of $\psi_{m,s}$ then this should also be the smallest air entry pressure considered to be relevant in the fracture. If the largest relevant aperture in the fracture continuum has an air entry pressure of $\psi_{f,s}$ and 99% of the fracture continuum has an air entry pressure greater than $\psi_{m,s}$, then this assumption will be forced providing λ_f is found from (recall equation 4.18)

$$\lambda_f = \frac{-2}{\log(\psi_{f,s}/\psi_{m,s})} \tag{4.36}$$

Generally, fracture flow appears to be insignificant as compared to matrix flow when pressure heads have fallen below -50 cm (*Wellings*, 1984a; *Hodnett and Bell*, 1990; *Cooper et al.*, 1990; *Mahamood-ul-Hassan and Gregory*, 2002). If $K_{f,s}$ is the saturated hydraulic conductivity of the fracture continuum and $K_{m,s}$ is the saturated hydraulic conductivity of the matrix continuum, then this assumption can be satisfied providing η_f is found from (recall equations 4.18 and 4.17)

$$\eta_f = \frac{1}{\lambda_f} \frac{\log(K_{m,s}/K_{f,s})}{\log(-\psi_{f,s}/50 \text{ cm})} \tag{4.37}$$

From our analysis of mercury intrusion curves we can assume that $\lambda_m = 2$ and $\psi_{m,s} = -3000$ cm. Because in the matrix the variation of hydraulic conductivity with pressure head is

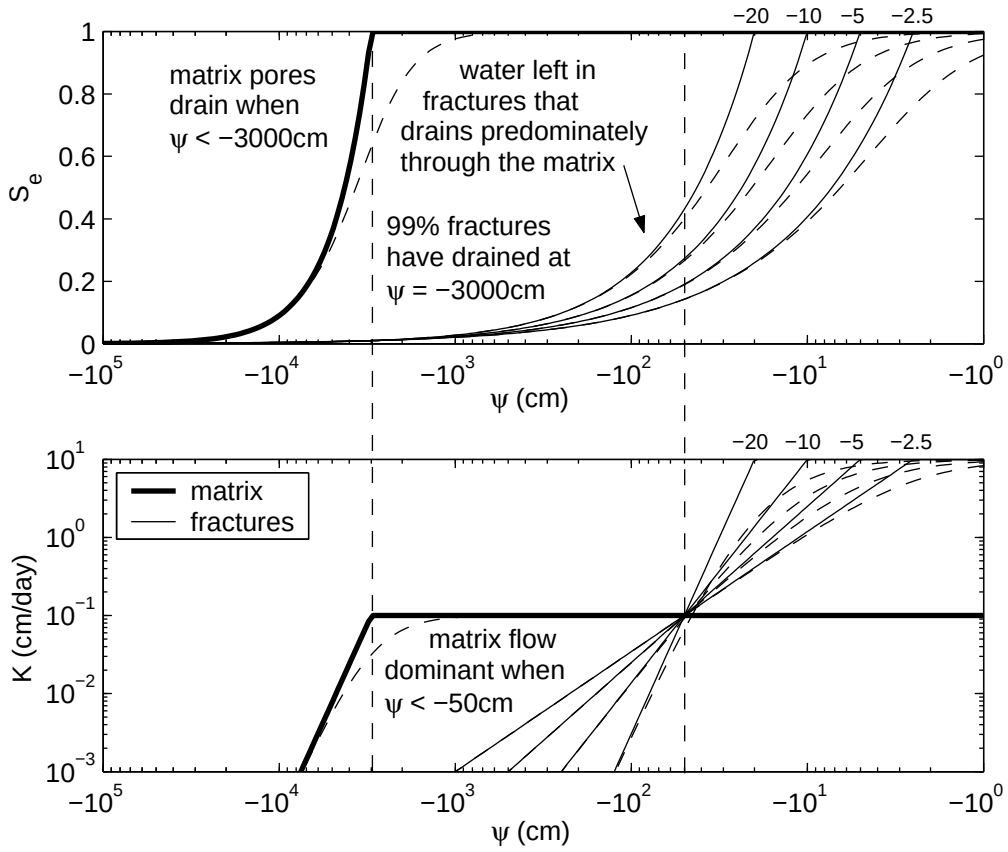

Figure 4.11 Matrix and fracture effective saturation, S_e and hydraulic conductivity, K curves for different values of $\psi_{f,s}$ as indicated on the top axis. The solid lines are using the *Brooks and Corey* (1966) S_e function while the dashed lines are using equivalent *van Genuchten* (1980) S_e functions. The hydraulic conductivity functions are calculated from corresponding Kozeny functions.

of less importance, we will assume that the *Mualem* (1976) model with $\eta = 0.5$ is a reasonable estimate. From equation (4.20), the corresponding value for the Kozeny model is therefore $\eta_m = 2.5$. If we then assume that $K_{m,s} = 0.1$ cm/day and $K_{f,s} = 10$ cm/day, values of λ_f and η_f can be obtained for different values of $\psi_{f,s}$ using equations (4.36) and (4.37). Some examples are shown in Table 4.4. Corresponding effective saturation curves and hydraulic conductivity curves are shown in Figure 4.11.

From Figure 4.11, it can be seen that $\psi_{f,s}$ controls how much storage is left after the fractures have drained to such an extent that their hydraulic conductivity is less than that in the matrix. The storage of water that drains at pressure heads greater than -50 cm can be associated with the specific yield one might observe during pumping tests. The rest of the water can then be attributed to part of the extra water which *Price et al.* (2000) was looking

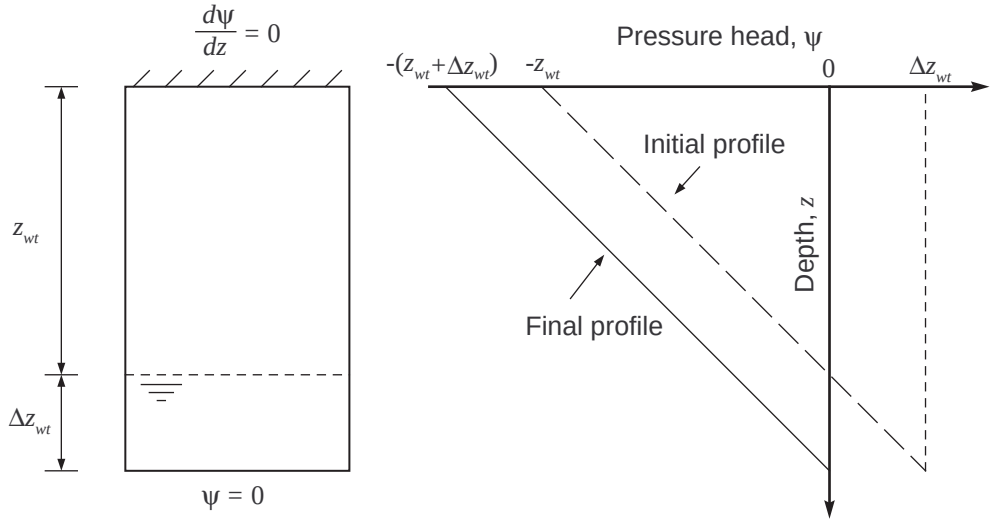

Figure 4.12 Schematic diagram of one-dimensional drainage model.

for to explain the base flow anomaly during droughts (observed by *Lewis et al.*, 1993).

4.8 Some drainage simulations

A major issue concerning studies of this sort is the lack of observed data available for model verification. To explore the validity of this approach further it is therefore pertinent to consider the simplest possible simulation scenario. To this end, we now consider one-dimensional flow through a $(3000 + \Delta z_{wt})$ cm deep homogenous Chalk column which is initially hydrostatic with a water table at Δz_{wt} above the column base. We then force the water table down to the base of the column such that any change in storage can be associated with a Δz_{wt} in groundwater head (see Figure 4.12). The column depth is set at $(3000 + \Delta z_{wt})$ cm such that at least Δz_{wt} of the column should eventually experience drainage of the matrix. *Narasimhan and Zhu* (1993) conducted similar numerical experiments to study the effects of slowly draining unsaturated zones on pumping test analysis in single porous medium aquifers.

Equation (4.3) was discretised in space using finite differences reducing the problem to a system of ordinary differential equations. These were solved using the stiff integrator, ODE15S available in the MATLAB Release 13 suite. The composite functions, $\theta(\psi)$, $C(\psi)$ and $K(\psi)$ were defined by equation (4.33) and S_e and k_r were defined by equations (4.21) (with $\alpha = -1/\psi_s$, $n = \lambda + 1$ and $m = 1 - 1/n$) and (4.17) for both the fracture and the matrix continua. The parameters used were those detailed in Table 4.4. The *van Genuchten* (1980)

Table 4.4 Parameters used in the drainage simulations

Item	Units	Matrix	Fractures			
ψ_s	(cm)	-3000	-2.5	-5	-10	-20
λ	(-)	2	0.65	0.72	0.81	0.92
η	(-)	2.5	2.37	2.78	3.54	5.47
S_s	(cm^{-1})	10^{-8}	10^{-7}	10^{-7}	10^{-7}	10^{-7}
θ_r	(-)	0	0	0	0	0
θ_s	(-)	0.35	0.01	0.01	0.01	0.01
K_s	(cm/day)	0.1	10	10	10	10

S_e function was used as opposed to the *Brooks and Corey* (1966) function because the *Brooks and Corey* (1966) function tends to become unstable close to the water table boundary due to the discontinuity at $\psi = \psi_s$.

The initial condition was set to

$$\psi(z, 0) = z - z_{wt} \tag{4.38}$$

such that the system is initially hydrostatic with the water table set at a depth of $z_{wt} = 3000$ cm.

The boundary conditions were

$$\left.\frac{\partial \psi}{\partial z}\right|_{z=0} = 0; \quad \psi(z_{wt} + \Delta z_{wt}, t) = 0 \tag{4.39}$$

such that there is zero net infiltration and the water table is instantaneously brought down to the bottom of the Chalk column at $z = 3000 + \Delta z_{wt}$ cm.

The specific yield, S_y can then be obtained from

$$S_y(t) = \frac{1}{\Delta z_{wt}} \left\{ \left[\int_0^{z_{wt}+\Delta z_{wt}} \theta(z) dz \right]_{\tau=0} - \left[\int_0^{z_{wt}+\Delta z_{wt}} \theta(z) dz \right]_{\tau=t} \right\} \tag{4.40}$$

Plots of specific yield against time are shown for each of the parameter sets listed in Table 4.4 for $\Delta z_{wt} = 100$ cm in Figure 4.13 and for $\Delta z_{wt} = 10$ cm in Figure 4.14. Both figures show different responses because the system is non-linear. However, in each curve it can be seen that prior to 1 day, most of the water in the fractures has drained although the 'full' specific yield of 0.01 is not achieved until tens of days afterwards. The speed of drainage is clearly sensitive to the selection of parameters from Table 4.4.

Also of interest is that the matrix does not appear to drain appreciably until after 100 days. Note that all of the times quoted from these simulations are likely to be underestimates

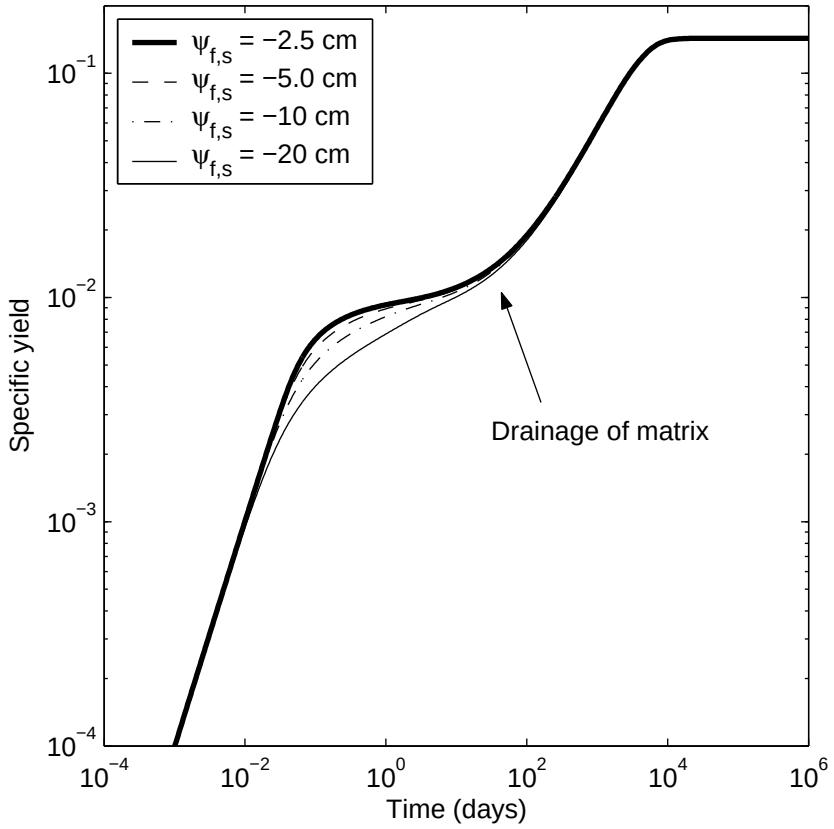

Figure 4.13 Variation of specific yield, S_y with time for a 3100 cm deep hydrostatic Chalk column subjected to a 100 cm drop in water table for a range of different $\psi_{f,s}$.

as compared to a model utilising the *Brooks and Corey* (1966) S_e function because the *van Genuchten* (1980) function tends to predict the drainage of pores at lower suctions (see Figure 4.11). In practice, the matrix is likely to take significantly longer to drain.

For a further illustration of the models behaviour, Figure 4.15 shows the variation of moisture content with elevation above the water table for different times for the case when $\Delta z_{wt} = 100$ cm and $\psi_{f,s} = -10$ cm. The righthand-side plot shows the fracture moisture content, where it can be seen that most of water has drained after around 1 day although the remainder of the water takes a further 9 days. The lefthand-side plot shows the matrix moisture content where it can be seen that matrix does not drain appreciably until around 100 days. Again it is emphasised that the *Brooks and Corey* (1966) S_e function would have predicted much longer times.

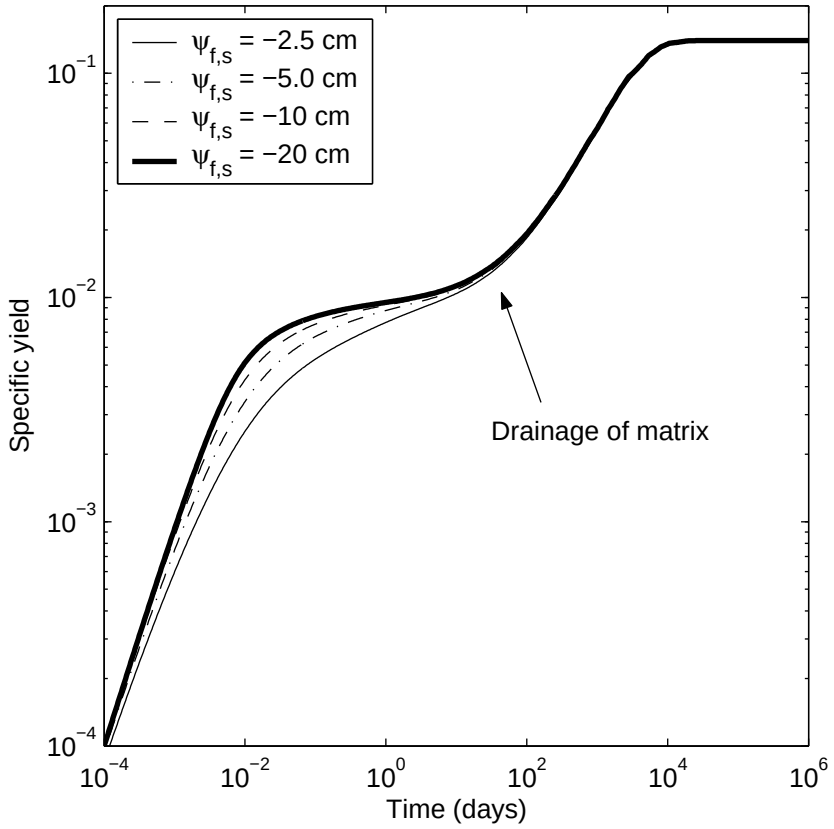

Figure 4.14 Variation of specific yield, S_y with time for a 3010 cm deep hydrostatic Chalk column subjected to a 10 cm drop in water table for a range of different $\psi_{f,s}$.

4.9 Drainage under ambient conditions

Earlier it was suggested that the extra water stored in the fractures for pressure heads less than -50 cm could partially explain the order of magnitude discrepancy in specific yield calculated by *Lewis et al.* (1993). However, from Figures 4.13 and 4.14 it would appear that the water in the fractures that drain when the pressure head falls below -50 cm is only a small fraction of the total water in the fractures.

Consider a case in which the water table falls by a certain amount. Water will initially be present in the narrower pores in the fractures (which only drain at pressure heads less than -50 cm) at higher elevations than in the wider pores. However if the water table drops by a certain amount, the water level in the narrow fracture pores and the wide fracture pores will drop by the same amount. Thus the yield from the wide and narrow pores would be in the relative proportions of the corresponding contributions to the fracture porosity and so the yield would predominantly come from the wider pores. It would not appear in any

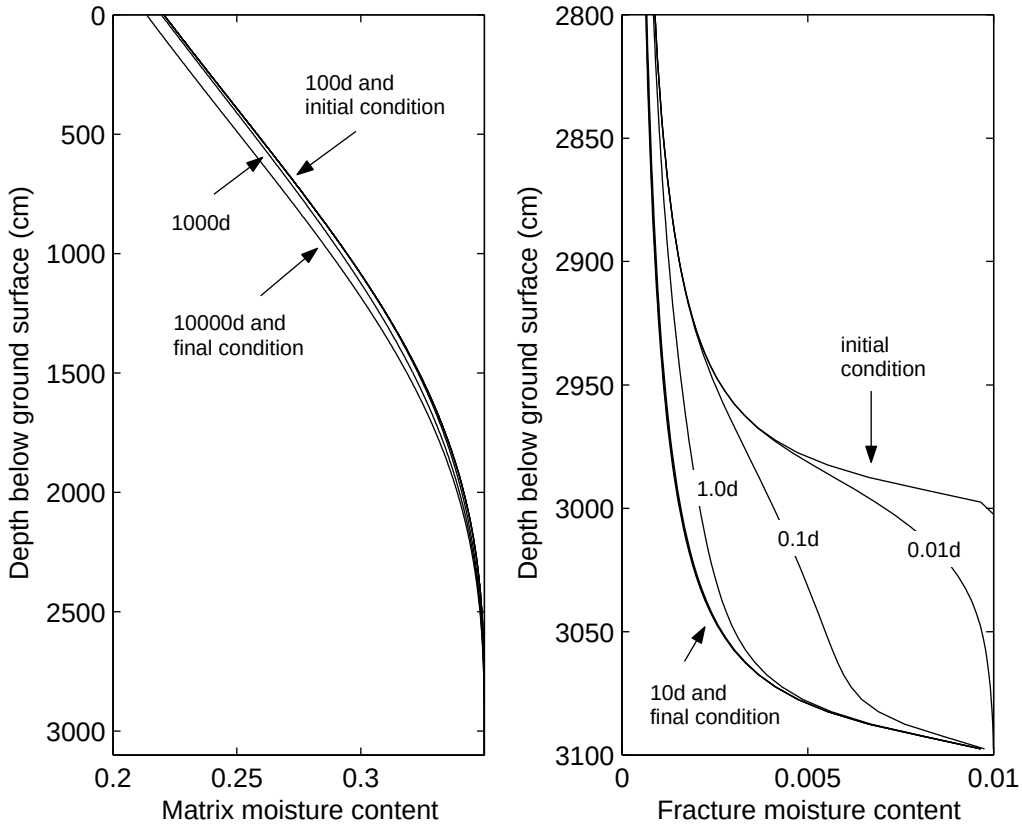

Figure 4.15 Variation of moisture content with depth for different times after a 3100 cm deep hydrostatic Chalk column is subjected to a 100 cm drop in water table when $\psi_{f,s} = -10$ cm.

circumstances more water would be obtained from the narrower pores than from the wider pores for a given drop in the water table. In short, for a Δz_{wt} drop in the water table, water drains from at most a Δz_{wt} thickness of the Chalk, although this Δz_{wt} thickness will come from different elevations for different diameter pores (see Figure 4.15).

However, a hydrostatic condition is rarely found in reality. *Ireson et al.* (2005) found that the vertical hydraulic gradient within the Chalk unsaturated zone ranged $-0.7 > J > -0.95$ over the period of November 2003 to August 2004 at a West Ilsley site, Berkshire.

Taking the hydraulic gradient J to be of order -0.7 to -0.95 would not be realistic for the model presented under drought conditions, because this model tends rapidly to hydrostatic conditions, coming close to such conditions in a few days (see Figure 4.15). The fact that such large gradients have been observed experimentally implies that water is being supplied to the fractures by some process not represented in the model (such as storage sites within near-surface layers of soil and weathered chalk).

Assuming the presence of such a gradient, it is possible that the yield of water measured

by *Lewis et al.* (1993) may have been a combination of the water released due to the change in the water table and the redistribution of water higher in the unsaturated zone as the system tends towards a hydrostatic condition.

To explore this further, we assume a uniform hydraulic gradient, J with depth such that the pressure head profile will take the form

$$\psi(z) = (J+1)(z - z_{wt}) \tag{4.41}$$

Assuming a *Brooks and Corey* (1966) type medium the moisture content of the profile will be defined by (recall equation 4.18)

$$S_e(z) = \frac{\theta(z) - \theta_r}{\theta_s - \theta_r} \begin{cases} \left[\dfrac{\psi_s}{(J+1)(z - z_{wt})}\right]^{\lambda}, & z - z_{wt} \leq \dfrac{\psi_s}{J+1} \\ 1, & z - z_{wt} > \dfrac{\psi_s}{J+1} \end{cases} \tag{4.42}$$

The total volume of drainable water present in the profile, $V_w(z_{wt}, J)$ can then be obtained from

$$\frac{V_w}{\theta_s - \theta_r} = \int_0^{z_{wt}} S_e(z)dz = \frac{-\psi_s}{J+1} + \int_{-z_{wt}}^{\psi_s/(J+1)} \left[\frac{\psi_s}{(J+1)(z - z_{wt})}\right]^{\lambda} d(z - z_{wt}) \tag{4.43}$$

which on evaluation, yields

$$\frac{V_w}{\theta_s - \theta_r} = \frac{\lambda\psi_s}{(J+1)(1-\lambda)} + \frac{z_{wt}}{(1-\lambda)}\left[\frac{-\psi_s}{(J+1)z_{wt}}\right]^{\lambda} \tag{4.44}$$

The change in storage, ΔV_w that would occur if the water table is dropped by a distance of Δz_{wt} and the system is then allowed to equilibriate (to the hydrostatic condition, i.e. $J = 0$) can then be found from

$$\frac{S_y}{\theta_s - \theta_r} = 1 + \frac{J\lambda(-\psi_s)}{(J+1)(1-\lambda)\Delta z_{wt}} + \frac{(-\psi_s)^{\lambda}}{(1-\lambda)\Delta z_{wt}}\left[\frac{z_{wt}^{1-\lambda}}{(J+1)^{\lambda}} - (z_{wt} + \Delta z_{wt})^{1-\lambda}\right] \tag{4.45}$$

where $S_y = -\Delta V_w / \Delta z_{wt}$.

Figure 4.16 shows the variation of normalised specific yield, $S_y/(\theta_s - \theta_r)$ (according to equation 4.45) against initial vertical hydraulic gradient, J for a range of water table drops Δz_{wt} assuming $\psi_s = -10$ cm, $\lambda = 0.81$ and $z_{wt} = 3000$ cm (the results were found to be largely insensitive to the selection of parameters from Table 4.4). It can be seen that the 'apparent' yield increases greatly with increasing negative initial hydraulic gradient. However, this does not fully explain the order of magnitude discrepancy in specific yield. For a $J = -0.7$, Δz_{wt} would have to be less than 30 cm, for an order of magnitude discrepancy to occur, according to Figure 4.16.

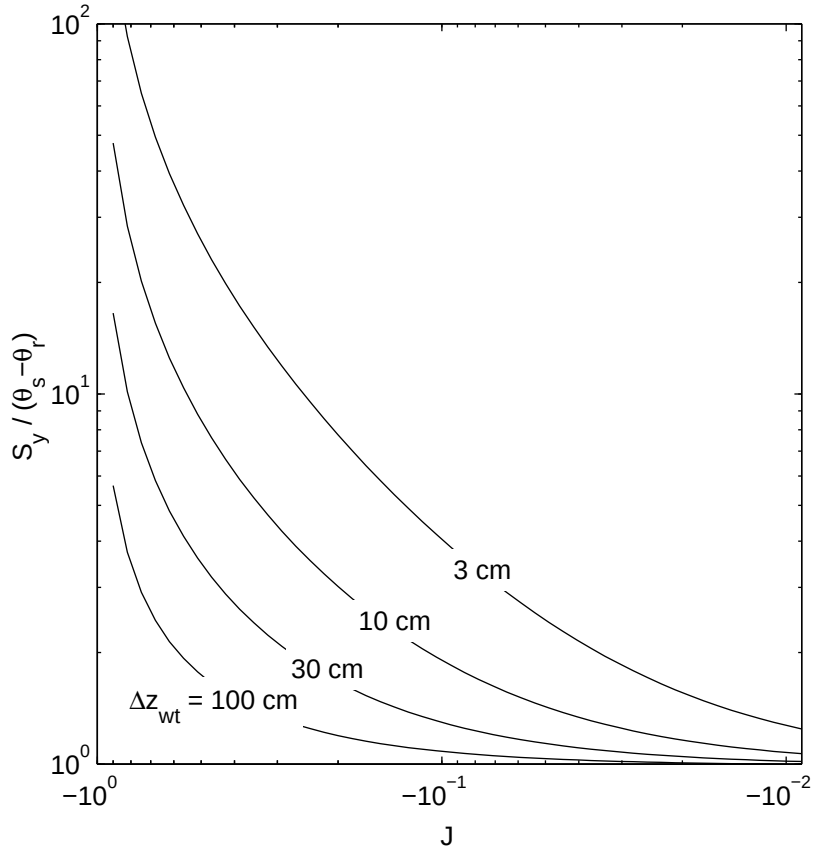

Figure 4.16 Plot of normalised specific yield, $S_y/(\theta_s - \theta_r)$ (according to equation 4.45) against initial vertical hydraulic gradient, J for a range of water table drops Δz_{wt} assuming $\psi_s = -10$ cm, $\lambda = 0.81$ and $z_{wt} = 3000$ cm.

4.10 Conclusions

A methodology for conceptualising and parameterising flow in the fractures and the matrix of the Chalk unsaturated zone has been presented. An issue that has hampered the development of this study is the lack of data available for model verification. Nevertheless, it has been demonstrated that the devised model satisfies all the known observations presented in the literature concerning the Chalk unsaturated zone. These include: the matrix pores not draining until pressure heads become less than -3000 cm; fracture flow becoming much less than matrix flow when pressure heads fall below -50 cm; the fracture continuum containing an element of storage that drains almost instantaneously and an element that drains more slowly (over a period of days to months). In the next chapter, this methodology is coupled with a solute transport model to study the effects of transient recharge on the development of solute profiles and breakthrough curves.

Chapter 5

Transient simulations of flow and transport in the Chalk unsaturated zone

5.1 Introduction

In this chapter all the findings from the previous chapters are collated so as to develop a numerical model of transient coupled flow and transport in the Chalk unsaturated zone. In Chapter 4, we were only interested in flow. Consequently it was reasonable to assume a single pressure head field. However, it is not possible to assume a single solute concentration field for solute transport, as was demonstrated in Chapter 2. Consequently, an explicit representation of a fracture and matrix is required for solute transport. (For completeness and compatibility, an explicit representation of a fracture and matrix is also considered for flow although this is not strictly necessary.) This greatly complicates the solution process because although our model is one-dimensional, we require a two dimensional representation of the matrix. The problem is solved using a modelling tool FLOWTRAN2D which has been developed specifically for this project. The development and verification of this model is described in detail in Appendix A. A purpose built code was considered preferable to a commercial code because it allowed greater flexibility in process representation.

To explore the behaviour of the model, a hypothetical scenario is developed. The one-dimensional model of the Chalk unsaturated zone features a fixed water table at 10 m depth (see Figure 5.1). At the top of the model various recharge time-series are applied for a number of years. A conservative solute (that could be tritium, chloride or nitrate) is applied to the

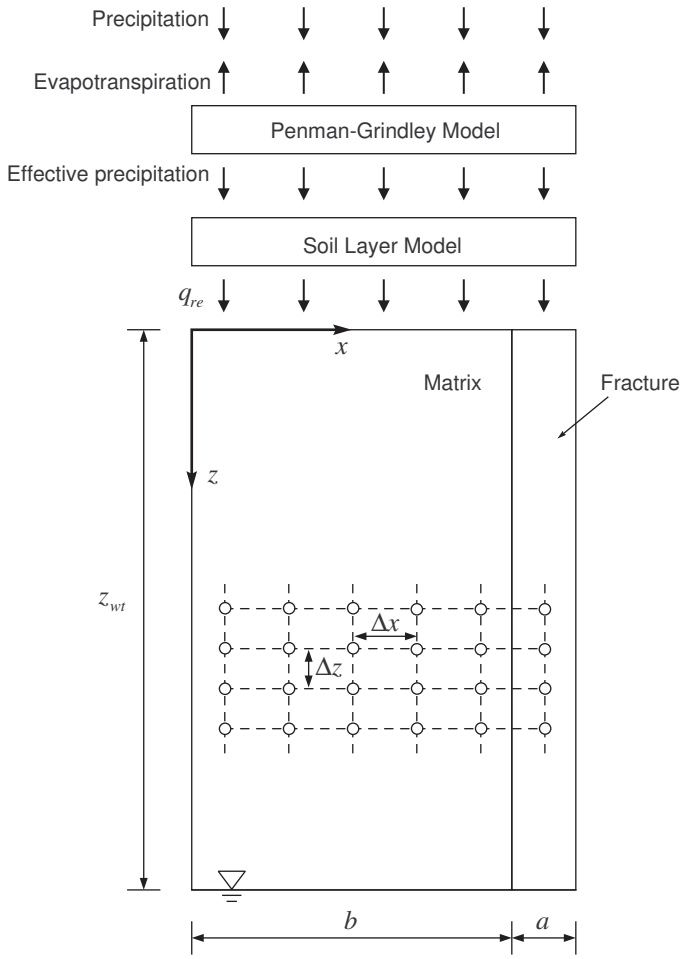

Figure 5.1 Schematic diagram of model structure used.

recharge for one year. Subsequent years involve the input of clean water. Solute profiles and breakthrough curves derived from the model are presented and discussed.

5.2 Governing equations

Identical slabs of matrix material are separated by equally spaced, rough surfaced fractures. Because of the symmetry of the model only a single, semi-infinite unit extending from the centre of a matrix block to the centre of a neighbouring fracture need be considered. Unsaturated flow in the fracture (subscript f) is governed by

$$C_f \frac{\partial \psi_f}{\partial t} = \frac{\partial}{\partial z}\left[K_f\left(\frac{\partial \psi_f}{\partial z} - 1\right)\right] - \frac{K_{m,x}}{a}\left.\frac{\partial \psi_m}{\partial x}\right|_{x=b} \tag{5.1}$$

and in the neighbouring matrix slab (subscript m) by

$$C_m \frac{\partial \psi_m}{\partial t} = \frac{\partial}{\partial x}\left[K_{m,x}\frac{\partial \psi_m}{\partial x}\right] + \frac{\partial}{\partial z}\left[K_{m,z}\left(\frac{\partial \psi_m}{\partial z} - 1\right)\right] \tag{5.2}$$

subject to the boundary conditions

$$\left.\frac{\partial \psi_m}{\partial x}\right|_{x=0} = 0; \quad \psi_m(b,z,t) = \psi_f(z,t) \tag{5.3}$$

where C is specific capacity and ψ is pressure head, θ is moisture content, K is hydraulic conductivity, a is the half-width of the fracture, b is the half-width of the matrix block, x is horizontal distance from the centre of the matrix block, z is depth and t is time. The x and z subscripts refer to the direction where applicable.

Moisture content is related to pressure head using the *Brooks and Corey* (1966) model

$$\frac{\theta - \theta_r}{\theta_s - \theta_r} = S_e = \begin{cases} (\psi_s/\psi)^{\lambda}, & \psi < \psi_s \\ 1, & \psi \geq \psi_s \end{cases} \tag{5.4}$$

where θ_r and θ_s are residual and saturated moisture contents respectively, S_e is the effective saturation, λ is an exponent that describes the variation of a pore-size distribution and ψ_s is an air entry pressure of the largest sized pore that has a significant presence.

Hydraulic conductivity is related to pressure head using the Kozeny approach (*Brutsaert*, 1967)

$$k_r = \frac{K}{K_s} = S_e^{\eta} \tag{5.5}$$

where K_s is the saturated hydraulic conductivity and η is an exponent that describes the growth of hydraulic conductivity with increasing effective saturation.

The specific capacity can be found from

$$C = \begin{cases} d\theta/d\psi, & \psi < \psi_s \\ S_s, & \psi \geq \psi_s \end{cases} \tag{5.6}$$

where S_s is specific storage associated with elastic (or compressible) storage.

The initial and boundary conditions of the flow model are:

$$\begin{aligned} &\psi_f = \psi_m = z_{wt} + \psi_{f,s} - z, && z > 0, && t = 0; \\ &\psi_f = \psi_m = \psi_{f,s}, && z = z_{wt}, && t > 0; \\ &K_{m,z}\left[\frac{\partial \psi_m}{\partial z} - 1\right] = q_{m,re}(t), && z = 0, && t > 0; \\ &K_f\left[\frac{\partial \psi_f}{\partial z} - 1\right] = q_{f,re}(t), && z = 0, && t > 0. \end{aligned} \tag{5.7}$$

where z_{wt} is the depth of a constant water table (set to 10m) and $q_{m,re}$ and $q_{f,re}$ are time varying recharge fluxes into the matrix block and fracture continuum found from

$$q_{m,re}(t) = \begin{cases} q_{re}(t), & q_{re} \leq K_{m,s} \\ K_{m,s}, & q_{re} > K_{m,s} \end{cases} \tag{5.8}$$

$$q_{f,re}(t) = \begin{cases} q_{re}(t), & q_{re} \leq K_{m,s} \\ \dfrac{b}{a}[q_{re}(t) - K_{m,s}] + q_{re}, & q_{re} > K_{m,s} \end{cases} \tag{5.9}$$

where q_{re} is the time varying recharge flux into the system derived using a simple soil moisture accounting model described in the next section. Note that the pressure in both the fractures and the matrix at the water table boundary is set to $\psi_{f,s}$ such that the boundary is actually the capillary fringe of the fractures. This makes a trivial difference but helps towards better model stability.

From the flow and moisture content fields calculated by the flow model, the solute transport model can be constructed using

$$\frac{\partial}{\partial t}(\theta_f c_f) = \frac{\partial}{\partial z}\left[\theta_f D_f \frac{\partial c_f}{\partial z} - q_f c_f\right] + \frac{1}{a}\left[\theta_m D_{m,x} \frac{\partial c_m}{\partial x} - q_{m,x} c_m\right]_{x=b} \tag{5.10}$$

and

$$\frac{\partial}{\partial t}(\theta_m c_m) = \frac{\partial}{\partial z}\left[\theta_m D_{m,z} \frac{\partial c_m}{\partial z} - q_{m,z} c_m\right] + \frac{\partial}{\partial x}\left[\theta_m D_{m,x} \frac{\partial c_m}{\partial x} - q_{m,x} c_m\right] \tag{5.11}$$

subject to the boundary conditions

$$\left[\theta_m D_{m,x} \frac{\partial c_m}{\partial x} - q_{m,x} c\right]_{x=0} = 0; \quad c_m(b, z, t) = c_f(z, t) \tag{5.12}$$

where D is the dispersion coefficient found from

$$D = D_A + \chi \frac{|q|}{\theta} \tag{5.13}$$

with D_A being the apparent diffusion coefficient and χ a dispersivity associated with hydrodynamic dispersion. Note that here, for simplicity, hydrodynamic dispersion is assumed to be linearly dependant on velocity. This is not always the case. For instance, if we consider hydrodynamic dispersion induced under laminar flow conditions in a pipe, the dispersion has a squared dependency on velocity due to the parabolic velocity profile (*Taylor*, 1953).

The initial and boundary conditions of the solute transport model are:

$$\begin{aligned} &c_f = c_m = 0, && z > 0, && t = 0; \\ &\theta_m D_{m,z} \frac{\partial c_m}{\partial z} = \theta_f D_{f,z} \frac{\partial c_f}{\partial z} = 0, && z = z_{wt}, && t > 0; \\ &\theta_m D_{m,z} \frac{\partial c_m}{\partial z} - q_{m,z} c_m = -q_{m,re} c_0 H(t_p - t), && z = 0, && t > 0; \\ &\theta_f D_{f,z} \frac{\partial c_f}{\partial z} - q_{f,z} c_f = -q_{f,re} c_0 H(t_p - t), && z = 0, && t > 0. \end{aligned} \tag{5.14}$$

where H denotes the Heaviside step function, c_0 is a constant tracer concentration (set to unity) and t_p is the duration of solute injection (set to 1 year).

All the above equations are integrated together in respect to time using the stiff integrator ODE15s available in any standard version of MATLAB (*Shampine and Reichelt*, 1997; *Shampine et al.*, 1999). ODE15s is a variable order method which employs an adaptive time grid (i.e. time steps are continuously adjusted such that the numerical error associated with each step is always below some specified tolerance). A stiff method (as opposed to a non-stiff method) was used because of the non-linearity of the problem.

Following the discussion in Chapter 4 the parameters in Table 5.1 are assumed throughout (unless otherwise stated) with a uniform space step of 2 cm in both directions. The dispersivity used for all simulations was 4 cm, a space step of 2 cm ensured that the Peclet number ($Pe = v\Delta x/D < \Delta x/\chi$) was always well below 2.0 which is needed for numerical stability when using a central difference approximation for advection (e.g. *Sun*, 1996). A 4 cm dispersivity was selected because we wanted hydrodynamic dispersion to be small as we were more interested in matrix diffusion effects. A 2 cm space step allowed simulations to be undertaken in a reasonable amount time.

Table 5.1 Base case model parameters

Item	Units	Fracture	Matrix
ψ_s	(cm)	-5	-3000
λ	(-)	0.72	2
η	(-)	2.78	2.5
S_s	(cm^{-1})	10^{-7}	10^{-8}
θ_r	(-)	0.0	0.0
θ_s	(-)	1.0	0.35
K_s	(cm/day)	1000	0.1
D_A	(m^2/s)	10^{-10}	10^{-10}
χ	(cm)	4	4
a	(cm)	0.1	N/A
b	(cm)	N/A	10

5.3 Description of recharge flux

Daily precipitation and monthly potential evaporation data from the Theale gauging station in the Kennet catchment from the 30th June 1993 to 29th June 1994 (provided by MORECS) was used to generate an effective precipitation time series using the Penman-Grindley model.

The model as given by *Ragab et al.* (1997), calculates the water that is potentially available for groundwater recharge, $EP = q_{re}$ as a difference between measured precipitation P, estimated actual evapotranspiration AE and the soil moisture deficit SMD.

Actual evaporation is calculated from

$$AE_k = \begin{cases} PE_k, & SMD_k < C_1 \quad \text{OR} \quad P_k \geq PE_k \\ P_k + C_3(PE_k - P_k), & C_2 > SMD_k \geq C_1 \quad \text{AND} \quad P_k < PE_k \\ P_k, & SMD_k = C_2 \quad \text{AND} \quad P_k < PE_k \end{cases} \tag{5.15}$$

where PE is potential evapotranspiration, C_1 is a root constant, C_2 is the SMD at wilting point and C_3 is an empirical constant relating actual to potential evapotranspiration when deficits are greater than the root constant.

A potential soil moisture deficit, $PSMD$ is calculated from

$$PSMD_{k+1} = SMD_k + AE_k - P_k \tag{5.16}$$

allowing effective precipitation and soil moisture deficit to be calculated from

$$EP_k = \begin{cases} -PSMD_{k+1}, & PSMD_{k+1} < 0 \\ 0, & PSMD_{k+1} > 0 \end{cases} \tag{5.17}$$

and

$$SMD_{k+1} = \begin{cases} 0, & PSMD_{k+1} < 0 \\ PSMD_{k+1}, & PSMD_{k+1} > 0 \end{cases} \tag{5.18}$$

The parameters used were $C_1 = 75$ mm, $C_2 = 150$ mm and $C_3 = 1/3$ and the results are shown in Figure 5.2.

5.4 Parameter sensitivity

Parameters to describe flow in Chalk fractures, established in Chapter 4, mostly relied on a common observation that fracture flow becomes much less than matrix flow when pressure heads fall below -50 cm (e.g. *Wellings*, 1984a; *Cooper et al.*, 1990; *Hodnett and Bell*, 1990). This resulted in a series of parameter sets, depending on an assumed value of $\psi_{f,s}$ (see Table 5.2). As $\psi_{f,s}$ increases, the moisture retention and hydraulic conductivity functions more closely approximate a step-function. Figure 5.3 shows solute profiles representing the mean concentration in the matrix after 1, 2, 3, 4 and 5 years using the model setup, parameters and conditions set out in Section 5.2, the recharge data presented in Figure 5.2 and the different fracture hydraulic parameter sets detailed in Table 5.2. Solute migration appears

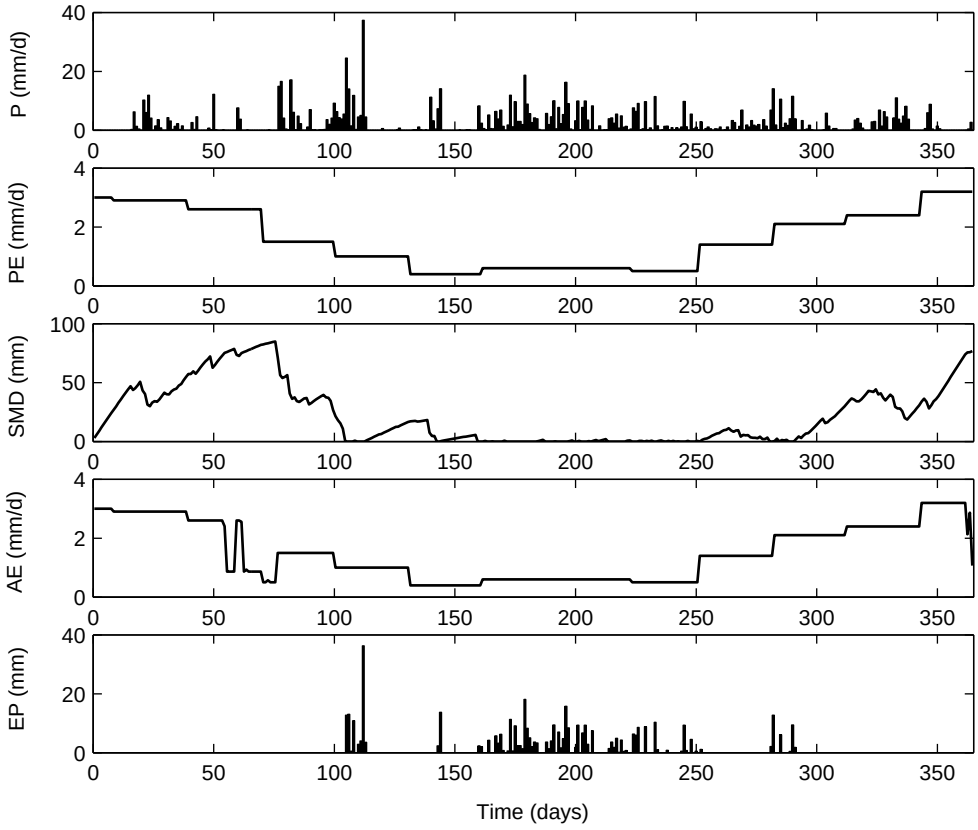

Figure 5.2 Output from the Penman-Grindley model for the Theale gauging station from the summer of 1993 to the summer of 1994.

to be insensitive to choice of fracture hydraulic parameters. This is because all the fracture parameter sets define a system whereby a fraction of fracture-water de-waters very quickly (in hours) while the remainder drains very slowly (over at least several days). It is also interesting to note that there is significant forward tailing due to solutes that enter the fractures penetrating much further than the advective solute front associated with the matrix.

Table 5.2 Possible hydraulic parameter combinations for Chalk fractures

$\psi_{f,s}$ (cm)	λ_f	η_f
-2.5	0.65	2.37
-5.0	0.72	2.78
-10.0	0.81	3.54
-20.0	0.92	5.50

Note that no warm up period was used because the simulation assumed a hydrostatic

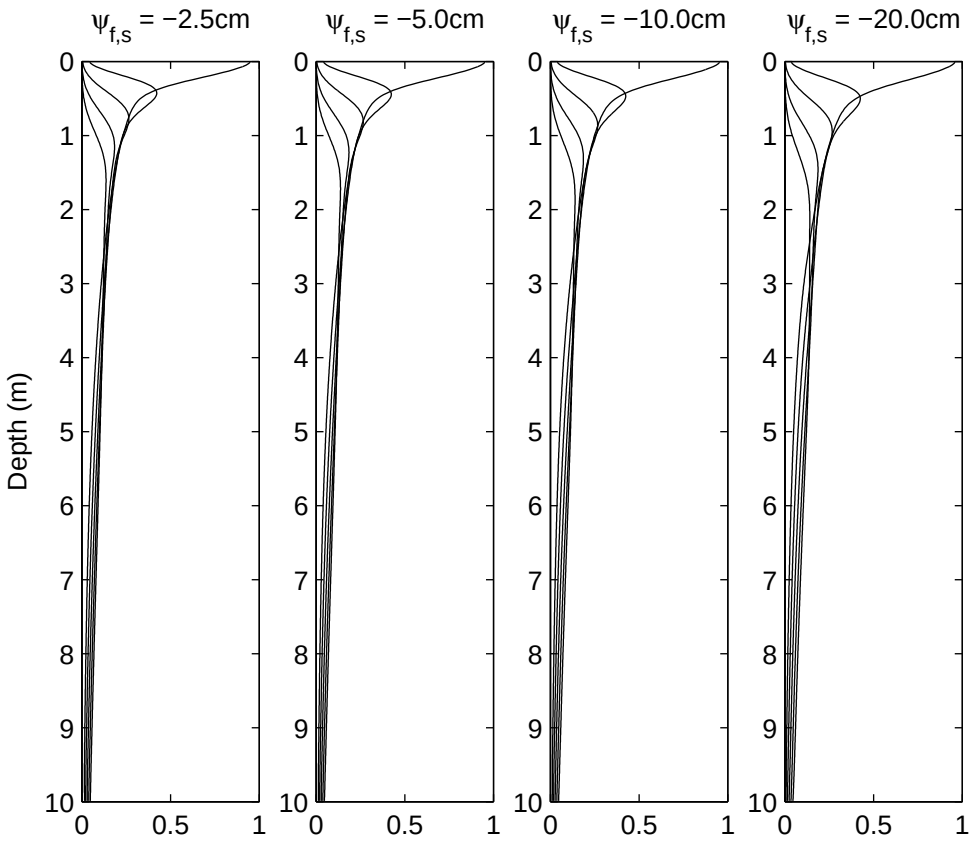

Figure 5.3 Sensitivity of solute profiles to fracture hydraulic parameters. The solute profiles represent the mean concentration in the matrix after 1, 2, 3, 4 and 5 years using a $\psi_{f,s}$ (and its associated values of λ and η) as detailed in each subplot title.

initial condition which was appropriate because simulations started in the middle of summer when there was no effective precipitation. Furthermore, because the matrix was always fully saturated (due to the capillary fringe) and the fractures had very little storage, the model was found to warm up in just a few days under heavy rainfall.

Another parameter of interest is the matrix hydraulic conductivity (previously taken as 0.1 cm/day). A range of different values from 0.1 to 0.6 cm/day have been observed at various Chalk sites (e.g. *Wellings*, 1984a; *Cooper et al.*, 1990; *Hodnett and Bell*, 1990). Figure 5.4 shows solute profiles representing the mean concentration in the matrix after 1, 2, 3, 4 and 5 years using the model setup, parameters and conditions set out in Section 5.2, the recharge data presented in Figure 5.2 but with $K_{m,s}$ = 0.0, 0.1, 0.2 and 0.3 cm/day. More mass is present and there is better peak preservation in the profiles with larger $K_{m,s}$, suggesting that fast solute bypass and forward tailing is more prevalent in systems with low $K_{m,s}$. In contrast, the solute peak can be seen to move faster in the profiles of larger $K_{m,s}$. The movement of

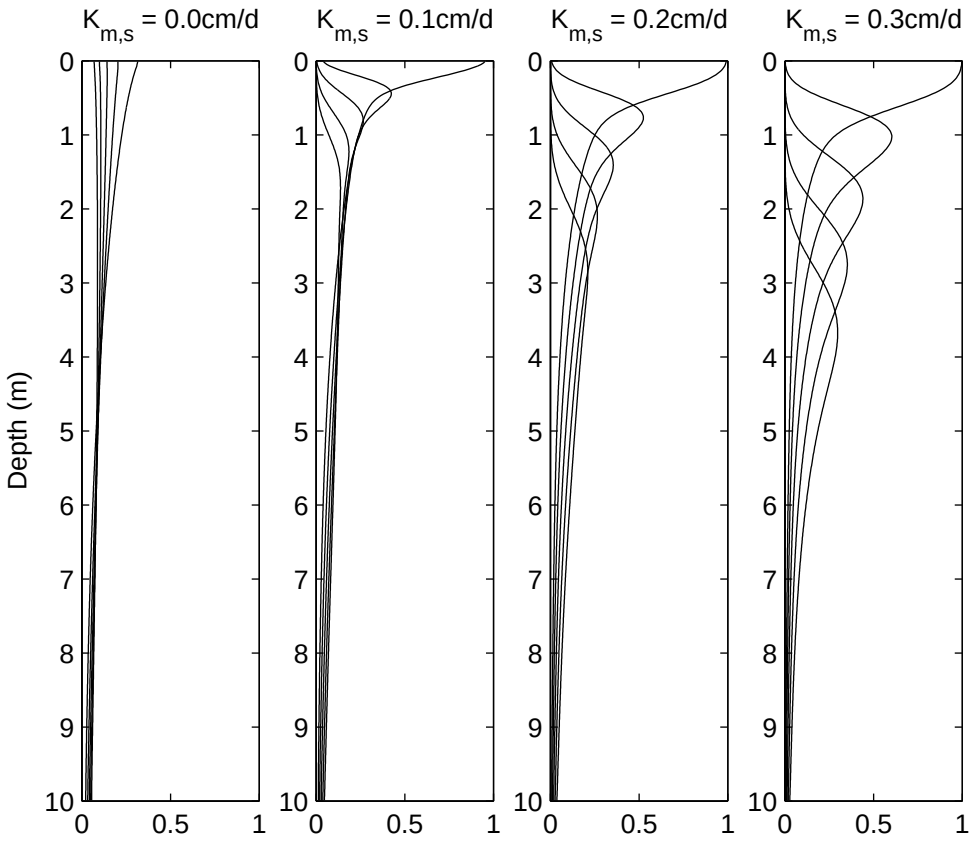

Figure 5.4 Sensitivity of solute profiles to matrix hydraulic conductivity at saturation. The solute profiles represent the mean concentration in the matrix after 1, 2, 3, 4 and 5 years using a $K_{m,s}$ as detailed in each subplot title.

the solute peak is mostly dependent on the advective travel times of the matrix. No peak is present in the profile where $K_{m,s} = 0$ because there is no advection in the matrix.

5.5 Sensitivity to temporal sampling

One of the main drivers of this study is to examine the sensitivity of the model to temporal sampling. To explore this systematically, the daily EP time series has been re-sampled at weekly, monthly, quarterly and yearly rates (see Figure 5.5). Figure 5.6 shows solute profiles representing the mean concentration in the matrix after 1, 2, 3, 4 and 5 years using the model setup, parameters and conditions set out in Section 5.2, and the different recharge data sets presented in Figure 5.5.

It can be seen that with increasing temporal sampling the profiles become increasingly dispersed with longer forward tails. This is due to increased infiltration rates (albeit more sparsely distributed) which have to go through the fractures. Another apparent feature is

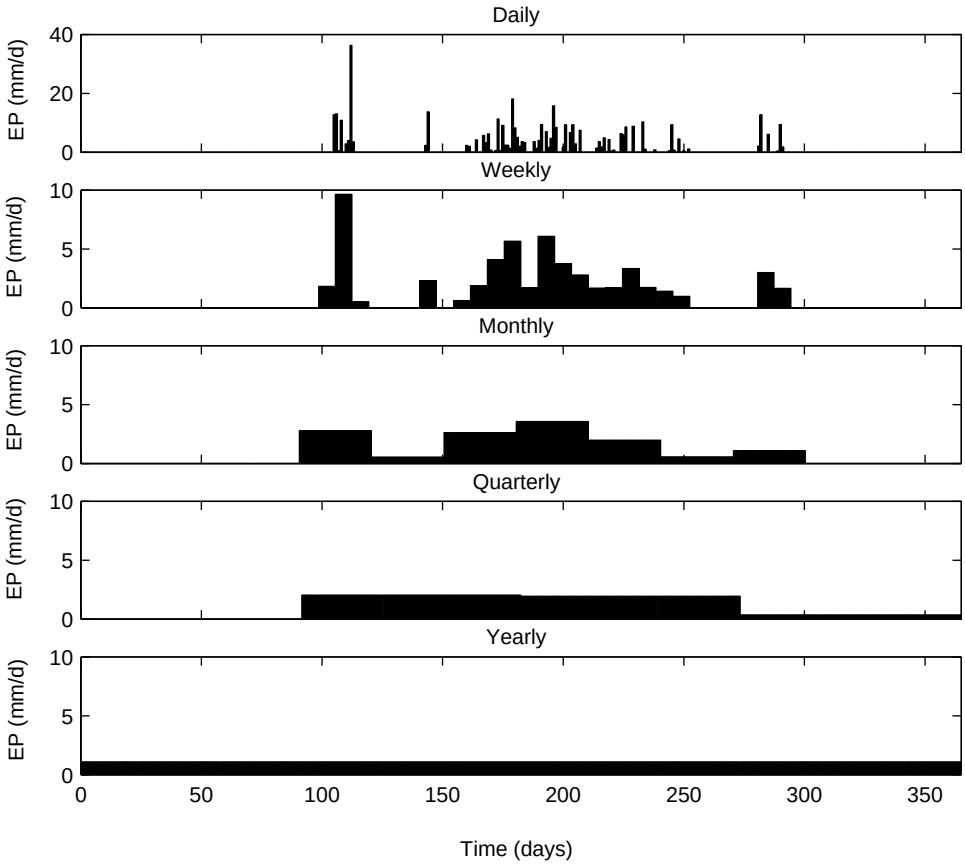

Figure 5.5 Different cumulative sampling rates of the effective precipitation time-series.

that the solute peak movement in the matrix increases with decreasing temporal sampling. This can be explained by more water (and solute mass) directly entering the matrix. The annual displacement of the solute peaks can be directly related to the annual infiltration that directly entered the matrix. Also of interest is that the profiles do not contain the same amount of mass. This is because substantially, more solute mass was able to penetrate the entire chalk column, as indicated in Table 5.3.

It can therefore be concluded that assuming steady state flow conditions can lead to erroneous data interpretation. Furthermore, these simulations show how sensitive the system must be to recharge attenuation by overlying soil and gravelly chalk layers.

5.6 Considerations of soil layers

To explore the attenuation effect of soil layers to the recharge input function, a single porous medium model was set up with the same initial and boundary conditions as used in the

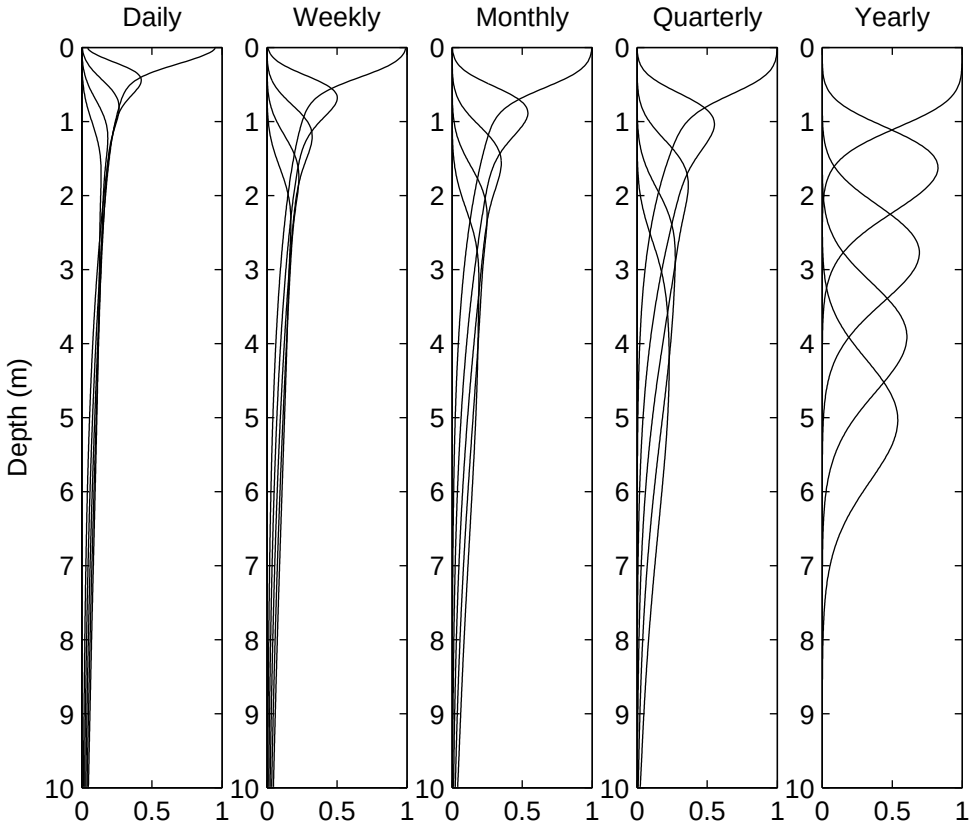

Figure 5.6 Sensitivity of solute profiles to temporal sampling of the effective precipitation time series. The solute profiles represent the mean concentration in the matrix after 1, 2, 3, 4 and 5 years using a sampling rate as detailed in each subplot title.

previous simulations.

Moisture content and hydraulic conductivity were related to pressure head using (*van Genuchten*, 1980)

$$\frac{\theta - \theta_r}{\theta_s - \theta_r} = S_e = \left[\frac{1}{1 + |\alpha\psi|^n}\right]^m \tag{5.19}$$

$$K(S_e) = K_s S_e^{0.5}[1 - (1 - S_e^{1/m})^m]^2 \tag{5.20}$$

where $m = 1 - 1/n$, θ_r and θ_s are residual and saturated moisture contents, K_s is the hydraulic conductivity at saturation, and α and n are empirical parameters.

The soil was assumed to behave like the Silt Loam G.E.3 reported by *van Genuchten* (1980) using the parameters set out in Table 5.4. Interestingly, *Van den Daele et al.* (2003) notes a 25 cm layer of sandy silt loam overlying the Chalk outcrop at the Fleam Dyke lysimeter.

Figure 5.7 shows the downward fluxes at various depths into the soil column following infiltration of the daily sampled recharge data presented in Figure 5.2. Figure 5.8 shows

Table 5.3 Cumulative mass that left the Chalk columns as a percentage of what went in.

Time (years)	Daily	Weekly	Monthly	Quarterly	Annually
1	3.8%	1.3%	0.0%	0.0%	0.0%
2	7.1%	3.3%	0.0%	0.0%	0.0%
3	11.1%	6.6%	0.5%	0.0%	0.0%
4	15.9%	11.1%	3.3%	1.0%	0.0%
5	21.7%	16.9%	8.3%	3.8%	0.0%

Table 5.4 Hydraulic parameters for soil layer.

Soil name	θ_r	θ_s	α (cm^{-1})	n	K_s (cm/day)	S_s (cm^{-1})
Silt Loam G.E.3	0.131	0.396	0.00423	2.06	4.96	10^{-7}

solute profiles representing the mean concentration in the matrix after 1, 2, 3, 4 and 5 years using the model, parameters and conditions set out in Section 5.2, and the different recharge data sets presented in Figure 5.7 (with $K_{m,s} = 0.1$ cm/day).

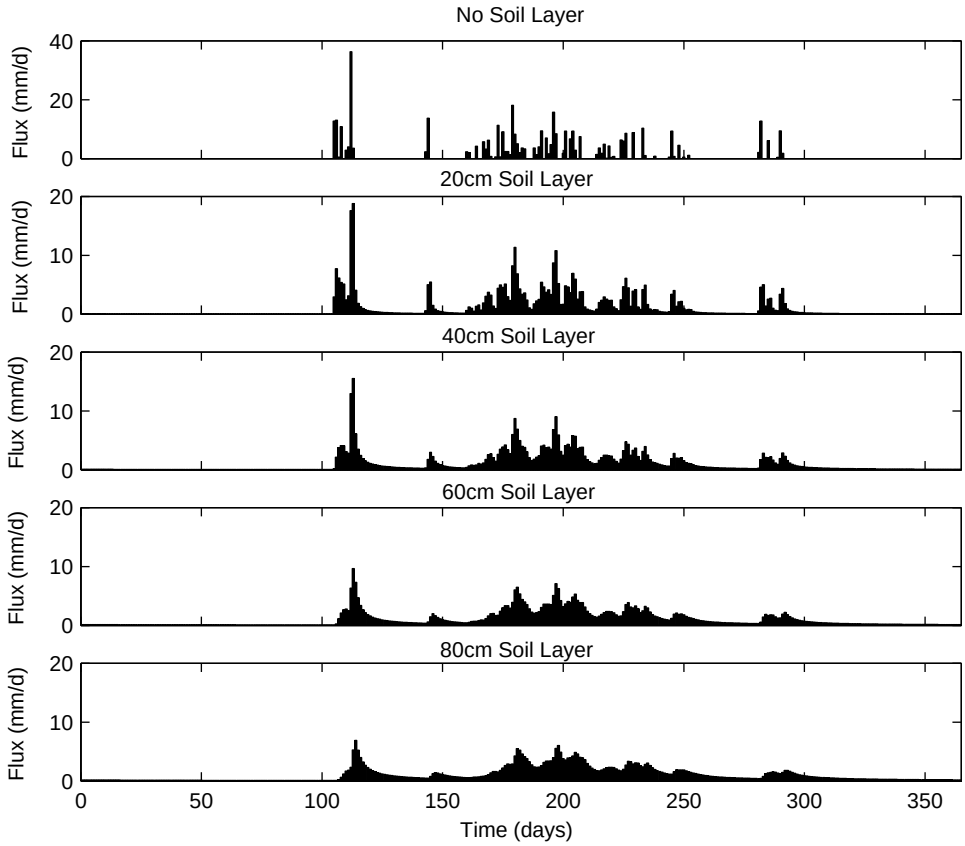

Figure 5.7 Effective precipitation time-series exiting soil layers of varying depths.

As with increasing temporal sampling, with decreasing thickness of overlying soil layers, the profiles become increasingly dispersed with longer forward tails. This effect appears more dramatic when $K_{m,s}$ is increased. Figure 5.9 shows solute profiles under exactly the same conditions used to get Figure 5.8 but with a $K_{m,s} = 0.3$ cm/day. For soil layers greater than 80cm, there is almost negligible forward tailing. The reason is that the infiltration rate into the Chalk column is predominately less than the matrix hydraulic conductivity such that flow in the fractures is almost negligible.

Figures 5.10 a and b show the solute breakthrough curves (BTC) at the water table (i.e. $z = 10$ m) in the matrix and the fractures with overlying soil layers of 20 cm and 40 cm respectively. The matrix BTCs are uni-modal although they plateaus every summer when there is negligible solute movement due to lack of infiltration. The matrix BTCs peak at 10 years suggesting a bulk movement of 1m/year which corresponds well with a number of field investigations (e.g. *Smith et al.*, 1970; *Oakes et al.*, 1981; *Barraclough et al.*, 1994).

In contrast, the fracture BTCs are multi-modal showing spikes which correspond to the

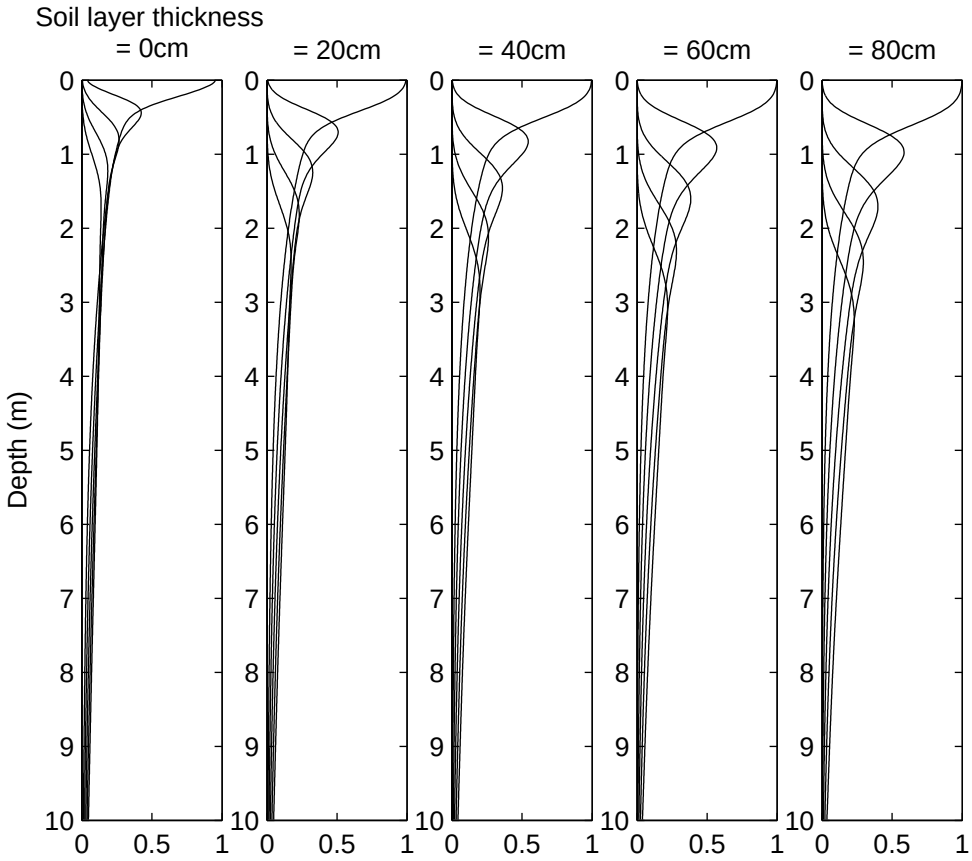

Figure 5.8 Sensitivity of solute profiles to depth of overlying soil layer. The solute profiles represent the mean concentration in the matrix after 1, 2, 3, 4 and 5 years using an overlying soil layer thickness as detailed in each subplot title, with a saturated matrix hydraulic conductivity of 0.1 cm/day.

peaks in the infiltration time-series. The peaks are less dramatic with the 40 cm soil layer because the associated infiltration is more attenuated (see Figure 5.7). For times up to the main solute peak the spikes are positive whereas for times after, they are negative. This is indicative of the fractures flushing out contaminated water from the matrix prior to the peak exit and flushing clean water after the peak exit.

The importance of these concentration fluctuations is hard to decipher because the fracture porosity is only 1% as opposed to the matrix porosity which is 35%. However, the spikes only occur where there are heavy infiltration rates, when water is travelling much faster in the fractures. This significance can be explored by considering the composite response of the columns summarised in figures 5.11 and 5.12.

The third subplots show the composite BTCs for the Chalk columns. It can be seen that the spikes often raise the composite solute concentration by three-fold with the 20 cm soil layer. With the 40 cm soil layer this is reduced. Also of interest is that the main peak

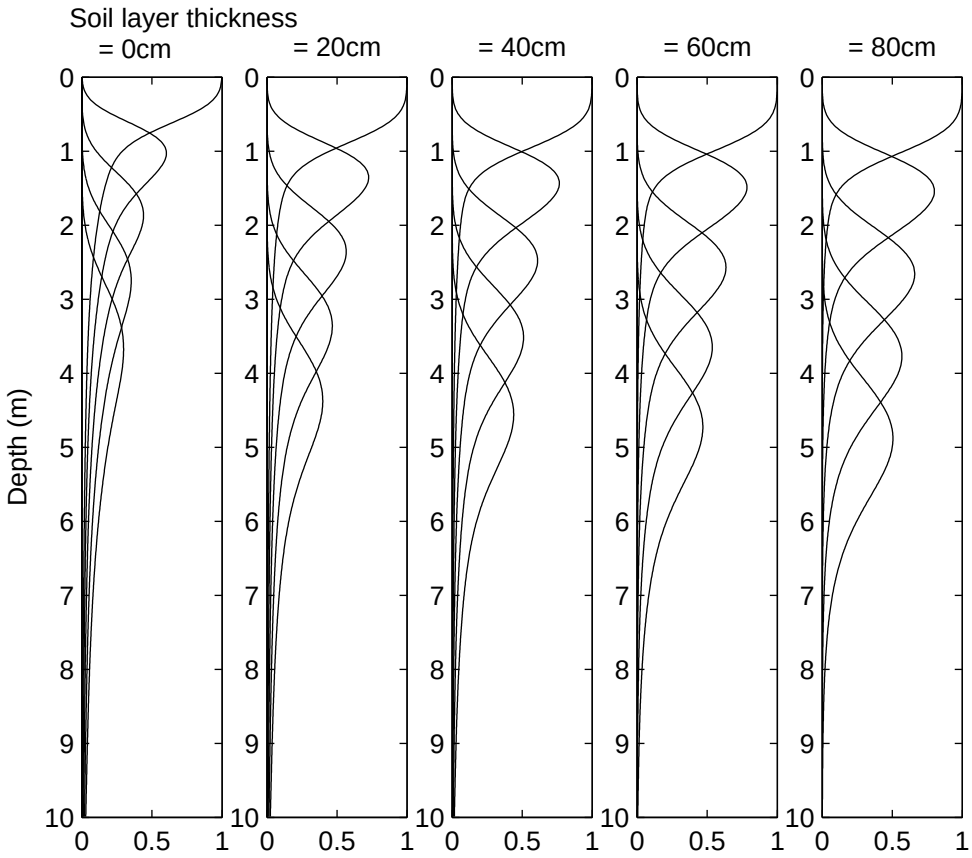

Figure 5.9 Sensitivity of solute profiles to depth of overlying soil layer. The solute profiles represent the mean concentration in the matrix after 1, 2, 3, 4 and 5 years using an overlying soil layer thickness as detailed in each subplot title, with a saturated matrix hydraulic conductivity of 0.3 cm/day.

concentration is higher with the 40 cm soil layer because of less forward tailing. The fourth subplots show the mass flux out of the columns. These are also very spiky and strongly correlated with the infiltration flux (see first subplots). Interestingly, mass spikes associated with the 38 mm/day infiltration event,at the beginning of each winter (see Figure 5.2), can be seen at the base of the Chalk column, with a 20 cm overlying soil layer, in the first year. With the 40 cm soil layer, these are not significant until around 5 years. However, both columns have almost identical breakthrough statistics see cumulative mass fluxes (normalised to the total input mass) in the fifth subplots and Table 5.5.

5.7 Water table response

In Chapter 3 the problems of models that ignore matrix flow was discussed. The issue was that for large fracture spacings, significant forward tailing occurred in the simulated solute

Table 5.5 Breakthrough statistics from long term simulations using a 20 cm and 40 cm overlying soil layer.

% breakthrough	20cm soil layer	40cm soil layer
5	4.40year	5.54year
50	9.50year	9.51year
95	12.48year	11.67year

profiles which was believed to be incompatible with the well preserved peaks observed in the pore waters of many Chalk sites across the United Kingdom. It was concluded that the inadequacies of the model were due to the assumption of ignoring matrix flow. In this chapter, matrix flow has been explicitly accounted for yet significant forward tailing is also observed in the simulated profiles. The only way that we have been able to reduce forward tailing has been by attenuating the infiltration time-series by assuming the existence of an overlying soil layer.

A question then arises as to whether the modelling framework developed within this thesis is still compatible with the fast water table response, characteristic of Chalk aquifers. The model described in this chapter is one-dimensional which constrains us to assume a fixed water table. To explicitly investigate water table response, at least a two-dimensional representation that considers a saturated zone would be needed.

Such a model would require a significant extra effort of work for at least two reasons. Firstly, each model simulation described in this chapter has taken several hours to run (the 19 year simulations took around 36 hours). A two-dimensional representation may involve a model domain that would be at least a hundred times larger. Consider a 1 km, hill-slope. Even if we assume a horizontal space step as large as 10m, we would still need at least a hundred vertical profiles. Secondly, water table response will be highly dependant on the vertical variation in hydraulic conductivity in the saturated zone (e.g. *Rushton et al.*, 1989). How to represent vertical heterogeneity in the saturated zone of the Chalk is not well understood, beyond the scope of this work and the primary subject of another project within the NERC thematic program, LOCAR.

Nevertheless, we can still speculate about the effect of infiltration attenuation on water table response by examining the water flux at the water table of our one-dimensional model. Figures 5.13 and 5.14 show the water table flux (fifth subplots) from the models with overlying soil layers of 20 cm and 40 cm plotted along side the daily sampled EP time-series from the Penman-Grindley model (first subplots). Both models dampen the EP time-series by around

four times. However, the offset between the peaks is less than three days. This is because the unsaturated zone model has an extremely small storage (less than 1%). The dampening is almost solely due to the overlying soil model (compare second and fifth subplots). Because the delay time between peaks is so small we can reasonably conclude that our model is still compatible with a fast water table response.

Figures 5.13 and 5.14 also show the variations of fracture and matrix flow with depth. For both models, significant fracture flow only occurs three times after the major infiltration events at around 110, 180 and 200 days. However, at the water table, most of the flow is through the fractures due to the presence of the fracture capillary fringe. Figure 5.15 shows the proportion of total flow that occurs in the fractures, over the year, plotted against depth. For the model with an overlying soil layer of 20 cm thickness, fracture flow represents between 20 and 30% to a depth of around 800 cm. For the model with an overlying soil layer of 40 cm thickness, fracture flow represents between 17 and 20% to a depth of around 800 cm. Below 800 cm, the proportion rises exponentially, to just under 90%. Again, this is due to the fracture capillary fringe where water preferentially leaves the matrix. This is because the fracture and matrix heads are close to equilibrium and the fracture hydraulic conductivity is several orders of magnitude greater than that of the matrix. Note that the percentages of fracture flow in the upper part of the column are predefined by the soil-layer attenuation and the saturated hydraulic conductivity of the matrix and are therefore of slightly trivial significance.

5.8 Conclusions

The developed model has a large parameter requirement. Different and similar effects are achieved by varying different parameters. However, the simulated solute profiles show that the extent of solute spreading is almost completely dependant on the amount of fracture flow. Fracture flow can be reduced by increasing the matrix hydraulic conductivity or attenuating the recharge time-series.

While the solute profiles look very smooth, the corresponding breakthrough curves at the water table are not. The presence of fracture flow causes large spikes to protrude the underlying long-term concentration trend associated with transport in the matrix. These spikes can be explicitly related to extreme events within the infiltration time-series which have skimmed off solute from matrix. However, studies of the cumulative mass flux at the water table suggest that in the context of total mass, these may not be important (compare

Figures 5.11 and 5.12 and Table 5.5).

In Chapter 3 it was suggested that the representation of matrix flow would solve the forward tailing conundrum associated with dual-porosity models. However, the magnitude of matrix flow is still very small as compared to the recharge estimates from the Penman-Grindley model. As a result most of the simulations described in this chapter show significant forward tailing. This could suggest that the Penman-Grindley model does not predict recharge in an appropriate manner for the Chalk. If our model is reasonable, and forward tailing is not something that should occur, then the recharge estimates must be substantially attenuated to allow more of the water to be absorbed by the matrix. This was illustrated by the exploration of various depths of soil layers (see Figure 5.7). It seems that a soil layer as deep as 80 cm is required to dampen the recharge sufficiently. Generally overlying soil layers on Chalk outcrops are very shallow ≈ 25 cm. However, the remaining 55 cm could be accounted for within the storage that might be expected in the weathered Chalk layers which can extend for several metres.

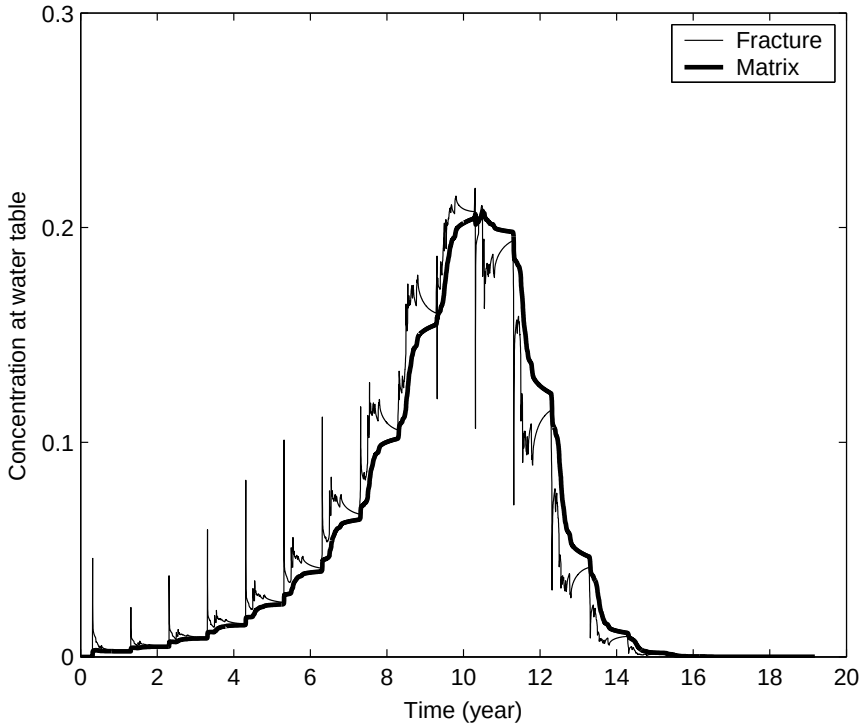

a) with an overlying soil layer of 20 cm

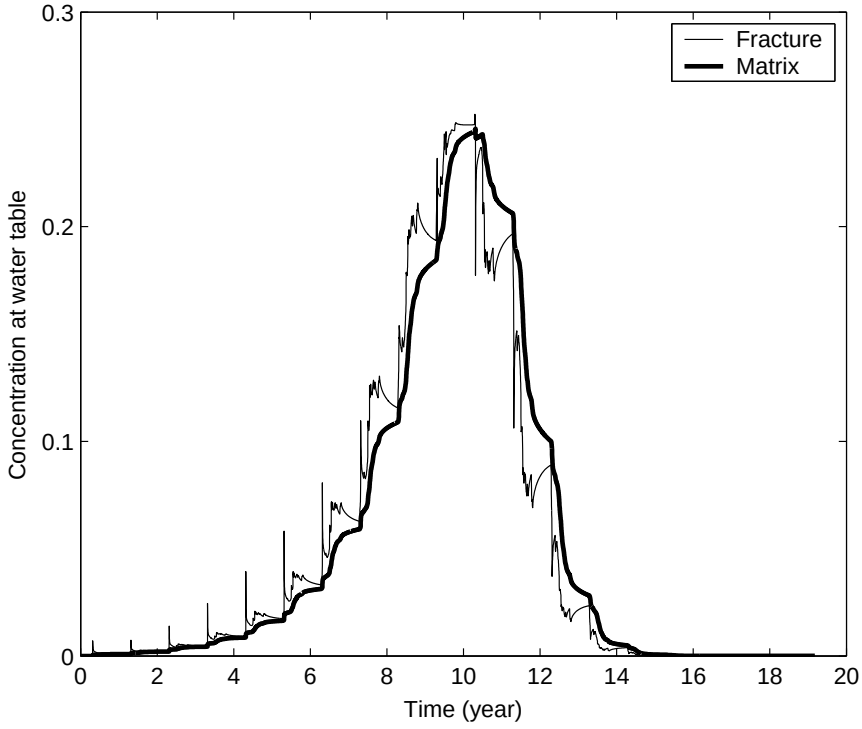

b) with an overlying soil layer of 40 cm

Figure 5.10 Solute concentrations in the fracture and the matrix block at the water table.

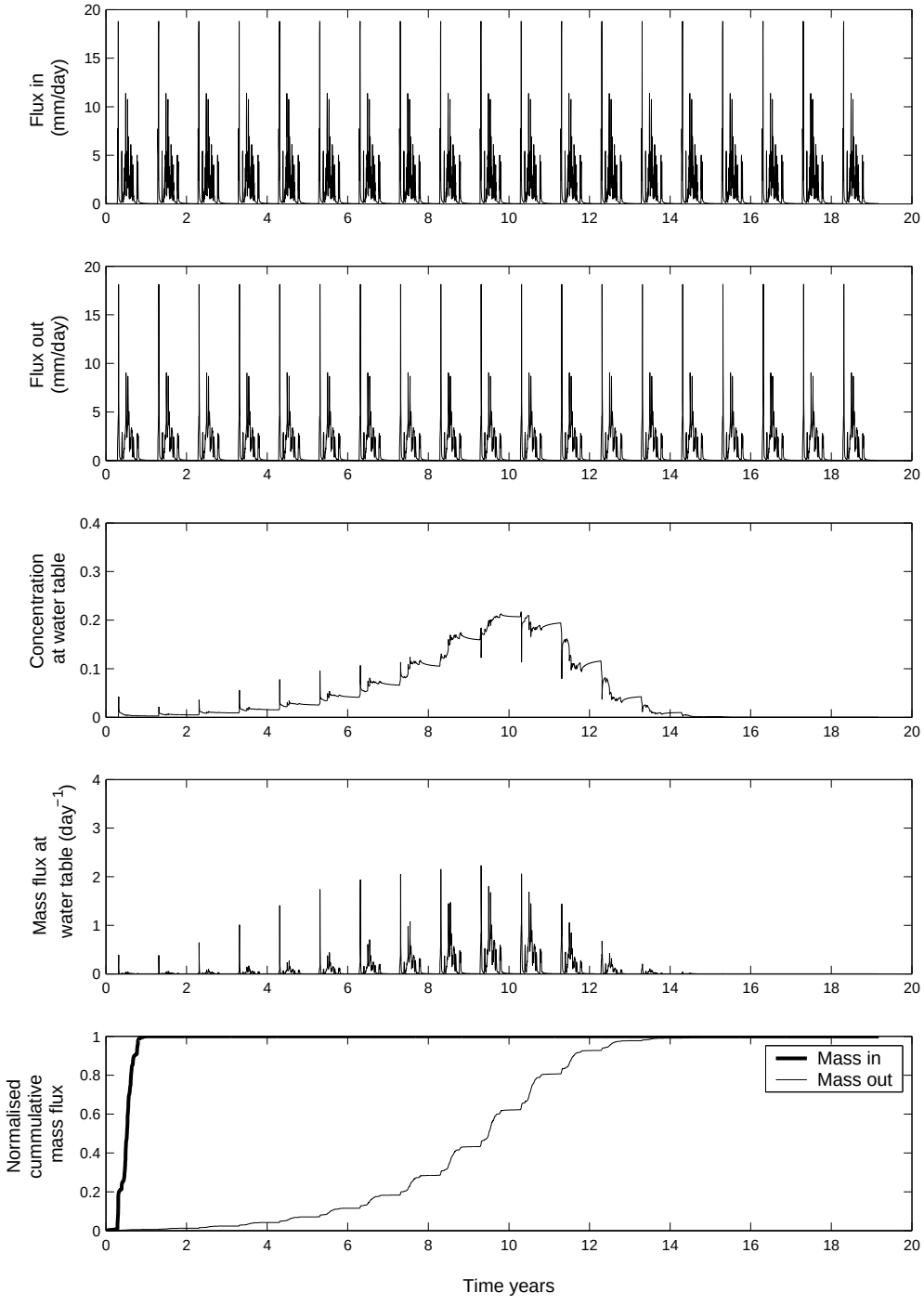

Figure 5.11 Input output data including the composite breakthrough curve from the 19 year simulation with an overlying soil layer of 20 cm.

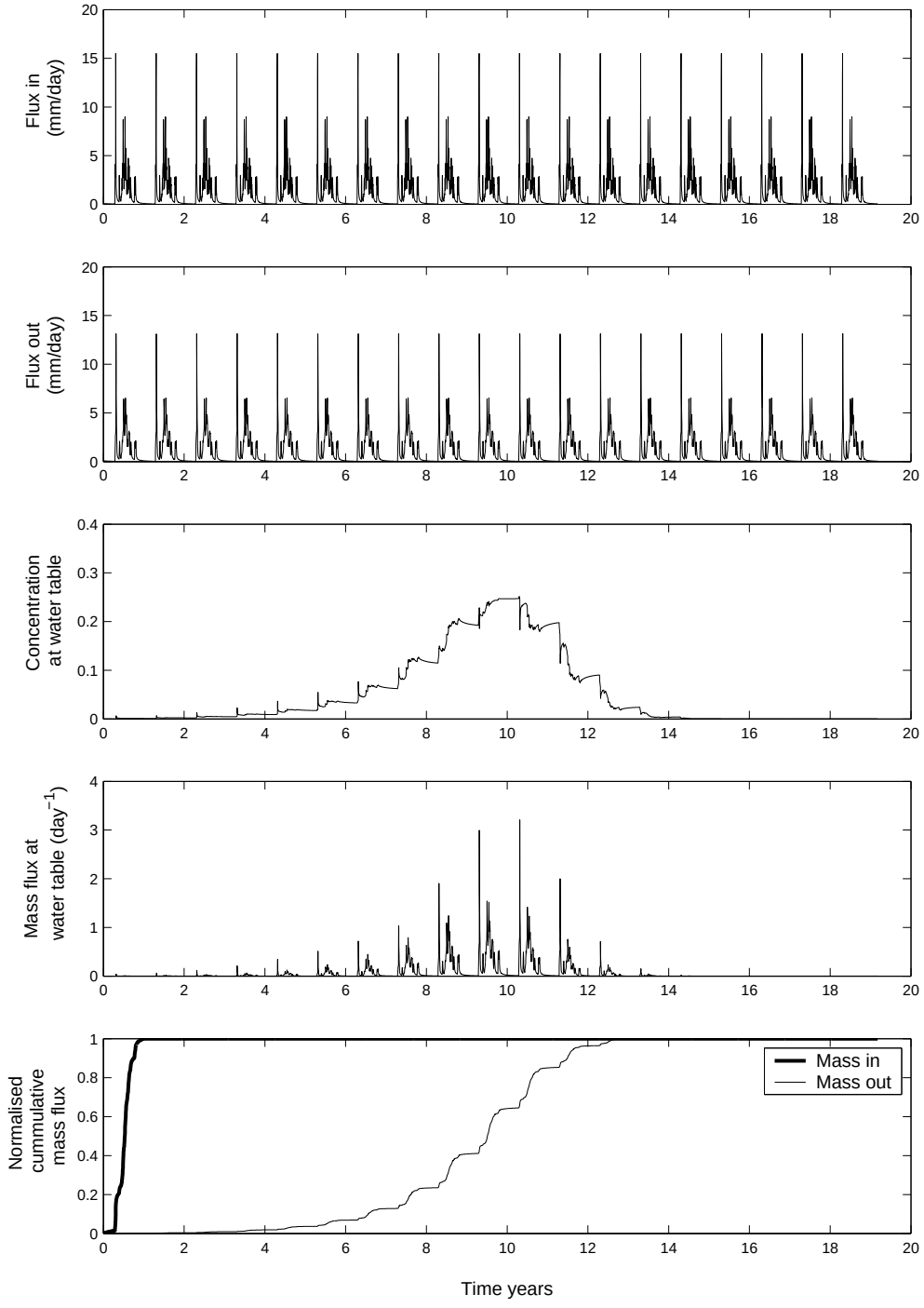

Figure 5.12 Input output data including the composite breakthrough curve from the 19 year simulation with an overlying soil layer of 40 cm.

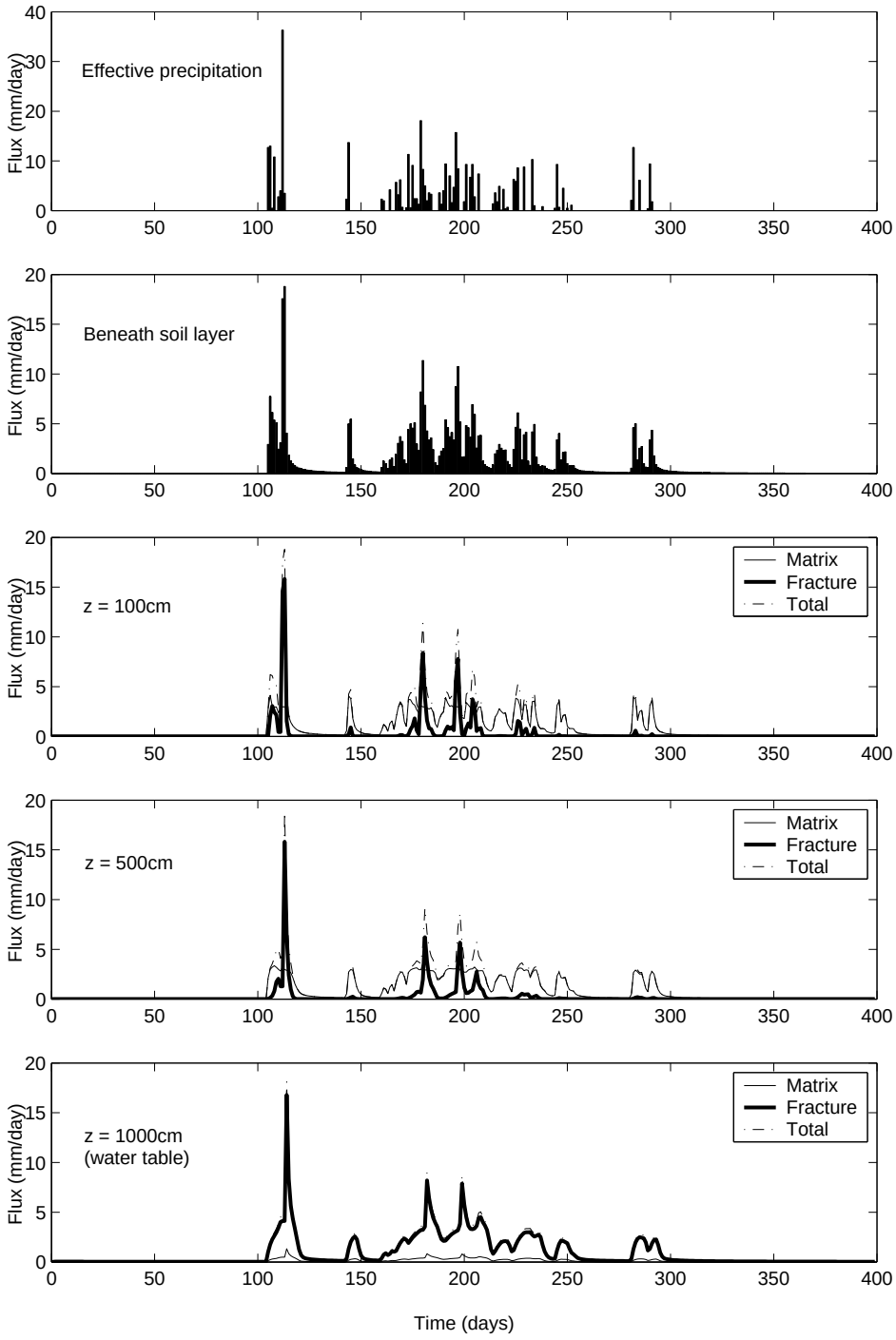

Figure 5.13 Plot of fluxes at various depths from the model with an overlying soil layer of 20 cm.

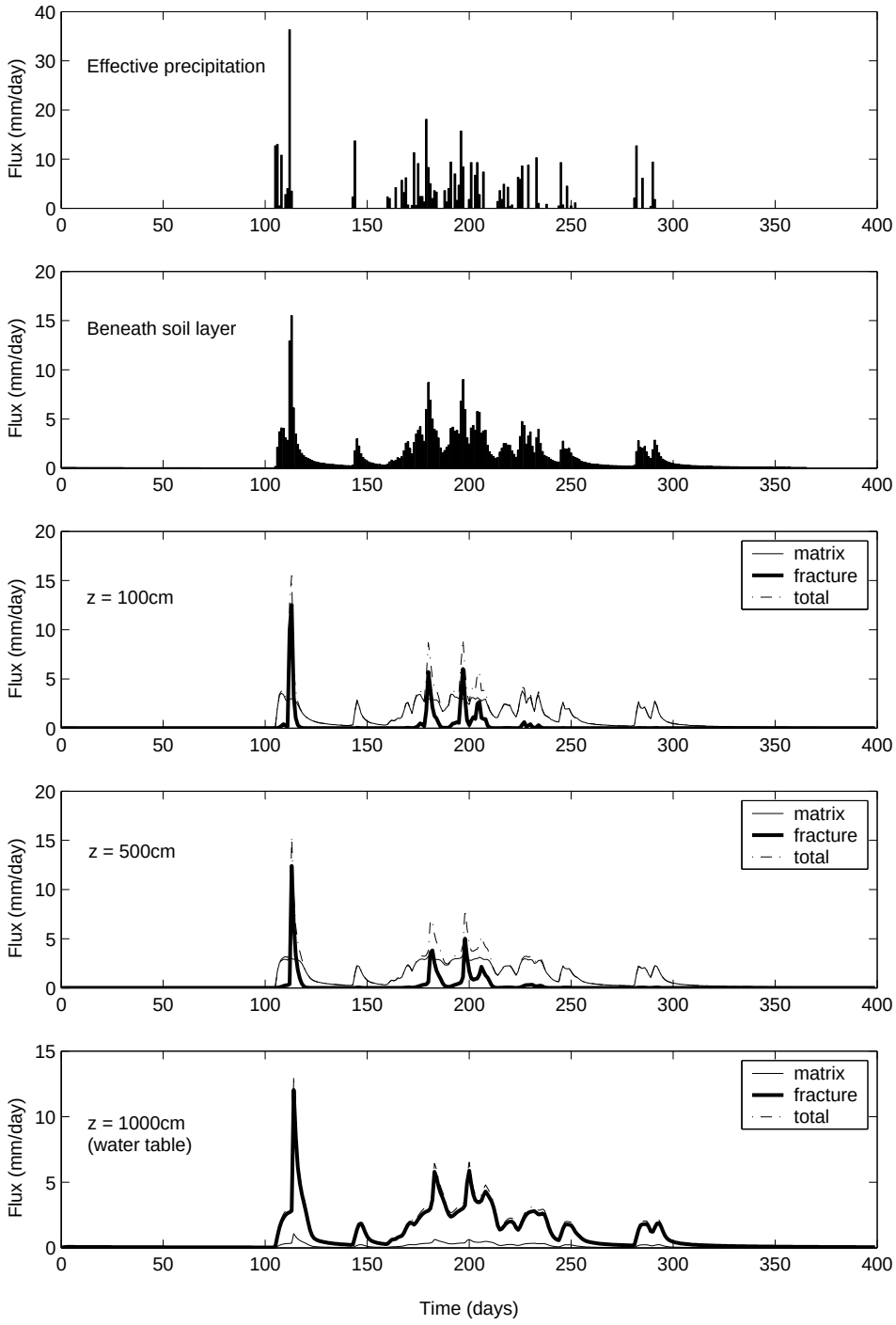

Figure 5.14 Plot of fluxes at various depths from the model with an overlying soil layer of 40 cm.

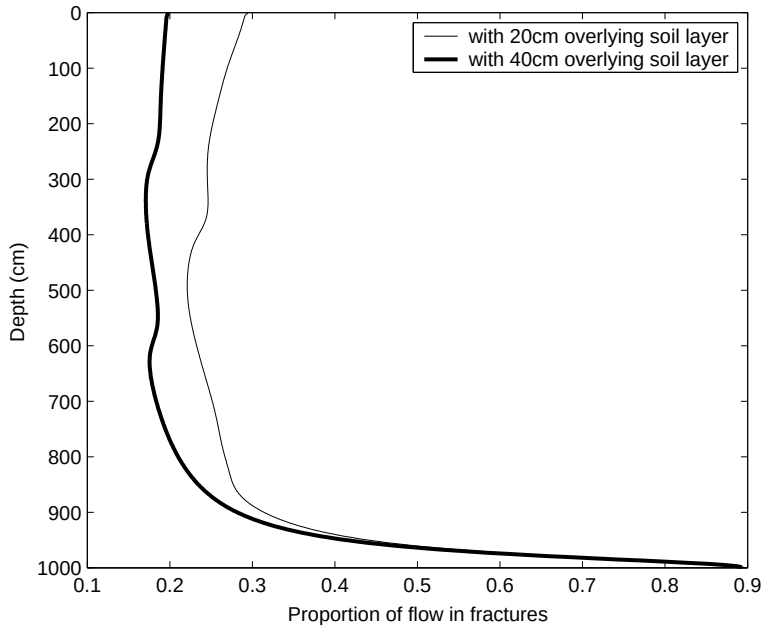

Figure 5.15 Proportion of total flow that occurs in the fractures over the year plotted against depth from the models with overlying soil layers of 20 cm and 40 cm.

Chapter 6

Summary and conclusions

6.1 Summary of thesis

Representing Fickian diffusion in numerical dual-porosity models

Prior to the findings in Chapter 3, we were originally unconvinced that significant flow occurred in the matrix of the Chalk unsaturated zone. Consequently, we were interested in developing a numerical dual-porosity model whereby longitudinal flow (parallel to the fractures) is assumed negligible in the rock matrix due to its much lower hydraulic conductivity (the sensibility of doing this in the unsaturated zone was discussed in Chapter 3). Within such models it is common to assume that fracture/matrix transfer is governed by Fickian diffusion. To avoid explicitly representing the matrix in terms of finite differences, many workers have sought to find approximations that lump a distributed matrix response into a single mean value that varies only in the direction of the fracture flow. One method of doing this is to assume that the fractures and matrix are in a quasi-steady-state (QSS) (*Barenblatt et al.*, 1960; *Warren and Root*, 1963). The diffusive flux between the fractures and matrix is then taken to be proportional to the difference between their concentrations. The problem is that when subjected to a step increase in fracture concentration, the QSS model is unable to replicate Fickian behaviour during early times. *Dykhuizen* (1990) and *Zimmerman et al.* (1993) (the Vermeulen model) proposed two alternative methods that work well during early times but are limited to monotonic fracture concentrations.

Often, these models are compared whilst assuming a step increase in fracture concentration (e.g. *Dykhuizen*, 1987, 1990; *Zimmerman et al.*, 1993). This is an unrealistic scenario as generally solute changes are less rapid. However, in systems where the characteristic block diffusion time is comparable to or greater than the timescale of change, the early time regime

is still important. For this reason, *Zimmerman et al.* (1993) also performed model comparisons with the fracture concentration increasing as a power law, an exponential law and a sinusoidal law with time but were not interested in the exponent (for power and exponential laws) or frequency (for the sinusoidal law) for which different models work better.

Natural solute functions are often periodic (and not monotonic) in nature due to climatic, seasonal or anthropogenic activities. In Section 2.5, a study was conducted to find out at what frequencies the QSS model ceases to be a good approximation to Fickian diffusion by application of a sinusoidal fracture concentration history. It was found that for dimensionless frequencies of $\Omega > 10$, the QSS model becomes an increasingly poor approximation of the Fickian model. In the context of conservative solute diffusing into Chalk blocks, this corresponds to a time period of $0.12 < t_p < 2000$ years. From this it was concluded that the QSS model is an inappropriate alternative for a Fickian model when simulating solute transport in fractured rocks where the characteristic block diffusion time, t_{cb} is greater than a year (such as in the Chalk).

Bibby (1981), *Little et al.* (1996) and *Carrera et al.* (1998) presented another lumped response model that works well for non-monotonic fracture concentrations and large values of t_{cb} because it represents a fully analytical solution to the Fickian model. However, their model considers an integral representation of Fick's second law. This requires the evaluation of a number of terms for its approximation to an infinite series. The number of terms required can be equated to the number of nodes needed for an equivalent finite difference solution. Nevertheless, our comparison study showed that the integral representation consistently offers more accurate results than our simple finite difference scheme with the same number of nodes/terms.

However, two major drawbacks of the integral representation are that it requires that the processes within the matrix are linear and that advective flow in the matrix is negligible. While the former is arguably true for the Chalk, in Chapter 2 it was concluded that the latter is not. Consequently, the finite difference method has been used to represent matrix diffusion in numerical model simulations described in the remainder of this thesis.

The significance of flow in the matrix of the Chalk unsaturated zone

All the models discussed in Chapter 2 assume that flow in the matrix is negligible. As discussed in Section 1.1, the respective contributions of flow in fractures and matrix to the behaviour of unsaturated Chalk has been the subject of much debate. Flow in the unsaturated zone of the Chalk was originally believed to be predominantly through fractures. Evidence

to support this included the observed rapid response of the water table after high intensity rainfall events (*Headworth*, 1972) and the appearance of bacteria in boreholes (*Maclean*, 1969). However, the slow migration of tritium observed in the pore-waters of the 40m deep Chalk unsaturated zone in Berkshire led *Smith et al.* (1970) to estimate that matrix flow accounted for up to 85% of the total flow.

However, although many modelling studies cite the work of *Smith et al.* (1970) as a good reason for using a fracture flow bypass of around 15%, in Chapter 3 it is suggested that this work is unsatisfactory in at least four respects: Firstly, the calculation of tritium input involved the assumption that actual evapotranspiration is the same as potential evaporation (albeit with an upper limit of soil moisture deficit). This could potentially result in an underestimation of tritium input. Secondly, *Smith et al.* (1970) do not report any consideration of decay in their mass-balance calculation, which would result in an overestimation of tritium input. Thirdly, it assumes that all tritium that had travelled through fractures remained present in the unsaturated zone profile shown in Figure 3.1. In reality, very fast flowing tritium may have flowed through the unsaturated zone and into the saturated zone. Fourthly, the errors associated with the measurements of tritium content were around $\pm 10\%$ while the values of tritium below 13m depth (assumed to be fracture flow derived) were only slightly elevated from values associated with background levels.

Troubled by the absence of surface runoff at Chalk sites, *Foster* (1975) speculated that the slow migration of tritium in the presence of a fracture-flow dominated system could be explained by retardation caused by lateral diffusion of solutes from fracture water to matrix water. This hypothesis was supported by the numerical simulations presented by *Barker and Foster* (1981). However, the sensitivity of this model was explored in Figure 3.4 using the Laplace transform solution of *Barker* (1982). It was shown that an increase in fracture spacing results in an increase in solute spreading. The extent of solute spreading for a fracture spacing of just 25cm is incompatible with the well preserved peaks in solute profiles presented by *Smith et al.* (1970), *Young et al.* (1976), *Oakes* (1977), *Oakes et al.* (1981) and *Barraclough et al.* (1994).

There is a consensus in more recent literature that flow in the Chalk unsaturated zone is a complex combination of matrix and fracture flow components (*Geake and Foster*, 1989; *Price et al.*, 2000; *Jones and Robins*, 1999; *Haria et al.*, 2003). However, the presence of significant matrix flow requires that water can easily travel across air-phase discontinuities in between the matrix blocks. No rigourous explanation for how this can occur is present in the previous literature. As has been pointed out by *Wang and Narasimhan* (1985) and *Hodnett*

and Bell (1990), these discontinuities are frequently interrupted by points of connectivity between matrix blocks. *Hodnett and Bell* (1990) suggest that as water flux increases the contact points wet up and the hydraulic conductivity increases such that they do not form a restriction to flow. However, these air phase discontinuities represent capillary barriers, which may only be overcome once pressure heads exceed the associated air entry pressures. Furthermore, as chalk blocks generally have rough surfaces this means that for most of the time there will still only be partial connection between the matrix blocks.

However, such a complicated hypothesis (which may or may not be true) is not needed (in the context of the feasibility of matrix flow). In Section 3.4 the effect of inter-block connectivity was explicitly explored using a three dimensional implementation of the Laplace equation. The equation was solved by applying a fixed head boundary at the top and bottom of a matrix block. An air-phase discontinuity was represented by applying a no-flow condition to the base of the block except at those nodes where there was connectivity to an underlying matrix block (here the fixed head condition remained). All other faces of the block were assumed impermeable due to symmetry effects caused by the assumption of equally spaced identical points of connectivity (see Figure 3.6). In this way, an effective hydraulic conductivity of the block could be calculated by dividing the total flux into the block by the overall hydraulic gradient (defined by the two fixed head conditions). The ratio of effective hydraulic conductivity over the local hydraulic conductivity (i.e. the node-scale conductivity of the matrix block) was then calculated for a range of different connectivities (the % area of the base that is connected to the underlying block). It was found that just 1% connectivity represented an effective pathway equivalent to 18% of the local rock hydraulic conductivity. *Pyrak-Nolte et al.* (1987) found that contact area within a single Stripa granite fracture ranged from 10% to 40% (depending on the effective stress). Accordingly, it was concluded that air-phase discontinuities have little effect on the feasibility of matrix flow.

In section 3.5, the impact of flow in the matrix on solute transport was then explicitly analysed by comparing the temporal moments of breakthrough curves derived from dual-porosity models (which ignore matrix flow) and equivalent dual-permeability models (which include matrix flow). It was found that the dual-permeability breakthrough curves could be well approximated by a dual-porosity model with a reduced characteristic block diffusion time. This is because as movement of water in the matrix reaches a similar velocity to water in the fractures, the two domains become closer to equilibrium with each another. Clearly, when there is no fracture flow, solute spreading is significantly reduced. However, this analysis shows that matrix flow reduces solute spreading in the presence of persistent fracture flow as

well.

All the above studies suggest that flow in the matrix of the Chalk unsaturated zone is significant and that ignoring it may result in a serious misunderstanding of the system. However, all the modelling analyses discussed so far assumed steady state flow conditions necessitating the use of annual mean estimates of infiltration. This makes it difficult to sensibly estimate the proportion of total infiltration that enters the matrix. The assumption of steady state flow also forces fracture flow to be either negligible or persistent whereas in reality it is likely to be intermittent (*Price et al.*, 2000). From this it became clear that we needed to explore the dual-permeability model under a transient flow regime.

Characterising flow in the Chalk unsaturated zone

Chapter 4 focused on the development and parametrisation of a transient flow model for the Chalk unsaturated zone. As discussed in Section 1.3, much work has been invested in the development of Richards' equation models for flow in unsaturated fractured rock as a whole. These models can be broadly classified into continuum and fracture network models (*Pruess et al.*, 1999). In this thesis, the continuum approach has been adopted due to the impracticalities of fracture-network models associated with the geometric characterisation of their fractures. In the continuum approach, fractures are considered to be sufficiently ubiquitous and distributed in such a manner that they can be meaningfully described statistically (*Bear*, 1993). The role of individual fractures in fractured media is considered to be similar to that of individual pores in porous media. Connected fractures and rock matrix are viewed as two or more overlapped interacting continua (*Liu et al.*, 2003b).

It is interesting to note that, while much effort has been focused on the acquisition of 'soil physics' data (pressure head, moisture content etc.) from Chalk sites (e.g. *Wellings*, 1984a; *Cooper et al.*, 1990; *Mahamood-ul-Hassan and Gregory*, 2002), there are no published applications of Richards' equation (with the exception of calculations of hydraulic conductivity using the instantaneous profile method) to the Chalk unsaturated zone. Chapter 4 considers all the published literature concerning characterisation of the Chalk unsaturated zone so as to derive moisture retention and relative permeability functions for both fracture and matrix continua for application to a Richards' equation model.

The first step was to conceptualise a parametric form through which to describe the continuous variations of moisture content and hydraulic conductivity with pressure head. Having reviewed the various options within the literature, a particularly simple method was selected whereby effective saturation is assumed to be defined by a power law relationship

with pressure head while relative permeability is assumed to be a power law of effective saturation. These models assume that both the fracture-aperture- and matrix pore-size frequency distributions are power functions and that hydraulic conductivity is proportional to some arbitrary power of aperture-/pore-size. Note that Poiseuille's law implies that hydraulic conductivity of a capillary tube is proportional to the tube diameter to the power of four. However, because soils and fractured rocks do not contain perfectly smooth tubes or fractures, the exponent (power) relating relative permeability to aperture-/pore-size is unknown (see Section 4.5).

Assuming that the matrix and fracture continua are homogeneous, both continua required the estimation of six parameters: residual and saturated moisture contents (θ_r and θ_s), a moisture retention exponent (λ), the air entry pressure of the largest pore/aperture with a significant presence (ψ_s), saturated hydraulic conductivity (K_s) and a relative permeability exponent η.

Characterising the matrix was relatively straightforward. Mercury intrusion experiments carried out by *Price et al.* (2000) on chalk samples from four different sites suggested that the matrix pore-size distribution is surprisingly similar across southern England. Inspection of the pore-size distributions suggested that the matrix continuum cutoff occurred at around 1 μm diameter, yielding $\psi_s = -30$ m. Fitting a power-law to the distribution then gave a moisture retention exponent of around $\lambda = 2$. Assuming a chalk porosity of 0.35 then yields $\theta_s = 0.35$ and $\theta_r = 0$. The matrix was then likened to a clay and the relative permeability exponent of $\eta = 2.5$ based on considerations of soil-physics literature (e.g. *Mualem*, 1976; *van Genuchten*, 1980). A saturated hydraulic conductivity of $K_s = 0.1$ cm/day was assumed based on observations made by (e.g. *Wellings*, 1984a; *Cooper et al.*, 1990).

Characterising the fractures was a much more subjective process. Assuming that matrix pores do not appreciably drain until pressure heads drop below -30 m, it follows that most field observations of changes in moisture content, from the Chalk unsaturated zone, represent what we have described as the fracture continuum. However, most observations of moisture content have shown very small changes (*Wellings*, 1984a; *Cooper et al.*, 1990; *Hodnett and Bell*, 1990). An exception to this are the measurements presented by *Mahamood-ul-Hassan and Gregory* (2002). However, *Mahamood-ul-Hassan and Gregory* (2002) only studied the near surface (top 1 m). This is unlikely to be representative of a further (potentially) 40 m of unsaturated zone. Consequently, we have chosen a more subjective, but more generic, approach to fracture continuum characterisation.

As with the matrix, to characterise moisture retention, we need to estimate three param-

eters: λ, ψ_s and θ_s (assuming that the fractures can completely drain, i.e. $\theta_r = 0$). We assumed a range of -20 cm$< \psi_s < -2.5$ cm on the basis that once film-flow is developed, the system acts as if 'fully saturated' (from a permeability point of view). Film flow has been seen to develop on a rock face of similar porosity to chalk for pressure heads > -10 cm (*Tokunaga and Wan*, 1997) and on glass (where there is no matrix imbibition) for pressure heads > -2.5 cm (*Tokunaga et al.*, 2000). We then made an assumption that at least 99% of the fracture continuum would have drained prior to the commencement of drainage of the matrix. The basis for this is that 'pores' in the fracture continuum, by definition, are larger (hence drain before) pores in the matrix. Having selected ψ_s, it was then possible to estimate a value for λ such that the moisture retention function satisfied the above assumptions. The saturated moisture content was then assumed to be 0.01 on the basis of specific yield estimates made from pumping tests (e.g. *Price et al.*, 1993).

Variations of fracture continuum hydraulic conductivity with pressure head were dealt with in a similar way. From considerations of the core-scale compressibility of chalk, it was estimated that fracture and matrix pressure heads should equilibrate within 10^{-2} days. It follows that pressure heads in the fractures and the matrix are essentially the same. Furthermore, most measurements of hydraulic conductivity suggest that the fracture flow starts to dominate over matrix flow once pressure heads exceed -50 cm (*Wellings*, 1984a; *Cooper et al.*, 1990; *Hodnett and Bell*, 1990; *Mahamood-ul-Hassan and Gregory*, 2002). It follows that the fracture continuum hydraulic conductivity becomes greater than that of the matrix continuum once pressure heads exceed -50 cm. Given an *a priori* constrained moisture retention curve and an estimate of saturated matrix and fracture continua hydraulic conductivity (assumed to be 0.1 and 10 cm/day), a corresponding estimate of η can be obtained.

Through some simple drainage simulations, it was shown that the above considerations result in a set of moisture retention and hydraulic conductivity functions that conform to the main observations that have been made at a number of unsaturated Chalk sites. These included: the matrix pores not draining until pressure heads become less than -3000 cm (*Price et al.*, 1976); fracture flow becoming much less than matrix flow when pressure heads fall below -50 cm (e.g. *Wellings*, 1984a; *Cooper et al.*, 1990); the fracture continuum containing an element of storage that drains almost instantaneously and an element that drains more slowly (over a period of days to months) (*Price et al.*, 2000).

Transient simulations of flow and transport in the Chalk unsaturated zone

In Chapter 5, the unsaturated flow model developed in Chapter 4 was coupled with a

solute transport model to study the effects of transient recharge on the development of solute profiles and breakthrough curves. To explore the behaviour of the model, a hypothetical scenario was developed. The one-dimensional model of the Chalk unsaturated zone featured a fixed water table at 10m depth. At the top of the model various recharge time-series were applied for a number of years. A conservative solute (that could be tritium, chloride or nitrate) was applied to the recharge for one year. Subsequent years involved the input of clean water. Although the model was essentially one-dimensional, a two-dimensional representation of the matrix continuum was required to describe the lateral diffusion of water and solute from the fracture continuum. Note that while water pressure can be expected to equilibrate within the matrix block in less than 10^{-2} days (see Section 4.3), solutes may take several years (see Section 2.5).

The recharge time-series was constructed using the Penman-Grindley model (as described by *Ragab et al.*, 1997). Daily potential evaporation and precipitation data from the Kennet catchment for the period of 30th June 1993 to 29th June 1994 was used. The same year was repeated for twenty five years so as to ensure that each year had the same annual total of recharge.

Despite the assumption of a homogenous fracture (with a randomly rough surface) lying alongside a homogenous matrix block, the developed model had a large number of parameters. These included: for both the matrix and fracture continua, the moisture retention and relative permeability function parameters (ψ_s, λ, η), the residual and saturated moisture contents (θ_r and θ_s), the saturated hydraulic conductivity (K_s), an apparent diffusion coefficient (D_A), a hydrodynamic dispersivity (α), in addition to a fracture-width ($2a$) and a fracture spacing ($2b$), i.e. 20 parameters in total.

In Section 4.7, fracture continuum parameter sets were derived for various assumed values of ψ_s. It was found that simulated solute profiles was generally insensitive to these. This is because all the fracture parameter sets define a system whereby a fraction of fracture-water de-waters very quickly while the remainder drains very slowly (see Section 5.4).

In Section 5.5, the sensitivity to temporal sampling was also explored. The recharge time-series was re-sampled to weekly, monthly, quarterly and yearly time-steps. It was found that with increasing temporal sampling, the profiles became increasingly dispersed with longer forward tails. This is due to increased infiltration rates (albeit more sparsely distributed) which have to go through the fractures. Another apparent feature was that the solute peak movement increased with decreasing temporal sampling. This can be explained by more water (and solute mass) directly entering the matrix. It also clearly shows that the steady

state flow assumption can lead to erroneous data interpretation.

The simulations also highlighted the potential significance of flow attenuation within an overlying soil layer. Section 5.6 explored the effects of overlying soil layers. The recharge time-series was applied to a Richards' equation model of a silt loam column. Water flux were recorded at 20, 40, 60 and 80 m depth and then applied to the top of the Chalk model. As with increasing temporal sampling, decreasing thickness of overlying soil layers caused the profiles to become increasingly dispersed with longer forward tails. It was found that, with an overlying soil layer of 80 cm and with the saturated hydraulic conductivity of the Chalk matrix set at 0.3 cm/day, there was almost negligible forward tailing. The reason was that variations in the infiltration rate had been attenuated to such an extent that it was predominately less than 0.3 cm/day and could therefore easily be accommodated by the matrix.

While the plotted solute profiles from all simulations looked very smooth, the corresponding breakthrough curves at the water table were not. The presence of fracture flow caused large spikes to protrude the underlying long-term concentration trend associated with transport in the matrix. These spikes can be explicitly related to extreme events within the infiltration time-series which have skimmed off solute from matrix. However, studies of the cumulative mass flux at the water table suggest that in the context of total mass, these may not be important.

In Chapter 3 it was suggested that the inclusion of matrix flow would solve the forward tailing conundrum associated with dual-porosity models. However, the magnitude of matrix flow is still very small as compared to the recharge estimates from the Penman-Grindley model. As a result most of the simulations described in Chapter 5 show significant forward tailing. This could suggest that the Penman-Grindley model does not predict recharge in an appropriate manner for the Chalk. If our model is reasonable, and forward tailing is not something that should occur, then the recharge estimates must be substantially attenuated to allow more of the water to be absorbed by the matrix. This was illustrated by the exploration of various thicknesses of overlying soil layers. It seems that a soil layer as deep as 80 cm is required to dampen the recharge sufficiently. Generally overlying soil layers on Chalk outcrops are very shallow ≈ 25 cm. However, the further attenuation could be accounted for through the storage that might be expected in the surficial weathered Chalk layers which can extend for several metres.

6.2 Conclusions

The objective of this thesis was to develop a unified physically-based modelling framework for unsaturated Chalk that is consistent with observed (often contradicting) phenomena at Chalk sites. These include: a fast water table response to rainfall events (in days) and an absence of surface run-off (*Headworth*, 1972); slow solute migration (in tens of years) with very little dispersion (*Oakes et al.*, 1981); specific yields that can vary an order of magnitude during droughts (*Price et al.*, 2000). Following the above discussion, it is believed that the model described in Chapter 5 meets these criteria.

Furthermore, the resulting work has given rise to some important conclusions regarding modelling and understanding flow and transport in the Chalk unsaturated zone. To summarise, these are that: given the current state of knowledge, the dual continua approach is a reasonable method for simulation of flow and transport in the Chalk unsaturated zone; the importance of transient effects has been previously neglected; overlying soil and weathered chalk layers are likely to cause significant attenuating effects on flow such that at depth, almost all flow occurs through the matrix.

6.3 Recommendations for future modelling

Useful recommendations for future modelling can be made through a discussion of the limitations in this thesis. Generally, limitations have been dealt with progressively, leading to the modelling studies detailed in Chapter 5. Consequently, this discussion is largely focused on the work detailed in Chapter 5. By far the largest limitation is the assumption of a homogenous matrix block lying alongside a homogenous fracture (albeit with a randomly rough surface).

The Chalk is highly heterogonous, specifically in respect to fracture spacing and fracture porosity (*Bloomfield*, 1996). Furthermore, the Chalk unsaturated zone can take many different forms. Often there is a loamy soil layer ($\approx$ 25 cm), followed by a weathered Chalk layer (up to several metres deep) followed by unweathered Chalk, which is likely to be punctuated by various marl seams and flint layers. Weathered Chalk is not a well defined description. Weathered Chalk can refer to putty Chalk (which is quite clayey), gravelly Chalk mixed with clayey deposits or something else (*Jones and Robins*, 1999). Similarly, unweathered Chalk can take many different forms in terms of fracture intensity and structure (*Bloomfield*, 1996).

Heterogeneity has been ignored because this thesis has been focused on the generic behaviour of unsaturated fractured Chalk in a modelling context. Although heterogeneity has

not been characterised, this thesis provides an idea as to how these affects might manifest themselves in solute concentration data. For example, Chapter 3 showed that increasing fracture spacing increases the matrix block diffusion time, and consequently the extent of dispersion in a solute plume. From Chapter 4, increased fracture density, increases water storage available in the unsaturated zone, which is likely to attenuate recharge at the surface. From Chapter 5, we know that such an effect will allow more water to travel through the Chalk matrix, thus reducing the dispersion of a solute plume.

In numerical simulations of flow and solute transport in a single porous medium, representing heterogeneity is achieved by assuming that the individual computational elements are assumed to be sufficiently large so that it is meaningful to assign suitably averaged effective properties to them (e.g. *Bear*, 1972). This can be achieved for dual-porosity media (where matrix flow is ignored) using the Multiple INteracting Continua (MINC) method (*Pruess and Narasimhan*, 1985). Within MINC, matrix blocks are discretised into nested shell-like cells. For example, consider Figure 6.1. All fractures are lumped into continuum 1, all matrix material within a certain distance from the fractures is lumped into continuum 2, matrix material at larger distance becomes continuum 3, and so on. The MINC model essentially offers an extra dimension which represents the distance of a point to its nearest fracture face. As a consequence, different fracture spacings can be suggested in a single element by specifying the space step between each nested matrix cell.

The problem with the Chalk unsaturated zone is that matrix flow cannot be ignored. Within the MINC model, a nested cell is only linked to its neighbouring cells within its element. If matrix flow is to be considered, nested cells must be linked to a global matrix of nested cells as well. It is not clear how to parameterise such a system using simple geometric considerations.

As a result, despite the inability of the QSS model to represent the early time behaviour associated with Fickian models (even in systems where early time behaviour is important) it has often been used in situations where matrix flow is an important factor (see *Doughty*, 1999). The QSS model represents a special case of the MINC model when there is only one nested cell for the matrix. For dual-permeability situations (where matrix flow is incorporated) these nested cells are linked together in exactly the same way as their associated fracture cells. Such an approach can be condoned when the effects of heterogeneity are more important than the early time behaviour associated with Fickian models. Clearly, there would be value in exploring the effects of weathered chalk layers using a QSS approximation. The governing equations for such a model were described by *Gerke and van Genuchten* (1996) and are

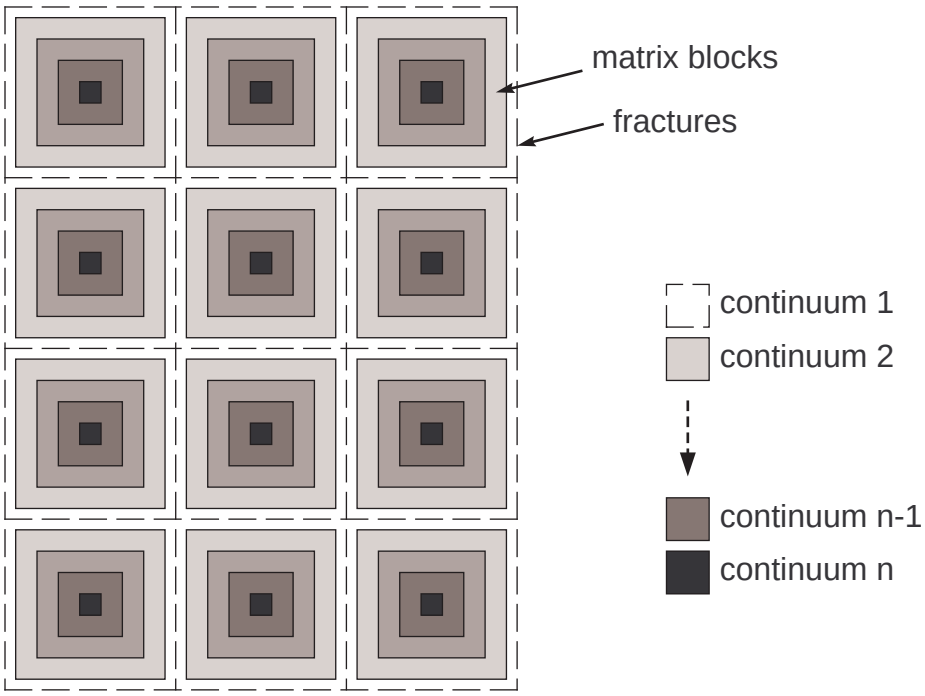

Figure 6.1 Subgridding in the method of 'multiple interacting continua' (MINC).

discussed further within Appendix A.

Another limitation associated with the model detailed in Chapter 5 is the assumption of a fixed water table boundary. The problem with one-dimensional vertical flow models is that they do not have enough information to dictate a variable depth water table. At least a two-dimensional representation is needed because the water table is dependant not only on infiltration, but also on the capacity for the saturated zone to move water away. An explicit representation of a variable water table depth is needed to properly understand how solute leaves the unsaturated zone and enters the saturated zone.

The Chalk saturated zone is known to be made up of almost discrete horizontal flow horizons (*Price et al.*, 1993). As the water table rises, new horizons are activated. It is speculated that as new horizons are activated, more solute from the SUZ (seasonal unsaturated zone) matrix is diffused into the groundwater. This is believed to explain the close correlation between the solute concentrations in abstraction water with water table depth fluctuations (*Callender*, 2002). The reason this has not been further explored is because each 5 year one-dimensional simulation takes at least 7 hours of computer time, using MATLAB release 13 with a Pentium 2.66 GHz processor. An equivalent two-dimensional model would potentially take months. Further work is needed to look at how to simplify the computation process.

Much time has been spent in optimising the source-code that describes FLOWTRAN2D (see attached CD) but improvements can always be made. It is possible that computer time could be reduced by developing a compiled executable using FORTRAN or C++.

To summarise: the possibility of reducing computation time by using a different code (FORTRAN, C++ etc.) should be explored; the effects of variability in fracture density should be investigated using a QSS approach; it would be interesting to explore the effects of a variable water table on solute concentrations in the saturated zone using a two-dimensional model (possibly also using the QSS approach).

6.4 Recommendations for future data collection

A general lack of observed data necessary to constrain the developed model has been a major issue throughout this project. This seems surprising given that the bulk of literature discussing the Chalk unsaturated zone (of which there is plenty) has been mostly concerned with the acquisition of data.

Field experiments conducted on the Chalk unsaturated zone can be broadly classified into two groups: solute transport and flow. Solute transport experiments have generally involved the collection of pore-water concentrations for tracers of concern (natural or applied) at various depths (*Smith et al.*, 1970; *Young et al.*, 1976; *Oakes*, 1977; *Oakes et al.*, 1981; *Wellings*, 1984b; *Geake and Foster*, 1989; *Barraclough et al.*, 1994; *Haria et al.*, 2003). Flow experiments have generally involved the collection of moisture content and pressure head at various depths and times along with other driving forces (such as precipitation and evaporation) (*Wellings and Bell*, 1980; *Wellings*, 1984a; *Cooper et al.*, 1990; *Hodnett and Bell*, 1990; *Mahamood-ul-Hassan and Gregory*, 2002; *Haria et al.*, 2003). Note that pore-water profile measurements are rarely sampled more than two or three times because they change very slowly (*Oakes et al.*, 1981; *Geake and Foster*, 1989). In contrast, the hydraulic profiles (moisture content and pressure head) change much faster.

Pore-water profiles alone, are not sufficient for constraining a coupled flow and transport model. Evidence for this can be seen in the excellent model fits presented by *Oakes et al.* (1981) using a uniform velocity solute transport model with a 15% bypass (which given the uncertainty associated with the contaminant inputs was probably not necessary). Successful calibration of a model to these pore-water profiles merely suggests that the model of concern might be capable of predicting the long-term trends in solute concentration. Little knowledge is gained in regards to the sub-annual dynamics of flow which is important when trying to

understand aquifer recharge on a daily time-scale.

To constrain a Richards' equation based flow model we need pressure head and moisture content data (both together are commonly referred to as soil physics data). Within the literature there are several detailed soil physics data collection studies looking explicitly at flow processes in the Chalk unsaturated zone (e.g. *Wellings*, 1984a; *Cooper et al.*, 1990; *Hodnett and Bell*, 1990; *Mahamood-ul-Hassan and Gregory*, 2002; *Haria et al.*, 2003). These data sets are generally limited to the near surface (< 3m depth) (with the exception of *Wellings*, 1984a) and low temporal frequency sampling (typically weekly) of moisture content (with the exception of *Mahamood-ul-Hassan and Gregory*, 2002).

The problem with these data sets is the lack of data covering periods when the Chalk is at its wettest. This is largely due to the temporal frequency of data sampling. While high temporal resolution is often achieved for the collection of pressure head data (through the use of pressure transducers), this is not the case for moisture content (with the exception of *Mahamood-ul-Hassan and Gregory*, 2002, who used a logged theta probe). Both are needed for accurate calculation of water fluxes which are helpful when trying to perform some form of model validation. This issue is being addressed within the NERC thematic programme, LOCAR, where a number of Chalk sites have been instrumented with a variety of different instruments that are being logged every 15 minutes. These data will be presented and analysed in a subsequent PhD thesis currently being undertaken by Andrew Ireson also at Imperial College London.

To further explore the role of weathered chalk layers on fracture flow attenuation, a particulary useful parameter that could be obtained from such data would be estimates of residual and saturated moisture contents at different depths. Assuming that the matrix pores do not drain (which can be checked from the pressure head record) the difference between the two is essentially an estimate of fracture porosity. Further assuming that all fractures contain randomly rough surfaces but are statistically homogenous (i.e. each fracture can be characterised with the same fracture-aperture distribution function) a corresponding estimate of fracture spacing can be obtained. It would therefore be possible to characterise the variation of fracture-matrix transfer coefficients with depth (associated with varying degrees of weathering) for use in a QSS dual-permeability modelling framework.

In short, the following recommendations can be made for future studies looking to acquire soil physics data describing the Chalk unsaturated zone: automatically logged instruments should be used for measuring moisture content and pressure head to properly capture events when the chalk is wettest; whereas in the past instrumentation has generally been restricted

to the near surface (< 3 m depth), deeper profiles should be explored, at least several metres beyond soil and weathered layers; furthermore, these measurements should be accompanied by monitoring of the water table; integrated instrumentation should also be continuous in time over several years to properly capture the seasonal dynamics.

6.5 Implications for catchment-scale nutrient modelling

Earlier in Section 1.4, it was stated that there is much interest in developing catchment-scale nutrient models (CSNM) for Chalk catchments in the United Kingdom. Complicated physically-based models are not practical for this purpose due to their large parameter requirements. More simple conceptual models are preferred. Typically, conceptual models separate catchments into conceptual stores. Each store is then treated as a continuously stirred tank reactor (CSTR) characterised by a resident time, obtained from calibration against observed data (*Whitehead et al.*, 1997, 1998).

The assumption of a completely mixed system (i.e. as assumed with a CSTR) has been found to be inappropriate even for river quality problems. This is largely due to the presence of dead-zones, associated with plant growth on the river bed, where there is generally a much slower flow of water. Two approaches have been developed to account for the incomplete mixing in river water: the aggregated dead zone model (ADZ) (*Beer and Young*, 1983) and the transient storage model (TS) (*Bencala and Walters*, 1983). The ADZ model is a box (CSTR style) model that considers a number of identical mixing tanks in series and an explicit time delay parameter. The TS model is a formulation of the advection dispersion equation with a first-order mass transfer term to characterise lateral diffusion of solute into a conceptualised dead zone.

The ADZ model is preferred because it has fewer parameters and is easier to implement (*Lees et al.*, 2000). The ADZ model is very much in line with the CSTR model structures commonly used in conceptual CSNMs (e.g. *Lees et al.*, 1998; *Whitehead et al.*, 1998). Recently, *Lees et al.* (2000) used a moment matching technique to examine relationships between parameters of two different in-stream solute transport models, the transient storage (TS) model and the aggregated dead zone (ADZ) model. Optimisation of the models against breakthrough curves obtained from in-stream tracer test data showed that both equations can characterise a breakthrough curve with very similar moments. On this basis *Lees et al.* (2000) speculated that analytical moment relationships between the two models can be used to infer parameters from one model to the other. Interestingly, the TS model equations are

mathematically analogous to those of the dual-porosity model often used for solute transport simulations in sandstone (*Coats and Smith*, 1964) and macroscopically aggregated soils (*van Genuchten and Wierenga*, 1976). Building on this analogy, *Mathias et al.* (2004) (also see Appendix B) explored the applicability of this approach for parameterising an ADZ model for a fractured rock system such as the Chalk.

Estimating ADZ parameters, that characterise subsurface environments, from closed-form relationships linking ADZ models to more physically-based models is appealing because no suitable method is available for obtaining observed data (such as input-output solute concentration time-series, see Section 1.4) to calibrate the ADZ resident and lag time parameters. However, *Mathias et al.* (2004) found that the extent of non-equilibrium between fractures and matrix was much larger than would be expected between dead and flowing zones in rivers. Consequently, it was concluded that the ADZ model was not suitable in this context. Furthermore, the model explored by *Mathias et al.* (2004) (along with the TS model explored by *Lees et al.*, 2000) assumed no flow in the matrix and steady state flow conditions. In Chapters 3 and 5 it has been shown that such assumptions can lead to erroneous results when dealing with the Chalk unsaturated zone. It is not clear how to modify the *Lees et al.* (2000) methodology for this purpose.

As a result, current research at Imperial College London is focusing on a more pragmatic approach, which accepts that solute mass and water movements behave extremely differently. Let us concentrate on three widely accepted characteristics of unconfined Chalk aquifers. Water table levels respond quickly to rainfall events (in days) (*Headworth*, 1972). Solutes migrate through the unsaturated zone very slowly (around 1 m/year) (*Oakes et al.*, 1981). Conversely, solutes in the saturated zone can be expected to travel much faster through saturated fractures (*Foster*, 1993). A simple conceptual modelling approach that satisfies these phenomena would be one where flow is dealt with an arrangement of linear stores (e.g. *Wheater et al.*, 2002) while solute mass arrives at a river reach according to some specified distribution of travel times. Given that solutes typically travel at 1m/year through the unsaturated zone, assuming that the saturated travel times are negligible (as compared to unsaturated zone travel times), an idea of the travel time distribution could be obtained from the statistical distribution of unsaturated zone thickness within a hillslope. Such data can be easily obtained using a GIS database of digital terrain data.

The above model essentially assumes a plug flow of solutes through the unsaturated. Although the simulated breakthrough curves in Chapter 5 show significant solute spreading and a complex array of spikes associated with fracture flow events, these need not be the case

in the field. A more realistic model (as compared to that in Chapter 5) would incorporate a soil layer, followed by a gradual grading of fracture density which gets smaller with depth. It can be anticipated that such a system would greatly attenuate infiltration allowing more flow to occur in the matrix which would then significantly reduce solute spreading to a level more in line with the field observations made by, among others, *Oakes et al.* (1981). Work is in hand (*Jackson et al.*, 2005) to investigate the performance of this conceptualisation further.

References

Abbot, M. B., J. C. Bathurst, J. A. Cunge, P. E. O'Connel, and J. Rasmussen (1986a), An introduction to the European Hydrological System - Systeme Hydrologique Europeen, "SHE", 1: History and philosophy of a physically-based, distributed modelling system, *J. Hydrol.*, *87*, 45–59.

Abbot, M. B., J. C. Bathurst, J. A. Cunge, P. E. O'Connell, and J. Rasmussen (1986b), An introduction to the European Hydrological System - Systeme Hydrologique Europeen, "SHE", 2: Structure of a physically-based, distributed modelling system, *J. Hydrol.*, *87*, 61–77.

Andrews, R. J., J. W. Lloyd, and D. N. Lerner (1997), Modelling of nitrate leaching from arable land into unsaturated soil and chalk 1. Development of a management model for applications of sewage sludge and fertiliser, *J. Hydrol.*, *200*, 179–197.

Aris, R. (1958), On the Dispersion of Linear Kinematic Waves, *Proc. of the Royal Soc. of London. Series A, Mathematical and Physical Sciences*, *245*(1241), 268–277.

Barenblatt, G. I., I. P. Zheltov, and I. N. Kochina (1960), Basic concepts in the theory of seepage of homogenous liquids in fissured rocks (strata), *J. Appl. Math. Mech.*, *24*, 1286–1303.

Barker, J. A. (1982), Laplace Transform Solutions for Solute Transport in Fissured Aquifers, *Adv. Water Resour.*, *5*, 98–104.

Barker, J. A. (1985), Block-geometry functions characterising transport in densely fissured media, *J. Hydrol.*, *77*, 263–279.

Barker, J. A. (1991), Transport in fractured rock, in *Applied Groundwater Hydrology*, edited by R. A. Downing and W. B. Wilkinson, pp. 199–216, Clarendon Press, Oxford.

Barker, J. A. (1993), Modelling groundwater flow and transport in the Chalk, in *The Hydrogeology of the Chalk of North-West Europe*, edited by R. A. Downing, M. Price, and G. P. Jones, pp. 59–66, Clarendon Press, Oxford.

Barker, J. A., and S. S. D. Foster (1981), A diffusion exchange model for solute movement in fissured porous rock, *Quart. J. Eng. Geol.*, *14*, 17–24.

Barker, J. A., T. E. J. Wright, and B. A. Fretwell (2000), A pulsed-velocity method of double-porosity solute transport modelling, in *Tracers and Modelling in Hydrogeology*, edited by A. Dassargues, 262, pp. 297–302, IAHS.

Barraclough, D., C. M. K. Gardner, S. R. Wellings, and J. D. Cooper (1994), A tracer investigation into the importance of fissure flow in the unsaturated zone of the British Upper Chalk, *J. Hydrol.*, *156*, 459–469.

Bear, J. (1972), *Dynamics of Fluids in Porous Media*, Elsevier, New York.

Bear, J. (1993), Modelling flow and contaminant transport in fractured rocks, in *Flow and Contaminant Transport in Fractured Rock*, edited by J. B. Bear, C. F. Tsang, and G. de Marsily, pp. 1–37, Academic Press, Inc., New York.

Beaulac, M. N., and K. M. Reckhow (1982), An examination of land use - nutrient export relationships, *Water Resource Bulletin*, *18*, 1013–1024.

Bechtel SAIC Company (2003), UZ Flow Models and Submodels, *Analysis Model Report MDL-NBS-HS-000006 REV01*, Bechtel SAIC Company, Las Vegas, Nevada.

Beer, T., and P. C. Young (1983), Longitudinal dispersion in natural streams, *J. Environ. Eng.*, *109*(5), 1049–1067.

Bell, F. G., J. C. Cripps, C. N. Edmonds, and M. G. Culshaw (1990), Chalk fabric and its relation to certain geotechnical properties, in *Chalk*, edited by J. B. Burland, pp. 187–194, Thomas Telford, London.

Bencala, K. E., and R. A. Walters (1983), Simulation of Solute Transport in a Mountain Pool-and-Riffle Stream: A Transient Storage Model, *Water Resour. Res.*, *19*(3), 718–724.

Bertels, S. P., D. A. DiCarlo, and M. J. Blunt (2003), Measurment of aperture distribution, capillary pressure, relative permeability, and in situ saturation in a rock fracture using computed tomography scanning, *Water Resour. Res.*, *37*(3), 649–662.

Beven, K., and P. C. Young (1988), An aggregated mixing zone model of solute transport through porous media, *J. Cont. Hydrol.*, *3*, 129–143.

Beven, K. J. (1989), Changing Ideas in Hydrology - The Case of Physically Based Models, *J. Hydrol.*, *105*, 157–172.

Bibby, R. (1981), Mass Transport of Solutes in Dual-Porosity Media, *Water Resour. Res.*, *17*(4), 1075–1081.

Binley, A. M., and K. J. Beven (1989), A physically based models of heterogeneous hillslopes 2. Effective hydraulic conductivities, *Water Resour. Res.*, *25*(6), 1227–1223.

Binley, A. M., J. Elgy, and K. J. Beven (1989), A physically based models of heterogeneous hillslopes 1. Runoff production, *Water Resour. Res.*, *25*(6), 1219–1226.

Birkinshaw, S. J., and J. Ewen (2000), Nitrogen transformation component for SHETRAN catchment nitrate transport modelling, *J. Hydrol.*, *230*, 1–17.

Bloomfield, J. (1996), Characterisation of hydrologically sigificant fracture distributions in the Chalk: an example from the Upper Chalk of southern England, *J. Hydrol.*, *184*, 355–379.

Bromwich, T. J. I., and T. M. Macrobert (1947), *Theory of Infinite Series*, Macmillan and Co., Limited.

Brooks, R. H., and A. T. Corey (1966), Properties of porous media affecting flow, *J. Irrig. Drain. Div. ASCE*, *92*(IR2), 61–88.

Brown, S. R., H. W. Stockman, and S. J. Reeves (1995), Applicability of the Reynolds equation for modelling fluid flow between rough surfaces, *Geophys. Res. Lett.*, *22*(18), 2537–2540.

Brutsaert, W. (1967), Some methods of calculating unsaturated permeability, *Trans. ASAE*, *10*, 400–404.

Buckley, K. M., A. M. Binley, and K. J. Beven (1995), Calibration and predictive uncertainty estimation of groundwater quality models: application to Twin Lake Tracer Test, in *Groundwater Quality Models*, 220, pp. 205–214, IAHS.

Burdine, N. T. (1953), Relative permeability calculation from size distribution data, *Trans. AIME*, *198*, 71–78.

Callender, I. J. (2002), *Modelling Time & Groundwater Level Dependant Nitrate Concentrations at Abstraction Wells in the Chalk*, MSc Thesis, Imperial College of Science, Technology and Medicine, London.

Carey, M. A., and J. W. Lloyd (1985), Modelling non-point sources of nitrate pollution of groundwater in the Great Ouse Chalk, U.K., *J. Hydrol.*, *78*, 83–106.

Carrera, J., X. Sanchez-Vila, I. Benet, A. Medina, G. Galarza, and J. Guimera (1998), ON matrix diffusion: formulations, solution methods and qualitative methods, *Hydrogeol. J.*, *6*, 178–190.

Carslaw, H. S., and J. C. Jaeger (1949), *Operational Methods in Applied Mathematics*, Oxford University Press, Oxford.

Carslaw, H. S., and J. C. Jaeger (1980), *Conduction of Heat in Solids*, Claredon Press, Oxford.

Cash, J. R., and A. H. Karp (1990), A variable order Runge-Kutta method for initial value problems with rapidly varying right-hand sides., *ACM Trans. on Mathematical Software*, *16*, 201–222.

Chapra, S. C., and R. P. Canale (1998), *Numerical Methods for Engineers*, WCB McGraw-Hill, London.

Coats, K. H., and B. D. Smith (1964), Dead-end pore volume and dispersion in porous media, *Soc. of Pet. Eng. J.*, *4*, 73–84.

Cooper, J. D., C. M. K. Gardner, and N. MacKensie (1990), Soil water controls on recharge to aquifers, *J. Soil Sci.*, *41*, 613–630.

Copson, E. T. (1947), On the problem of the electrified disc, *Proc. Edinburgh Math. Soc.*, *8*, 14–19.

Crank, J. (1975), *The Mathematics of Diffusion*, Clarendon, Oxford.

Dahan, O., R. Nativ, E. M. Adar, and B. Berkowitz (1998), A measurement system to determine water flux and solute transport through fractures in the unsaturated zone, *Groundwater*, *36*, 444–449.

Dahan, O., R. Nativ, E. M. Adar, B. Berkowitz, and Z. Ronen (1999), Field observation of flow in a fracture intersecting unsaturated chalk, *Water Resour. Res.*, *35*(11), 3315–3326.

Dahan, O., R. Nativ, E. M. Adar, and B. Berkowitz (2001), Water Flow and Solute Transport in Unsaturated Fractured Chalk, in *Flow and Transport Through Unsaturated Fractured Rock, Second Edition*, edited by D. D. Evans, T. J. Nicholson, and T. C. Rasmussen, Geophysical Monograph 42, pp. 183–196, AGU, Washington, DC.

Davis, P. M., and T. C. Atkinson (2000), Longitudinal dispersion in natural channels: 3. An aggregated dead zone model applied to the River Severn, UK, *Hydrol. Earth Syst. Sci.*, *4*(3), 373–381.

de Hoog, F. R., J. H. Knight, and A. N. Stokes (1982), An improved method for numerical inversion of Laplace transforms, *S.I.A.M. J. Sci. and Stat. Comput.*, *3*, 357–366.

de Marsily, G. (1986), *Quantitative Hydrogelogy*, Academic Press, Inc.

Doughty, C. (1999), Investigation of conceptual and numerical approaches for evaluating moisture, gas, chemical, and heat transport in fractured unsaturated rock, *J. Cont. Hydrol.*, *38*, 69–106.

Downing, R. A., M. Price, and G. P. Jones (1993), The making of an aquifer, in *The Hydrogeology of the Chalk of North-West Europe*, edited by R. A. Downing, M. Price, and G. P. Jones, pp. 1–13, Clarendon Press, Oxford.

Dragila, M. I., and S. W. Wheatcraft (2003), Free-Surface Films, in *Conceptual Models of Flow and Transport in the Fractured Vadose Zone*, pp. 217–241, National Academy Press, Washington, D.C.

Dunn, S. M., A. J. A. Vinten, A. Lilly, J. DeGroote, M. A. Sutton, and M. McGechan (2004), Nitrogen Risk Assessment Model for Scotland: I. Nitrogen leaching, *Hydrol. Earth Syst. Sci.*, *8*(2), 191–204.

Dykhuizen, R. C. (1987), Transport of solutes through unsaturated fractured media, *Water Res.*, *21*(12), 1531–1539.

Dykhuizen, R. C. (1990), A new coupling term for double-porosity models, *Water Resour. Res.*, *26*(2), 351–356.

Ewen, J. (1997), 'Blueprint' for the UP Modelling System for Large Scale Hydrology, *Hydrology and Earth System Sciences*, *1*, 55–69.

Ewen, J., G. Parkin, and P. E. O'Connell (2000), SHETRAN: Distributed river basin flow and transport modelling system, *Journal of Hydrological Engineering*, *229*, 265–280.

Fabryka-Martin, J. T., A. V. Wolfsberg, P. R. Dixon, S. Levy, J. Musgrave, and H. J. Turin (1996), Summary report of chlorine-36 studies: sampling, analysis and simulation of chlorine-36 in the Exploratory Studies Facility, Los Alamos National Laboratory Report LA-CST-TIP-96-002., *Tech. rep.*, Los Alamos National Laboratory.

Flint, A. L., L. E. Flint, G. S. Bodvarsson, E. M. Kwicklis, and J. Fabryka-Martin (2001), Evolution of the conceptual model of unsaturated zone hydrology at Yucca Mountain, Nevada, *J. Hydrol.*, *247*, 1–30.

Foster, S. S. D. (1975), The Chalk groundwater tritium anomaly - a possible explanation, *J. Hydrol.*, *25*, 159–65.

Foster, S. S. D. (1993), The Chalk aquifer - its vulnerability to pollution, in *The Hydrogeology of the Chalk of North-West Europe*, edited by R. A. Downing, M. Price, and G. P. Jones, pp. 93–112, Clarendon Press, Oxford.

Foster, S. S. D., and A. Smith-Carington (1980), The Interpretation of Tritium in the Chalk Unsaturated Zone, *J. Hydrol.*, *46*, 343–364.

Fretwell, B. A., W. Burgess, and J. A. Barker (2000), Contaminant retardation within the seasonally unsaturated zone of the Chalk aquifer: the SUZ process, in *Tracers and Modelling in Hydrogeology*, edited by A. Dassargues, 262, pp. 385–390, IAHS.

Geake, A. K., and S. S. D. Foster (1989), Sequential isotope and solute profiling in the unsaturated zone of British Chalk, *Hydrol. Sci. J.*, *34*(1), 79–95.

Gentier, S. (1986), Morphologie et comportment hydromecanique d'une fracture naturelle dans un granite sous constrainte normale, Ph.D. thesis, Univ. D'Orleans, Orleans, France.

Gerke, H. H., and M. T. van Genuchten (1993a), A dual-porosity model for simulating the preferential movement of water and solutes in structured porous media, *Water Resour. Res.*, *29*(2), 305–319.

Gerke, H. H., and M. T. van Genuchten (1993b), Evaluation of a first-order water transfer term for variably saturated dual-porosity flow models, *Water Resour. Res.*, *29*(2), 1225–1238.

Gerke, H. H., and M. T. van Genuchten (1996), Macroscopic representation of structural geometry for simulating water and solute movement in dual-porosity media, *Adv. Water Resour.*, *19*(6), 343–357.

Glass, R. J., M. J. Nicholl, and V. C. Tidwell (1995), Challenging models for flow in unsaturated, fractured rock through exploration of small scale processes, *Geophys. Res. Lett.*, *22*(11), 1457–1460.

Gooddy, D. C. (2003), Controls on the distribution of dense non-aqueous phase liquids in the matrix of permo-triassic sandstones, Ph.D. thesis, University College London, London.

Gooddy, D. C., D. G. Kinniburgh, and J. A. Barker (1995), Development of a Rapid Method for Determining Apparent Diffusion Coefficients for Chloride in Chalk, *Hydrogeological Series Technical Report WD/95/66*, British Geological Survey.

Grindley, J. (1969), The Calculation of Actual Evaporation and Soil Moisture Deficit over Specified Catchment Areas, *Hydrological Memorandum 38*, Meteorological Office.

Haria, A. H., M. G. Hodnett, and A. C. Johnson (2003), Mechanism of groundwater recharge and pesticide penetration to a chalk aquifer in southern England, *J. Hydrol.*, *275*, 122–137.

Hayes, C. R., and L. A. Greene (1984), The evaluation of eutrophic impact in public water supply reservoirs in East Anglia, *Water Pollution Control*, *83*(1), 42.

Headworth, H. G. (1972), The analysis of natural groundwater fluctuations in the chalk of Hampshire, *J. Inst. Water Eng.*, *26*, 107–124.

Heathwaite, A. L., T. P. Burt, and S. T. Trudgill (1993), Overview - the Nitrate Issue, in *Nitrate : processes, patterns, and management*, edited by T. P. Burt, A. L. Heathwaite, and S. T. Trudgill, pp. 3–22, John Wiley And Sons, Chichester.

Hill, D. (1984), Diffusion coefficients of nitrate, chloride, sulphate and water in cracked and uncracked Chalk, *J. Soil Sci.*, *35*, 27–33.

Hillel, D. (1980), *Fundamentals of Soil Physics*, Academic Press, London.

Hodnett, M. G., and J. P. Bell (1990), Processes of Water Movement Through a Chalk Coombe Deposit in Southeast England, *Hydrol. Process.*, *4*, 361–372.

Hoffmann-Reim, H., M. T. van Genuchten, and H. Fluhler (1999), General model for the hydraulic conductivity of unsaturated soils, in *Chracterization and Measurement of the Hydraulic Properties of Unsaturated Porous Media: Proceedings of the International Workshop*, edited by M. T. van Genuchten, F. J. Leij, and L. Wu, pp. 31–42, Riverside, California.

Hollenbeck, K. J. (1998), *INVLAP.M: A matlab function for numerical inversion of Laplace transforms by the de Hoog algorithm*, http://www.isva.dtu.dk/staff/karl/invlap.htm.

Hough, M. N., and R. J. A. Jones (1997), The United Kingdom Meteorological Office rainfall and evaporation calculation system: MORECS version 2.0 - an overview, *Hydrol. Earth Syst. Sci.*, *1*(2), 227–239.

Ireson, A. M., H. S. Wheater, A. P. Butler, J. Finch, J. D. Cooper, and S. A. Mathias (2005), Hydrological processes in the Chalk unsaturated zone - insights from an intensive field monitoring programme, *Submitted to J. Hydrol.*

Jackson, B. M., H. S. Wheater, N. McIntyre, A. P. Butler, P. Whitehead, and A. Wade (2004), Calibration and undertainty issues arising from a process-based integrated nitrogen model (INCA) placed within a subjective probability framework, in *Hydrology: Science & Practice for the 21st Century*, vol. 2, pp. 123–129, British Hydrological Society.

Jackson, B. M., H. S. Wheater, N. McIntyre, A. P. Butler, and S. A. Mathias (2005), A simple model of variable residence time flow and nutrient transport in the Chalk, *Submitted to J. Hydrol.*

Johnes, P. J. (1996), Evaluation and management of the impact of land use change on the nitrogen and phosphorous load delivered to surface waters: the export coefficient modelling approach, *J. Hydrol.*, *183*, 323–349.

Johnes, P. J., and T. P. Burt (1993), Overview - the Nitrate Issue, in *Nitrates in Surface Waters*, edited by T. P. Burt, A. L. Heathwaite, and S. T. Trudgill, pp. 269–320, John Wiley And Sons, Chichester.

Johnes, P. J., and A. L. Heathwaite (1997), Modelling the impact of land use change on water quality in agricultural catchments, *Hydrol. Process.*, *11*, 269–286.

Johnes, P. J., B. Moss, and G. Phillips (1996), The determination of total nitrogen and total phosphorous concentrations in freshwaters from land use, stock headage and population data: testing of a model for use in conservation and water quality management, *Freshwater Biology*, *36*, 451.

Jones, D. R., C. D. Perttunen, and B. E. Stuckman (1993), Lipschitzian Optimization Without the Lipschitz Constant, *JOTA*, *79*.

Jones, H. K., and N. S. Robins (1999), *The Chalk aquifer of the South Downs*, Hydrogeological Report Series of the British Geological Survey.

Kwicklis, E. M., and R. W. Healey (1993), Numerical investigation of steady liquid water flow in a variably saturated fracture network, *Water Resour. Res.*, *29*(12), 4091–4102.

Landereau, P., B. Noetinger, and M. Quintard (2001), Quasi-steady two-equation models for diffusive transport in fractured porous media: large-scale properties for densely fractured systems, *Adv. Water Resour.*, *24*, 863–876.

Lees, M. J., L. A. Comacho, and P. G. Whitehead (1998), Extension of the QUASAR river water quality model to incorporate dead-zone mixing, *Hydrology and Earth System Sciences*, *2*(2), 353–365.

Lees, M. J., L. A. Comacho, and S. Chapra (2000), On the relationship of transient storage and aggregated dead zone models of longitudinal solute transport in streams, *Water Resour. Res.*, *36*(1), 213–224.

Leij, F. J., and J. H. Dane (1990), Analytical Solutions of the One-Dimensional Advection Equation and Two- or Three-Dimensional Dispersion Equation, *Water Resour. Res.*, *26*(7), 1475–1482.

Lever, D. A., M. H. Bradbury, and S. J. Hemingway (1983), Modelling the Effect of Diffusion into the Rock Matrix on Radionuclide Migration, *Prog. in Nuclear Res.*, *12*(1), 85–117.

Lewis, M. A., H. K. Jones, D. M. J. Macdonald, M. Price, J. A. Barker, J. A. Shearer, T. R. Wesselink, and D. J. Evans (1993), Groundwater storage in British aquifers: Chalk, *R&D Note 169*, National Rivers Authority, Bristol.

Little, R., E. Muller, and R. Mackay (1996), Modelling of contaminant migration in a chalk aquifer, *J. Hydrol.*, *175*, 473–509.

Liu, H. H., C. Doughty, and G. S. Bodvarsson (1998), An active fracture model for unsaturated flow and transport in fractured rocks, *Water Resour. Res.*, *34*(10), 2633–2646.

Liu, H. H., G. S. Bodvarsson, and S. Finsterle (2003a), A note on unsaturated flow in two-dimensional fracture networks, *Water Resour. Res.*, *38*, 1176 DOI: 10.1029/2001WR000,977.

Liu, H. H., C. B. Haukwa, C. F. Ahlers, G. S. Bodvarsson, A. L. Flint, and W. B. Guertal (2003b), Modeling flow and transport in unsaturated fractured rock: an evaluation of the continuum approach, *J. Cont. Hydrol.*, *62-63*, 173–188.

Liu, H. H., G. Zhang, and G. S. Bodvarsson (2003c), The Active Fracture Model: Its Relation to Fractal Flow Patterns and an Evaluation Using Field Observations, *Vadose Zone J.*, *2*, 259–269.

Maclean, R. D. (1969), The effects of tipped domestic refuse on groundwater quality: a survey in north Kent, *Proc. Soc. Water Treat. Exam.*, *18*, 18–34.

Mahamood-ul-Hassan, M., and P. J. Gregory (2002), Dynamics of water movement on Chalkland, *J. Hydrol.*, *257*, 27–41.

Marshall, T. J. (1959), Relations between water and soil, *Tech. Comm. 50*, Bur. Soils, Comm. Agric. Bur., Farnham Royal, England.

Marshall, T. J., and J. W. Holmes (1979), *Soil Physics*, Cambridge University Press.

Massey, B. S. (1995), *Mechanics of Fluids, Sixth edition*, Chapman & Hall, London.

Mathias, S. A., and R. W. Zimmerman (2003), Laplace transform inversion for late-time behaviour of groundwater flow problems, *Water Resour. Res.*, *39*, 1283.

Mathias, S. A., A. P. Butler, N. McIntyre, and H. S. Wheater (2004), Applicability of box model to dual porosity systems, in *Hydrology: Science & Practice for the 21st Century*, vol. 1, pp. 315–321, British Hydrological Society.

Mathias, S. A., A. P. Butler, N. McIntyre, and H. S. Wheater (2005), The sigificance of flow in the matrix in the Chalk unsaturated zone, *J. Hydrol*, *310*, 62–77.

Mualem, Y. (1976), A new model of predicting hydraulic conductivity of unsaturated porous media, *Water Resour. Res.*, *12*, 513–522.

Narasimhan, T. N., and M. Zhu (1993), Transient flow of water to a well in an unconfined aquifer: Applicability of some conceptual models, *Water Resour. Res.*, *29*(1), 179–191.

Nativ, R., and I. Nissim (1992), Chracterisation of a desert aquitard: Hydrologic and hydrochemical considerations, *Groundwater*, *30*, 598–606.

Nativ, R., E. M. Adar, O. Dahan, and M. Geyh (1995), Water recharge and solute transport through the vadose zone of fractured chalk under desert conditions, *Water Resour. Res.*, *31*(2), 253–261.

Neal, C. (2002), *Assessing nitrogen dynamics in catchments across Europe within an INCA modelling framework*, Hydrology and Earth System Sciences.

Neitsch, S. L., J. G. Arnold, J. R. Kiniry, J. R. Williams, and K. W. King (2002), Soil and water assessment tool theoretical documentation, version 2000, *Tech. rep.*, Texan Water Resources Institute, Texas.

Nicholl, M. J., R. J. Glass, and S. W. Wheatcraft (1994), Gravity-driven infiltration instability in initially dry nonhorizontal fractures, *Water Resour. Res.*, *30*(9), 2533–2546.

Nitao, J., and T. Buscheck (1991), Infiltration of a liquid front in an unsaturated, fractured porous mdium, *Water Resour. Res.*, *27*(8), 2099–2112.

Oakes, D. B. (1977), The movement of water and solutes through the unsaturated zone of the Chalk of the United Kingdom, *Proc. 3rd Int. Hydrol. Symp. Colo. State Univ. (Fort Collins)*.

Oakes, D. B., C. P. Young, and S. S. D. Foster (1981), The effects of farming practices on groundwater quality in the United Kingdom, *Sci. Tot. Environ.*, *21*, 17–30.

Papoulis, A. (1984), *Probability, Random Variables, and Stochastic Process, 2nd ed*, McGraw-Hill.

Parsons, R. (1959), *Handbook of Electro-chemical Constants*, Butterworth Scientific Publishers, London.

Payne, B. R. (1972), Isotope hydrology, *Adv. Hydrosci.*, *8*, 95–138.

Penman, H. L. (1950), Evaporation over the British Isles, *Quart. Jl. Roy. Met. Soc.*, *LXXVI, 330*, 372–383.

Peters, R. R., and E. A. Klavetter (1988), A Continuum Model for Water Movement in an Unsaturated Fractured Rock Mass, *Water Resour. Res.*, *24*(3), 416–430.

Price, M., M. J. Bird, and S. S. D. Foster (1976), Chalk pore size measurements and their sigificance, *Water Services*, *80*, 596–600.

Price, M., R. A. Downing, and W. M. Edmunds (1993), The Chalk as an aquifer, in *The Hydrogeology of the Chalk of North-West Europe*, edited by R. A. Downing, M. Price, and G. P. Jones, pp. 35–58, Clarendon Press, Oxford.

Price, M., R. G. Low, and C. McCann (2000), Mechanisms of water storage and flow in the unsaturated zone of the Chalk aquifer, *J. Hydrol.*, *233*, 54–71.

Pruess, K. (1999), A mechanistic model for water seepage through thick unsaturated zones in fractured rocks of low matrix permeability, *Water Resour. Res.*, *35*(4), 1039–1051.

Pruess, K., and T. N. Narasimhan (1985), A practical method for modeling heat and fluid flow in fractured porous media, *Soc. Pet. Eng. J.*, *25*, 14–26.

Pruess, K., and Y. W. Tsang (1990), On two-phase relative permeability and capillary pressure of rough-walled rock fractures, *Water Resour. Res.*, *26*(9), 1915–1926.

Pruess, K., B. Faybishenko, and G. S. Bodvarsson (1999), Alternative concepts and approaches for modeling flow and transport in thick unsaturated zones of fractured rocks, *J. Cont. Hydrol.*, *38*, 281–322.

Pyrak-Nolte, L., J. L. Myer, N. G. W. Cook, and P. A. Witherspoon (1987), Hydraulic and mechanical properties of natural fractures in low permeability rock., in *Proc. Int. Cong. Int. Soc. Rock Mech.*, pp. 225–231.

Ragab, R., J. Finch, and R. Harding (1997), Estimation of groundwater recharge to Chalk and sandstone aquifers using simple soil models, *J. Hydrol.*, *190*, 19–41.

Reeves, M. J. (1979), Recharge and pollution of the English Chalk: some possible mechanisms, *Eng. Geol.*, *14*, 231–240.

Richards, L. A. (1931), Capillary conduction of liquids through porous mediums, *Physics*, *1*, 318–333.

Ritter, H. L., and L. C. Drake (1945), Pore-size distribution in porous materials, *Ind. Eng. Chem.: Analytical Edition*, *17*, 782–786.

Ross, C. T. F. (1996), *Mechanics of Solids*, Prentice Hall, London.

Rushton, K. R., B. J. Connorton, and L. M. Tomlinson (1989), Estimation of the groundwater resources of the Berkshire Downs supported by mathematical modelling, *Quart. J. Eng. Geol.*, *22*, 329–341.

Schaap, M. G., and F. J. Leij (2000), Improved Prediction of Unsaturated Hydraulic Conductivity with the Mualem-van Genuchten Model, *Soil Sci. Soc. Am. J.*, *64*, 843–851.

Shampine, L. F., and M. W. Reichelt (1997), The MATLAB ODE Suite, *SIAM J. Sci. Comp.*, *18*, 1–22.

Shampine, L. F., M. W. Reichelt, and J. A. Kierzenka (1999), Solving Index-1 DAEs in MATLAB and Simulink, *SIAM J. Sci. Comp.*, *41*, 538–552.

Simunek, J., N. J. Jarvis, M. T. van Genuchten, and A. Gardenas (2003), Review and comparison of models for describing non-equilibrium and preferential flow and transport in the vadose zone, *J. Hydrol.*, *272*, 14–35.

Sloan, W. T., and J. Ewen (1999), Modelling long-term contaminant migration in a catchment at fine spatial and temporal scales suing the UP system, *Hydrol. Process.*, *13*, 823–846.

Smith, D. B., P. L. Wearn, H. J. Richards, and P. C. Rowe (1970), Water movement in the unsaturated zone of high and low permeability strata using natural tritium, in *Isotope Hydrology*, pp. 73–87, Atomic Energy Agency, Vienna.

Smith, R. M. S., and H. S. Wheater (2004), Multiple objective evaluation of a simple phosphorous transfer model, *Hydrol. Proc.*, *18*, 1703–1720.

Smith, R. M. S., D. J. Evans, and H. S. Wheater (2004), Evaluation of two hybrid metric-conceptual models for simulating phosphorous transfer from agricultural land in the river enborne, a lowland UK catchment, *J. Hydrol.*, *in press*, 1–15.

Sneddon, I. N. (1966), *Mixed boundary value problems in potential theory*, John Wiley & Sons, Inc., New York.

Snow, D. T. (1968), Rock fracture spacings, openings and porosities, *J. Soil Mech. Found. Div., ASCE*, *94*(SM1), 73–91.

Su, G. W., J. T. Geller, K. Pruess, and F. Wen (1999), Experimental studies of water seepage and intermittent flow in unsaturated, rough-walled fractures, *Water Resour. Res.*, *35*(4), 1019–1037.

Su, G. W., J. T. Geller, K. Pruess, and J. R. Hunt (2001), Solue transport along preferential flow paths in unsaturated fractures, *Water Resour. Res.*, *37*(10), 2481–2491.

Sudicky, E. A., and E. O. Frind (1982), Contaminant Transport in Fractured Porous Media: Analytical Solutions for a System of Parallel Fractures, *Water Resour. Res.*, *18*(6), 1634–1642.

Sun, N. Z. (1996), *Mathematical modeling of groundwater pollution*, Springer, New York.

Taylor, G. I. (1953), The dispersion of soluble matter in solvent flowing slowly through a tube, *Proc. Roy. Soc. Lond.*, *219A*, 186–203.

Tokunaga, T. K., and J. Wan (1997), Water film flow along fracture surface of porous rock, *Water Resour. Res.*, *33*(6), 1287–1295.

Tokunaga, T. K., J. Wan, and S. R. Sutton (2000), Transient film flow on rough fracture surfaces, *Water Resour. Res.*, *36*(7), 1737–1746.

Trudgill, S. T. (1995), *Solute Modelling in Catchment Systems*, John Wiley and Sons, Chichester.

Valocchi, A. J. (1985), Validity of the Local Equilibrium Assumption for Modeling Sorbing Solute Transport Through Homogeneous Soils, *Water Resour. Res.*, *21*(6), 808–820.

Van den Daele, G. H., J. A. Barker, T. C. Atkinson, and L. C. Connell (2003), A Tracer investigation into the importance of diffusive exchange in the unsaturated zone of the British chalk, in *Groundwater in Fractured Rocks - IHP-VI Series on Groundwater, Vol. 7*, edited by J. Krasny, Z. Hrkal, and J. Bruthans, pp. 301–302.

van Genuchten, M. T. (1980), A Closed-form Equation for Predicting the Hydraulic Conductivity in Unsaturated Soils, *Soil Sci. Soc. of America J.*, *44*, 892–898.

van Genuchten, M. T., and F. N. Dalton (1986), Models for simulating salt movement in aggregated field soils, *Geoderma*, *38*, 165–183.

van Genuchten, M. T., and P. J. Wierenga (1976), Mass Transfer Studies in Sorbing Porous Media I. Analytical Solutions, *Soil Sci. Soc. of America J.*, *40*(4), 473–480.

Vavra, C. L., J. G. Kaldi, and R. M. Sneider (1992), Geological applications of capillary pressure: a review, *American Assoc. Pet. Geol. Bull.*, *76*, 840–850.

Vermeulen, T. (1953), Theory of irreversible and constant-pattern solid diffusion, *Ind. Eng. Chem.*, *45*, 1664–1670.

Vogel, T., H. H. Gerke, R. Zhang, and M. T. van Genuchten (2000), Modeling flow and transport in a two-dimensional dual-permeability system with spatially variable hydraulic properties, *J. Hydrol.*, *238*, 78–89.

Wade, A. J., P. G. Whitehead, H. P. Jarvie, C. Neal, H. Prior, and P. J. Johnes (2004), Nutrient monitoring, simulation and management within a major lowland UK river system: the Kennet, *Math. Comp. Sim.*, *64*, 307–317.

Wang, J. S. Y., and T. N. Narasimhan (1985), Hydrological Mechanisms Governing Fluid Flow in a Partially Saturated, Fractured, Porous Medium, *Water Resour. Res.*, *21*(12), 1861–1874.

Wang, J. S. Y., and T. N. Narasimhan (1993), Unsaturated Flow in Fractured Porous Media, in *Flow and Contaminant Transport in Fractured Rock*, edited by J. B. Bear, C. F. Tsang, and G. de Marsily, pp. 325–394, Academic Press, Inc., New York.

Warren, J. E., and P. E. Root (1963), The behaviour of naturally fractured reservoirs, *Soc. of Pet. Eng. J.*, *3*, 245–255.

Watson, K. K. (1966), An instantaneous profile method for determining the hydraulic conductivity of unsaturated porous media, *Water Resour. Res.*, *2*, 709–715.

Wellings, S. R. (1984a), Recharge of the Upper Chalk aquifer at a site in Hampshire, England, 1. Water balance and unsaturated flow, *J. Hydrol.*, *69*, 259–273.

Wellings, S. R. (1984b), Recharge of the Upper Chalk aquifer at a site in Hampshire, England, 2. Solute Movement, *J. Hydrol.*, *69*, 275–285.

Wellings, S. R., and J. P. Bell (1980), Movement of water and nitrate in the unsaturated zone of the Upper Chalk near Winchester, Hants., England, *J. Hydrol.*, *48*, 119–136.

Wheater, H. S., A. J. Jakeman, and K. J. Beven (1993), Progress and Directions in Rainfall-runoff Modelling, in *Modelling Change in Environmental Systems*, edited by A. J. Jakeman, M. B. Beck, and M. J. McAleer, pp. 101–132, John Wiley And Sons, Chichester.

Wheater, H. S., J. A. Tomkins, M. van Leeuwen, and A. P. Butler (2000), Uncertainty in groundwater flow and transport modeling - a stochastic analysis of well-protection zones, *Hydrol. Process.*, *14*, 2019–2029.

Wheater, H. S., S. Boxall, and T. Wagener (2002), Regionalisation of rainfall-runoff models: an application to the Thames Basin, in *Proceedings BHS 8th National Hydrology Symposium*, pp. 199–206, British Hydrol. Soc., Birmingham.

Whitehead, P. G., R. J. Williams, and G. M. Hornberger (1986), On the identification of pollutant or tracer sources using dispersion theory, *J. Hydrol.*, *84*, 273–286.

Whitehead, P. G., R. J. Williams, and D. R. Lewis (1997), Quality simulation along river systems (QUASAR): model theory and development, *Sci. Tot. Environ.*, *194/195*, 447–456.

Whitehead, P. G., E. J. Wilson, and D. Butterfield (1998), A semi-distributed Integrated Nitrogen model for multiple source assessment in Catchments (INCA): Part I - model structure and process equations, *Sci. Tot. Environ.*, *210/211*, 547–558.

Whitehead, P. G., P. J. Johnes, and D. Butterfield (2002), Steady state and dynamic modelling of nitrogen in the River Kennet: impacts of land use change since the 1930s, *Sci. Tot. Env.*, *282-283*, 417–434.

Winslow, D. N., M. D. Cohen, D. Bentz, K. A. Snyder, and E. J. Garboczi (1994), Percolation and pore structure in mortars and concrete, *Cement and Concrete Research*, *24*(1), 25–37.

Young, C. P., D. B. Oakes, and W. B. Wilkinson (1976), Prediction of Future Nitrate Concentrations in Ground Water, *Groundwater*, *14*(6), 426–438.

Zhu, J. L., S. Mishra, and J. C. Parker (1990), Effective properties for modelling unsaturated flow in large-scale heterogeneous porous media, in *Field-scale Water and Solute Flux in soils*, edited by K. Roth, H. Flhler, W. A. Jurg, and J. C. Parker, Birkhuser: Basel, Switzerland.

Zimmerman, R. W., and G. S. Bodvarsson (1996), Effective transmissivity of two-dimensional fracture networks, *Int. J. Rock Mech. Min. Sci.*, *33*, 433–438.

Zimmerman, R. W., G. Chen, T. Hadgu, and G. S. Bodvarsson (1993), A Numerical Dual-Porosity Model With Semianalytical Treatment of Fracture/Matrix Flow, *Water Resour. Res.*, *29*(7), 2127–2137.

Zimmerman, R. W., T. Hadgu, and G. S. Bodvarsson (1996), A new lumped-parameter model for flow in unsaturated dual-porosity media, *Adv. Water Resour.*, *19*(5), 317–327.

Appendix A

Development and testing of FLOWTRAN2D

A.1 Introduction

FLOWTRAN2D solves the governing equations of two-dimensional flow and solute transport in variably saturated porous media within the MATLAB programming environment. This is the model used for the simulations detailed in Chapter 5. In this appendix, the salient points of the model are described followed by a series of verification exercises.

A.2 Model development

The governing equations of two-dimensional (2D) flow and solute transport are

$$\frac{\partial \theta}{\partial t} = -\frac{\partial q_x}{\partial x} - \frac{\partial q_z}{\partial z} \tag{A.1}$$

and

$$\frac{\partial (\theta c)}{\partial t} = -\frac{\partial q_{s,x}}{\partial x} - \frac{\partial q_{s,z}}{\partial z} \tag{A.2}$$

where θ is moisture content, q_x and q_z are water fluxes in the x and z directions, c is solute concentration, $q_{s,x}$ and $q_{s,z}$ are solute fluxes in the x and z directions, x is a horizontal distance, z is depth and t is time.

The water fluxes are found from Darcy's Law:

$$q_x = -K_x(\psi)\frac{\partial h}{\partial x}, \quad q_z = -K_z(\psi)\frac{\partial h}{\partial z} \tag{A.3}$$

where $K_x(\psi)$ and $K_z(\psi)$ are the hydraulic conductivities in the x and z direction, h is hydraulic head and ψ is pressure head. Note that x and z are assumed to be the principal

axes of anisotropy throughout.

The solute fluxes are found from the addition of advective and dispersive fluxes:

$$q_{s,x} = q_x c - \theta D_x \frac{\partial c}{\partial x}, \quad q_{s,z} = q_z c - \theta D_z \frac{\partial c}{\partial z} \tag{A.4}$$

where D_x and D_z are dispersion coefficients in the x and z directions.

Hydraulic head is related to pressure head through

$$h = \psi - z \tag{A.5}$$

while rates of change in moisture content are related to rates of change in pressure head through

$$\frac{\partial \theta}{\partial t} = C(\psi)\frac{\partial \psi}{\partial t}, \quad C(\psi) = \frac{d\theta}{d\psi} \tag{A.6}$$

where $C(\psi)$ is often referred to as the specific capacity function.

Within the model, it is further assumed that the dispersion coefficients are found from:

$$D_x = \frac{\chi_x |q_x|}{\theta} + D_A, \quad D_z = \frac{\chi_z |q_z|}{\theta} + D_A \tag{A.7}$$

where χ_x and χ_z are dispersivities in the x and z directions and D_A is the apparent diffusion coefficient.

Equations (A.1) and (A.2) are discretised in space using a block centred finite difference approach such that

$$\left.\frac{d\theta}{dt}\right|_{i,j} = \left[\frac{(q_{x,i-1/2,j} - q_{x,i+1/2,j})}{\Delta x_{i,j}}\right] + \left[\frac{(q_{z,i,j-1/2} - q_{z,i,j+1/2})}{\Delta z_{i,j}}\right] \tag{A.8}$$

and

$$\left.\frac{d}{dt}(\theta c)\right|_{i,j} = \left[\frac{(q_{s,x,i-1/2,j} - q_{s,x,i+1/2,j})}{\Delta x_{i,j}}\right] + \left[\frac{(q_{s,z,i,j-1/2} - q_{s,z,i,j+1/2})}{\Delta z_{i,j}}\right] \tag{A.9}$$

where

$$q_{x,i-1/2,j} = K_{x,i-1/2,j}\left[\frac{(\psi_{i-1/2,j} - \psi_{i,j})}{\Delta x_{i-1/2,j}}\right] \tag{A.10}$$

$$q_{x,i+1/2,j} = K_{x,i+1/2,j}\left[\frac{(\psi_{i,j} - \psi_{i+1/2,j})}{\Delta x_{i+1/2,j}}\right] \tag{A.11}$$

$$q_{z,i,j-1/2} = K_{z,i,j-1/2}\left[\frac{(\psi_{i,j-1/2} - \psi_{i,j})}{\Delta z_{i,j-1/2}} + 1\right] \tag{A.12}$$

$$q_{z,i,j+1/2} = K_{z,i,j+1/2}\left[\frac{(\psi_{i,j} - \psi_{i,j+1/2})}{\Delta z_{i,j+1/2}} + 1\right] \tag{A.13}$$

and

$$q_{s,x,i-1/2,j} = \theta_{x,i-1/2,j} D_{x,i-1/2,j}\left[\frac{(c_{i-1/2,j} - c_{i,j})}{\Delta x_{i-1/2,j}}\right] + q_{x,i-1/2,j} c_{i-1/2,j} \tag{A.14}$$

$$q_{s,x,i+1/2,j} = \theta_{x,i+1/2,j} D_{x,i+1/2,j} \left[\frac{(c_{i,j} - c_{i+1/2,j})}{\Delta x_{i+1/2,j}} \right] + q_{x,i+1/2,j} c_{i+1/2,j} \tag{A.15}$$

$$q_{s,z,i,j-1/2} = \theta_{z,i,j-1/2} D_{z,i,j-1/2} \left[\frac{(c_{i,j-1/2} - c_{i,j})}{\Delta z_{i,j-1/2}} \right] + q_{z,i,j-1/2} c_{i,j-1/2} \tag{A.16}$$

$$q_{s,z,i,j+1/2} = \theta_{z,i,j+1/2} D_{z,i,j+1/2} \left[\frac{(c_{i,j} - c_{i,j+1/2})}{\Delta z_{i,j+1/2}} \right] + q_{z,i,j+1/2} c_{i,j+1/2} \tag{A.17}$$

The model solves for ψ and c which are obtained by virtue of

$$\frac{d\psi}{dt} = \frac{1}{C} \frac{d\theta}{dt} \tag{A.18}$$

and

$$\frac{dc}{dt} = \frac{1}{\theta} \left[\frac{d}{dt}(\theta c) - c \frac{d\theta}{dt} \right] \tag{A.19}$$

which are integrated together in respect to time using the stiff integrator ODE15s available in any standard version of MATLAB (*Shampine and Reichelt*, 1997; *Shampine et al.*, 1999).

FLOWTRAN2D also has the capability to model several domains simultaneously. Fracture and matrix coupling is then achieved by coupling two model domains together through their boundary conditions. Multiple continua systems can also be considered by setting up multiple model domains and coupling them using discrete sink and source terms.

A.3 1D steady state flow with 2D dispersion

As a first verification exercise FLOWTRAN2D's capability for solving solute transport problems with 1D steady state flow with 2D dispersion was checked against an existing analytical solution derived by *Leij and Dane* (1990).

Transport in a homogenous and isotropic medium during one-dimensional steady state flow with two-dimensional dispersion is given by (*Leij and Dane*, 1990)

$$\frac{\partial c}{\partial t} = D_L \frac{\partial^2 c}{\partial x^2} - v \frac{\partial c}{\partial x} + D_T \frac{\partial^2 c}{\partial y^2} \tag{A.20}$$

where c is the solute concentration, t is time, D_L and D_T are the coefficients of longitudinal and transverse dispersion, respectively, v is the pore-water velocity and x and y are positions along the coordinate axes parallel and perpendicular to the direction of flow. The initial and

boundary conditions are:

$$\begin{aligned}
&c(x,y,0) = c_i, && 0 < x < \infty, && -\infty < y < \infty;\\
&\left.\frac{\partial c}{\partial x}\right|_{x\to\infty} = 0, && -\infty < y < \infty, && t > 0;\\
&c(0,y,t) = c_L, && y < 0, && t > 0;\\
&c(0,y,t) = 0.5(c_L + c_R), && y = 0, && t > 0;\\
&c(0,y,t) = c_R, && y > 0, && t > 0;\\
&\left.\frac{\partial c}{\partial y}\right|_{y\to\pm\infty} = 0, && 0 < x < \infty, && t > 0.
\end{aligned} \tag{A.21}$$

The solution to this problem is (*Leij and Dane*, 1990)

$$\begin{aligned}
c(x,y,t) = {} & \frac{x}{(4\pi D_L)^{1/2}} \int_0^t \tau^{-3/2} \left\{ \frac{c_L}{2} \mathrm{erfc}\left[\frac{y}{(4D_T\tau)^{1/2}}\right] \right.\\
& \left. + \frac{c_R}{2} \mathrm{erfc}\left[-\frac{y}{(4D_L\tau)^{1/2}}\right] \right\} \exp\left[-\left(\frac{x - v\tau}{(4D_L\tau)^{1/2}}\right)^2\right] d\tau\\
& - \frac{c_i}{2} \left\{ \mathrm{erfc}\left[\frac{x - vt}{(4D_L t)^{1/2}}\right] + \exp\left(\frac{vx}{D_L}\right) \right.\\
& \left. \cdot \mathrm{erfc}\left[\frac{x + vt}{(4D_L t)^{1/2}}\right] \right\} + c_i
\end{aligned} \tag{A.22}$$

FLOWTRAN2D was compared to a snapshot obtained from equation (A.22) at $t = 0.50$ d with $D_L = 25$ cm^2/day, $D_T = 5$ cm^2/d, $v = 50$ cm/day, $c_L = 1$ and $c_R = c_i = 0$ (i.e. *Leij and Dane*, 1990, Figure 3) (see Figure A.1). To approximate the infinite boundaries no flow boundaries were placed at $y = \pm 20$ cm and $x = 40$ cm. A uniform space step of 1.0 cm was used throughout. FLOWTRAN2D approximates the solution well and the approximation becomes better as the space step reduces.

A.4 1D steady state flow in a dual-porosity medium

This verification exercise tests the fracture and matrix coupling achieved by coupling two model domains together through their boundary conditions for solute transport under steady state conditions.

Barker (1982) presents a set of assumptions and equations to describe solute transport in a dual-porosity medium. Identical slabs of matrix material are separated by equally spaced, planar fractures. The matrix is homogenous and saturated with immobile water. Solute transfer between the fractures and matrix and within the matrix occurs by molecular diffusion in the immobile water in a direction perpendicular to the plane of the fractures. There is

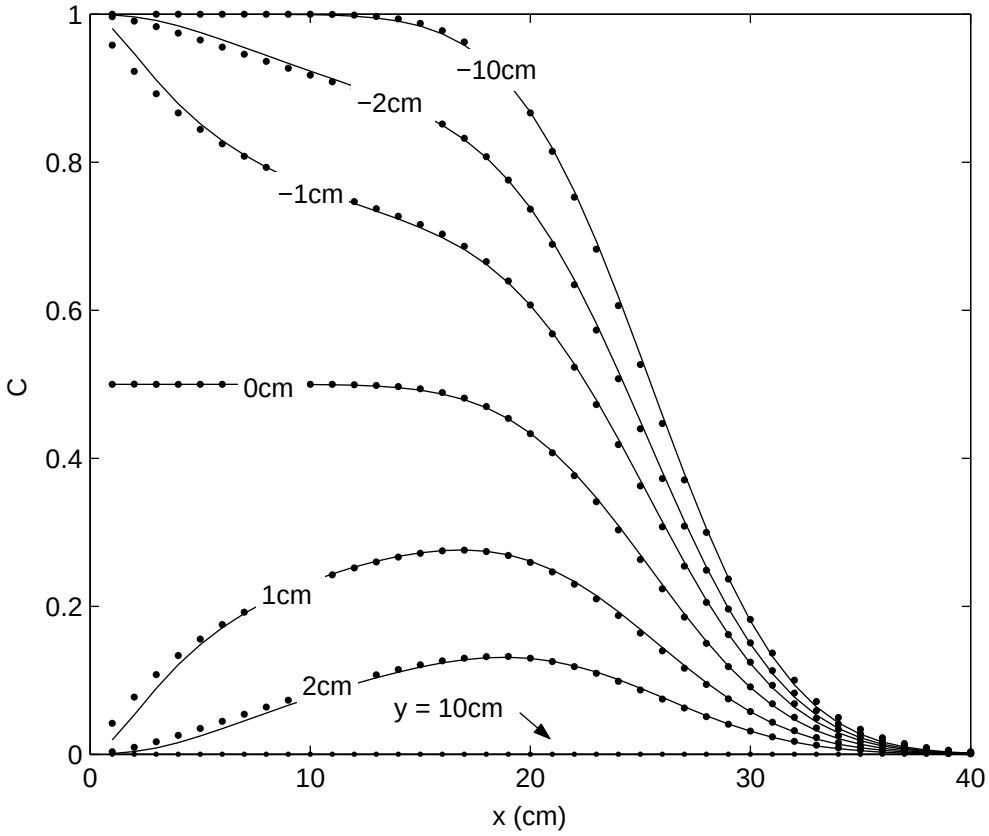

Figure A.1 Comparison of FLOWTRAN2D (the dots) with the analytical solution of (*Leij and Dane*, 1990) (the solid lines) for various y values as indicated.

no concentration gradient across the fractures. The flow velocity in the fractures is uniform while no flow occurs in the matrix.

Because of the symmetry of the model only a single, semi-infinite unit extending from the centre of a matrix block to the centre of a neighbouring fracture need be considered. Let $c_f(Z,T)$ be the solute concentration in the fracture water and $c_m(X,Z,T)$ be the concentration in the matrix water. Further ignoring longitudinal dispersion, the movement of a conservative non-sorbing solute in a fracture is then described by

$$\frac{\partial c_f}{\partial T} + \frac{\partial c_f}{\partial Z} + \sigma \left.\frac{\partial c_m}{\partial X}\right|_{X=1} = 0 \tag{A.23}$$

where the dimensionless variables represent

$$X = x/a; \qquad T = D_A t/b^2$$
$$Z = D_A z/(vb^2); \quad \sigma = \phi b/a$$

and x is lateral distance from the centre of the matrix block, z is longitudinal distance, t

is time, a and b are the fracture and matrix half-widths, ϕ is the matrix porosity, v is the velocity of water flowing in the fracture and D_A is the apparent molecular diffusion coefficient of a solute in the matrix.

Solute concentrations in the matrix are then described by

$$\frac{\partial c_m}{\partial T} - \frac{\partial^2 c_m}{\partial X^2} = 0 \tag{A.24}$$

subject to the boundary conditions

$$\left.\frac{\partial c_m}{\partial X}\right|_{X=0} = 0; \quad c_m(1, Z, T) = c_f(Z, T) \tag{A.25}$$

Assuming the following initial and additional boundary conditions

$$c_f(0, T) = 1; \quad c_f(\infty, T) = 0; \quad c_m(X, Z, 0) = c_f(Z, 0) = 0 \tag{A.26}$$

the Laplace transform solution describing solute concentrations in the fracture is (*Barker*, 1982)

$$\hat{c}_f(Z, s) = \frac{1}{s} \exp(-\hat{\lambda}(s) Z) \tag{A.27}$$

where

$$\hat{\lambda}(s) = s \left[1 + \sigma \frac{\tanh(s^{1/2})}{s^{1/2}} \right] \tag{A.28}$$

and s, $\hat{c}_f$, $F(s)$ are the corresponding Laplace transforms of T, c_f and $f(T)$.

The Laplace transform solution describing the mean solute concentration in the matrix is (*Barker*, 1982)

$$\hat{\bar{c}}_m(Z, s) = \frac{\tanh(s^{1/2})}{s^{1/2}} \hat{c}_f(Z, s) \tag{A.29}$$

where

$$\bar{c}_m(Z, T) = \int_0^1 c_m(X, Z, T) dX \tag{A.30}$$

Equivalent model output from FLOWTRAN2D is compared to breakthrough curves derived from numerical Laplace transform inversions of equations (A.27) and (A.29), using the *de Hoog et al.* (1982) method, at $Z = 1, 2, 3, 4$ with $\sigma = 140$ in Figure A.2. Five nodes were used in the lateral direction for the matrix block plus an additional node for the fracture domain. Space steps of $\Delta Z = 0.05$ were used in the vertical direction. To approximate the infinite boundary a no flow boundary was placed at $Z = 8$. FLOWTRAN2D approximates the solution almost perfectly.

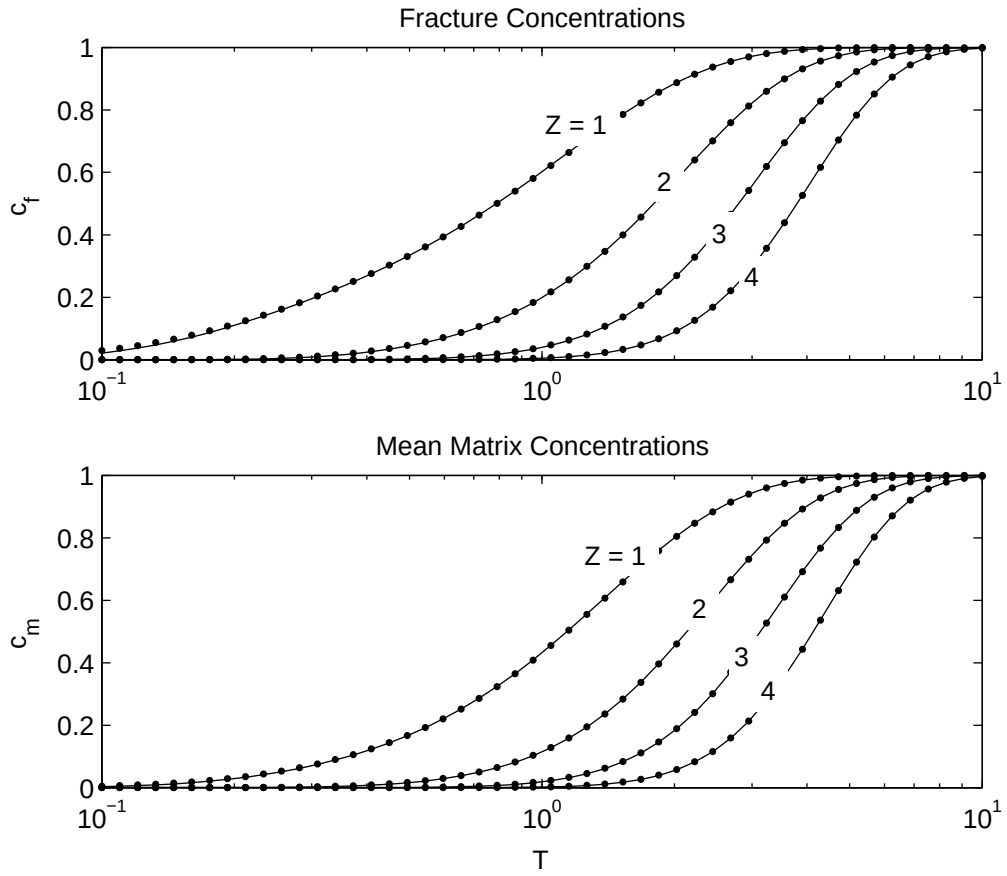

Figure A.2 Comparison of FLOWTRAN2D (the dots) with the analytical solution of (*Barker*, 1982) (the solid lines) for various Z values as indicated.

A.5 1D unsaturated flow in a dual-permeability medium

This verification exercise tests the fracture and matrix coupling achieved by coupling two model domains together through their boundary conditions for unsaturated flow.

Gerke and van Genuchten (1993b) describe a system in which unsaturated flow in a fracture (subscript f) is governed by

$$C_f \frac{\partial \psi_f}{\partial t} = \frac{\partial}{\partial z}\left[K_f\left(\frac{\partial \psi_f}{\partial z} - 1\right)\right] - \frac{K_{m,x}}{a}\left.\frac{\partial \psi_m}{\partial x}\right|_{x=b} \tag{A.31}$$

and in a neighbouring matrix slab (subscript m) by

$$C_m \frac{\partial \psi_m}{\partial t} = \frac{\partial}{\partial x}\left[K_{m,x}\frac{\partial \psi_m}{\partial x}\right] + \frac{\partial}{\partial z}\left[K_{m,z}\left(\frac{\partial \psi_m}{\partial z} - 1\right)\right] \tag{A.32}$$

subject to the boundary conditions

$$\left.\frac{\partial \psi_m}{\partial x}\right|_{x=0} = 0; \quad \psi_m(b,z,t) = \psi_f(z,t) \tag{A.33}$$

where C is specific capacity and ψ is pressure head, θ is moisture content, K is hydraulic conductivity, a is the half-width of the fracture, b is the half-width of the matrix block, z is depth and t is time. The x and z subscripts refer to the direction where applicable.

Moisture content and hydraulic conductivity are related to pressure head using (*van Genuchten*, 1980)

$$\frac{\theta - \theta_r}{\theta_s - \theta_r} = S_e = \left[\frac{1}{1 + |\alpha\psi|^n}\right]^m \tag{A.34}$$

$$K(S_e) = K_s S_e^{0.5}[1 - (1 - S_e^{1/m})^m]^2 \tag{A.35}$$

where $m = 1 - 1/n$, θ_r and θ_s are residual and saturated moisture contents, K_s is the hydraulic conductivity at saturation, and α and n are empirical parameters.

Specific capacity is found from

$$C = S_e S_s + \frac{d\theta}{d\psi} \tag{A.36}$$

where S_s is specific storage.

The particular scenario that we will try and copy utilised the parameters in Table A.1 and the following initial and additional boundary conditions:

$$\begin{aligned}
&\psi_f = \psi_m = -1000\text{cm}, && z > 0.0\text{cm}, \quad t = 0;\\
&\psi_f = \psi_m = -1000\text{cm}, && z = 40\text{cm}, \quad t > 0;\\
&K_{m,z}\left[\frac{\partial \psi_m}{\partial z} - 1\right] = 0, && z = 0.0\text{cm}, \quad t > 0;\\
&K_f\left[\frac{\partial \psi_f}{\partial z} - 1\right] = 1000\text{cm/day}, && z = 0.0\text{cm}, \quad t > 0.
\end{aligned} \tag{A.37}$$

In addition it was assumed that $a = 0.05$ cm, $b = 1.0$ cm while $\Delta z = \Delta x = 0.2$ cm.

Table A.1 Assumed hydraulic parameters from *Gerke and van Genuchten* (1993b).

Pore System	θ_r	θ_s	α (cm^{-1})	n	K_s (cm/d)	S_s (cm^{-1})
Matrix (z dir.)	0.105	0.5	0.005	1.5	1.05	10^{-7}
Matrix (x dir.)	0.105	0.5	0.005	1.5	0.1	10^{-7}
Fracture	0.0	0.5	0.1	2.0	2000	10^{-7}

Model output from FLOWTRAN2D (using a uniform space step of 0.2 cm in both the x and y directions) is compared to the numerical solution of *Gerke and van Genuchten* (1993b) in Figure A.3. It can be seen that FRM1D (with the heavier lines) appears to slightly underestimate the wetting front movement. However, it was found (by mistake) that a much better match with *Gerke and van Genuchten* (1993b) can be obtained when the fracture

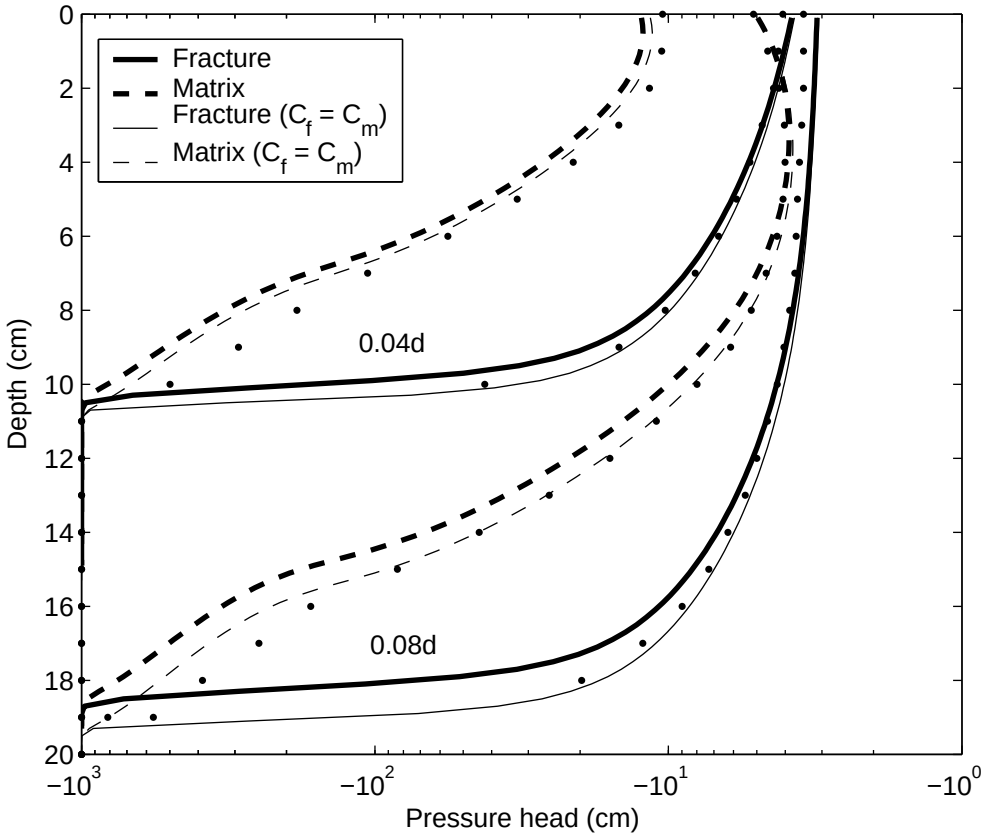

Figure A.3 Comparison of FLOWTRAN2D (the lines) with the numerical solution of *Gerke and van Genuchten* (1993b) (the dots).

specific capacity, $C_f(\psi_f)$ is replaced with $C_m(\psi_m)$. This could be because *Gerke and van Genuchten* (1993b) got it wrong or as a result of other unknown numerical inconsistencies.

A.6 1D coupled unsaturated flow and solute transport in a dual-permeability medium using the QSS approximation

To test FLOWTRAN2D capability for coupling flow with solute transport, the model was further adapted to model a dual continua using a quasi-steady-state approximation for fracture-matrix transfer such that it could be compared to the numerical solutions of *Gerke and van Genuchten* (1993a).

One-dimensional vertical water flow in a dual-permeability medium can be approximated using *Gerke and van Genuchten* (1993a)

$$C_f \frac{\psi_f}{\partial t} = \frac{\partial}{\partial z}\left[K_f\left(\frac{\partial \psi_f}{\partial z} - 1\right)\right] - \frac{\Gamma_w}{w_f} \tag{A.38}$$

$$C_m \frac{\psi_m}{\partial t} = \frac{\partial}{\partial z}\left[K_m\left(\frac{\partial \psi_m}{\partial z} - 1\right)\right] + \frac{\Gamma_w}{1 - w_f} \tag{A.39}$$

where everything is as defined in the previous section with the exception of the volumetric weighting factor found from

$$w_f = \frac{a}{a + b} \tag{A.40}$$

and the water transfer term, Γ_w found from

$$\Gamma_w = \alpha_w(\psi_f - \psi_m) \tag{A.41}$$

with a and b being the fracture and matrix half-widths and α_w a first-order transfer coefficient for water.

Similarly solute transport can be approximated using (*Gerke and van Genuchten*, 1993a)

$$\frac{\partial}{\partial t}(\theta_f c_f) = \frac{\partial}{\partial z}\left(\theta_f D_f \frac{\partial c_f}{\partial z} - q_f c_f\right) - \frac{\Gamma_s}{w_f} \tag{A.42}$$

$$\frac{\partial}{\partial t}(\theta_m c_m) = \frac{\partial}{\partial z}\left(\theta_m D_m \frac{\partial c_m}{\partial z} - q_m c_m\right) + \frac{\Gamma_s}{1 - w_f} \tag{A.43}$$

where c is solute concentration, D is a dispersion coefficient found from

$$D = D_A + \chi|v| \tag{A.44}$$

with D_A being an apparent diffusion coefficient, χ a dispersivity and $v = q/\theta$ a pore-water velocity.

The volumetric flow rate, q is found from

$$q = K\left(\frac{\partial \psi}{\partial z} - 1\right) \tag{A.45}$$

and Γ_s is the solute transfer term found from (*Gerke and van Genuchten*, 1996)

$$\Gamma_s = (1 - d)\Gamma_w \phi_f c_f + d\Gamma_w \phi_m c_m + (1 - w_f)\alpha_s \theta_m (c_f - c_m) \tag{A.46}$$

where

$$\phi_f = w_f \frac{\theta_f}{\theta}; \quad \phi_m = (1 - w_f)\frac{\theta_m}{\theta}; \quad d = 0.5\left(1 - \frac{\Gamma_w}{|\Gamma_w|}\right) \tag{A.47}$$

and α_s is a first-order transfer coefficient for solute.

The first-order transfer coefficients are found from

$$\alpha_w = \frac{\omega}{b^2}\gamma_w K_a; \quad \alpha_s = \frac{\omega}{b^2} D_A \tag{A.48}$$

where b is the matrix block half width, ω is a matrix block geometry factor, K_a and D_A are the hydraulic conductivity and apparent diffusion coefficient of the matrix block close to the fracture interface and γ_w is an empirical factor.

Gerke and van Genuchten (1993b) performed a detailed analysis to examine the optimum method for defining the parameters ω, K_a and γ_w such that the simple model using a first-order fracture-matrix transfer function (known as the Quasi-Steady-State (QSS) model (*Barker*, 1991)) (i.e. equations A.38 and A.39) can approximate the diffusive type model (i.e. equations A.31, A.32 and A.33). By studying the limit of a Laplace transform solution to Fick's second law as $s \rightarrow 0$, *Gerke and van Genuchten* (1993b) concluded that $\omega = 3$ for a slab-like matrix geometry. By studying 1-D Richards' simulations of a single matrix block, *Gerke and van Genuchten* (1993b) concluded that K_a is best obtained from the arithmetic mean

$$K_a = 0.5[K_a(\psi_f) + K_a(\psi_m)] \tag{A.49}$$

Finally, by comparing model outputs from equations (A.38) and (A.39) with equations (A.31), (A.32) and (A.33), *Gerke and van Genuchten* (1993b) found that application of the empirical factor $\gamma_w = 0.4$ yielded the closest correspondence. Not all of these conclusions are sensible as is discussed in the next section. Nevertheless, *Gerke and van Genuchten* (1993a) do provide a uniquely detailed account of a coupled flow and solute transport simulation such that we can use it to check the flow and transport coupling capability of FLOWTRAN2D.

The particular scenario that we will try and copy utilised the parameters in Table A.2 and the following initial and additional boundary conditions:

$$\begin{aligned}
&\psi_f = \psi_m = -1000\text{cm}, && z > 0.0\text{cm}, && t = 0;\\
&\psi_f = \psi_m = -1000\text{cm}, && z = 40\text{cm}, && t > 0;\\
&K_{m,z}\left[\frac{\partial \psi_m}{\partial z} - 1\right] = 0, && z = 0.0\text{cm}, && t > 0;\\
&K_f\left[\frac{\partial \psi_f}{\partial z} - 1\right] = 1000\text{cm/d}, && z = 0.0\text{cm}, && t > 0;\\
&c_f = c_m = 1, && z > 0.0\text{cm}, && t = 0;\\
&c_f = c_m = 1, && z = 40.0\text{cm}, && t > 0;\\
&\theta_m D_{m,z}\frac{\partial c_m}{\partial z} - q_{m,z}c_m = 0, && z = 0.0\text{cm}, && t > 0;\\
&\theta_f D_{f,z}\frac{\partial c_f}{\partial z} - q_{f,z}c_f = 0, && z = 0.0\text{cm}, && t > 0.
\end{aligned} \tag{A.50}$$

In addition it was assumed that $a = 0.05$, $b = 1.0$ cm and $\Delta z = 0.2$ cm.

Model output from FLOWTRAN2D is compared to the numerical solution of *Gerke and van Genuchten* (1993a) in Figure A.4. It can be seen that there is excellent correspondence between the two models for both pressure head and solute concentration. However, also shown in the solute concentration is another FLOWTRAN2D simulation which utilises the corrected expression of fracture-matrix solute transfer

$$\Gamma_s = (1-d)\Gamma_w c_f + d\Gamma_w c_m + (1-w_f)\alpha_s\theta_m(c_f - c_m) \tag{A.51}$$

Table A.2 Assumed hydraulic and solute transport parameters from *Gerke and van Genuchten* (1993a).

Pore System	θ_r	θ_s	α (cm^{-1})	n	K_s (cm/day)	S_s (cm^{-1})	D_A (cm^2/d)	χ (cm)
Matrix	0.105	0.5	0.005	1.5	1.05	10^{-7}	0.5	2
Interface	N/A	N/A	0.005	1.5	0.01	N/A	0.05	N/A
Fracture	0.0	0.5	0.1	2.0	2000	10^{-7}	0.5	2

found in *Gerke and van Genuchten* (1996). The expression given by (*Gerke and van Genuchten*, 1993a) in equation (A.46) is wrong.

For this simulation, the matrix concentrations are relatively unchanged when using the corrected expression (equation A.51) while the fracture solute fronts are much sharper. This is because clean water is being injected into a contaminated system causing the advective solute fluxes to be predominately zero. However, if the system is reversed such that contaminated water is injected into clean, equation (A.46) grossly overestimates the adjective transfer. But the main point is that this exercise has verified the coupling of the flow and solute transport models within FLOWTRAN2D.

A.7 1D coupled unsaturated flow and solute transport in a dual-permeability medium using a diffusive-type model

By comparing model outputs from equations (A.38) and (A.39) with equations (A.31), (A.32) and (A.33), *Gerke and van Genuchten* (1993b) found that application of an empirical factor $\gamma_w = 0.4$ was necessary to get an appropriate correspondence.

Mathias and Zimmerman (2003) showed that *Gerke and van Genuchten* (1993b) made a mistake in deriving the block geometry factor. *Gerke and van Genuchten* (1993b) assume that for large times (i.e. $t \to \infty$) it is appropriate to only to consider small values of the Laplace transform variable, s (i.e. $s \to 0$) which led them to believe that $\beta = 3$ for a slab-type matrix. There is no basis for this approach. Following a more rigourous approach, *Mathias and Zimmerman* (2003) verified that in fact, $\beta = \pi^2/4$. This would suggest an equivalent empirical factor of $\gamma_w = 0.4863$ would be needed. However, for the scenario depicted by the parameters in Table A.1, no factor is needed. Figure A.5 compares pressure head profiles from the QSS model (with $\beta = \pi^2/4$ and $\gamma_w = 1.0$) and the diffusive type model using the conditions and parameters set out in Section A.5. The correspondence between the two

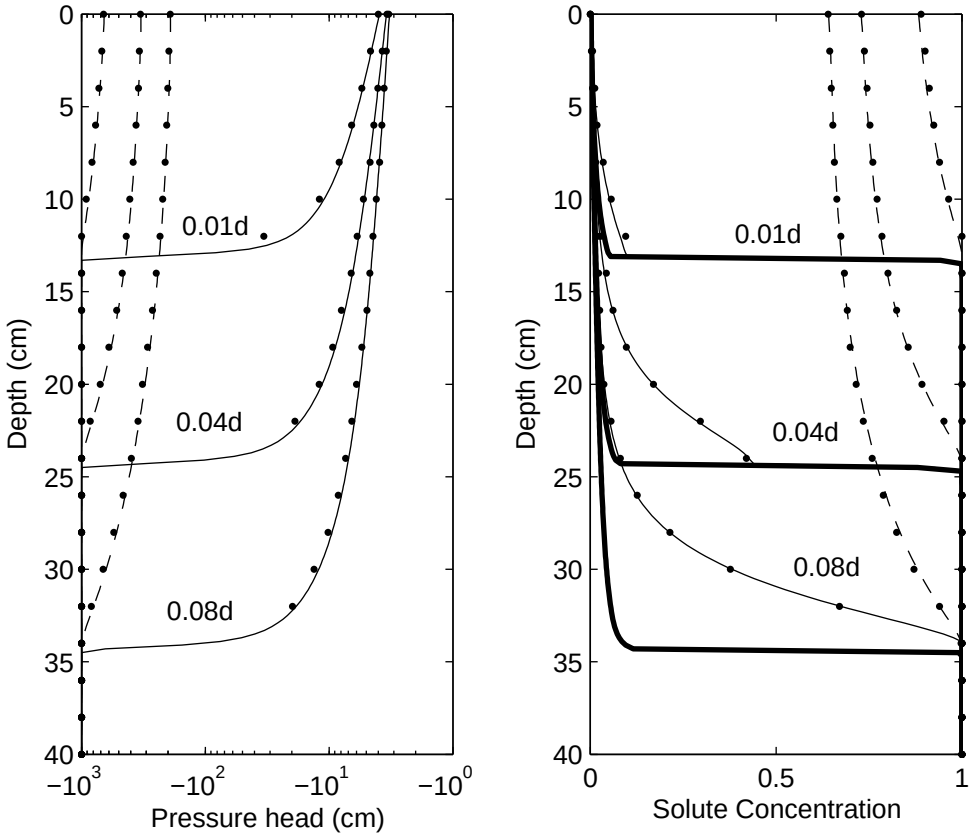

Figure A.4 Comparison of FLOWTRAN2D (the solid lines show the fractures and the dashed lines show the matrix) with the numerical solution of *Gerke and van Genuchten* (1993a) (the dots). The heavier line in the solute concentration plot show FLOWTRAN2D with the correct approximation for advective fracture-matrix solute transfer.

fracture profiles is very good. The matrix curves are slightly different as was also found by *Gerke and van Genuchten* (1993b).

Interestingly, while model output from QSS and diffusive type models for unsaturated flow and solute transport (under steady state flow) have been extensively compared (e.g. *Gerke and van Genuchten*, 1993b) there are no published comparisons of solute transport modelling under transient flow conditions.

Consider the unsaturated flow system previously described in section A.5, the equations governing solute transport over the transient flow regime would be

$$\frac{\partial}{\partial t}(\theta_f c_f) = \frac{\partial}{\partial z}\left[\theta_f D_f \frac{\partial c_f}{\partial z} - q_f c_f\right] + \frac{1}{a}\left[\theta_m D_{m,x} \frac{\partial c_m}{\partial x} - q_{m,x} c_m\right]_{x=b} \tag{A.52}$$

and

$$\frac{\partial}{\partial t}(\theta_m c_m) = \frac{\partial}{\partial z}\left[\theta_m D_{m,z}\frac{\partial c_m}{\partial z} - q_{m,z}c_m\right] + \frac{\partial}{\partial x}\left[\theta_m D_{m,x}\frac{\partial c_m}{\partial x} - q_{m,x}c_m\right] \tag{A.53}$$

subject to the boundary conditions

$$\left[\theta_m D_{m,x}\frac{\partial c_m}{\partial x} - q_{m,x}c\right]_{x=0} = 0 \quad c_m(b,z,t) = c_f(z,t) \tag{A.54}$$

where D is the dipsersion coefficient found from

$$D = D_A + \chi\frac{|q|}{\theta} \tag{A.55}$$

with D_A being the apparent diffusion coefficient and χ is the dispersivity.

The following initial and boundary conditions are also needed:

$$\begin{aligned}
&c_f = c_m = 1, && z > 0.0\text{cm}, && t = 0;\\
&c_f = c_m = 1, && z = 40.0\text{cm}, && t > 0;\\
&\theta_m D_{m,z}\frac{\partial c_m}{\partial z} - q_{m,z}c_m = 0, && z = 0.0\text{cm}, && t > 0;\\
&\theta_f D_{f,z}\frac{\partial c_f}{\partial z} - q_{f,z}c_f = 0, && z = 0.0\text{cm}, && t > 0.
\end{aligned} \tag{A.56}$$

with $D_A = 0.5\text{cm}^2/\text{d}$, $\chi = 2\text{cm}$.

The equivalent solute profiles are also shown in Figure A.5 alongside an equivalent QSS simulation with $\gamma_w = 1.0$ and $\omega = \pi^2/4$. It can be seen that the solute profiles from the QSS model have much sharper fronts than those obtained from the diffusive type model. This is because the QSS model overestimates the rate of solute transfer due to its fully-mixed approximation of the matrix.

A.8 Conclusions

A two-dimensional coupled flow and solute transport numerical dual-porosity model in variably saturated porous media, FLOWTRAN2D has been developed. FLOWTRAN2D also has the capability to model several domains simultaneously. Fracture and matrix coupling is then achieved by coupling two model domains together through their boundary conditions. Multiple continua systems can also be considered by setting up multiple model domains and coupling them using discrete sink and source terms. All the different facets of the model have been rigourously tested against several analytical solutions and published numerical solutions. This is the model that is used extensively in Chapter 6.

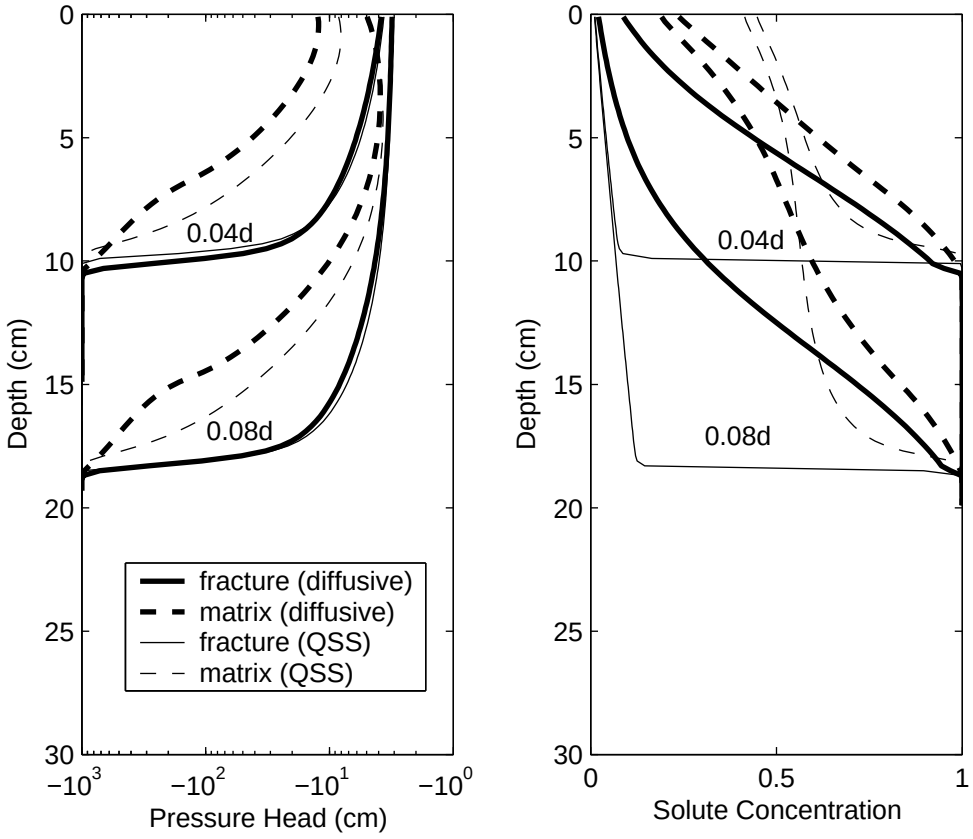

Figure A.5 Comparison of FLOWTRAN2D using a diffusive model and a QSS approximation for fracture-matrix transfer for the scenario presented by *Gerke and van Genuchten* (1993b).

Appendix B

Applicability of box models to dual-porosity systems

Adapted from *Mathias et al.* (2004) (this is the paper referred to in sections 3.5 and 6.5)

B.1 Introduction

With the availability of conceptual, catchment-scale solute transport models such as INCA (*Whitehead et al.*, 1998) there is a growing trend to model subsurface solute transport using simple arrangements of box models (see also *Buckley et al.*, 1995). When dealing with Chalk catchments this can be problematic due to, among other things, the complex nature of dual porous flow. Traditionally, solute transport in the Chalk has been investigated using dual-porosity (DP) models (*Barker*, 1993).

Recently, *Lees et al.* (2000) used a moment matching technique to examine relationships between parameters of two different in-stream solute transport models, the transient storage (TS) model (*Bencala and Walters*, 1983) and the aggregated dead zone (ADZ) model (*Beer and Young*, 1983). The ADZ model is a box model that considers a number of identical mixing tanks in series and an explicit time delay parameter. The TS model is a formulation of the advection dispersion equation with a first-order mass transfer term to characterise lateral diffusion of solute into a conceptualised dead zone. Optimisation of the models against breakthrough curves obtained from in-stream tracer test data showed that both equations can characterise a breakthrough curve with very similar moments. On this basis *Lees et al.* (2000) speculate that analytical moment relationships between the two models can be used to infer parameters from one model to the other.

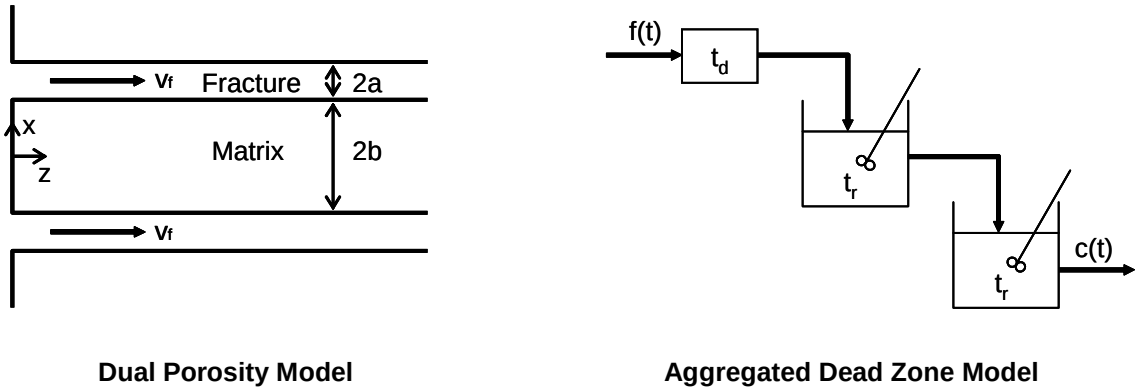

Figure B.1 Schematic diagrams of a dual-porosity model and an aggregated dead zone model.

Inspection of the TS model equations shows that it is mathematically analogous to the DP model used for solute transport simulations in sandstone (*Coats and Smith*, 1964) and macroscopically aggregated soils (*van Genuchten and Wierenga*, 1976). The reader is referred to *Davis and Atkinson* (2000) for further discussion on this subject. This study looks at how temporal moment relationships can be used to give insight into the applicability of using box models to simulate solute transport in Chalk.

Barker (1991) distinguishes between two types of DP models; the diffusive type and the quasi-steady-state (QSS) type model. The TS is a QSS type. Diffusive type DP models characterise exchange of solute between the fractures and the matrix (or storage zone) in terms of Fickian diffusion within the matrix block. The QSS type DP model can be looked at as an approximation of the diffusive type DP model when changes within mobile zones are slow in relation to the time for diffusive equilibrium across immobile zones (*Barker*, 1991). This happens quite rapidly (i.e. in hours) when dealing with very fine fracture spacing or macroscopically aggregated soils, but for the scenarios presented by Chalk it can take several years. Accordingly, it is deemed more appropriate to look at the moment relationships between the ADZ model and a diffusive type DP model.

B.2 A dual-porosity model

Barker (1982) presents a set of assumptions and equations to describe solute transport in a fractured porous medium. Consider the model geometry illustrated in Figure B.1. Identical slabs of matrix material are separated by equally spaced, planar fractures. The matrix is homogenous and saturated with immobile water. Solute transfer between the fractures

and matrix and within the matrix occurs by molecular diffusion in the immobile water in a direction perpendicular to the plane of the fractures. There is no concentration gradient across the fractures. The flow velocity in the fractures is uniform while no flow occurs in the matrix. Longitudinal dispersion in the fractures is characterised by a constant dispersion coefficient.

Because of the symmetry of the model only a single, semi-infinite unit extending from the centre of a matrix block to the centre of a neighbouring fracture need be considered. Let $c_f(z,t)$ be the solute concentration in the fracture water and $c_m(x,z,t)$ be the concentration in the matrix water. The movement of a conservative non-sorbing solute in a fracture is then described by

$$\frac{\partial c_f}{\partial t} - D_L \frac{\partial^2 c_f}{\partial z^2} + v_f \frac{\partial c_f}{\partial z} + \frac{\phi D_A}{a} \left.\frac{\partial c_m}{\partial x}\right|_{x=b} = 0 \tag{B.1}$$

where x is lateral distance from the centre of the matrix block, z is longitudinal distance, t is time, a is the half-width of the fracture, b is the half-width of the matrix block, ϕ is the matrix porosity, v_f is the velocity of water flowing in the fracture, D_L is a hydrodynamic dispersion coefficient for solute in the fracture water and D_A is the apparent molecular diffusion coefficient for solute in the matrix.

Solute concentrations in the matrix are then described by

$$\frac{\partial c_m}{\partial t} - D_A \frac{\partial^2 c_m}{\partial x^2} = 0 \tag{B.2}$$

subject to the boundary conditions

$$\left.\frac{\partial c_m}{\partial x}\right|_{x=0} = 0; \quad c_m(b,z,t) = c_f(z,t) \tag{B.3}$$

Following *Barker et al.* (2000), we introduce a pore-volume ratio, σ, an advective travel time, t_a and a characteristic block diffusion time, t_{cb} which are found from

$$\sigma = \phi \frac{b}{a}; \quad t_a = \frac{L}{v_f}(1+\sigma); \quad t_{cb} = \frac{b^2}{D_A} \tag{B.4}$$

where L is the distance along a fracture being considered.

Applying the following transformations

$$T = \frac{t}{t_a}; \quad Z = \frac{z}{L}; \quad Pe = \frac{v_f L}{D_L}; \quad X = \frac{x}{b}; \quad \gamma = \frac{t_a}{t_{cb}} \tag{B.5}$$

then yields the set of dimensionless equations

$$\frac{\partial c_f}{\partial T} - \frac{(1+\sigma)}{Pe} \frac{\partial^2 c_f}{\partial Z^2} + (1+\sigma) \frac{\partial c_f}{\partial Z} + \sigma\gamma \left.\frac{\partial c_m}{\partial X}\right|_{X=1} = 0 \tag{B.6}$$

$$\frac{\partial c_m}{\partial T} - \gamma \frac{\partial^2 c_m}{\partial X^2} = 0 \tag{B.7}$$

$$\left.\frac{\partial c_m}{\partial X}\right|_{X=0} = 0; \quad c_m(1, Z, T) = c_f(Z, T) \tag{B.8}$$

Applying the additional boundary and initial conditions

$$c_f(0, T) = f(T); \quad c_f(\infty, T) = 0; \quad c_m(X, Z, 0) = c_f(Z, 0) = 0 \tag{B.9}$$

the Laplace transform solution describing solute concentrations in the fracture water is (*Barker*, 1982)

$$\hat{c}_f(Z, s) = \hat{f}(s) \exp\left[\frac{ZP}{2}\left(1 - \left(1 + \frac{4}{Pe}\hat{\lambda}(s)\right)^{1/2}\right)\right] \tag{B.10}$$

where

$$\hat{\lambda}(s) = \frac{s}{(1+\sigma)}\left[1 + \sigma\frac{\gamma^{1/2}}{s^{1/2}}\tanh\left(\frac{s^{1/2}}{\gamma^{1/2}}\right)\right] \tag{B.11}$$

and s, $\hat{c}_f$, $\hat{f}(s)$ are the corresponding Laplace transforms of T, c_f and $f(T)$.

Two interesting limiting cases are when there is negligible longitudinal dispersion (i.e. $D_L \to 0$)

$$\lim_{Pe\to\infty} \hat{c}_f = \hat{f}(s) \exp[-Z\hat{\lambda}(s)] \tag{B.12}$$

or when there is negligible characteristic block diffusion time (i.e. $D_A \to \infty$ and/or $b \to 0$)

$$\lim_{\gamma\to\infty} \hat{\lambda}(s) = s \tag{B.13}$$

B.3 An aggregated dead zone model

The aggregated dead zone (ADZ) model was originally developed to overcome the failure of the conventional advection dispersion equation (ADE) to explain transport processes in river reaches (*Beer and Young*, 1983). Consider the schematic diagram of an ADZ model in Figure B.1. The ADZ model considers a river reach to be incompletely mixed, allowing a dissolved pollutant to undergo pure advection followed by dispersion in a lumped active mixing zone.

The governing equation for a first-order ADZ model is

$$\frac{dc}{dt} = \frac{1}{t_r}\left[f(t - t_d) - c(t)\right] \tag{B.14}$$

where $f(t)$ and $c(t)$ are the concentrations upstream and downstream of a given reach respectively, t_r is the reach residence time and t_d is a delay time representing pure advection.

Without loss of generality, equation (14) can also be normalised with respect to the advective travel time, t_a such that

$$\frac{dc}{dT} = \frac{1}{T_r}\left[f(T - T_d) - c(T)\right] \tag{B.15}$$

where $T_r = t_r/t_a$ and $T_d = t_d/t_a$.

For a zero concentration initial condition the Laplace transform solution of equation (B.15) with N number identical CSTRs (continuously stirred tank reactors) in series is

$$\hat{c}(s) = \frac{\hat{f}(s)\exp(-T_d s)}{(1+T_r s)^N} \tag{B.16}$$

where s and $\hat{f}(s)$ are the Laplace transforms of T, $c(T)$ and $f(T)$. This resembles the ADZ model structure that was compared with the TS model by *Lees et al.* (2000). Many other model structures are also possible that consider both parallel and series combinations of non-identical CSTRs (e.g. *Beven and Young*, 1988).

B.4 Moment generating equations

Absolute temporal moments (those about the origin) for a given function, $\eta(t)$ can be obtained from

$$\mu'_m = \int_0^\infty t^m \eta(t) dt \tag{B.17}$$

Similarly, central moments (those about the mean) can be obtained from

$$\mu_m = \int_0^\infty (t-\mu'_1)^m \eta(t) dt \tag{B.18}$$

Providing these moments exist, the same absolute moments can be obtained from a function's Laplace transform using (*Aris*, 1958)

$$\mu'_m = (-1)^m \left[\frac{d^m}{ds^m}\hat{\eta}(s)\right]_{s=0} \tag{B.19}$$

By application of a binomial transform, the second and third central moments can be retrieved from (*Papoulis*, 1984, p.146)

$$\mu_2 = -{\mu'_1}^2 + \mu'_2 \tag{B.20}$$

and

$$\mu_3 = 2{\mu'_1}^3 - 3\mu'_1\mu'_2 + \mu'_3 \tag{B.21}$$

To derive the temporal moments of a mathematical model it is common to assume a boundary condition of $f(T) = \delta(T)$, the δ operator denotes the Dirac delta function. The advantage of using such a function is that its zeroth moment $\mu'_0 = 1$ and $\mu'_1 = \mu_2 = ... = \mu_m = 0$. Thus these moments are normalised and represent the changes in centroid position, variance and skewness incurred to any general boundary condition (*Valocchi*, 1985).

To further aid derivation of the temporal moments for equation (B.10) we consider the Taylor series representation of the hyperbolic tangent function (p.83 Abramowitz and Stegun, 1972)

$$\tanh(y) = y - \frac{1}{3}y^3 + \frac{2}{15}y^5 - \frac{17}{315}y^7 + \frac{62}{2835}y^9 - ... \tag{B.22}$$

Because the *Aris* (1958) method only looks at the limits of function as $s \to 0$, to find the first three temporal moments only the first three terms are required such that equation (B.11) can be approximated using

$$\lambda = s\left[1 + \sigma\left(1 - \frac{1}{3}\frac{s}{\gamma} + \frac{2}{15}\frac{s^2}{\gamma^2}\right)\right] \tag{B.23}$$

The temporal moments for the DP model (B.10) calculated using equations (B.19) to (B.22) are therefore

$$\mu_1' = Z \tag{B.24}$$

$$\mu_2 = \frac{2Z}{Pe} + \frac{2}{3}\frac{Z}{\gamma}\frac{\sigma}{(1+\sigma)} \tag{B.25}$$

$$\mu_3 = \frac{12Z}{Pe^2} + \frac{4Z}{Pe\gamma}\frac{\sigma}{(1+\sigma)} + \frac{4Z}{5\gamma^2}\frac{\sigma}{(1+\sigma)} \tag{B.26}$$

Equivalent results have been obtained for spherical matrix blocks by *Valocchi* (1985).

Interestingly, the first moment, μ_1' is independent of D_A. This appears strange because intuitively we know that when $D_A = 0$ (i.e. $\gamma = 0$), the matrix pore-space is no longer connected to the fractures, and therefore μ_1' should be equal to $Z/(1+\sigma)$. However, this intuitive analysis is wrong. The first moments are independent of D_A because diffusion is a second-order process. When D_A is infinitesimally small, an infinitesimal part of solute will diffuse into the matrix. Because D_A is so small, it will then take an infinitely long time to come out. Consequently, this infinitesimal part of solute causes the variance and skewness of a breakthrough curve to increase (see equations B.25 and B.26) such that its centroid remains at $\mu_1' = Z$ (also see the long tails produced by models with low γ in Figure B.2).

A similar application to equation (B.16) gives the equivalent set of temporal moments for the ADZ model (*Lees et al.*, 2000)

$$\mu_1' = T_d + nT_r \tag{B.27}$$

$$\mu_2 = nT_r^2 \tag{B.28}$$

$$\mu_3 = 2nT_r^3 \tag{B.29}$$

If ADZ model parameters are estimated from

$$T_d = \mu_1' - nT_r, \quad T_r = \frac{\mu_3}{2\mu_2} \quad \text{and} \quad N = \frac{\mu_2}{T_r^2} \tag{B.30}$$

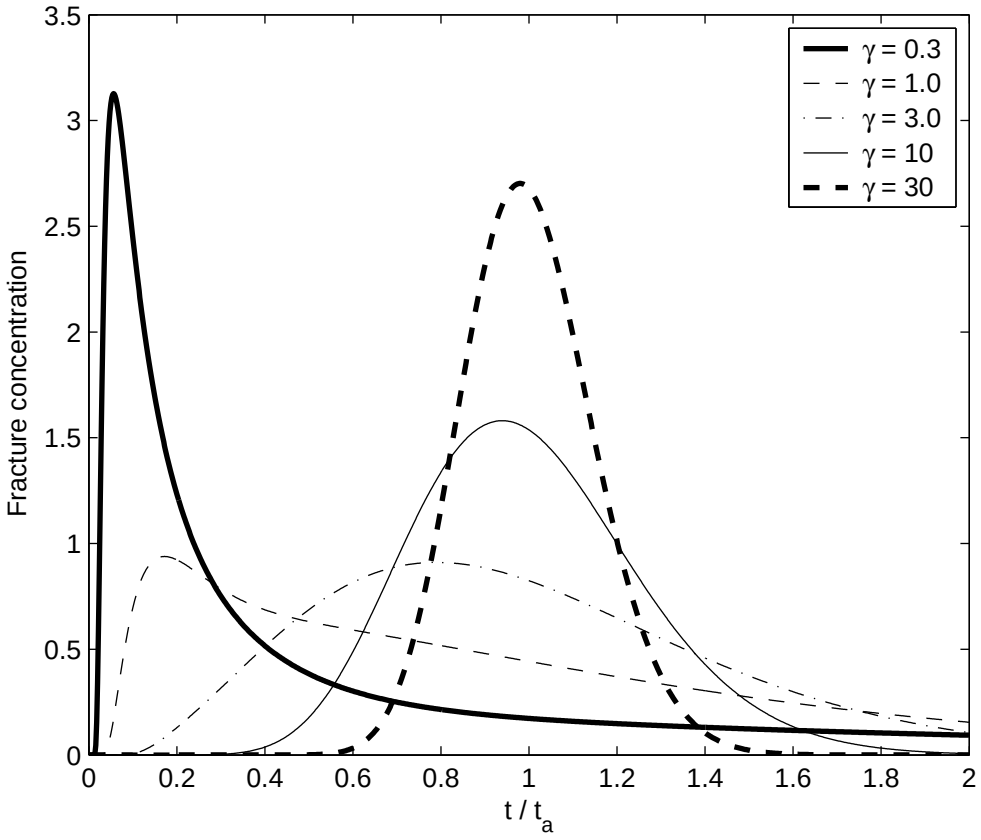

Figure B.2 Breakthrough curves from the DP model with $Pe = \infty$, $Z = 1$, $\sigma = 140$ and γ as indicated. All breakthrough curves have the same centroid (or μ_1').

where μ_1', μ_2 and μ_3 are found from equations (B.24) to (B.26), breakthrough curves from the ADZ model should have identical centroid position, variance and skewness as equivalent curves derived from the DP model.

B.5 Moment matching without hydrodynamic dispersion

For situations when hydrodynamic dispersion is negligible as compared to the spreading caused by matrix diffusion we can consider the limiting case when $Pe \to \infty$. Application of equation (B.30) in conjunction with equations (B.24) to (B.26) then yields

$$T_d = Z\left[1 - \frac{10}{9}\frac{\sigma}{(1+\sigma)}\right], \quad T_r = \frac{3}{5\gamma} \quad \text{and} \quad N = \frac{50}{27}Z\gamma\frac{\sigma}{(1+\sigma)} \quad \text{as} \quad Pe \to \infty \quad \text{and} \quad \sigma < 9 \tag{B.31}$$

Whenever $\sigma > 9$, the delay time, T_d is negative. This is not a sensible parameter value and causes equation (B.16) to become unstable. For this case, it is better to set $T_d = 0$ and

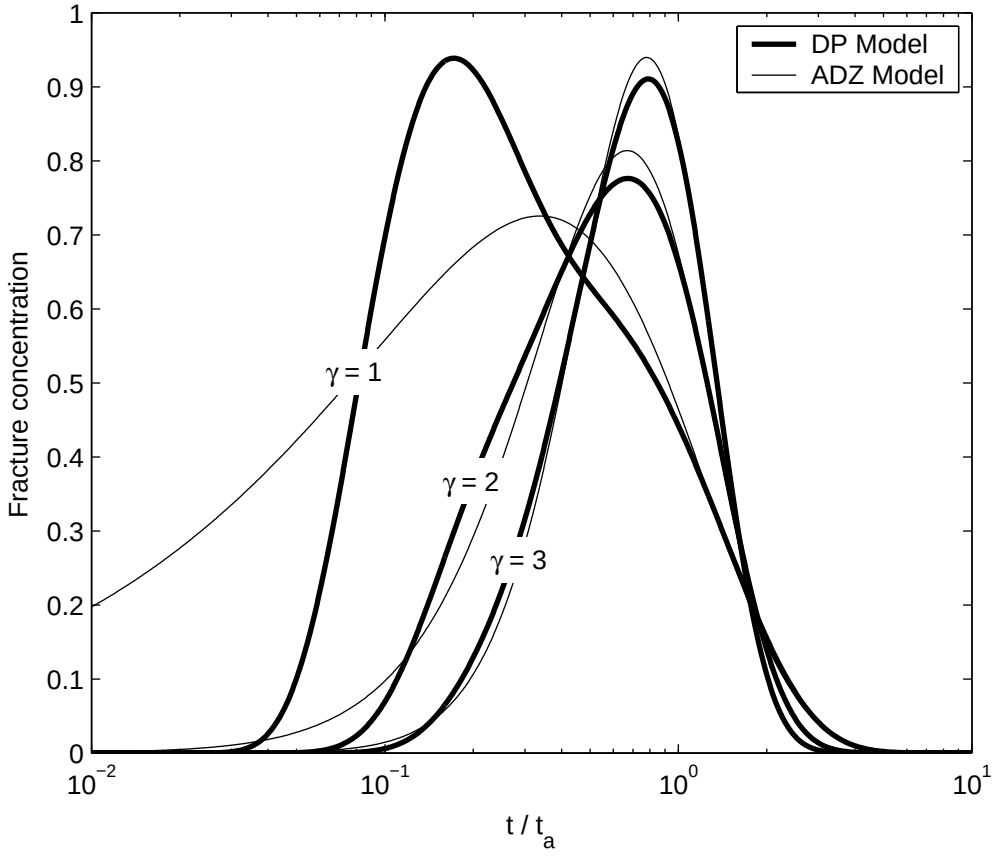

Figure B.3 Breakthrough curves from the DP model and the ADZ model with $Pe = \infty$, $Z = 1$, $\sigma = 140$ and γ as indicated.

equate just the first two moments of both models which yields

$$T_d = 0, \quad T_r = \frac{2}{3\gamma}\frac{\sigma}{(1+\sigma)} \quad \text{and} \quad N = \frac{3\gamma}{2}\frac{(1+\sigma)}{\sigma}Z \quad \text{as} \quad Pe \to \infty \quad \text{and} \quad \sigma \geq 9 \tag{B.32}$$

Consider an example, based on parameters typical for the Chalk where $\phi = 0.35$, $a = 0.00025$m and $b = 0.1$m (*Foster*, 1993). This gives a σ of 140, hence we must use equation (32) to match the ADZ and DP moments. Figure B.3 shows breakthrough curves for the DP model and the ADZ model as $Pe \to \infty$ while $\sigma = 140$, $Z = 1$ with $\gamma = 1$, $\gamma = 2$ and $\gamma = 3$. It can be seen that equation (B.32) is reasonably appropriate providing

$$\gamma = \frac{t_a}{t_{cb}} > 1 \tag{B.33}$$

which suggests that the advective travel time must be longer than the characteristic block diffusion time. When this condition is not satisfied the DP model exhibits an almost bi-modal breakthrough curve which the ADZ model (as defined in this chapter) is incapable of achieving.

Model simulations were achieved by numerically inverting the Laplace transform solutions in equations (B.10) and (B.16) using a MATLAB implementation of the *de Hoog et al.* (1982) algorithm developed by *Hollenbeck* (1998). For simplicity, both simulations assumed an input function of the form $f(T) = \delta(T)$.

Providing the condition stated in equation (B.33) is satisfied, equation (B.32) appears be very efficient at estimating ADZ model parameters from DP model parameters. Bringing equation (B.32) back to a dimensional time axis we get

$$t_d = 0, \quad t_r = \frac{2}{3}\frac{\sigma}{(1+\sigma)}t_{cb} \quad \text{and} \quad N = \frac{3}{2}\frac{(1+\sigma)}{\sigma}\frac{z}{L}\frac{t_a}{t_{cb}} \tag{B.34}$$

where it can be seen that the residence time is proportional to the characteristic block diffusion time while the number of CSTRs needed is also dependant on the advective travel time.

B.6 Moment matching with hydrodynamic dispersion

Barker et al. (2000) suggest that dispersivity, χ (from $D_L = \chi|v_f|$) is typically one-tenth of the distance being considered, L (i.e. $Pe = 10$). Given this criterion, *Barker et al.* (2000) further suggest that hydrodynamic dispersion should be negligible if the effective dispersivity $\chi^* = L/Pe^*$ (where Pe^* is the dimensionless Pe parameter a model without matrix diffusion) is greater than the distance travelled (i.e. $Pe^* < 1$). An effective dispersivity can be found by equating the second central moment of the DP model with an equivalent moment where t_{cb} is assumed to be zero, as follows

$$\frac{2Z}{Pe} + \frac{2}{3}\frac{Z}{\gamma}\frac{\sigma}{(1+\sigma)} = \frac{2Z}{Pe^*} \tag{B.35}$$

which can be rearranged to get

$$\frac{1}{Pe} + \frac{1}{3}\frac{t_{cb}}{t_a}\frac{\sigma}{(1+\sigma)} = \frac{1}{Pe^*} \tag{B.36}$$

It can therefore be ascertained that hydrodynamic dispersion may be significant when

$$\gamma = \frac{t_a}{t_{cb}} > \frac{1}{3}\frac{\sigma}{(1+\sigma)} \approx \frac{1}{3} \tag{B.37}$$

which is always the case providing the condition in equation (B.33) is satisfied. Consequently we must consider the ADZ-DP moment matching relationships when hydrodynamic dispersion is not negligible.

For situations when the characteristic block diffusion time is small the limiting case when $\gamma \to \infty$ can be adopted. Application of equation (B.30) in conjunction with equations (B.24)

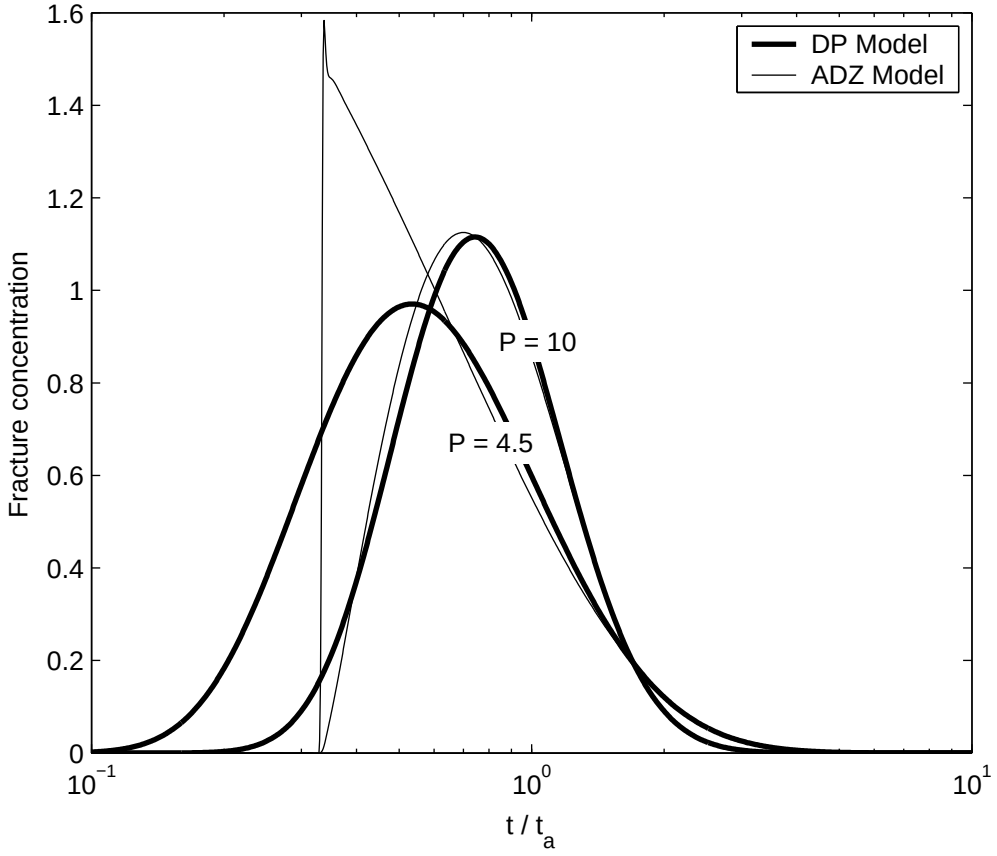

Figure B.4 Breakthrough curves from the DP model and the ADZ model with $\gamma = \infty$, $Z = 1$, $\sigma = 140$ and Pe as indicated.

to (B.26) then yields

$$T_d = \frac{Z}{3}, \quad T_r = \frac{3}{Pe} \quad \text{and} \quad N = \frac{2}{9}ZP \quad \text{as} \quad \gamma \to \infty \tag{B.38}$$

The ADZ model tends to be unstable for $N < 1$. Hence another limiting condition for the ADZ model to appropriately approximate DP model breakthrough curves must be that

$$Pe \geq \frac{9}{2Z} \tag{B.39}$$

Figure B.4 shows breakthrough curves for the DP model and the ADZ model when $\gamma = \infty$, $\sigma = 140$, $Z = 1$ with $Pe = 10$ and $Pe = 9/2$. It can be seen that the ADZ model approximates the DP model well when $Pe = 10$. As Pe approaches $9/2$, the ADZ model appears to truncate the head of the curve, which is then compensated for by an overestimate of the peak. Figure B.5 explores the efficiency of equation (B.30) in estimating ADZ parameters from DP parameters when there is hydrodynamic dispersion and spreading due to matrix diffusion. It can be seen that the ADZ parameter estimates are still plausible providing the conditions in equations (B.33) and (B.39) are satisfied.

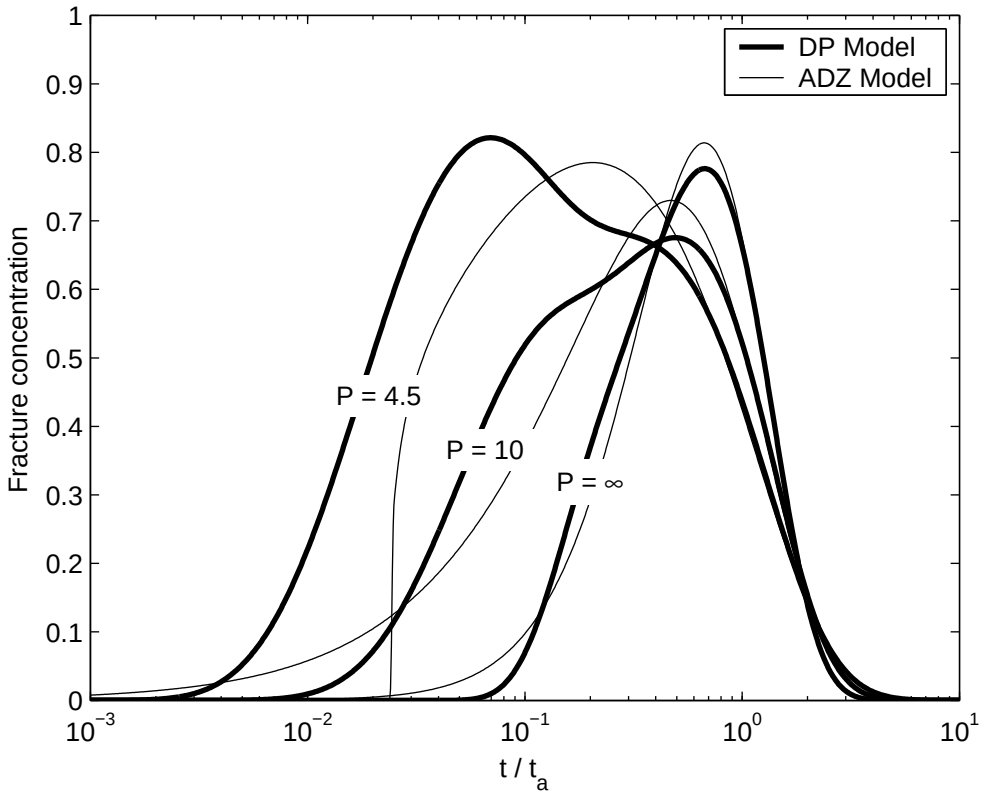

Figure B.5 Breakthrough curves from the DP model and the ADZ model with $\gamma = 2$, $Z = 1$, $\sigma = 140$ and Pe as indicated.

B.7 Conclusions

Analytical expressions have been derived that relate aggregated dead zone (ADZ) model parameters to parameters describing a diffusive type dual-porosity (DP) model. It has been shown that as long as the advective travel time, t_a is greater than the matrix block diffusion time, t_{cb} and as long as the hydrodynamic dispersivity, χ is not greater than 2/9 of the distance being considered (recall equation B.39 and that $\chi = Z/Pe$), the ADZ model appears to be a plausible substitute for the DP model. If we consider solute (such as tritium, nitrate or chloride, i.e. $D_A \approx 10^{-10}$ m^2/s) diffusing into Chalk blocks with half-widths of around 10 cm, this gives a $t_{cb} = 1000$ days. Taking $\sigma = 140$, for a stretch of 100 m, the maximum velocity in the fractures (i.e. v_f) that can be considered is 14 m/day (*Foster*, 1993, considers a range from 10 to 1000 m/day). The ADZ model fails to represent DP systems well when $t_a < t_{cb}$, because this condition causes the DP model to produce a 'shouldered' breakthrough curve. The ADZ model would only be able to approximate this by considering two non-identical series of CSTRs in parallel causing a doubling in parameter requirement.

From this we can conclude that the moment matching procedure for estimating ADZ

model parameters using knowledge of DP model parameters, as suggested by *Lees et al.* (2000), is not as useful when looking at fractured porous media such as the Chalk. *Lees et al.* (2000) were interested in solute transport through rivers where the equivalent t_{cb} (associated with dead zones) would be much smaller allowing a greater flexibility in advective travel times that can be considered (recall equation B.33). However, alternative ADZ model structures where parameters are estimated by calibration against observed data may often be more suitable than the DP model (*Beven and Young*, 1988).